REDOX HOMEOSTASIS AND METABOLIC REPROGRAMMING IN SKELETAL MUSCLE: EXPLORING THE ROLE OF THE CYSTINE/GLUTAMATE ANTIPORTER

Michel Kanaan

A thesis submitted to the University of Ottawa
in partial fulfillment of the requirements for the
Doctorate in Philosophy degree in Biochemistry

Department of Biochemistry, Microbiology, and Immunology
Faculty of Medicine
University of Ottawa

ABSTRACT

Skeletal muscle regeneration is a highly regulated process that primarily relies on the activity of muscle satellite cells (MuSCs). The functions and fates of MuCSs are highly sensitive to alterations in cellular redox, as different phases of the myogenic program are redox-sensitive. Glutathione (GSH), a major antioxidant in muscle cells, plays a key role in myogenesis by maintaining redox homeostasis. Redox homeostasis is often disrupted in muscle injury, aging, and diseases such as muscular dystrophies. Cysteine is the rate-controlling amino acid in the synthesis of GSH in the cytosol. Cystine, the predominant form of free cysteine in blood, is imported into cells by the plasma membrane antiporter, xCT, which imports cystine and exports glutamate. As such, this antiporter plays a central role in controlling intracellular GSH levels. xCT can also regulate cellular metabolism by modulating the intracellular availability of cysteine and glutamate, which impact a number of metabolic pathways. Therefore, xCT, through its dual redox and metabolic roles, can profoundly impact skeletal muscle health and its regenerative capacity.

The first project of my doctoral research aimed to elucidate the role of xCT in regulating MuSC myogenic programming processes. It also explored the implications of xCT in the context of exercise training. Given the well-recognized redox role of xCT, we hypothesized that xCT controls skeletal muscle regeneration by modulating GSH redox. To test this hypothesis, we employed a multifaceted approach, including bioinformatic analyses, *in vitro* studies using the murine C2C12 muscle cell line and mouse primary muscle cells, as well as *in vivo* experiments with xCT-mutant mice ($Slc7a11^{sut/sut}$). Our findings revealed that xCT is indispensable for MuSC proliferation and self-renewal processes, while its expression is downregulated during myotube differentiation. Strikingly, xCT deficiency enhanced myogenic differentiation *in vitro*

and *in vivo*. Furthermore, xCT-mutant mice displayed improved insulin sensitivity pre- and post-exercise training and had blunted muscle mitochondrial biogenesis and respiration in response to exercise training. These findings highlight the role of xCT in skeletal muscle regenerative capacity and metabolism, which may help inform novel therapeutic approaches for muscle wasting and dysfunction observed in metabolic diseases and aging.

MuSC proliferation is an essential myogenic phase for stem cell pool maintenance and successful muscle repair. Disruptions in metabolic processes during MuSC proliferation, particularly a decreased supply of amino acids, can impair MuSC growth and function and compromise muscle health. Thus, my second project investigated the metabolic consequences of xCT deficiency in proliferating MuSCs. We hypothesized that loss of xCT perturbs redox balance, disrupts mitochondrial structure, and alters metabolic pathways in proliferating MuSCs. By leveraging complementary bioinformatic, metabolomic, and mechanistic approaches, our findings revealed that xCT-deficient MuSCs have impaired GSH redox and lower glycolytic and oxidative capacities associated with DRP1-mediated mitochondrial fragmentation. To compensate for dysregulated xCT transport activity, MuSCs underwent metabolic reprogramming, directing glycolytic intermediates toward serine and cysteine biosynthesis. Additionally, xCT-deficient MuSCs channeled excess glutamate toward proline biosynthesis to maintain cellular redox and balance between oxidative and reductive pathways. These findings emphasize the role of xCT in driving metabolic adaptations in MuSCs, further confirming the link between redox regulation and cellular metabolism.

In conclusion, these projects provide novel insights into the dual role of xCT in skeletal muscle redox and metabolism during various myogenic stages. A better understanding of xCT function

in skeletal muscle may pave the way for therapeutic interventions aimed at restoring/improving muscle health in conditions characterized by dysregulated redox and metabolism.

ACKNOWLEDGEMENTS

First and foremost, I express my profound gratitude to **Jesus Christ** and the **Virgin Mary** for their unwavering presence and countless blessings. Their grace has supported me during the toughest times, making this thesis possible.

Pursuing a PhD is never an easy task, particularly during a global pandemic, while I witnessed the ongoing crisis in my homeland, Lebanon. This journey has challenged me in many ways, and it would not have been achievable without the support of many individuals.

I would like to sincerely thank my supervisor, **Dr. Mary-Ellen Harper**, for believing in a young man from Lebanon who came with nothing but hope and determination. Your trust, mentorship, and scientific insight have profoundly shaped my development as a researcher. I am grateful for the knowledge I have gained under your guidance and the dedication you represent as a scientist.

My heartfelt appreciation also goes to **Dr. Chantal Pileggi**, whose expertise and leadership in the lab have taught me immensely.

To my current and former colleagues in the Harper lab and from other labs: thank you for your support and for the many shared laughs and invaluable moments during long days in the lab. A special thanks to **Charbel Karam**, **Luke Kennedy**, **Claire Fong-McMaster**, **Dhanuddara Mohottalage**, **Dr. Rajaa Sebaa**, **Dr. Alessandra Gentile**, **Dr. David Patten**, **Dr. Gaganvir Parmar**, **Dr. William Chen**, **Dr. Jamie Whitcomb**, **Dr. Lara Gharibeh**, **Danny Farhat**, and **Jian Xuan**. Your presence has enriched this journey in ways I cannot fully express.

To all my friends, near and far, who have supported me through the years: thank you from the depths of my heart. I wish I could name each of you, but I would need several more pages to do so.

To my mother, **Marcelle**; my brother, **Dr. Georges Kanaan**; my aunts, **Micheline** and **Antoinette**; and my entire family: your love, encouragement, and faith in me have never faded. You have given me the strength to persevere, even when things felt impossible. I feel incredibly blessed to have you all in my life.

Finally, to my father, **Nicolas:** more than anything, I wish you could be here today for my defense. Your memory has accompanied me throughout every step of the way. This thesis is dedicated to you and to all those who stood by me.

TABLE OF CONTENTS

ABSTRACT ii

ACKNOWLEDGEMENTS v

TABLE OF CONTENTS vii

LIST OF ABBREVIATIONS xiv

LIST OF TABLES xix

LIST OF FIGURES xx

LIST OF SUPPLEMENTARY FIGURES xxi

CHAPTER 1: GENERAL INTRODUCTION 1

1.1 Skeletal Muscle Structure 1

1.2 Skeletal Muscle Functions 4

1.2.1 The Neuromuscular Junction 4

1.2.2 Force Generation 5

1.3 Skeletal Muscle Fiber Heterogeneity 5

1.4 Skeletal Muscle Energy Metabolism 8

1.4.1 Glycolysis 8

1.4.2 Mitochondrial Oxidative Pathways 9

1.4.3 Skeletal Muscle Metabolic Flexibility 15

1.4.4 Mitochondrial Structure and Dynamics 16

1.4.5 Mitochondrial Biogenesis 17

1.4.6 Mitophagy 18

1.5 Skeletal Muscle Growth 21

1.5.1 Skeletal Muscle Hypertrophy 21

1.5.2 Skeletal Muscle Atrophy 22

1.5.3 Myogenesis 23

1.6 Redox Homeostasis in Skeletal Muscle 27

1.6.1 Reactive Oxygen and Nitrogen Species 27

1.6.2 Different Cellular ROS Producers in Skeletal Muscle 28

1.6.3 Antioxidant Systems in Skeletal Muscle 29

1.7 Cysteine 34

1.7.1 Cysteine Bioavailability and Sources 34

1.7.2 Non-specific Cysteine Transporters 35

1.7.3 Cystine/glutamate Antiporter, System Xc- 36

1.8 Metabolic and Redox Implications in Skeletal Muscle Regeneration 42

1.8.1 Metabolic Regulation of Myogenesis 42

1.8.2 Redox Regulation of Myogenesis 43

1.9 Glutathione Redox and ROS in Skeletal Muscle-related Diseases 46

1.9.1 Muscular Dystrophies 46

1.9.2 Metabolic Diseases 47

1.9.3 Sarcopenia 49
1.10 Aims and Hypotheses 50
1.11 References 52
CHAPTER 2: 77
2.1 STATEMENT OF MANUSCRIPT STATUS AND CONTRIBUTIONS 78
2.1.1 Statement of Manuscript Status 78
2.1.2Acknowledgements 78
2.1.3 Author Contributions 78
2.1.4 Funding 79
2.1.5 Conflict of Interests 79
2.2 Abstract 80
2.3 Introduction 81
2.4 Experimental Procedures 83
2.4.1 Bioinformatic Analysis of C2C12 Transcriptomics Differentiation Profiles 83
2.4.2 Correlation Analysis 84
2.4.3 Hierarchical Clustering 84
2.4.4 Enrichment Analysis 84
2.4.5 Animals 84
2.4.6 Measurements of Body Composition, Food Intake, Volitional Activity, and Indirect Calorimetry 85

2.4.7 Oral Glucose Tolerance Test and Intraperitoneal Insulin Tolerance Test 85

2.4.8 Exercise Training Protocol 86

2.4.9 Muscle Injury Protocol 86

2.4.10 C2C12 Cell Culture 86

2.4.11 Mouse Primary Muscle Cell Isolation and Culture 86

2.4.12 Immunostaining of Primary Muscle Cells 87

2.4.13 GSH and GSSG Measurements 88

2.4.14 Extracellular Flux Determinations of Cellular Bioenergetics 89

2.4.15 In situ Determinations of Oxygen Consumption in Cultured Primary Cells during Proliferation and Differentiation 90

2.4.16 Glucose Uptake in Primary Muscle Cells 90

2.4.17. Cell Death and Growth Assays 90

2.4.18 High-resolution Respirometry of ex vivo Muscle 91

2.4.19 Muscle Tissue Immunohistochemistry 91

2.4.20 Muscle Cross-sectional Area Determinations 92

2.4.21 Protein Extraction 92

2.4.22 Western Blot Analyses 92

2.4.23 Enzymatic Activity Analyses 93

2.4.24 Statistics 94

2.5 Results 95

2.5.1 xCT controls GSH Redox during Myogenic Proliferation.....95

2.5.2 Absence of Functional xCT Inhibits Proliferation but Potentiates Myogenesis ..101

2.5.3 In vivo Evidence of Enhanced Myogenesis in the Absence of xCT Function.....109

2.5.4 Increased Insulin Sensitivity and Impaired Muscle Mitochondrial Energetics Response to Exercise Training in xCT deficient Mice.....114

2.6 Discussion 118

2.7. References 123

2.8 Supplementary Figures.....131

CHAPTER 3: 139

3.1 STATEMENT OF MANUSCRIPT STATUS AND CONTRIBUTIONS 140

3.1.1 Statement of Manuscript Status 140

3.1.2Acknowledgements 140

3.1.3 Author Contributions.....140

3.1.4 Funding 141

3.1.5 Conflict of Interests.....141

3.2 Abstract 142

3.3 Introduction 144

3.4 Experimental Procedures 146

3.4.1. Animals 146

3.4.2. Mouse Primary Muscle Cell isolation and Culture 146

3.4.3. Immunostaining of Primary Muscle Cells 147

3.4.5. Cystine and Glucose Uptake in Primary Muscle Cells 147

3.4.6. GSH and GSSG Measurements 148

3.4.7. Cellular Bioenergetics 148

3.4.8. Citrate Synthase Activity 149

3.4.9. Cellular Protein Levels 149

3.4.10. Western Blot Analyses 150

3.4.11. Mitochondrial H_2O_2 Emission 151

3.4.12. Metabolomic Stable Isotope Tracer Analysis (SITA) and LC-MS 151

3.4.13. Metabolomic Profiling 152

3.4.14. Analysis of Metabolomic Profiling Data 153

3.4.15. Statistics 154

3.5 Results 155

3.5.1. xCT Controls GSH Levels and Redox in Proliferating Muscle Cells 155

3.5.2. Impaired cellular bioenergetics accompanied by fragmented mitochondrial structure in Slc7a11$^{sut/sut}$ MuSCs 159

3.5.3. Metabolomic Profiling Analysis Reveals Distinct Phenotypes Including Differences in Branched Chain Amino Acids, Cysteine, Methionine, and Proline in Slc7a11$^{sut/sut}$ MuSCs 163

3.5.4. xCT Deficiency Upregulates Glucose Uptake and Promotes Cellular de novo Serine Synthesis 169

3.5.5. Increased Proline Biosynthesis in the Absence of Functional xCT 173

3.6. Discussion 177

3.7. References 184

3.8. Supplementary Figures 193

CHAPTER 4: GENERAL DISCUSSION 200

4.1 References 214

CHAPTER 5: APPENDIX 223

LIST OF ABBREVIATIONS

2ME	2-mercaptoethanol
3MST	3-mercaptopyruvate sulfurtransferase
3PG	3-phosphoglycerate
AARE	Amino acid response element
ACC	Acetyl-CoA carboxylase
ACh	Acetylcholine
ADP	Adenosine diphosphate
α-KG	α-ketoglutarate
AMP	Adenosine monophosphate
AMPK	AMP-activated protein kinase
ARE	Antioxidant response element
ASCT	Alanine-serine-cysteine transporter
ATF4	Activating transcription factor 4
ATF5	Activating transcription factor 5
ATP	Adenosine triphosphate
BAP1	BRCA1-associated protein 1
BAT	Brown adipose tissue
BAX	BCL-associated X
BCAA	Branched-chain amino acids
BCAT	Branched-chain amino acid aminotransferase
BCKAs	Branched-chain keto acids
BCKDH	Branched-chain keto acid dehydrogenase
BRD4	Bromodomain-containing protein 4
CAT	Catalase
CBR1	Carbonyl reductase 1
CBS	Cystathionine β-synthase
CD36	Cluster of differentiation 36
CHOP	C/EBP homologous protein
CO_2	Carbon dioxide
CoQ	Coenzyme Q
CoQH•	Ubisemiquinone
CPT1	Carnitine palmitoyltransferase 1
CPT2	Carnitine palmitoyltransferase 2
CTH	Cystathionine γ-lyase
CTX	Cardiotoxin
DEM	Diethyl maleate
DMD	Duchenne muscular dystrophy
DRP1	Dynamin-related protein 1

DTT	Dithiothreitol
DUOX	Dual oxidase
EAATs	Excitatory amino acid transporter
ECM	Extracellular matrix
EGFR	Epidermal growth factor receptors
eIF2B	Eukaryotic translation initiation factor 2B
eIF2α	Eukaryotic translation initiation factor 2 alpha
eIF4E-4EBP1	Eukaryotic translation initiation factor 4E binding protein 1
EpRE	Electrophile response element
ER	Endoplasmic reticulum
ERR-α	Estrogen-related receptor-α
ETC	Electron transport chain
FABP3	FA binding protein 3
$FADH_2$	Flavine adenine dinucleotide
FAK	Focal adhesion kinase
FAO	Fatty acid oxidation
FAP	Fibro-adipogenic progenitor
FA	Fatty acid
FBXO40	F-box protein 40
Fe/S	Iron-sulfur
FGF21	Fibroblast growth factor 21
FIS1	Fission 1 protein
FMN	Flavin mononucleotide
FOXO	Forkhead box O
GAPDH	Glyceraldehyde-3-phosphate dehydrogenase
GCL	Glutamate-cysteine ligase
GDF15	Growth differentiation factor 15
GLS	glutaminase
GLUT4	Glucose transporter 4
GPX	Glutathione peroxidase
GR	Glutathione reductase
GRE	Glucocorticoid response element
GRX	Glutaredoxin
GSH	Glutathione
GSHee	GSH ethyl ester
GSK3β	Glycogen synthase kinase-3 beta
GSS	Glutathione synthetase
GSSG	Glutathione disulfide
GST	Glutathione s-transferase
GYS1	Glycogen synthase 1
Gαi2	G protein subunit alpha i2

H_2O	Water
H_2O_2	Hydrogen peroxide
H_2S	Hydrogen sulfide
H4K16	Histone H4 lysine 16
HAT	Heterodimeric amino acid transporter
HDAC1	Histone deacetylase complex 1
HKII	Hexokinase 2
HO•	Hydroxyl radicals
HOCl	Hypochlorous acid
IGF1	Insulin-like growth factor 1
IGF1R	Insulin-like growth factor 1 receptor
IKE	Imidazole ketone erastin
IL	Interleukin
IMM	Inner mitochondrial membrane
IMS	Intermembrane space
IRS1	Insulin receptor substrate
JAK/STAT	Janus kinase/signal transducers and activators of transcription
KEAP1	Kelch-like ECH-associated protein 1
Kg	Kilogram
LDH	Lactate dehydrogenase
LDHA	Lactate dehydrogenase A-subunit
l-OPA1	Long form of optic atrophy protein 1
LPS	Lipopolysaccharide
MBD2	Methyl CpG-binding protein
MFF	Mitochondrial fission factor
MFN1	Mitofusin 1
MFN2	Mitofusin 2
MIRO	Mitochondrial Rho GTPase
MRF4/Myf6	Myogenic regulatory factor 4
MRF	Myogenic regulatory factor
MRP1	Multidrug resistance protein 1
mtDNA	Mitochondrial DNA
mtISR	Mitochondrial integrated stress response
mTOR	Mammalian target of rapamycin
mTORC1	Mammalian target of rapamycin complex 1
mTORC2	Mammalian target of rapamycin complex 2
mtPTP	Mitochondrial permeability transition pore
mtROS	Mitochondrial ROS
mtTFA	Mitochondrial transcription factor A
MURF1	Muscle RING-finger protein-1

MuSC	Muscle satellite cell
Myf5	Myogenic factor 5
MyHC	Myosin heavy chain
MyoD	Myoblast determination protein 1
MyoG	Myogenin
NAC	N-acetyl cysteine
NADH	Nicotinamide adenine dinucleotide
NADPH	Nicotinamide adenine dinucleotide phosphate
NFκB	Nuclear factor-kappa B
NMJ	Neuromuscular junction
NNT	Nicotinamide nucleotide transhydrogenase
NO•	Nitric oxide
NOD2	Nucleotide-binding oligomerization domain protein-2
NOS	Nitric oxide synthase
NOX	NADPH oxidase
NRF1	Nuclear respiratory factor 1
NRF2	Nuclear factor erythroid 2-related factor 2
O_2^-	Superoxide anion
OMM	Outer mitochondrial membrane
$ONOO^-$	Peroxynitrite
OPA1	Optic atrophy protein 1
OXPHOS	Oxidative phosphorylation
P13K	Phosphatidylinositol-3-kinase
p38 MAPK	p38 mitogen-activated protein kinase
PAR	Partitioning-defective
Pax7	Paired-box transcription factor 7
PDH	Pyruvate dehydrogenase
PDK	Pyruvate dehydrogenase kinase
PFKM	Phosphofructokinase
PGC-1α	Peroxisome proliferator-activated receptor gamma coactivator 1 alpha
PGK	Phosphoglycerate kinase
PHGDH	Phosphoglycerate dehydrogenase
Pi	Inorganic phosphate
PINK1	Phosphatase and tensin homolog-induced putative kinase 1
PIP3	Phosphatidylinositol-3,4,5 triphosphate
PITX2	Paired-like homeodomain transcription factor 2
PITX3	Paired-like homeodomain transcription factor 3
PMF	Proton motive force
PPARγ	Peroxisome proliferator-activated receptor gamma
PPP	Pentose phosphate pathway
PRC1	Polycomb repressive complex 1

PRX	Peroxiredoxin
PSAT1	Phosphoserine aminotransferase 1
PSPH	Phosphoserine phosphatase
RET	Reverse electron transfer
RNS	Reactive nitrogen species
RO•	Alkoxyl
ROO•	Peroxyl
ROOH	Organic hydroperoxides
ROS	Reactive oxygen species
S6K1	S6 kinase 1
SHMT	Hydroxymethyltransferase
SIRT-1	Sirtuin 1
SMAD2/3	SMA- and MAD-related protein 2 and
SOD	Superoxide dismutase
s-OPA1	Short form of optic atrophy protein 1
T2DM	Type 2 diabetes mellitus
TCA	Tricarboxylic acid
TGF-β	Transforming growth factor
TNFα	Tumor necrosis factor alpha
TRX	Thioredoxins
TRXR	Thioredoxin reductase
Ub	Ubiquitin
VDAC	Voltage-dependent anion-selective channel
Wnt	Wingless-related integration site
XOR	Xanthine oxidoreductase
XRE	Xenobiotic response element
Zip1	Zinc transporter 1

LIST OF TABLES

Table 1.1. Skeletal Muscle Fiber Types......7

Table 2.1. Metabolic Phenotyping of WT and Slc7a11$^{sut/sut}$.....102

Table 3.1. List of significantly different metabolites between WT and Slc7a11$^{sut/sut}$ MuSCs......168

LIST OF FIGURES

Figure 1.1. Skeletal Muscle Structure 3

Figure 1.2. Metabolic Pathways Activated in Skeletal Muscle During Exercise 14

Figure 1.3. Mitochondrial Structure, Dynamics, Biogenesis and Mitophagy 20

Figure 1.4. Skeletal Muscle Regeneration 25

Figure 1.5. Various Sources of Cysteine and GSH Biosynthesis 38

Figure 1.6. Molecular Regulators of xCT Induction and Suppression 41

Figure 2.1. xCT Controls GSH Redox During Myogenic Proliferation 100

Figure 2.2. Absence of Functional xCT Inhibits Proliferation but Potentiates Myogenesis 108

Figure 2.3. Absence of xCT Enhances myogenesis Following Cardiotoxin-induced Muscle Injury 113

Figure 2.4. Increased Insulin Sensitivity and Impaired Muscle Mitochondrial Energetics in Response to Exercise Training in Slc7a11$^{sut/sut}$ mice 117

Figure 3.1. xCT Controls GSH Levels and Redox in Proliferating Muscle Cells 158

Figure 3.2. Impaired cellular bioenergetics accompanied by fragmented mitochondrial structure in Slc7a11$^{sut/sut}$ MuSCs 162

Figure 3.3. Metabolomic Profiling Analysis Reveals Distinct Phenotypes Including Differences in Branched Chain Amino Acids, Cysteine, Methionine, and Proline in Slc7a11$^{sut/sut}$ MuSCs 166

Figure 3.4. xCT Deficiency Upregulates Glucose Uptake and Promotes Cellular *de novo* Serine Synthesis 172

Figure 3.5. Increased Proline Biosynthesis in the Absence of Functional xCT 176

LIST OF SUPPLEMENTARY FIGURES

Supplementary Figure 2.1. 132

Supplementary Figure 2.2. 135

Supplementary Figure 2.3. 136

Supplementary Figure 2.4. 138

Supplementary Figure 3.1. 193

Supplementary Figure 3.2. 195

Supplementary Figure 3.3. 197

Supplementary Figure 3.4. 199

CHAPTER 1: GENERAL INTRODUCTION

Skeletal muscle tissue accounts for slightly less than half of the body mass in lean adults and consists of over 600 muscles that enable movement and stability [1]. Skeletal muscle function and health can be compromised by injury, disease, or disuse, resulting in reduced mobility and poor quality of life at any age [2]. This introduction will explore the interconnected roles of redox balance and metabolic pathways in maintaining skeletal muscle homeostasis and regulating its regenerative capacity.

1.1 Skeletal Muscle Structure

Skeletal muscle is a highly organized tissue made of thousands of muscle fibers known as myofibers that are arranged into fascicles. The sarcomere is the contractile unit of skeletal muscle, and it mainly consists of proteins responsible for muscle contraction, such as actin and myosin. A group of sarcomeres arranges together to form myofibrils, which are further grouped to create myofibers[3] (**Figure 1.1**). In muscle anatomy, the sarcolemma refers to the cell membrane of a myofiber, and the sarcoplasm is the cytoplasm within that muscle fiber. The sarcoplasm contains the sarcoplasmic reticulum that acts as a reservoir for calcium (Ca^{2+}), whereas, the sarcolemma contains structural invaginations known as T-tubules that facilitate ion exchange during muscle contraction [4].

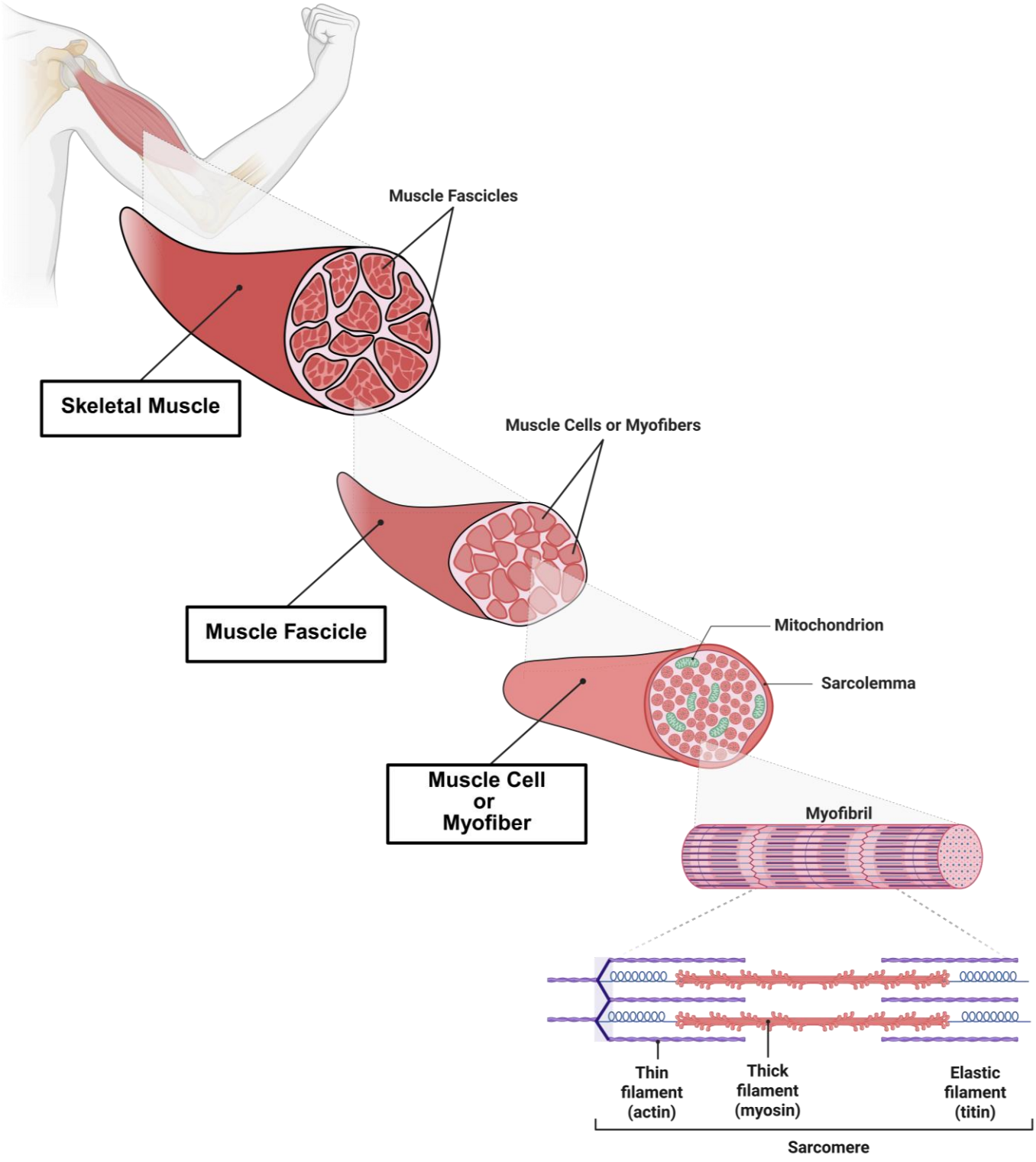
Muscle Fascicles
Skeletal Muscle
Muscle Cells or Myofibers
Muscle Fascicle
Mitochondrion
Sarcolemma
Muscle Cell
or
Myofiber
Myofibril
Thin
filament
(actin)
Thick
filament
(myosin)
Elastic
filament
(titin)
Sarcomere

Figure 1.1. Skeletal Muscle Structure
Skeletal muscle has a hierarchical organization composed of fascicles, myofibers, myofibrils, and sarcomeres. Muscle tissue is made up of bundles of fascicles, which are surrounded by connective tissue, nerve fibers, and blood vessels. Each fascicle contains a group of myofibers, which are the fundamental units of skeletal muscle. Within each myofiber are multiple myofibrils, which are cylindrical structures formed by the assembly of sarcomeres. Sarcomeres, the basic contractile units of muscles, are composed of organized arrays of actin (thin filaments) and myosin (thick filaments). This figure was created with BioRender.com

1.2 Skeletal Muscle Functions

The primary function of skeletal muscle is to convert chemical energy into mechanical energy to generate force, which allows the tissue to support movement and maintain posture [2]. Skeletal muscle also plays an important role in regulating whole body metabolism by contributing to basal energy metabolism, acting as a reservoir for amino acids and carbohydrates, blood glucose homeostasis, regulating core temperature, and accounting for most of the body's oxygen and fuel consumption during physical activity and exercise [5,6].

1.2.1 The Neuromuscular Junction

The neuromuscular junction (NMJ) transmits signals from motor neurons to myofibers and consists of three distinct compartments: the presynaptic nerve terminal, the synaptic cleft, and the postsynaptic motor end plate [7]. In response to an action potential, acetylcholine (ACh) binds to nicotinic receptors and mediates Na^+ influx into the sarcoplasm and signal transmission through T-tubules, inducing Ca^{2+} release from the sarcoplasmic reticulum to initiate excitation-contraction coupling. These chemical changes support the sliding of myofibrils past each other without changing their length, a process known as the filament model of contraction. Troponin is another protein that plays a pivotal role in muscular contraction along with actin and myosin.

At rest, low levels of Ca^{2+} keep tropomyosin in place, blocking myosin-binding sites on actin and preventing contraction. During excitation, tropomyosin is displaced after Ca^{2+} binding to troponin C, which allows myosin heads to form cross-bridges with actin and to drive filament sliding. However, muscle contraction is over when ACh is degraded by acetylcholinesterase, leading to the repolarization of the sarcolemma and the reabsorption of Ca^{2+} by the sarcoplasmic reticulum [8].

1.2.2 Force Generation

The contraction of a sarcomere is driven by the cross-bridge cycle, a phenomenon that involves the movement of myosin filaments along actin filaments [9]. The cross-bridge cycle occurs following six enzymatic steps that allow myosin heads to move along actin filaments, generating force throughout the muscle. The first step of muscular contraction is mediated by the binding of cytosolic Ca^{2+} to troponin, followed by a conformational change that exposes myosin-binding sites on actin. Consequently, the myosin head binds to the actin filament at a 45° angle (rigid state). Then, adenosine triphosphate (ATP) binds to myosin, causing its detachment from the actin filament. The hydrolysis of ATP to adenosine diphosphate (ADP) and inorganic phosphate (Pi), catalyzed by myosin ATPase activity, allows the myosin filament to re-attach weakly to actin at a 90° angle (cross-bridge). The release of Pi provides sufficient power for the myosin head to rotate, pushing the actin filament. When this process is completed, the myosin head releases ADP and returns to its rigid state, prepared for the next cycle [10].

1.3 Skeletal Muscle Fiber Heterogeneity

The capacity of skeletal muscle to adapt to various mechanical and metabolic demands is partly attributable to the tissue diversity in the mechanical and biochemical characteristics of individual myofibers. Muscle fibers can be classified into two major types: slow-twitch (type I) and fast-twitch (type II) which are characterized by distinct expression patterns of sarcomere myosin heavy chain (MyHC) isoforms (**Table 1.1**). Slow-twitch or type I fibers are rich in mitochondria and display a high oxidative capacity. This metabolic characteristic makes type I fibers fatigue-resistant and suitable for prolonged low-force contractions like marathon running and lower-intensity swimming. Type II fibers can be further classified into subtypes, such as IIA, IIX, and IIB [11]. Type IIA and IIX fibers are found in humans and rodents, whereas type IIB fibers are exclusively present in rodents [12]. Type IIA fibers are fast oxidative glycolytic fibers, whereas type IIX and IIB fibers are purely fast glycolytic fibers. Type

II fibers are less fatigue-resistant and support contractions with short anaerobic bursts, such as those during powerlifting and sprinting [12]. Type IIA fibers are metabolically the closest to type I fibers since they exhibit high mitochondrial content with a greater dependence on oxidative metabolism in mitochondria compared to other type II fibers.

Although most nuclei within the same myofiber transcribe a single MyHC isoform, a minority of myofibers can be hybrid [13]. Hybrid myofibers co-express different MyHC isoforms, enabling further functional adaptations ranging from the slowest and most oxidative to the fastest and most glycolytic pathways (I → I/IIA → IIA → IIA/IIX → IIX) [14]. Myofibers can undergo remodeling and change their composition, abundance, and functional characteristics in response to conditions such as exercise, inactivity, disease, and aging. Various types of exercise training can differently impact myofiber composition. It has been reported that endurance training increases the abundance or proportion of type I fibers, whereas resistance training downregulates *MyHC7* gene expression without altering the corresponding type I fibers abundance [15]. Moreover, it has been shown that exercise training shifts myofibers towards a less hybrid phenotype. For instance, endurance and resistance training promote hybrid myofiber compositions towards type I and type IIA, respectively [16]. Furthermore, it has been demonstrated that fast glycolytic muscle fibers are more prone to age-related muscle wasting [17]. However, other studies conducted in mice and humans have shown that aging causes a reduction in the size of all fiber types, irrespective of fiber type specificity [18,19].

Fiber Type	**I**	**IIA**	**IIX**	**IIB**
MyHC Gene	*MyHC7*	*MyHC2*	*MyHC1*	*MyHC4*
MyHC Isoform	MyHC I	MyHC IIA	MyHC IIX	MyHC IIB
Contractile Speed	Slow	Moderate	Fast	Very Fast
Mitochondrial Density	High	Intermediate	Low	Low
Metabolism	Oxidative	Oxidative/Glycolytic	Glycolytic	Glycolytic
Fatigability	Low	Moderate	High	Highest

Table 1.1. Skeletal Muscle Fiber Types.
Different muscle fiber types are classified based on their expression of MyHC isoforms. Skeletal muscle is a heterogeneous tissue where each muscle fiber type displays distinct metabolic and functional characteristics. Different MyHC isoforms can also be co-expressed within the same muscle fiber, generating a hybrid myofiber. Due to their mixed composition, hybrid myofibers can exhibit remarkable functional and metabolic adaptations.

1.4 Skeletal Muscle Energy Metabolism

ATP availability is essential for multiple key cellular processes that drive skeletal muscle function such as Ca^{2+} storage (Ca^{2+} ATPase), membrane excitability (Na^{+}/ K^{+} ATPase), and myofilament cross-bridge cycling (myosin ATPase). Energy in the form of ATP is essential for supporting muscle contraction throughout all types of activities, with distinct intensity levels and durations. However, skeletal muscle ATP storage capacity is extremely small (~5 mmol per kg muscle), therefore, the tissue relies on various metabolic pathways to produce ATP [20]. In response to metabolic stress, the decrease in ATP levels elevates the adenosine monophosphate (AMP): ATP and ADP: ATP ratios, leading to the activation of the energy sensor, AMPK. Once activated, AMPK helps restore cellular energy balance by suppressing ATP-consuming pathways while stimulating ATP-generating pathways [21]. To produce ATP, skeletal muscle can use a variety of substrates as fuel including carbohydrates (glucose and muscle glycogen) and fats (plasma-free fatty acids and muscle triglycerides). The two major pathways for muscle ATP generation are glycolysis and oxidative phosphorylation (OXPHOS). However, these pathways do not function in isolation; they can operate simultaneously or to some extent in relative isolation during physical activity, and this depends mainly on contraction intensities [5].

1.4.1 Glycolysis

Glycolysis is a major metabolic pathway that enables skeletal muscle tissue to rapidly produce ATP in response to increasing energy demands. Glycolysis can occur aerobically or anaerobically in the sarcoplasm following ten reactions that lead to pyruvate production. These reactions can be split into two phases: the preparatory phase and the energy-yielding phase [22]. In the first phase, two ATP molecules are utilized in the reactions catalyzed by hexokinase (HKII) and phosphofructokinase (PFK). In the second phase, four ATP molecules are produced by the reactions catalyzed by phosphoglycerate kinase (PGK) and pyruvate kinase (PK), yielding a net gain of two ATP molecules [23]. In anaerobic

glycolysis, pyruvate is converted into lactate in a reaction catalyzed by lactate dehydrogenase (LDH). NAD^+, produced by this LDH-mediated reaction, supports glycolysis continuation by serving as a cofactor for the key glycolytic enzyme glyceraldehyde 3-phosphate dehydrogenase (GAPDH). In aerobic glycolysis, the pyruvate is transported into mitochondria where the pyruvate dehydrogenase complex converts it to acetyl-CoA to be utilized by the tricarboxylic acid (TCA) cycle [5]. Glucose is taken up by skeletal muscle through sarcolemmal glucose transporter 4 (GLUT4). Insulin stimulation and muscular contraction drive GLUT4 translocation from intracellular vesicles to the sarcolemmal membrane where it exerts its transport activity [24].

Type II fibers, except for type IIA, use predominantly glycolytic ATP production rather than OXPHOS for short, intense bursts of activity, particularly when blood flow and oxygen are limited (hypoxia). Anaerobic glycolysis is the dominant source of ATP during high-intensity and sustained activity, such as weightlifting and sprints [25]. Conversely, muscles rely on aerobic glycolysis and OXPHOS during low-intensity exercises like walking and low-intensity running [26].

Glucose can be stored as glycogen in skeletal muscle through a process catalyzed by glycogen synthase 1 (GYS1). Depending on metabolic needs, phosphorylase, and debranching enzymes can break down glycogen to release glucose-1-phosphate, which is then converted to glucose-6-phosphate that can enter glycolysis [27]. Disrupted glycogen storage and breakdown can lead to glycogen storage diseases in skeletal muscle. These diseases are often associated with exercise intolerance caused by glycogen accumulation and limited energy supply. Acidification resulting from lactate accumulation also seems to contribute to glycogen storage disease pathology [28].

1.4.2 Mitochondrial Oxidative Pathways

In addition to ATP generated through glycolysis, skeletal muscles rely on mitochondrial oxidative metabolic pathways to meet their energy demands. These oxidative pathways can metabolize glycolytic

byproducts, lipids, and amino acids to produce nicotinamide adenine dinucleotide (NADH) and flavin adenine dinucleotide ($FADH_2$), which subsequently support ATP synthesis by OXPHOS (**Figure 1.2**). In most cell types, mitochondria consume 85-90% of cellular oxygen, mainly as a result of OXPHOS [29].

Pyruvate is a key metabolite that links cytosolic glycolysis to the TCA cycle and OXPHOS [30]. Through the mitochondrial pyruvate carrier, pyruvate can be transported into the mitochondria, where it is converted by PDH to acetyl-CoA for the TCA cycle entry [31]. Additionally, skeletal muscle can import fatty acids (FA) and oxidize them through fatty acid β-oxidation (FAO) to support OXPHOS. It is well recognized that FAO is the primary source of reducing equivalents driving OXPHOS in skeletal muscle during prolonged endurance exercise and during resting periods between meals when blood glucose levels decline [32,33,31]. Individuals with obesity have been reported to have impaired FAO capacity, which is commonly accompanied by impaired insulin-stimulated glucose uptake [34]. Such impairments can be improved by exercise training, further confirming the metabolic importance of skeletal muscle [35,36]. In contrast, other studies have shown that excessive FAO can contribute to obesity-induced insulin resistance in skeletal muscle by impairing the ability to shift from fat to carbohydrate utilization during the transition from fasting to the feeding state [37].

The initial step of FAO involves the import of FAs into skeletal muscle followed by their transport to the mitochondria. FA uptake is mediated via multiple FA transporters like cluster of differentiation 36 (CD36) and FA binding protein 3 (FABP3) in skeletal muscle tissue, where a CoA group is added in the sarcoplasm by fatty acyl-CoA synthase to generate long-chain acyl-CoA. Then, long-chain acyl-CoA is converted by carnitine palmitoyltransferase 1 (CPT1) to long-chain acylcarnitine, which can be transported across the inner mitochondrial membrane (IMM). Once inside the mitochondria, carnitine

palmitoyltransferase 2 (CPT2) converts long-chain acylcarnitine back to long-chain acyl-CoA to be metabolized through FAO, generating acetyl-CoA, which can enter the TCA cycle [38,39].

Beyond glycolytic products and FAs, skeletal muscle can utilize amino acids as a source of energy, particularly during exercise [40]. When exercise is prolonged and the carbohydrate supply is inadequate, skeletal muscles oxidize amino acids that can be taken up from blood or derived from increased protein degradation. However, short-term resistance exercise also induces amino acid oxidation but involves protein catabolism to a lesser extent [41,22]. The reliance on amino acid oxidation when muscle glycogen is depleted contributes to muscle fatigue by degrading structural and contractile proteins, compromising muscle integrity and function [42].

Branched-chain amino acids (BCAAs), valine, leucine, and isoleucine, can be catabolized in skeletal muscle, producing metabolic intermediates that replenish the TCA cycle. BCAAs are transformed into branched-chain keto acids (BCKAs) by branched-chain amino acid aminotransferase (BCAT). Then, branched-chain keto acid dehydrogenase (BCKDH) catalyzes the conversion of BCKAs to branched-chain acyl-CoA, which is further oxidized to acetyl-CoA and propionyl CoA for TCA cycle entry as succinyl CoA [43]. Glutamine is another amino acid that can serve as an energy substrate and can be oxidized by the TCA cycle. In a reaction catalyzed by glutaminase (GLS), glutamine is converted to glutamate, which is then transformed into α-ketoglutarate (α-KG) to enter the TCA cycle [44].

The mitochondrial oxidation of various substrates through the TCA cycle generates NADH and $FADH_2$. These reduced coenzymes donate reducing equivalents (i.e., electrons) to the electron transport chain (ETC) which is comprised of the four respiratory complexes (complex I-IV). The ultimate electron acceptor in the ETC is molecular oxygen, which is then reduced to water (H_2O) [45]. The transfer of electrons through different respiratory complexes is accompanied by proton (H^+) pumping from the matrix toward the intermembrane space (IMS) of mitochondria. Specifically, a total of ten H^+ is pumped

through complex I (four H^+), complex III (four H^+), and complex IV (two H^+) to establish a proton motive force (PMF). The PMF, made up of an electrochemical gradient and a pH gradient, powers ATP synthase or complex V to synthesize ATP from ADP and Pi. [46]. However, OXPHOS energetic efficiency is highly variable due to a process called H^+ leak. While the mechanisms are still poorly understood, H^+ can return to the matrix in ways different than ATP synthase. Thus, H^+ leak can result in the dissociation between the PMF and ATP synthesis, thereby decreasing the efficiency of OXPHOS [47]. H^+ leak occurs in mitochondrial of all cell types and altogether accounts for 30-50% of the resting metabolic rate [47,48]. H^+ leak can be mediated by specialized proteins such as uncoupling proteins (UCPs) and adenine nucleotide translocases (ANTs) [49–51]. However, despite the substantial body of literature that demonstrates a link between mitochondrial uncoupling and cellular processes such as autophagy, ROS production, and thermogenesis in physiological and pathophysiological settings, mechanistic aspects are still poorly understood. Lastly, electrons can leak from the ETC, leading to the one-electron reduction of oxygen, which produces superoxide (O_2^-), the main reactive oxygen species (ROS) precursor [52]. This phenomenon will be discussed in detail later.

Mitochondrial oxidative metabolic pathways are tightly controlled by the peroxisome proliferator-activated receptor gamma (PPARγ) and peroxisome proliferator-activated receptor gamma coactivator 1-alpha (PGC-1α). Activated PGC-1α upregulates the transcription of mitochondrial genes involved in OXPHOS and FAO [53]. Additionally, the activation of PGC-1α promotes the generation of new mitochondria, a process known as mitochondrial biogenesis [54]. Furthermore, PGC-1α activity can be controlled by the master metabolic sensor, AMPK, either directly through phosphorylation or indirectly by activating the deacetylase sirtuin 1 (SIRT1). Importantly, it has been reported that physical activity can mitigate the impaired oxidative mitochondrial capacity observed in various metabolic diseases by initiating PGC-1α activity [55].

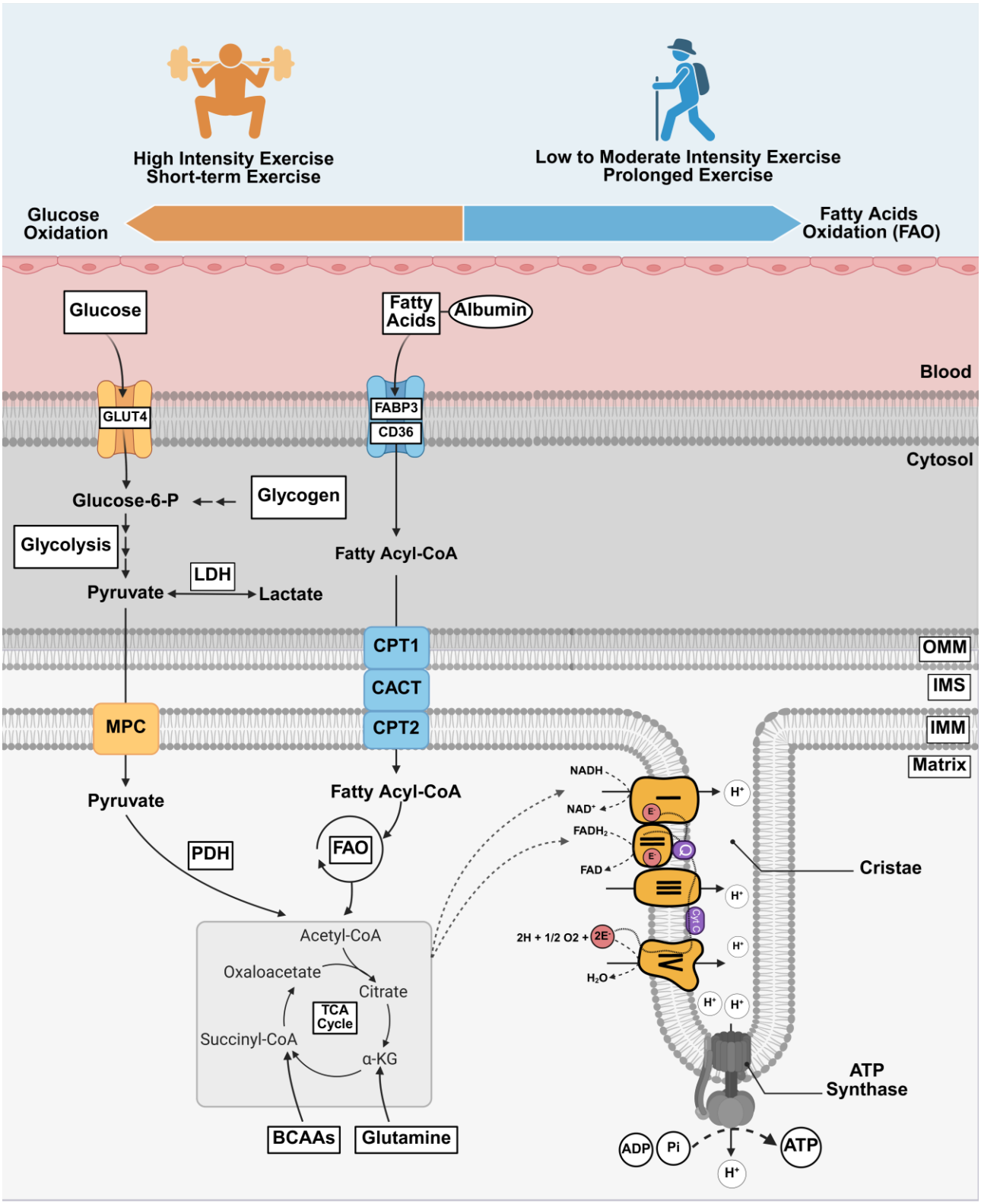
High Intensity Exercise
Short-term Exercise
Low to Moderate Intensity Exercise
Prolonged Exercise
Glucose Oxidation
Fatty Acids Oxidation (FAO)
Glucose
Fatty Acids
Albumin
Blood
GLUT4
FABP3
CD36
Cytosol
Glucose-6-P
Glycogen
Glycolysis
Fatty Acyl-CoA
LDH
Pyruvate
Lactate
CPT1
CACT
CPT2
OMM
IMS
IMM
Matrix
MPC
Pyruvate
Fatty Acyl-CoA
PDH
FAO
Acetyl-CoA
Oxaloacetate
Citrate
TCA Cycle
Succinyl-CoA
α-KG
BCAAs
Glutamine
NADH
NAD+
FADH2
FAD
2H + 1/2 O2 +
H2O
H+
Cristae
ATP Synthase
ADP
Pi
ATP

Figure 1.2. Metabolic Pathways Activated in Skeletal Muscle During Exercise
Skeletal muscle relies on a variety of metabolic substrates including glucose, fat, and amino acids to ensure adequate ATP supply during different types of exercise training. These substrates are oxidized in the TCA cycle to generate the reduced coenzymes NADH and $FADH_2$. These electron carriers donate electrons to be transferred through different respiratory complexes of the ETC, driving proton pumping across the IMM. The resulting PMF powers ATP synthase to produce ATP. Abbreviations: ADP, adenosine diphosphate; α-KG, α-ketoglutarate; ATP, adenosine triphosphate; BCAAs, branched-chain amino acids; CACT, carnitine acylcarnitine translocase; CD36, cluster of differentiation 36; CPT1, carnitine palmitoyltransferase 1; CPT2, carnitine palmitoyltransferase 2; Cyt c, cytochrome c; e-, electron; FABP3, FA binding protein 3; FAO, fatty acid oxidation; FAD(H2), flavin adenine dinucleotide (hydrogen); GLUT4, glucose transporter 4; H+, proton; H2O, water; IMM, inner mitochondrial membrane; IMS, intermembrane space; MPC, mitochondrial pyruvate carrier; NAD(H), nicotinamide adenine dinucleotide (hydrogen); O2, molecular oxygen; OMM, outer mitochondrial membrane; PDH, pyruvate dehydrogenase; Q, coenzyme Q.. This figure was created with BioRender.com

1.4.3 Skeletal Muscle Metabolic Flexibility

Metabolic flexibility defines the ability of skeletal muscles to switch between fuel sources to meet their energetic needs. Commonly this refers to the capacity of muscle to switch from glucose following meals to FA between meals, and it allows skeletal muscle to adapt to variable physiological conditions, such as substrate availability, and exercise intensity [56]. Serving as metabolic hubs, mitochondria play a central role in metabolic flexibility. Mitochondrial metabolism responds to changes in nutrient availability. For example, after a carbohydrate-rich meal, glycolysis and pyruvate oxidation increase, and FAO decreases. The glycolysis-derived metabolite, malonyl-CoA, prevents FAs from being transported into mitochondria for FAO by inhibiting CPT1. High pyruvate production through glycolysis promotes further glucose oxidation by inhibiting the activity of (PDK), upregulating the activity of PDH [57]. Conversely, during fasting, AMPK lowers malonyl-CoA levels by inhibiting acetyl-CoA carboxylase (ACC), increasing transport of FA into the mitochondria through CPT1 for FAO. When FAO is favoured, acetyl-CoA and NADH levels increase and inhibit PDH activity [58]. Additionally, the high availability of lipids can result in increased citrate levels, which in turn downregulate glucose transport and metabolism by inhibiting several factors involved in these processes such as GLUT4 and phosphofructokinase [59].

Beyond ATP production, mitochondria participate in many other biochemical processes including the synthesis of iron-sulfur (Fe/S) clusters and heme, ROS management, and drug detoxification. Mitochondria can also influence the epigenome by producing key metabolites such as acetyl-CoA, hydroxy-ketoglutarate, succinate, and fumarate, which can directly affect nuclear processes, including DNA methylation and histone acetylation [60,61]. Lastly, mitochondria can control whole-body metabolism through inter-organ communication mediated by hormone-like circulating factors called “mitokines” [62,63]. An increasing body of evidence shows that mitochondrial dysfunction can impact

metabolism in distant organs. For instance, in some mitochondrial diseases that affect muscle, “mitokines” have been reported to modulate glucose uptake and mitochondrial biogenesis in the brain [64].

1.4.4 Mitochondrial Structure and Dynamics

Mitochondria are versatile organelles that act as metabolic and redox hubs in all eukaryotic cells containing them [65]. Despite originating from the common bacterial ancestor alpha-proteobacterium, mitochondria display great functional and structural diversity [66]. The nuclear genome encodes roughly 99% of the mitochondrial proteome, comprising approximately 1100 proteins. The mitochondrial genome contains 37 genes that encode 13 proteins involved in OXPHOS, 22 tRNAs, and 2 rRNAs [67]. Mitochondria have two membranes: the outer mitochondrial membrane (OMM) and IMM which create two distinct functional compartments: the IMS and the matrix (**Figure 1.3A**). The OMM is relatively permeable and contains membrane proteins such as mitochondrial fission factor (MFF) and mitochondrial Rho GTPase (MIRO) that regulate mitochondrial behaviour and cellular communication through binding to dynamin. Additionally, the OMM contains voltage-dependent anion-selective channels (VDACs) through which metabolites and small molecules can be transported [68]. The IMS comprises roughly 5% of mitochondrial proteins and plays a crucial role in various cellular processes such as metal metabolism, redox homeostasis, protein and lipid synthesis, and mitochondrial structure and dynamics [69]. The highly selectively impermeable IMM folds to form invaginated structures known as cristae, where the ETC proteins are embedded [45]. The mitochondrial matrix is the second functional compartment where crucial metabolic pathways take place such as the TCA cycle, FAO, urea cycle, and multiple biosynthetic mechanisms [70].

Mitochondria are dynamic reticular structures that continuously undergo cycles of fission and fusion. Mitochondrial fission is the process through which one mitochondrion is split into two or more daughter

mitochondria. Fission is a mitochondrial quality control process that can separate healthy mitochondria from irreversibly damaged ones that will be selectively degraded by mitophagy [71,72]. However, excessive fission is harmful and can be associated with pathological consequences such as impaired mitochondrial bioenergetics, elevated oxidative stress, and cell death [73]. Mitochondrial fission is mainly regulated by the GTPase dynamin-related protein 1 (DRP1), which is translocated from the cytoplasm to the OMM to bind to several membrane proteins such as MFF and mitochondrial fission 1 protein (FIS1) [74–76]. FIS1 inhibits mitochondrial fusion by binding to mitofusin proteins and suppressing their GTPase activity [77].

Mitochondrial fusion is the process by which 2 or more mitochondria fuse by merging their outer and inner membranes. Fusion is driven by GTPase regulatory proteins: optic atrophy protein 1 (OPA1) and mitofusin proteins, MFN1 and MFN2 [78,79]. Mitochondrial fusion starts with merging the OMM of different mitochondria in a process mediated by MFN1 and MFN2. Then, the long form of OPA1 (L-OPA1) induces the fusion of the IMM through its interaction with cardiolipins. L-OPA1 is cleaved to generate the short isoform (s-OPA1), which further promotes IMM fusion by interacting with l-OPA1 [80,81]. One of the fundamental roles of mitochondrial fusion is to enable the mixing and the transfer of content between mitochondria [82] (**Figure 1.3B**).

1.4.5 Mitochondrial Biogenesis

Mitochondrial biogenesis is the process of producing new mitochondria, which is primarily regulated by the coactivator PGC-1α. PGC-1α was initially identified as a master regulator of mitochondrial content in skeletal muscle and brown adipose tissue (BAT) upon exposure to cold [83]. Several studies have confirmed the implications of PGC-1α as a driver of mitochondrial biogenesis and oxidative capacity in skeletal muscle. For instance, muscle-specific overexpression of PGC-1α has been shown to increase the oxidative capacity of the tissue in mice [84]. In contrast, muscle isolated from PGC-1α knockout mice

displayed decreased levels of mitochondrial metabolic markers (e.g., citrate synthase and succinate dehydrogenase) and mtDNA [85,86].

Mitochondrial biogenesis involves various pathways and factors essential for synthesizing new mitochondria such as mtDNA replication, mtDNA-encoded proteins, and nuclear-encoded mitochondrial proteins. In response to cellular stressors like exercise and nutrient deprivation, PGC-1α is activated and translocated from the sarcoplasm to the nucleus [87]. In the nucleus, PGC-1α upregulates the expression of the nuclear respiratory factor 1 (NRF1) and NF-E2-related factor 2 (NRF-2), inducing the transcription of genes encoding subunits of various mitochondrial respiratory complexes. Additionally, NRF1 and NRF2 initiate the expression of mitochondrial transcription factor A (mtTFA), essential for mtDNA replication and transcription. Thus, the PGC-1α-NRF1/2-mtTFA axis plays an instrumental role in the formation of new mitochondria [88,89].

1.4.6 Mitophagy

In contrast to the synthesis of new mitochondria through mitochondrial biogenesis, mitophagy is a form of autophagy in which irreversibly dysfunctional mitochondria are selectively degraded through the lysosomal pathway. Mitophagy is facilitated by fission that sorts out damaged mitochondria for degradation [90]. However, excessive mitophagy can lead to cell death by substantial depletion of mitochondria [91]. At fission sites, the interaction between DRP1 and the mitochondrial zinc (Zn^{2+}) transporter, Zip1, initiates the import of Zn^{2+} into the matrix and causes a localized decline in mitochondrial membrane potential, triggering mitophagy [92]. Mitophagy and ROS are interconnected; moderate levels of ROS trigger selective mitophagy, while high levels of ROS induce autophagy [93,94]. Mitophagy occurs through multiple sequential stages, including a decrease in mitochondrial membrane potential, mitophagosome formation, transport of the mitophagosome to the lysosome, and degradation and recycling of mitochondrial components [95]. Mitophagy can occur through ubiquitin (Ub)-

dependent and Ub-independent pathways. The phosphatase and tensin homolog-induced putative kinase 1 (PINK1)-Parkin pathway is the most studied Ub-dependent mechanism. When mitochondrial membrane potential decreases, PINK1 accumulates on the OMM, phosphorylates ubiquitin, and recruits Parkin, which amplifies ubiquitination and triggers mitophagy [96] (**Figure 1.3C**). Mitophagy can also occur in an Ub-independent way when PINK1 directly recruits several factors involved in mitophagy independently of Parkin [97].

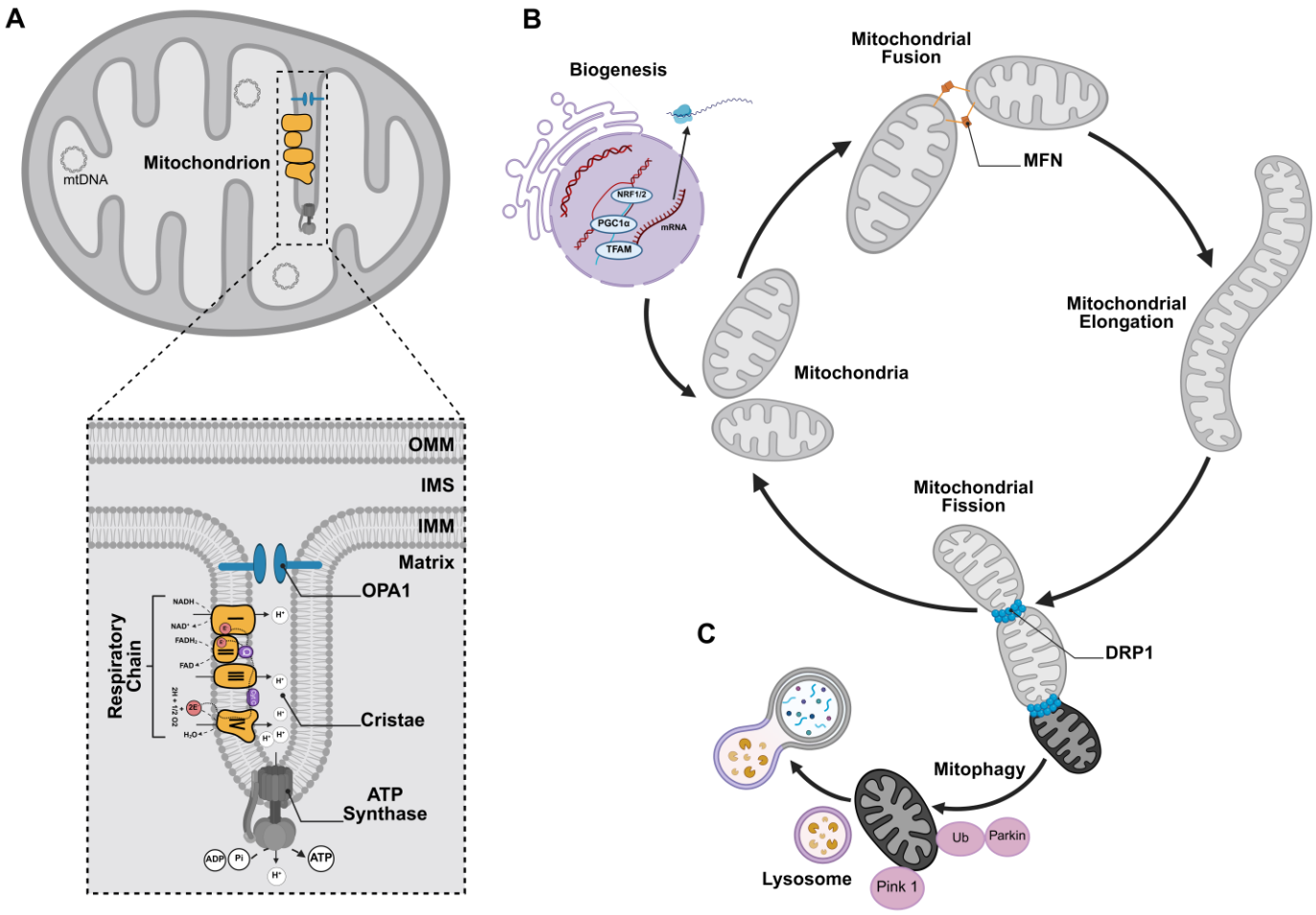

Figure 1.3. Mitochondrial Structure, Dynamics, Biogenesis and Mitophagy
A) A representative scheme showing different mitochondrial membranes and compartments. The respiratory chain is embedded in the IMM, particularly within the cristae. B) Mitochondrial biogenesis involves various factors essential for synthesizing different mitochondrial components such as PGC1α, NRF1/2, and TFAM. Mitochondria undergo continuous cycles of fission and fusion that are controlled by key regulatory proteins such as DRP1, MFN, and OPA1. C) During mitophagy, PINK1 accumulates on the OMM and recruits Parkin. Activated Parkin ubiquitinates OMM proteins, marking the damaged mitochondrion for encapsulation and subsequent degradation. Abbreviations: DRP1, dynamin-related protein 1; IMM, inner mitochondrial membrane; IMS, intermembrane space; MFN, mitofusin; mtDNA, mitochondrial DNA; NRF1/2, nuclear respiratory factor 1/2; OMM, outer mitochondrial membrane; OPA1, optic atrophy 1; PGC1α, peroxisome proliferator-activated receptor gamma coactivator-1 alpha; Pink1, PTEN-induced kinase 1; TFAM, mitochondrial transcription factor A; Ub, ubiquitin. This figure was created with BioRender.com

1.5 Skeletal Muscle Growth

Maintaining muscle mass is a complex and multifactorial process influenced by various synthetic and catabolic mechanisms. Different mechanical, nutritional, and oxidative stresses modulate signaling pathways that converge on protein and organelle turnover, affecting the dynamic balance between skeletal muscle growth and loss. Exercise training stimulates synthetic pathways in skeletal muscle, leading to hypertrophy. Conversely, muscle disuse triggers catabolic pathways that cause muscle wasting and atrophy. [98–100].

1.5.1 Skeletal Muscle Hypertrophy

Skeletal muscle hypertrophy can be initiated by chemical signals such as hormones and growth factors, as well as by mechanical signals resulting from resistance muscle work and training. At a molecular level, the IGF1-AKT-mTOR pathway is well-known to regulate muscle mass and protein synthesis [101]. Insulin-like growth factor 1 (IGF1) binds to its receptor, IGF1R, and activates a signaling pathway through insulin receptor substrate (IRS1) and its downstream target, phosphatidylinositol-3-kinase (P13K). Upon P13K activation, phosphatidylinositol-3,4,5 triphosphate (PIP3) activates AKT, which promotes protein synthesis by activating the mammalian target of rapamycin (mTOR). mTOR forms two complexes: mTORC1, which triggers protein translation via ribosomal S6 kinase 1 (S6K1) activation and deactivation of the eukaryotic translation initiation factor 4E binding protein 1 (eIF4E-4EBP1) inhibitor, and mTORC2, which promotes cell growth. Additionally, activated AKT inhibits glycogen synthase kinase-3 beta (GSK3β), which no longer suppresses the eukaryotic translation initiation factor 2B (eIF2B), further increasing protein synthesis [102]. Additionally, skeletal muscle growth can be induced through AKT-independent pathways such as guanine nucleotide-binding protein (G-protein) signaling via G protein subunit alpha i2(Gαi2) activation and myostatin inhibition. Myostatin, which is a member of the transforming growth factor beta (TGF-β) family, suppresses muscle growth via the

SMA- and MAD-related protein 2 and 3 (SMAD2/3) pathway [103]. The inhibition of myostatin induces hyper-muscularity in mice [104]. In humans, earlier studies have reported undesirable side effects when myostatin inhibitors were tested [105]. However, more recent studies have shown that bimagrumab (BYM-338), a dual-specific monoclonal antibody targeting the myostatin/activin-follistatin pathway, safely improves lean mass and decreases fat mass in patients with T2D in response to exercise and diet [106,107]. Other promising compounds that inhibit myostatin, such as trevogrumab (REGN-1033), are still under development and testing [108]. Thus, beyond the IGF1-AKT-mTOR pathway, Gαi2 signaling pathway activation and myostatin blockade are two distinct pathways that promote muscle growth by directly regulating mTOR downstream targets independently of AKT [109].

1.5.2 Skeletal Muscle Atrophy

Muscle atrophy, characterized by decreased muscle mass and strength, can be induced by several catabolic conditions that promote muscle protein loss such as prolonged immobility, cancer, and unhealthy aging. It is a multifactorial process that involves multiple proteolytic and apoptotic pathways, which lead to lower protein content, smaller cross-sectional area of myofibers, and loss of muscle mass and volume. When AKT is deactivated, forkhead box O (FOXO) transcription factors promote muscle atrophy by upregulating key drivers of atrophy such as Atrogin-1 and muscle RING-finger protein-1 (MURF1) [110]. Pro-inflammatory factors like interleukin 1 (IL-1), IL-6, and tumor necrosis factor-alpha (TNFα), upregulate Atrogin-1 and MURF1, which promotes muscle atrophy by activating the p38 mitogen-activated protein kinase (p38 MAPK), nuclear factor-kappa B (NFκB), and the janus kinase/signal transducers and activators of transcription (JAK/STAT) signaling pathways [111,98,112]. It has been shown that IL-6 can initiate a catabolic muscle state through STAT3 activation, whereas its inhibition helps mitigate atrophy [113]. Furthermore, F-box protein 40 (FBXO40) promotes muscle atrophy by activating IRS1 ubiquitination, which inhibits the PI3K/AKT signaling pathway [114].

Elevated Ca^{2+} levels also contribute to muscle atrophy, by activating the Ca^{2+}-regulated proteases, calpains, that degrade cytoskeletal proteins and induce muscle necrosis [115,116]. Lastly, the overactivation of apoptotic enzymes, particularly caspase 3, has been reported to be a major driver of muscle atrophy[117].

1.5.3 Myogenesis

While hypertrophy increases the size of existing myofibers, myogenesis is the process by which new muscle fibers are generated to support muscle growth during childhood and young adulthood, and to repair damaged tissue. Myogenesis is a hallmark of healthy skeletal muscle tissue that can expand and regenerate upon injury (**Figure 1.4**). This reparative capacity is driven by a special population of resident stem cells called muscle satellite cells (MuSCs) found beneath the basal lamina of myofibers in a state of quiescence [118,119]. In response to myofiber injury or chronic regeneration that is commonly observed in muscular dystrophies, quiescent MuSCs become activated and express myogenic progenitors that drive myogenesis and facilitate muscle repair. Additionally, exercise, particularly resistance training, stimulates MuSC activation, promoting muscle adaptation to exercise manifested by hypertrophy and muscle function enhancement [120,121].

1.5.3.1 Myogenic Transcriptional Program

Quiescent MuSCs are characterized by the expression of the paired-box transcription factor 7 (Pax7), which is a crucial myogenic factor for muscle regeneration that suppresses differentiation genes [122]. Quiescent MuSCs also display several sarcolemmal membrane receptors that are unevenly distributed on the cellular surface, serving as sensors to integrate niche-derived signals through cell-cell communication, paracrine signaling, and extracellular matrix adhesion [123,124]. As MuSCs break quiescence, they become activated and start to express a family of transcription factors known as myogenic regulatory factors (MRFs). The MRFs include myogenic factor 5 (Myf5), myoblast

determination protein 1 (MyoD), myogenin (MyoG), and myogenic regulatory factor 4 (MRF4/Myf6). These MRFs, which are expressed in an orchestrated way, play a crucial role in defining lineage specification and regulating myogenic fate. Myf5 is exclusively expressed in undifferentiated myoblasts, while MyoD is expressed in activated MuSCs until the early stage of differentiation. MyoG and MRF4 expression lasts until the late stages of commitment and differentiation. Activated MuSCs that proceed toward differentiation downregulate Pax7 expression levels. Finally, the fusion of myoblasts into multinucleated myofibers is mediated by two muscle-specific membrane proteins called myomaker and myomerger [125].

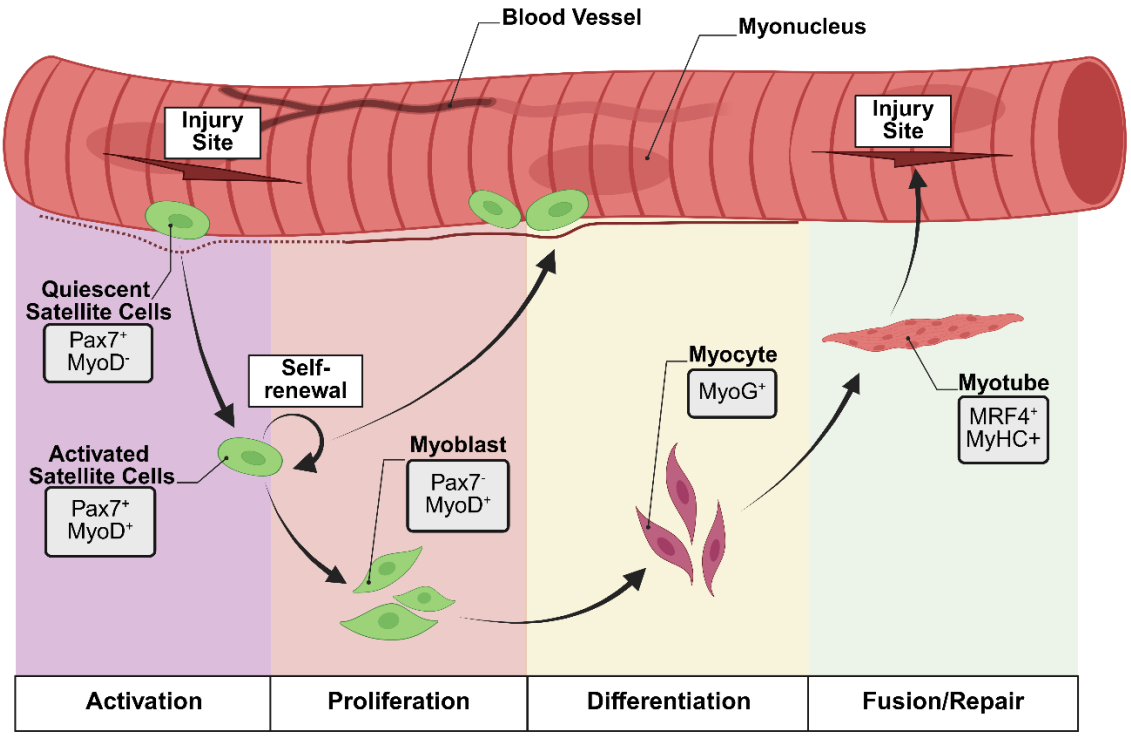

Figure 1.4. Skeletal Muscle Regeneration
Satellite cell activation upon injury undergoes sequential myogenic phases to self-renew and differentiate. Key myogenic regulators drive the activation and differentiation of satellite cells to repair the injured area. Abbreviations: MRF4, myogenic regulatory factor 4; MyHc, myosin heavy chain; MyoD, myoblast determination protein 1; MyoG, myogenin; Pax7, paired box 7. This figure was created with BioRender.com

1.5.3.2 The MuSC Microenvironment

The MuSC microenvironment or niche is complex and contains multiple cell types and extracellular matrix (ECM) elements. Surrounding myofibers and cells including endothelial cells, pericytes, macrophages, and fibro-adipogenic progenitors (FAPs) continuously influence MuSCs through membrane-bound and secreted factors. Thus, MuSC behaviour and fate are regulated by their interaction with different elements of the surrounding microenvironment [126,127].

1.5.3.3 MuSC Division Patterns

To balance self-renewal and commitment to differentiation, MuSCs can divide asymmetrically or symmetrically. Upon activation, MuSCs undergo asymmetric divisions to generate one committed progenitor and one daughter stem cell to sustain self-renewal. MuSCs can also undergo symmetric divisions to produce 2 stem cells or 2 progenitors [123]. Structural and mechanical signals spatially arrange these divisions by controlling proteins involved in the mitotic spindle. It has been reported that dystrophin, responsible for myofiber membrane stability, regulates asymmetric divisions and self-renewal. Dystrophin controls p38 MAPK activity and MyoD expression in MuSCs through the cellular polarization of the partitioning-defective (PAR) complex. Epidermal growth factor receptors (EGFR) can also promote asymmetric division and self-renewal through their polarized localization at the basal surface of quiescent MuSCs, [128]. Additionally, the MuSC niche influences symmetric and asymmetric divisions throughout different myogenic stages. During the early stage of regeneration, symmetric divisions are predominant to ensure the expansion of the myogenic progenitor population. During the terminal phase of regeneration, asymmetric divisions are predominant and lead to the production of uncommitted MuSCs dedicated to the replenishment of stem cell pool [129].

1.6 Redox Homeostasis in Skeletal Muscle

Redox is a term that refers to all reduction and oxidation reactions that involve electron transfer between chemical species [130]. Redox reactions are indispensable for all living organisms given their central roles in biological processes [131,132]. For instance, the electron transfer through different respiratory complexes of the ETC is driven by a sequence of redox reactions. This electron flow is due to the differences in the redox potential between the donor and the acceptor molecules with molecular oxygen as the ultimate electron acceptor [133]. Cellular redox involves many redox couples in the forms of coenzymes, essential to maintaining cellular function and homeostasis. For example, the NADH / NAD^+ redox couple serves as a major electron carrier and signaling system [134]. Moreover, the reversible oxidation of sulfur-containing amino acids in proteins plays a key role in redox signaling transduction, modulating the function of proteins in response to various intrinsic and extrinsic cues [135]. However, during redox reactions, electrons can slip to interact with oxygen, generating highly reactive molecules with unpaired electrons and high oxidizing capacity. These reactive molecules generated in all aerobic processes are essential for redox signaling mechanisms when produced at controlled physiological levels. Conversely, when these species are available at very low or high concentrations, redox signaling and homeostasis become disrupted [136].

1.6.1 Reactive Oxygen and Nitrogen Species

ROS is a collective term for various O_2-derived species that differ in nature, reactivity, and half-life. These molecules can be classified into 2 groups, radical species with unpaired electrons in their outer orbital like superoxide anions (O_2^-), hydroxyl radicals (HO•), peroxyl (ROO•), and alkoxyl (RO•), and non-radical species like hydrogen peroxide (H_2O_2), hypochlorous acid (HOCl), and organic hydroperoxides (ROOH). While $O_2^-$is known to be the precursor of all ROS, H_2O_2 serves as a major mediator in many redox-sensitive pathways [137]. Additionally, nitric oxide (NO•) is another oxidant

compound that can be produced from L-arginine by nitric oxide synthase (NOS). NO• reactivity is low, but it can generate a group of more reactive derivatives, known as reactive nitrogen species (RNS). For example, NO• can form highly reactive and harmful molecules such as peroxynitrite ($ONOO^-$) by interacting with O_2^- [138,139]. In the following section, the major sources of ROS within skeletal muscle tissue are described.

1.6.2 Different Cellular ROS Producers in Skeletal Muscle

Mitochondria are the primary source of ROS in skeletal muscle. Complexes I and III of the ETC are involved in mitochondrial ROS (mtROS) emissions, as they represent sites of electron leakage. [140,141]. mtROS emitted by complex I are oriented toward the matrix side of the IMM, whereas those generated by complex III are released on both sides of the membrane [142]. More specifically, 10 sites were identified as major ROS producers in the mitochondria including two sites in complex I, one site in complex III, one site in complex II, and six dehydrogenases [143].

At complex I, electrons can be leaked through flavin mononucleotide (FMN) and CoQ to interact with molecular oxygen and generate O_2^- . Similarly, at complex III, ubisemiquinone (CoQH•) within the Qo site contributes to O_2^- generation [144,145]. Additionally, under low coenzyme Q pool and elevated PMF conditions, complex I can produce O_2^- through reverse electron transfer (RET) from CoQH2 to NAD^+, accompanied by increased levels of succinate. Clinically, RET is commonly observed during ischemia-reperfusion, which occurs in the heart, the brain, and other organs [146,147]. The levels of mtROS produced at these different sites vary depending on tissues. ROS can damage all cellular components, causing lipid peroxidation, protein carbonylation, and DNA guanine oxidation. However, mtDNA is the most vulnerable due to its proximity to ROS sources [148]. When mtROS levels exceed cellular antioxidant capacity, the resulting oxidative stress can trigger the opening of the mtPTP through oxidative modification of key structural proteins. When mtPTP is transiently opened, it facilitates the

release of ROS and Ca^{2+} and prevents their accumulation in mitochondria. When mtPTP opening is prolonged, this can cause a secondary burst of ROS production, leading to cellular damage and death [149]. Therefore, oxidative stress through mtROS, can be a major contributor to the pathophysiology of many diseases, including neurodegenerative disorders, cardiovascular diseases, metabolic diseases, and cancer [150].

Muscle cells also have non-mitochondrial ROS producers. The nicotinamide adenine dinucleotide phosphate (NADPH) oxidase (NOX) family of proteins are membrane-bound enzymes that mediate electron transfer through membranes. There are seven NOX isoforms, all known to produce O_2^- in phagocytic cells and non-phagocytic cells, including skeletal muscle cells [151]. In skeletal muscle, NOX2 and NOX4 are located in the sarcolemma and T-tubules, and NOX4 is located in the mitochondria. NOX2 and NOX4 are involved in regulating Ca^{2+} metabolism and ROS production during muscular contraction [152]. Xanthine oxidoreductase (XOR) is another non-mitochondrial ROS source in skeletal muscle. XOR can produce O_2^- as a byproduct of hypoxanthine oxidation into uric acid [153]. The role of XOR as ROS producer was confirmed using a specific XOR inhibitor called allopurinol [154]. Furthermore, several studies have identified XOR as a source of ROS in muscle atrophy and age-related muscle mass loss [155]. In addition to mitochondria, NOX, and XOR, the sarcoplasmic reticulum can contribute to ROS generation under specific conditions such as prolonged periods of inactivity or exercise involving intense contractile activity [156]. Lastly, the sarcoplasmic enzyme phospholipase A2 can be a source of ROS production through NOX activation in a calcium-dependent and independent manner [157].

1.6.3 Antioxidant Systems in Skeletal Muscle

Oxidative stress occurs when ROS production surpasses the cellular antioxidant capacities [158]. Cells employ a network of enzymatic and non-enzymatic antioxidant defenses to detoxify excess ROS and

prevent oxidative damage but still allow normal ROS signaling. These defenses can scavenge ROS directly or convert ROS to less harmful molecules. The following sections describe the main antioxidant systems in skeletal muscle.

1.6.3.1 Antioxidant Enzymes

To counteract oxidative stress, cells use a set of antioxidant enzymes like superoxide dismutase (SOD), catalase (CAT), thioredoxins (TRX), and peroxiredoxins (PRX). The SOD family is composed of 3 isoforms: SOD1, SOD2, and SOD3. These isoforms catalyze the dismutation of O_2^- into H_2O_2 in different cellular compartments [159]. SOD1 is localized in the cytosol and IMS, whereas SOD2 is exclusively located in the mitochondrial matrix. The remaining isoform SOD3 exerts its enzymatic function in the extracellular space [160]. It has been demonstrated that SOD1 is crucial for skeletal muscle health maintenance, as its deletion contributes to the loss of muscle mass associated with aging [161]. CAT is a 4-subunit enzyme that utilizes iron as a cofactor for its catalytic function [162]. CAT is predominantly found in peroxisomes where it catalyzes the degradation of H_2O_2 into H_2O and O_2. Decreases in CAT activity are associated with elevated H_2O_2 and with the onset of age-mediated muscle wasting [163]. Lastly, TRX and PRX, which share a similar structure, are mainly responsible for protein disulfide reduction [164]. The TRX system contains 2 oxidoreductases, TRX1 and TRX2, and thioredoxin reductase (TRXR). TRX1 and TRXR1 are present in the cytosol, where TRX1 can translocate to the nucleus to regulate the redox status of transcription factors. TRX2 and TRXR2 are found in the mitochondria [165]. TRX receives electrons from NADPH to exert its antioxidant function and reduce protein disulfide. TRX can also donate electrons to PRX, catalyzing the reduction of peroxides [166]. Studies have shown that muscle cells can secrete TRX1 as a “myokine” and its downregulated expression contributes to the oxidative damage observed in atrophic muscles [167,168].

1.6.3.2 Glutathione

Glutathione (GSH) is the most abundant non-enzyme antioxidant molecule in mammalian cells and is found at millimolar levels [169,170]. In skeletal muscle, GSH acts as an antioxidant and regulates redox-sensitive signaling pathways [171]. The oxidative type I fibers contain the highest levels of GSH, whereas the glycolytic type II fibers have lower concentrations [172]. Interestingly, research has revealed that GSH depletion disrupts muscle cell differentiation by activating NF-κB [173]. Furthermore, multiomic approaches have identified dysregulated GSH metabolism as a key driver of MuSC dysfunction associated with aging [174]. More importantly, restoring GSH synthesis has been able to rescue the defective regenerative capacity of aged MuSCs [174]. In contrast, excessive GSH levels induced by additions of N-acetyl cysteine (NAC) or GSH ethyl ester (GSHee) leads to reductive stress and impairs myogenic differentiation [175]. Therefore, GSH intracellular levels need to be tightly controlled in skeletal muscle.

1.6.3.2.1 Glutathione Synthesis

GSH is a tripeptide composed of cysteine, glutamate, and glycine, where the availability of cysteine is the rate-controlling precursor for GSH biosynthesis. Due to the reducing environment within the cells, about 98% of total glutathione (GSH + GSSG) exists in its reduced form (GSH); the remaining 2% exists in its oxidized form (GSSG or glutathione disulfide) [176]. Therefore, the GSH: GSSG ratio can be used to determine the GSH redox potential [177]. Also relevant is that GSSG can be exported to the extracellular space through multidrug resistance protein 1 (MRP1) to prevent its intracellular accumulation during prolonged oxidative stress conditions [178].

GSH is distributed unequally across various cellular organelles, with a concentration ranging from 1-10 mM in the cytosol, 5-10 mM in the mitochondria, and smaller concentrations in the nucleus and the ER [179]. GSH synthesis occurs in the cytosol following two ATP-demanding steps. The first step is the

formation of γ-glutamylcysteine by glutamate-cysteine ligase (GCL), a reaction that can be inhibited by GSH-mediated feedback. GCL has 2 subunits: a heavy subunit (GCLc) that exclusively catalyzes the ligation process, and a modifier subunit (GCLm) that increases the substrate affinity and reduces sensitivity to GSH inhibition. The second step is catalyzed by GSH synthetase (GSS) and leads to GSH production after ligating γ-glutamylcysteine with glycine. Unlike GCL, GSS activity cannot be inhibited by GSH-mediated feedback [180–182].

1.6.3.2.2 Glutathione-mediated Direct Detoxification

GSH directly neutralizes a wide range of free radicals and pro-oxidant compounds. *In vitro* studies have indicated that GSH can interact with various oxygen-derived radicals, transition metals, and carbon-centered radicals to form intermediate products. GSH can non-enzymatically react with O_2^- and H_2O_2 to reduce them, but at a slower rate than other enzymatic antioxidant systems [182,183].

1.6.3.2.3 Glutathione Peroxidases

The GSH peroxidase (GPX) enzymes neutralize H_2O_2 and other peroxides using GSH as a co-substrate. GPX antioxidant activity is coupled to the oxidation of GSH to GSSG, which is converted back to its reduced form by the NADPH-dependent enzyme, GSH reductase (GR) [184]. Therefore, maintaining a high NADPH: NADP+ ratio through the pentose phosphate pathway (PPP) is essential for regulating GSH: GSSG ratios and the cellular redox state. [182,185]. In addition to PPP, nicotinamide nucleotide transhydrogenase (NNT) found in the IMM contributes to maintaining NADPH pools in the mitochondrial matrix [186]. Among the eight isoforms of GPXs, GPX4 appears to be the most important due to its cytosolic, mitochondrial, and nuclear localization and its role in detoxifying lipid hydroperoxides [184]. GPX4 suppresses ferroptosis, an iron-dependent cell death, by neutralizing lipid peroxides [187]. NADPH and selenium are necessary for inhibiting ferroptosis since NADPH acts as a reducing agent and selenium is essential for the synthesis and catalytic activity of GPX4 [188].

1.6.3.2.4 Glutathione S-transferases

GSH is also a cofactor for GSH-S-transferase (GST), which detoxifies electrophilic compounds by making them more hydrophilic and less toxic [184]. GST isoforms neutralize a wide range of non-polar electrophilic compounds derived from exogenous and endogenous sources [189]. Among different isoforms, cytosolic GSTs are the most enzymatically active compared to those found in other cellular compartments like mitochondria and microsomes. Xenobiotics induce the expression of the GSTs through regulatory elements in their gene promoter regions, including the antioxidant response element (ARE), xenobiotic response element (XRE), and glucocorticoid response element (GRE) [190,191].

1.6.3.2.5 Protein S-glutathionylation

Protein S-glutathionylation (protein S-SG) is a reversible post-translational modification that protects proteins from irreversible oxidation and involves the enzymatic or non-enzymatic formation of a disulfide bond between GSSG and cysteine thiol groups of the targeted protein [192]. This post-translational modification plays a central role in the transduction of redox signals and the regulation of cellular behavior by modulating the activity of the targeted proteins. For example, in oxidative stress, S-glutathionylation transiently inhibits the activity of glycolytic enzymes such as aldolase, GAPDH, phosphoglycerate kinase (PGK), and enolase, to support NADPH pool replenishment through PPP and ROS neutralization [193,194]. Within oxidatively stressed mammalian mitochondria, s-glutathionylation of cysteine residues (Cys-531 and Cys-704) on the 75-KDa subunit of complex I of the ETC, downregulates its activity while simultaneously protecting it from oxidative damage [195]. When redox homeostasis is re-established, the glutaredoxin enzymes (GRXs) detect these changes and initiate deglutathionylation to return key enzymes and metabolic processes to their active state [196]. GSH can reverse protein s-glutathionylation (protein-SSG) and protein sulfenylation (protein-SOH) to restore protein function. However, sulfenic acids are highly reactive and can be irreversibly oxidized to form

sulfinic acid residues (protein-SO_2H) and sulfonic acid residues (protein-SO_3H), which can lead to protein dysfunction. Therefore, the production of sulfinic and sulfonic acids is an indication of severe oxidative damage of proteins [197].

1.7 Cysteine

Cysteine is a thiol-containing semi-essential amino acid that plays a role in the synthesis of numerous proteins and in maintaining cellular redox by being the rate-controlling precursor for GSH biosynthesis. [198]. This section explores cysteine bioavailability, sources, and transport mechanisms.

1.7.1 Cysteine Bioavailability and Sources

Although cysteine is not abundantly present in human food, dietary intake of free cysteine remains the primary source of this amino acid for cells. The oxidative environment in the plasma drives the dimerization of free cysteine into cystine, making it the most bioavailable form for cellular uptake [199,200]. Cysteine concentration in plasma ranges between 200-300 μM and is distributed as follows: 65% of total plasma cysteine is bound to proteins via s-cysteinylation [201], 30% exists in its oxidized dimer form as cystine, and less than 5% is present in its reduced monomer form as cysteine [202]. Many reports have shown that aging is associated with increased levels of cystine in plasma and decreased GSH levels in various tissues, including muscles [203,204,202]. Low intracellular availability of cysteine may contribute to this age-related GSH decline, elevated oxidative stress, and apoptosis in muscle cells [205,206]. However, dietary cysteine supplementation and a cysteine-rich diet showed beneficial effects in the elderly by increasing muscle strength and improving muscle health [207,208].

While dietary intake is important, protein degradation, GSH breakdown, and the transsulfuration pathway are endogenous sources of intracellular cysteine [209,210]. The first step of the transsulfuration pathway is the production of homocysteine from dietary methionine. Then, homocysteine and serine condense to form cystathionine by cystathionine β-synthase (CBS). Next, cystathionine γ-lyase (CTH)

mediates the production of cysteine from cystathionine, along with ammonia and α-ketoglutarate [211]. *De novo* cysteine synthesis involves serine biosynthesis from glucose-derived 3-phosphoglycerate (3PG) in a 3-step process catalyzed sequentially by phosphoglycerate dehydrogenase (PHGDH), phosphoserine aminotransferase 1 (PSAT1), and phosphoserine phosphatase (PSPH). Then, serine can either enter the transsulfuration pathway for cysteine biosynthesis or be converted to glycine by serine hydroxymethyltransferase (SHMT) [212].

Cysteine can also serve as a cellular precursor for the synthesis of hydrogen sulfide (H_2S), which is a gasotransmitter involved in diverse physiological functions. The endogenous generation of H_2S can be catalyzed by 3 enzymes: CBS, CTH, and 3-mercaptopyruvate sulfurtransferase (3MST) [213]. CBS and CTH are found in the cytosol and use cysteine as a substrate, whereas 3MST is mitochondrial and uses homocysteine as a substrate [214]. H_2S has been shown to improve skeletal muscle health in Duchenne muscular dystrophy (DMD) mouse models through its antioxidant, anti-inflammatory, and anti-apoptotic properties [215,216].

1.7.2 Non-specific Cysteine Transporters

As previously mentioned, only a small fraction of circulating cysteine exists in its reduced monomer form. The uptake of cysteine from the extracellular environment occurs through non-specific transporters such as excitatory amino acid transporters (EAATs) and alanine-serine-cysteine transporters (ASCTs). The primary function of EAATs is to import glutamate and aspartate in neurons. However, skeletal muscle cells can use EAAT3 to import cysteine in exchange for glutamate [217]. Additionally, ASCTs belong to a family of Na^+-dependent transporters that can import multiple neutral amino acids, including cysteine. The two isoforms ASCT1 (SLC1A4) and ASCT2 (SLC1A5) preferentially import the reduced cysteine monomer [218].

1.7.3 Cystine/glutamate Antiporter, System Xc-

1.7.3.1 System Xc-Function and Structure

System Xc-, also known as cystine/glutamate antiporter, is a specific transport system responsible for importing cystine, the oxidized dimer form of cysteine [219] (**Figure 1.5**). System Xc- was initially discovered in human fetal lung fibroblasts in 1980 [220]. This antiporter exchanges extracellular cystine for intracellular glutamate in a 1: 1 ratio [221]. System Xc- can transport each amino acid in both directions. However, due to the rapid intracellular reduction of cystine into cysteine and the higher intracellular glutamate concentration, system Xc- transport activity is predominantly directed toward cystine import and glutamate export [222]. System Xc^- transport activity can be inhibited by extracellular glutamate, structurally related endogenous compounds, and various pharmacological agents such as erastin, sulfasalazine, imidazole ketone erastin (IKE), sorafenib, and HG106 [223]. Despite their lack of specificity and off-target effects, all of these pharmacological inhibitors can induce ferroptosis, a unique iron-dependent cell death modality [223,224].

System Xc^- has a heterodimeric structure composed of a light chain xCT (SLC7A11) and a heavy chain 4F2hc (CD98/SLC3A2), linked together by a disulfide bond [225]. The 4F2hc subunit, which is shared by multiple amino acid transport systems, facilitates the proper membrane localization of the transporter system. In contrast, the light chain xCT, exclusively bound to 4F2hc, is specific to cystine-glutamate exchange. The murine xCT subunit is encoded by the *SLC7A11* gene and made of 502 amino acids, displaying high sequence similarity with other light chains of heterodimeric amino acid transporters (HATs) [226]. Studies have predicted xCT to have 12 transmembrane domains, with both N- and C-termini facing the cytoplasm [227]. Furthermore, it has been documented that the human version of xCT protein is 501 amino acids long with 89% identity and 93% similarity with the murine isoform of xCT [228].

In our studies, we used subtle gray (Slc7a11$^{sut/sut}$) mice, which are genetically null for xCT, alongside background–matched controls (C3H/HeSnJ). These mice carry a spontaneous mutation in the last exon of *Slc7a11* that causes both a truncation and a substitution, producing a non-functional xCT protein. As a result, Slc7a11$^{sut/sut}$ mice produce less pheomelanin, the cysteine-dependent yellow pigment in melanocytes, giving them their characteristic subtle grey fur [229]. In addition, they exhibit a moderate platelet storage pool deficiency, making them a relevant model for studying Hermansky-Pudlak syndrome, an autosomal recessive disorder characterized by prolonged bleeding, albinism, and immune dysfunction [230].

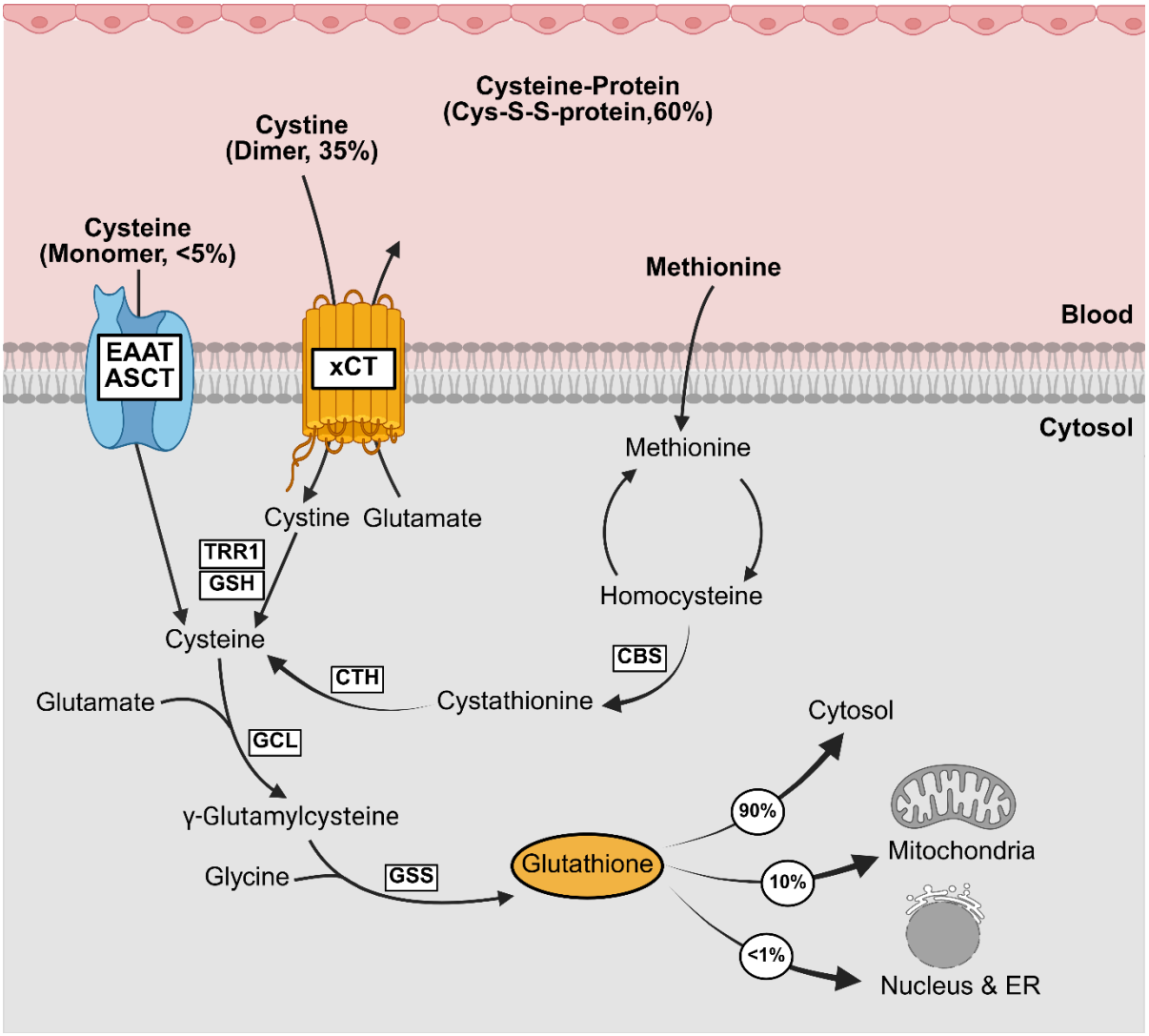

Figure 1.5. Various Sources of Cysteine and GSH Biosynthesis
Specific and non-specific transporters of cyste(i)ne, the rate-limiting substrate of GSH biosynthesis in the cytosol. Abbreviations: ASCT1, alanine serine cysteine transporter 1; CBS, cystathionine beta-synthase; CTH, cystathionine gamma-lyase; EAAT, excitatory amino acid transporter; ER, endoplasmic reticulum; GCL, glutamate-cysteine ligase; GSH, glutathione; GSS, glutathione synthase; TRR1, thioredoxin reductase. This figure was created with BioRender.com

1.7.3.2 System Xc-Molecular Regulation

System Xc- activity can be induced by various stressors. Standard cell culture conditions with atmospheric oxygen (21%) trigger system Xc- activity in several cell types [231–233]. System Xc- activity can be also induced by factors and reagents that cause oxidative insults such as glucose oxidase, paraquat, diethyl maleate (DEM), and heavy metals [225,234]. Cystine starvation has been found to induce system Xc- activity by depleting intracellular levels of GSH. Other than the cysteine dimer, cystine, decreased levels of other amino acids can upregulate system Xc- activity [235]. Additionally, inflammatory stimuli such as the bacterial lipopolysaccharides (LPS) and TNFα have been reported as potent inducers of system Xc- activity [236]. However, a substantial amount of research has demonstrated that system Xc- activity is mainly driven by the light chain xCT expression rather than the expression of its heavy chain 4F2hc [237,238,226]. At a molecular level, it has been documented that xCT expression can be regulated by various transcriptional, post-transcriptional, and post-translational mechanisms.

At a transcriptional level, the master regulator of anti-oxidative responses, NRF2, activates xCT expression in response to oxidative stress conditions [239]. In the absence of oxidative stress, Kelch-like ECH-associated protein 1 (KEAP1) degrades NRF2 to maintain its levels low. However, oxidative stress disrupts KEAP1-mediated degradation, allowing NRF2 to activate target gene expression through antioxidant response elements (AREs), also known as electrophile response elements (EpREs) [240]. Additionally, the stress response regulator activating transcription factor 4 (ATF4) controls xCT expression in response to amino acid starvation. When amino acid levels are depleted, activated ATF4 binds to amino acid response elements (AAREs) in the promoter region of its downstream target xCT, to initiate its expression [235,241,242]. ATF4 also plays a crucial role in the mitochondrial reparative response known as mitochondrial integrated stress response (mtISR) [243]. This response promotes

cellular recovery in response to mitochondrial stressors by mediating transcriptional and metabolic reprogramming [244]. Once activated, the phosphorylation of the eukaryotic translation initiation factor 2 alpha (eIF2α) suppresses global protein synthesis and selectively activates the translation of ATF4 and other stress-responsive factors such as ATF5 and C/EBP homologous protein (CHOP) [245–247]. These alterations at the translational level attempt to minimize cellular energy demands and mitigate mitochondrial dysfunction. When stress conditions are severe, the mt-ISR can activate apoptotic pathways to remove irreversibly damaged cells [244,248].

Post-transcriptional mechanisms can also modulate the expression of xCT. For example, microRNAs such as miR-27a, miR-26b, and miR-375 have been shown to degrade xCT mRNA through nonsense-mediated mRNA decay [249–251]. Histone 2 A mono-ubiquitination mediated by BRCA1-associated protein 1 (BAP1) or polycomb repressive complex 1 (PRC1) can suppress xCT expression [252,253]. Protein-protein interaction and various post-translation modifications are also involved in controlling xCT expression and transport activity. The glycoprotein variant, CD44v, has been found to stabilize xCT and support its transport activity [254]. Moreover, it has been shown that EGFR interacts with xCT to support its insertion into the plasma membrane [255]. Conversely, mTORC2 binds to the cytosolic N terminal side of xCT and suppresses its transport activity by phosphorylation at serine 26 [256] (**Figure 1.6**).

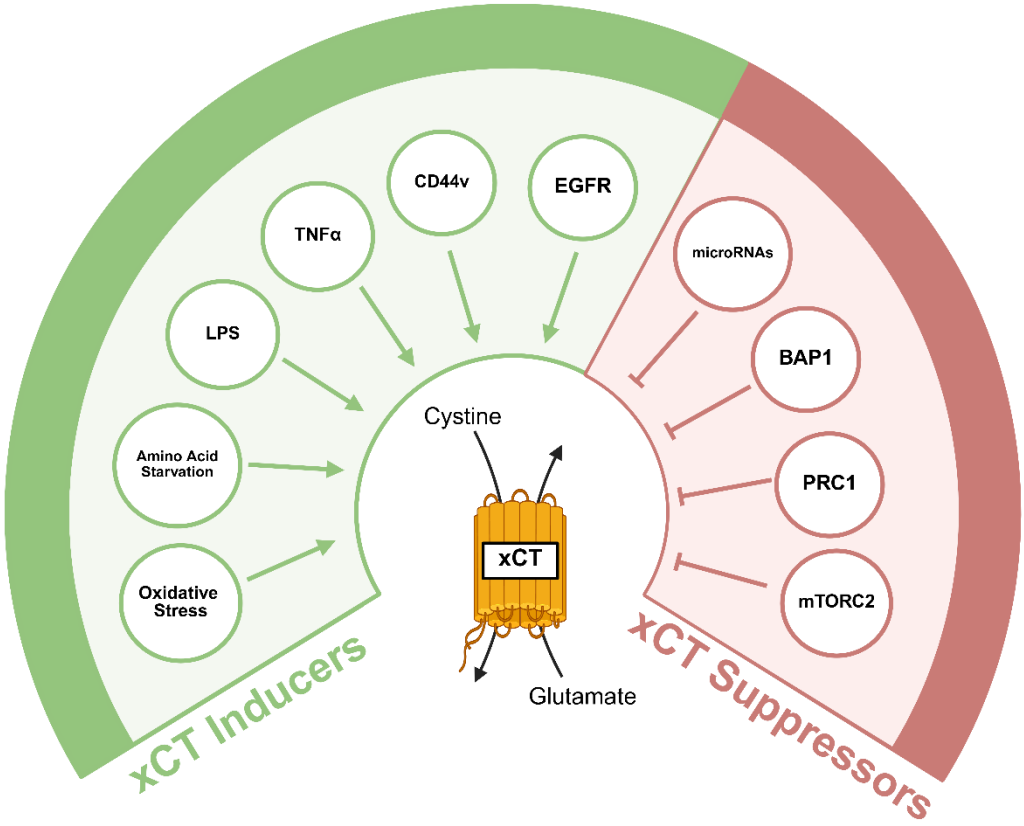

Figure 1.6. Molecular Regulators of xCT Induction and Suppression
Different pathways and factors involved in regulating xCT expression and activity at transcriptional, post-transcriptional, and post-translational levels. Abbreviations: BAP1, BRCA1-associated protein 1; CD44v, variant isoform of the CD44 protein; EGFR, epidermal growth factor receptor; LPS, lipopolysaccharides; mTORC2, mammalian target of rapamycin complex 2; PRC1, polycomb repressive complex 1; TNFα, tumor necrosis factor alpha. This figure was created with BioRender.com

1.8 Metabolic and Redox Implications in Skeletal Muscle Regeneration

1.8.1 Metabolic Regulation of Myogenesis

Metabolic processes play key roles within stem cell populations by determining stem identity, fate, and function [257–260]. In this section, the implications of metabolic regulation of myogenesis will be explored.

The capacity of quiescent MuSCs to inactivate their catabolic pathways enables them to survive up to 30 days post-mortem [261]. It has been demonstrated through RNA-seq analyses that quiescent MuSCs have a high expression of genes involved in FA transport and oxidation and a relatively low expression of genes implicated in glycolytic metabolism [262]. It is well established that mitochondrial FAO supports MuSC quiescence by maintaining high levels of NAD^+, which are required for SIRT1-mediated histone H4 lysine 16 (H4K16) deacetylation that in turn suppresses the transcription of myogenic factors [263]. Additionally, it has been reported that FAO inducers and NAD^+ supplementation enhance MuSCs function, whereas FAO inhibition leads to premature MuSCs differentiation [264]. Moreover, a short-term 40% caloric restriction diet in young and old mice has been shown to improve MuSCs engraftment post-transplantation, but its direct contribution to quiescence is still underexplored [265,266]. High FAO and low glycolysis in quiescent MuSCs deplete acetyl-CoA levels, which also limits histone and protein acetylation processes needed for myogenic activation [267]. Furthermore, it is thought that the reliance of quiescent MuSCs on FAO contributes to regenerative capacity maintenance by maintaining low levels of ROS emissions [268].

MuSC activation is characterized by a metabolic shift from OXPHOS and FAO toward anaerobic glycolysis [263,269]. Studies have shown that the pharmacological inhibition of glycolysis or the genetic suppression of lactate dehydrogenase A-subunit (LDHA) disrupts MuSCs expansion and self-renewal capacity. In contrast, LDHA overexpression enhances glycolysis and supports MuSC proliferation. It has

also been documented that AMPKα1 genetic suppression can improve MuSCs proliferation by impairing mitochondrial function and shifting cellular metabolism toward glycolysis [270]. The metabolic reprogramming in activated MuSCs is somewhat similar to the Warburg effect in cancer cells, where aerobic glycolysis upregulates glucose uptake to channel glucose-derived carbons into anabolic processes. This metabolic adaptation promotes *de novo* biosynthesis of macromolecules including nucleotides, amino acids, proteins, and lipids, and supports cell growth and proliferation [271].

Lastly, during differentiation, MuSCs shift their metabolism back to OXPHOS, accompanied by an upregulation of mitochondrial biogenesis. This remarkable reliance on oxidative metabolic pathways during differentiation has been further validated by evidence showing that suppression of the key driver of mitochondrial biogenesis, mtTFA, significantly impairs myogenic differentiation. Furthermore, upon muscle injury ROS emitted from mitochondrial ETC and cytosolic NOX, contribute to the regulation of myogenic differentiation [269]. Controlling ROS levels through various cellular antioxidant defenses is essential for effective muscle repair. In line with this notion, inhibition of the antioxidant genes, paired-like homeodomain transcription factor 2 (PITX2) and PITX3, has been associated with impaired regenerative potential and premature differentiation in MuSCs [272]. Finally, the phosphorylation of p38a has been proposed as a mechanism by which ROS regulates MuSC differentiation. This idea is supported by studies revealing that either p38a phosphorylation inhibition or NAC-mediated ROS neutralization disrupts myogenic differentiation [269].

1.8.2 Redox Regulation of Myogenesis

Redox signaling plays a pivotal role in driving different phases of the myogenic program. ROS can influence gene expression and modulate key transcriptional factors involved in myogenesis. For example, the suppression of NOS has been shown to inhibit MuSCs activation, whereas, NO• donation rescues defective activation and increases the number of Pax7+ cells [273]. NO• has also been reported

to support MuSCs self-renewal by regulating their migration and polarity [274]. As previously mentioned, the high dependency on glycolytic metabolism in activated MuSCs depletes NAD^+ levels needed for SIRT1 activity, which triggers *MyoD* transcription through elevated H4K16 acetylation [263]. Moreover, increased levels of ROS in differentiating MuSCs have been shown to promote focal adhesion kinase (FAK) translocation to the nucleus, where it interacts with methyl CpG-binding protein 2 (MBD2) [275]. This interaction induces *MyoG* expression through the dissociation of MBD2 with the histone deacetylase complex 1 (HDAC1) and methyl CpG sites in the *MyoG* promoter [275].

At the translational and protein post-translational levels, redox-sensitive pathways further regulate MuSC function and fate. For example, inhibition of the Notch pathway has been reported to cause impaired MuSC activation. It is well-recognized that Notch signaling in non-muscle cells can be influenced by NOX1-produced ROS, suggesting that Notch may impact myogenesis in a redox-dependent manner [276,277]. Additionally, several studies have shown that the activity of the Wnt/β-catenin pathway, which plays a role in stem cell fate, can be modulated for example by TRX, nucleoredoxin, and selenium [278,279]. Selenium is important through its antioxidant role as an essential component of several GPX enzymes [280].

Protein signaling cascades are also regulated by cellular redox and thus influence MuSC transition from one myogenic phase to another. During quiescence, MuSCs maintain redox balance by upregulating antioxidant genes such as GPX3 and TRXR1 [281]. This characteristic of quiescent MuSCs indicates the importance of redox homeostasis in maintaining the stem cell pool. Cellular redox also regulates multiple pathways involved in MuSCs transition from quiescence to activation. For instance, early studies demonstrated that low levels of O_2^- and H_2O_2 induce mammalian cell proliferation [282]. In contrast, it has been reported that NOX suppression and NAC treatment impair MuSCs proliferation by modulating cyclin D1 expression through PI3K/AKT and NF-κB pathways [283,284]. Additionally, the

implications of cellular redox in the control of MuSCs proliferation have been extensively studied using various mouse genetic models. For instance, it has been observed that MuSCs isolated from GPX1-deficient and SOD1-G93A mice exhibit impaired proliferation compared to wild-type counterparts [285,286]. During differentiation*, in vitro* studies have revealed that MuSCs display a decreased expression of NOX4. Furthermore, the overexpression and inhibition of the NOX subunit, DUOXA1, have been shown to impair and induce myogenic differentiation, respectively [287]. Additionally, it has been documented that treating cultured MuSCs with reducing agents like dithiothreitol (DTT) and resveratrol promotes differentiation, whereas excessive levels of H_2O_2 interfere with myogenesis [288,289]. *In vivo*, various pathways involved in GSH redox and metabolism, such as NF-κB and NRF2-GCL/GR-GSH, play a key role in myogenic differentiation [290]. It has been observed that NRF2 deficiency in mice perturbs muscle recovery post-cardiotoxin (CTX) injury by impairing the balance between MuSC proliferation and differentiation [291]. Furthermore, inhibiting NRF2 downstream target gene, carbonyl reductase 1 (CBR1) has been associated with elevated ROS levels and aberrant muscle regeneration [292]. Consistently, deleting the ROS inducer P66 (ShcA) has been shown to induce faster muscle regeneration following hind limb ischemia [293].

However, contrary to the conventional concept of ROS as detrimental molecules, mtROS, particularly H_2O_2, are necessary for myogenic differentiation progression. It has been demonstrated that inhibiting mtROS production with mitochondria-targeted antioxidant reagents like MitoQ or MCAT disrupts MuSCs differentiation [294]. Moreover, this critical role of ROS in myogenesis has been further confirmed through skeletal muscle regeneration studies conducted in conditional mutants of the antioxidant genes PITX2/3. Loss of PITX2/3 has been shown to increase MuSCs senescence by downregulating NRF1 expression and elevating ROS emission levels. However, this phenotype could be rescued by NAC treatment in a dose-dependent manner [272]. Altogether, these studies indicate that

the myogenic program is largely influenced by redox signaling, where ROS can either promote or suppress the process depending on their concentration and timing.

1.9 Glutathione Redox and ROS in Skeletal Muscle-related Diseases

It is well known that oxidative stress largely contributes to the pathogenesis of many skeletal muscle diseases such as muscular dystrophies, metabolic disorders, and sarcopenia. Therefore, understanding the significance of redox homeostasis in skeletal muscle function in the development of diseases is essential.

1.9.1 Muscular Dystrophies

Muscular dystrophy is a group of genetically inherited muscle disorders with diverse clinical and molecular characteristics. The main clinical characteristics of dystrophic muscles are atrophy and functional decline. DMD is the most severe and prevalent form of muscular dystrophy. DMD is an X-linked recessive disorder caused by a mutation in the *dystrophin* gene that encodes the cytoskeleton protein dystrophin. This mutation interferes with muscle cell integrity and makes myofibers highly vulnerable to mechanical stress, with defective reparative capacity [295]. Various disrupted cellular processes can contribute to DMD progression, including dysregulated Ca^{2+} metabolism, chronic inflammation, mitochondrial stress, and excessive ROS production [296,297]. In this section, we will explore several studies that have revealed the implications of redox stress in DMD pathophysiology.

The mdx mouse model, which carries a spontaneous mutation of the *dystrophin* gene, has been extensively used in research as a model for DMD since its first description in 1984 [298]. Interestingly, myofibers isolated from mdx mice have been shown to have a pronounced susceptibility to oxidative damage [299]. Additionally, it has been reported that muscle of DMD patients and mdx mice displays an upregulated expression of various antioxidant enzymes, in a failed attempt to restore dysregulated redox homeostasis [300]. Consistently, muscle biopsies from DMD patients demonstrate an increased activity

of NOX2 and elevated levels of ROS, especially during the early stages of the disease [301]. Another study has emphasized the contribution of oxidative stress to DMD progression by showing that NAC treatment can mitigate muscle degeneration in mdx mice [302]. Furthermore, it has been shown that the pharmacological suppression of bromodomain-containing protein 4 (BRD4), which regulates the KEAP1/NRF2 pathway, can lower oxidative stress and muscle damage in mdx mice [303]. Additionally, treating the mdx mice with the synthetic mimetic of SOD and CAT, EUK-134, has been associated with a decrease in oxidative stress levels in the diaphragm muscle [304]. Importantly, research has revealed that hind limb muscles of mdx mice have a defective GSH synthesis, low GSH: GSSG ratio, and increased GR activity [305,304]. Increased levels of Ca^{2+} can exacerbate DMD-associated oxidative stress by disrupting mitochondrial function and increasing ROS production. Furthermore, the damaged sarcolemma typically observed in DMD triggers mast cell degranulation, which increases oxidative stress levels due to excessive ROS emitted by activated neutrophils and macrophages [306].

1.9.2 Metabolic Diseases

Skeletal muscle is the primary site for insulin-stimulated glucose uptake, accounting for 70-90% of insulin-stimulated glucose disposal at the whole body level [307]. Insulin resistance in skeletal muscles, manifested by impaired insulin-stimulated glucose uptake is the main driver of type 2 diabetes (T2DM) [308]. Oxidative stress impacts the pathogenesis of skeletal muscle insulin resistance and related metabolic diseases [309]. The first direct evidence of a causal link between oxidative stress and insulin resistance was demonstrated in 2006, using TNFα and dexamethasone to induce insulin resistance in adipocytes [310]. Consistent with this finding, ROS scavenging has been shown to restore insulin sensitivity [310]. Furthermore, muscle from patients with T2DM and high-fat diet-fed mice display mitochondrial dysfunction associated with elevated mtROS emission [311,312]. Other studies have revealed that the activation of nucleotide-binding oligomerization domain protein-2 (NOD2) contributes

to insulin resistance by increasing mtROS generation [313]. Research has also shown a correlation between insulin sensitivity and the expression levels of the mitochondrial deacetylase SIRT3, which is known to regulate skeletal muscle metabolism, AMPK activation, and ROS levels [314–316]. Interestingly, SIRT3 downregulation in human endothelial cells and obese mice has been associated with increased mtROS production and dysregulated insulin signaling [317]. Another study has demonstrated that the first-line antidiabetic medication, metformin enhances insulin-dependent muscle glucose uptake in a SIRT3-AMPK-dependent manner, further indicating the importance of ROS signaling in glucose metabolism [318].

Beyond mtROS, cytosolic NOX isoforms can also be involved in the development of skeletal muscle insulin resistance. Under normal healthy conditions, NOX2-generated ROS are required as signaling molecules to regulate many cellular processes, including glucose uptake, insulin signaling, and Ca^{2+} metabolism. When cellular homeostasis is perturbed, NOX2 becomes over-activated by angiotensin II and disrupts insulin signaling in muscle cells [319]. Aligned with this notion, it has been reported that muscles from high-fat diet-induced insulin-resistant C57BL/6 mice display upregulated levels of NOX2 [320]. Conversely, NOX2 inhibition with apocynin in heart failure mouse models has been found to enhance skeletal muscle insulin sensitivity by upregulating serine phosphorylation of AKT and promoting GLUT4 translocation [321]. Lastly, XOR-produced ROS can also modify skeletal muscle insulin sensitivity. Studies have shown that inhibiting XOR can mitigate insulin resistance by decreasing oxidative stress and enhancing mitochondrial function in streptozotocin-induced diabetic mice and male Wistar rats fed a high-fat diet [322,323]. These findings indicate that ROS produced by different sources within muscle cells play a crucial role in regulating insulin sensitivity and maintaining metabolic homeostasis. While these findings highlight a significant role of ROS in promoting insulin resistance, some studies suggest that ROS implications are secondary rather than causal in this metabolic

dysfunction. Specifically, some studies have shown that ROS can enhance insulin signaling. For example, it has been reported that GPX1 knockout mice are protected from high-fat diet-induced insulin resistance, suggesting a potential insulin-sensitizing effect of ROS [324].

1.9.3 Sarcopenia

Sarcopenia is an age-related decline in muscle mass and function that leads to a compromised quality of life and higher mortality rates in older adults [325]. Sarcopenia begins around age 40, with a muscle mass loss rate of 8% per decade, which increases to 15 % per decade after the age of 70 [326]. Although sarcopenia is often linked to aging, it can also be caused by other chronic pathological conditions such as cancer and cardiovascular diseases where it is referred to as secondary sarcopenia [327,328]. Sarcopenia-related muscle loss is often associated with the buildup of lipids within muscle fibers. Moreover, there appear to be effects on MuSCs, which can transition to adipogenic phenotypes. This transition is mediated at least in part by ROS [329]. Altogether, sarcopenia leads to muscle atrophy, characterized by fewer muscle fibers and a smaller cross-sectional area of remaining fibers, as well as accumulation of lipids in muscles, as observed in both rodents and humans [330].

With specific regard to aging-associated processes, elevated oxidative stress and mitochondrial dysfunction are key contributors [325,331]. It has been demonstrated that increased oxidative stress in aged muscles disrupts signaling pathways and impairs the maintenance of muscle mass [332]. Indeed, MuSCs during aging display a decline in their proliferative and self-renewal capacities, leading to diminished regenerative potential [333–335]. Quiescent MuSCs show minimal mitochondrial metabolism, increased ROS production, and reduced antioxidant capacities during aging [336]. MuSCs from older adults also exhibit low activity of antioxidant enzymes such as CAT and GSTs [337]. Recently, it has been demonstrated in MuSCs isolated from aged C57BL/6 mice that impaired GSH synthesis and metabolism are key drivers of defective regenerative capacity. Specifically, authors

reported that perturbed GSH levels and redox in aged MuSCs increase pro-inflammatory and pro-aging responses, as evidenced by enrichment in the target genes of NF-kB and SMAD3 [174]. Furthermore, many redox-sensitive signaling pathways such as Notch, Wnt, p38MAPK, and JAK/STAT3 are dysregulated in aged MuSCs [338–340]. Oxidative stress in old MuSCs can disrupt protein homeostasis function by altering the ubiquitin-proteasome system, autophagy, and chaperone activity [341]. Lastly, mitochondrial dysfunction and subsequent excess of ROS observed in sarcopenic muscle, have been reported to trigger proteolytic and apoptotic pathways, leading to MuSC senescence in rat gastrocnemius muscle [342]. Despite substantial research indicating a correlation between ROS and age-related muscle loss, some studies challenge this association, suggesting that ROS may not be the primary driver of sarcopenia. For instance, while SS31 decreased mtROS and enhanced mitochondrial integrity and mitophagy in the skeletal muscle of old C57BL/6 mice, it did not reverse sarcopenic muscle mass and loss of strength [18]. Therefore, further research is needed to enhance our understanding of ROS implications in sarcopenia-related muscle wasting.

1.10 Aims and Hypotheses

Despite the recent advances in understanding the implications of cellular redox in skeletal muscle homeostasis, there are many unanswered questions. In particular, the role of the cystine/glutamate antiporter, xCT has been poorly understood. Therefore, the overarching goal of my research has been to explore the role of xCT in the regulation of skeletal muscle redox, metabolism, and regeneration. The overall hypothesis was that xCT controls skeletal muscle redox and plays a crucial role in skeletal muscle metabolism and regeneration.

Aim 1: To elucidate the role of xCT during myogenic differentiation.

Hypothesis: Cystine/glutamate antiporter xCT controls skeletal muscle regeneration and metabolism through modulating GSH redox.

Aim 2: To examine the impact of impaired or inhibited xCT activity on metabolic pathways, cellular bioenergetics, and mitochondrial morphology in proliferating MuSCs.

Hypothesis: xCT deficiency perturbs redox balance, disrupts mitochondrial dynamics, and alters metabolic pathways in proliferating MuSCs.

1.11 References

[1] S.V. Brooks, S.D. Guzman, L.P. Ruiz, Chapter 1 - Skeletal muscle structure, physiology, and function, in: D.S. Younger (Ed.), Handb. Clin. Neurol., Elsevier, 2023: pp. 3–16. https://doi.org/10.1016/B978-0-323-98818-6.00013-3.

[2] R.R. Wolfe, The underappreciated role of muscle in health and disease2, Am. J. Clin. Nutr. 84 (2006) 475–482. https://doi.org/10.1093/ajcn/84.3.475.

[3] M. Ramachandran, Basic Orthopaedic Sciences, CRC Press, 2018.

[4] J. Allen, M. Ramsden, S. Nisar, Skeletal muscle structure, function and pathology, Orthop. Trauma 38 (2024) 137–144. https://doi.org/10.1016/j.mporth.2024.03.004.

[5] M. Hargreaves, L.L. Spriet, Skeletal muscle energy metabolism during exercise, Nat. Metab. 2 (2020) 817–828. https://doi.org/10.1038/s42255-020-0251-4.

[6] C. McCuller, R. Jessu, A.L. Callahan, Physiology, Skeletal Muscle, in: StatPearls, StatPearls Publishing, Treasure Island (FL), 2025. http://www.ncbi.nlm.nih.gov/books/NBK537139/ (accessed April 22, 2025).

[7] R.L. Ruff, Endplate contributions to the safety factor for neuromuscular transmission, Muscle Nerve 44 (2011) 854–861. https://doi.org/10.1002/mus.22177.

[8] M.H. Wilson, M.R. and Deschenes, The neuromuscular junction: Anatomical features and adaptations to various forms of increased, or decreased neuromuscular activity, Int. J. Neurosci. 115 (2005) 803–828. https://doi.org/10.1080/00207450590882172.

[9] H.E. Huxley, The Mechanism of Muscular Contraction, Science 164 (1969) 1356–1366. https://doi.org/10.1126/science.164.3886.1356.

[10] A.M. Gordon, E. Homsher, M. Regnier, Regulation of Contraction in Striated Muscle, Physiol. Rev. 80 (2000) 853–924. https://doi.org/10.1152/physrev.2000.80.2.853.

[11] S. Schiaffino, C. Reggiani, Fiber Types in Mammalian Skeletal Muscles, Physiol. Rev. 91 (2011) 1447–1531. https://doi.org/10.1152/physrev.00031.2010.

[12] M.A. Pellegrino, M. Canepari, R. Rossi, G. D'Antona, C. Reggiani, R. Bottinelli, Orthologous myosin isoforms and scaling of shortening velocity with body size in mouse, rat, rabbit and human muscles, J. Physiol. 546 (2003) 677–689. https://doi.org/10.1113/jphysiol.2002.027375.

[13] M. Dos Santos, S. Backer, B. Saintpierre, B. Izac, M. Andrieu, F. Letourneur, F. Relaix, A. Sotiropoulos, P. Maire, Single-nucleus RNA-seq and FISH identify coordinated transcriptional activity in mammalian myofibers, Nat. Commun. 11 (2020) 5102. https://doi.org/10.1038/s41467-020-18789-8.

[14] D. Bloemberg, J. Quadrilatero, Rapid Determination of Myosin Heavy Chain Expression in Rat, Mouse, and Human Skeletal Muscle Using Multicolor Immunofluorescence Analysis, PLOS ONE 7 (2012) e35273. https://doi.org/10.1371/journal.pone.0035273.

[15] N.J. Pillon, B.M. Gabriel, L. Dollet, J.A.B. Smith, L. Sardón Puig, J. Botella, D.J. Bishop, A. Krook, J.R. Zierath, Transcriptomic profiling of skeletal muscle adaptations to exercise and inactivity, Nat. Commun. 11 (2020) 470. https://doi.org/10.1038/s41467-019-13869-w.

[16] S. Medler, Mixing it up: the biological significance of hybrid skeletal muscle fibers, J. Exp. Biol. 222 (2019) jeb200832. https://doi.org/10.1242/jeb.200832.

[17] M. Murgia, L. Toniolo, N. Nagaraj, S. Ciciliot, V. Vindigni, S. Schiaffino, C. Reggiani, M. Mann, Single Muscle Fiber Proteomics Reveals Fiber-Type-Specific Features of Human Muscle Aging, Cell Rep. 19 (2017) 2396–2409. https://doi.org/10.1016/j.celrep.2017.05.054.

[18] G.K. Sakellariou, T. Pearson, A.P. Lightfoot, G.A. Nye, N. Wells, I.I. Giakoumaki, A. Vasilaki, R.D. Griffiths, M.J. Jackson, A. McArdle, Mitochondrial ROS regulate oxidative damage and

mitophagy but not age-related muscle fiber atrophy, Sci. Rep. 6 (2016) 33944. https://doi.org/10.1038/srep33944.
[19] G. Gouspillou, N. Sgarioto, S. Kapchinsky, F. Purves-Smith, B. Norris, C.H. Pion, S. Barbat-Artigas, F. Lemieux, T. Taivassalo, J.A. Morais, M. Aubertin-Leheudre, R.T. Hepple, Increased sensitivity to mitochondrial permeability transition and myonuclear translocation of endonuclease G in atrophied muscle of physically active older humans, FASEB J. 28 (2014) 1621–1633. https://doi.org/10.1096/fj.13-242750.
[20] J.A. Hawley, M. Hargreaves, M.J. Joyner, J.R. Zierath, Integrative Biology of Exercise, Cell 159 (2014) 738–749. https://doi.org/10.1016/j.cell.2014.10.029.
[21] R.M. Esquejo, B. Albuquerque, A. Sher, M. Blatnik, K. Wald, M. Peloquin, J. Delmore, E. Kindt, W. Li, J.D. Young, K. Cameron, R.A. Miller, AMPK activation is sufficient to increase skeletal muscle glucose uptake and glycogen synthesis but is not required for contraction-mediated increases in glucose metabolism, Heliyon 8 (2022). https://doi.org/10.1016/j.heliyon.2022.e11091.
[22] J.S. Baker, M.C. McCormick, R.A. Robergs, Interaction among Skeletal Muscle Metabolic Energy Systems during Intense Exercise, J. Nutr. Metab. 2010 (2010) 905612. https://doi.org/10.1155/2010/905612.
[23] M. Dashty, A quick look at biochemistry: Carbohydrate metabolism, Clin. Biochem. 46 (2013) 1339–1352. https://doi.org/10.1016/j.clinbiochem.2013.04.027.
[24] P.L. Evans, S.L. McMillin, L.A. Weyrauch, C.A. Witczak, Regulation of Skeletal Muscle Glucose Transport and Glucose Metabolism by Exercise Training, Nutrients 11 (2019) 2432. https://doi.org/10.3390/nu11102432.
[25] L.L. Spriet, Anaerobic metabolism in human skeletal muscle during short-term, intense activity, Can. J. Physiol. Pharmacol. 70 (1992) 157–165. https://doi.org/10.1139/y92-023.
[26] E.A. Richter, W. Derave, J.F.P. Wojtaszewski, Glucose, exercise and insulin: emerging concepts, J. Physiol. 535 (2001) 313–322. https://doi.org/10.1111/j.1469-7793.2001.t01-2-00313.x.
[27] T.E. Jensen, E.A. Richter, Regulation of glucose and glycogen metabolism during and after exercise, J. Physiol. 590 (2012) 1069–1076. https://doi.org/10.1113/jphysiol.2011.224972.
[28] R. Godfrey, R. Quinlivan, Skeletal muscle disorders of glycogenolysis and glycolysis, Nat. Rev. Neurol. 12 (2016) 393–402. https://doi.org/10.1038/nrneurol.2016.75.
[29] E. Gnaiger, Capacity of oxidative phosphorylation in human skeletal muscle: New perspectives of mitochondrial physiology, Int. J. Biochem. Cell Biol. 41 (2009) 1837–1845. https://doi.org/10.1016/j.biocel.2009.03.013.
[30] J.C. Schell, D.R. Wisidagama, C. Bensard, H. Zhao, P. Wei, J. Tanner, A. Flores, J. Mohlman, L.K. Sorensen, C.S. Earl, K.A. Olson, R. Miao, T.C. Waller, D. Delker, P. Kanth, L. Jiang, R.J. DeBerardinis, M.P. Bronner, D.Y. Li, J.E. Cox, H.R. Christofk, W.E. Lowry, C.S. Thummel, J. Rutter, Control of intestinal stem cell function and proliferation by mitochondrial pyruvate metabolism, Nat. Cell Biol. 19 (2017) 1027–1036. https://doi.org/10.1038/ncb3593.
[31] J.C. Schell, J. Rutter, The long and winding road to the mitochondrial pyruvate carrier, Cancer Metab. 1 (2013) 6. https://doi.org/10.1186/2049-3002-1-6.
[32] G. van Hall, M. Sacchetti, G. Rådegran, B. Saltin, Human Skeletal Muscle Fatty Acid and Glycerol Metabolism During Rest, Exercise and Recovery, J. Physiol. 543 (2002) 1047–1058. https://doi.org/10.1113/jphysiol.2002.023796.
[33] C. Roepstorff, C.H. Steffensen, M. Madsen, B. Stallknecht, I.-L. Kanstrup, E.A. Richter, B. Kiens, Gender differences in substrate utilization during submaximal exercise in endurance-trained

subjects, Am. J. Physiol.-Endocrinol. Metab. 282 (2002) E435–E447. https://doi.org/10.1152/ajpendo.00266.2001.
[34] E.E. Blaak, Basic disturbances in skeletal muscle fatty acid metabolism in obesity and type 2 diabetes mellitus, Proc. Nutr. Soc. 63 (2004) 323–330. https://doi.org/10.1079/PNS2004361.
[35] J. Jeppesen, A.B. Jordy, K.A. Sjøberg, J. Füllekrug, A. Stahl, L. Nybo, B. Kiens, Enhanced Fatty Acid Oxidation and FATP4 Protein Expression after Endurance Exercise Training in Human Skeletal Muscle, PLOS ONE 7 (2012) e29391. https://doi.org/10.1371/journal.pone.0029391.
[36] C.A. Pileggi, D.P. Blondin, B.G. Hooks, G. Parmar, I. Alecu, D.A. Patten, A. Cuillerier, C. O'Dwyer, A.B. Thrush, M.D. Fullerton, S.A. Bennett, É. Doucet, F. Haman, M. Cuperlovic-Culf, R. McPherson, R.R.M. Dent, M.-E. Harper, Exercise training enhances muscle mitochondrial metabolism in diet-resistant obesity, eBioMedicine 83 (2022) 104192. https://doi.org/10.1016/j.ebiom.2022.104192.
[37] T.R. Koves, J.R. Ussher, R.C. Noland, D. Slentz, M. Mosedale, O. Ilkayeva, J. Bain, R. Stevens, J.R.B. Dyck, C.B. Newgard, G.D. Lopaschuk, D.M. Muoio, Mitochondrial Overload and Incomplete Fatty Acid Oxidation Contribute to Skeletal Muscle Insulin Resistance, Cell Metab. 7 (2008) 45–56. https://doi.org/10.1016/j.cmet.2007.10.013.
[38] R.J.A. Wanders, J.P.N. Ruiter, L. IJlst, H.R. Waterham, S.M. Houten, The enzymology of mitochondrial fatty acid beta-oxidation and its application to follow-up analysis of positive neonatal screening results, J. Inherit. Metab. Dis. 33 (2010) 479–494. https://doi.org/10.1007/s10545-010-9104-8.
[39] A.-M. Lundsgaard, A.M. Fritzen, B. Kiens, Molecular Regulation of Fatty Acid Oxidation in Skeletal Muscle during Aerobic Exercise, Trends Endocrinol. Metab. 29 (2018) 18–30. https://doi.org/10.1016/j.tem.2017.10.011.
[40] R.J. DeBerardinis, A. Mancuso, E. Daikhin, I. Nissim, M. Yudkoff, S. Wehrli, C.B. Thompson, Beyond aerobic glycolysis: Transformed cells can engage in glutamine metabolism that exceeds the requirement for protein and nucleotide synthesis, Proc. Natl. Acad. Sci. 104 (2007) 19345–19350. https://doi.org/10.1073/pnas.0709747104.
[41] Y. Shimomura, T. Murakami, N. Nakai, M. Nagasaki, R.A. Harris, Exercise Promotes BCAA Catabolism: Effects of BCAA Supplementation on Skeletal Muscle during Exercise1, J. Nutr. 134 (2004) 1583S-1587S. https://doi.org/10.1093/jn/134.6.1583S.
[42] N. Ørtenblad, H. Westerblad, J. Nielsen, Muscle glycogen stores and fatigue, J. Physiol. 591 (2013) 4405–4413. https://doi.org/10.1113/jphysiol.2013.251629.
[43] B.H. Choi, S. Hyun, S.-H. Koo, The role of BCAA metabolism in metabolic health and disease, Exp. Mol. Med. 56 (2024) 1552–1559. https://doi.org/10.1038/s12276-024-01263-6.
[44] Q. Chen, K. Kirk, Y.I. Shurubor, D. Zhao, A.J. Arreguin, I. Shahi, F. Valsecchi, G. Primiano, E.L. Calder, V. Carelli, T.T. Denton, M.F. Beal, S.S. Gross, G. Manfredi, M. D'Aurelio, Rewiring of Glutamine Metabolism Is a Bioenergetic Adaptation of Human Cells with Mitochondrial DNA Mutations, Cell Metab. 27 (2018) 1007-1025.e5. https://doi.org/10.1016/j.cmet.2018.03.002.
[45] M. Wikström, C. Pecorilla, V. Sharma, Chapter Two - The mitochondrial respiratory chain, in: L.S. Kaguni, F. Tamanoi (Eds.), The Enzymes, Academic Press, 2023: pp. 15–36. https://doi.org/10.1016/bs.enz.2023.05.001.
[46] W.S. Kunz, Control of oxidative phosphorylation in skeletal muscle, Biochim. Biophys. Acta BBA - Bioenerg. 1504 (2001) 12–19. https://doi.org/10.1016/S0005-2728(00)00235-8.
[47] R.K. Porter, M.D. Brand, Body mass dependence of H+ leak in mitochondria and its relevance to metabolic rate, Nature 362 (1993) 628–630. https://doi.org/10.1038/362628a0.

[48] M. Jastroch, A.S. Divakaruni, S. Mookerjee, J.R. Treberg, M.D. Brand, Mitochondrial proton and electron leaks, Essays Biochem. 47 (2010) 53–67. https://doi.org/10.1042/bse0470053.
[49] A.M. Bertholet, E.T. Chouchani, L. Kazak, A. Angelin, A. Fedorenko, J.Z. Long, S. Vidoni, R. Garrity, J. Cho, N. Terada, D.C. Wallace, B.M. Spiegelman, Y. Kirichok, H+ transport is an integral function of the mitochondrial ADP/ATP carrier, Nature 571 (2019) 515–520. https://doi.org/10.1038/s41586-019-1400-3.
[50] F. Bouillaud, M.-C. Alves-Guerra, D. Ricquier, UCPs, at the interface between bioenergetics and metabolism, Biochim. Biophys. Acta BBA - Mol. Cell Res. 1863 (2016) 2443–2456. https://doi.org/10.1016/j.bbamcr.2016.04.013.
[51] M.D. Brand, J.L. Pakay, A. Ocloo, J. Kokoszka, D.C. Wallace, P.S. Brookes, E.J. Cornwall, The basal proton conductance of mitochondria depends on adenine nucleotide translocase content, Biochem. J. 392 (2005) 353–362. https://doi.org/10.1042/BJ20050890.
[52] M. Jastroch, A.S. Divakaruni, S. Mookerjee, J.R. Treberg, M.D. Brand, Mitochondrial proton and electron leaks, Essays Biochem. 47 (2010) 53–67. https://doi.org/10.1042/bse0470053.
[53] S. Srivastava, F. Diaz, L. Iommarini, K. Aure, A. Lombes, C.T. Moraes, PGC-1α/β induced expression partially compensates for respiratory chain defects in cells from patients with mitochondrial disorders, Hum. Mol. Genet. 18 (2009) 1805–1812. https://doi.org/10.1093/hmg/ddp093.
[54] D.M. Muoio, T.R. Koves, Skeletal muscle adaptation to fatty acid depends on coordinated actions of the PPARs and PGC1α: implications for metabolic disease, Appl. Physiol. Nutr. Metab. 32 (2007) 874–883. https://doi.org/10.1139/H07-083.
[55] C. Cantó, J. Auwerx, PGC-1α, SIRT1 and AMPK, an energy sensing network that controls energy expenditure, Curr. Opin. Lipidol. 20 (2009) 98. https://doi.org/10.1097/MOL.0b013e328328d0a4.
[56] B. Saltin, P.D. Gollnick, Skeletal Muscle Adaptability: Significance for Metabolism and Performance, in: Compr. Physiol., John Wiley & Sons, Ltd, 2011: pp. 555–631. https://doi.org/10.1002/cphy.cp100119.
[57] D.M. Muoio, Metabolic Inflexibility: When Mitochondrial Indecision Leads to Metabolic Gridlock, Cell 159 (2014) 1253–1262. https://doi.org/10.1016/j.cell.2014.11.034.
[58] M.C. Sugden, M.J. and Holness, Mechanisms underlying regulation of the expression and activities of the mammalian pyruvate dehydrogenase kinases, Arch. Physiol. Biochem. 112 (2006) 139–149. https://doi.org/10.1080/13813450600935263.
[59] L.L. Spriet, New Insights into the Interaction of Carbohydrate and Fat Metabolism During Exercise, Sports Med. 44 (2014) 87–96. https://doi.org/10.1007/s40279-014-0154-1.
[60] O. Matilainen, P.M. Quirós, J. Auwerx, Mitochondria and Epigenetics – Crosstalk in Homeostasis and Stress, Trends Cell Biol. 27 (2017) 453–463. https://doi.org/10.1016/j.tcb.2017.02.004.
[61] U. Mühlenhoff, J.J. Braymer, S. Christ, N. Rietzschel, M.A. Uzarska, B.D. Weiler, R. Lill, Glutaredoxins and iron-sulfur protein biogenesis at the interface of redox biology and iron metabolism, Biol. Chem. 401 (2020) 1407–1428. https://doi.org/10.1515/hsz-2020-0237.
[62] A. Suomalainen, J.M. Elo, K.H. Pietiläinen, A.H. Hakonen, K. Sevastianova, M. Korpela, P. Isohanni, S.K. Marjavaara, T. Tyni, S. Kiuru-Enari, H. Pihko, N. Darin, K. Õunap, L.A. Kluijtmans, A. Paetau, J. Buzkova, L.A. Bindoff, J. Annunen-Rasila, J. Uusimaa, A. Rissanen, H. Yki-Järvinen, M. Hirano, M. Tulinius, J. Smeitink, H. Tyynismaa, FGF-21 as a biomarker for muscle-manifesting mitochondrial respiratory chain deficiencies: a diagnostic study, Lancet Neurol. 10 (2011) 806–818. https://doi.org/10.1016/S1474-4422(11)70155-7.

[63] Quantitative Fluxomics of Circulating Metabolites: Cell Metabolism, (n.d.). https://www.cell.com/cell-metabolism/fulltext/S1550-4131(20)30371-5 (accessed March 31, 2025).
[64] S. Forsström, C.B. Jackson, C.J. Carroll, M. Kuronen, E. Pirinen, S. Pradhan, A. Marmyleva, M. Auranen, I.-M. Kleine, N.A. Khan, A. Roivainen, P. Marjamäki, H. Liljenbäck, L. Wang, B.J. Battersby, U. Richter, V. Velagapudi, J. Nikkanen, L. Euro, A. Suomalainen, Fibroblast Growth Factor 21 Drives Dynamics of Local and Systemic Stress Responses in Mitochondrial Myopathy with mtDNA Deletions, Cell Metab. 30 (2019) 1040-1054.e7. https://doi.org/10.1016/j.cmet.2019.08.019.
[65] K.J. Vandiver, P.D. Neufer, Chapter 7 - Mitochondria: connecting oxygen to life, in: M.J. Joyner, J.A. Dempsey (Eds.), Oxyg., Academic Press, 2025: pp. 191–210. https://doi.org/10.1016/B978-0-443-21877-4.00007-3.
[66] T. Gabaldón, M.A. Huynen, Lineage-specific gene loss following mitochondrial endosymbiosis and its potential for function prediction in eukaryotes, Bioinformatics 21 (2005) ii144–ii150. https://doi.org/10.1093/bioinformatics/bti1124.
[67] N. Lane, W. Martin, The energetics of genome complexity, Nature 467 (2010) 929–934. https://doi.org/10.1038/nature09486.
[68] E.L. Eberhardt, A.V. Ludlam, Z. Tan, M.A. Cianfrocco, Miro: A molecular switch at the center of mitochondrial regulation, Protein Sci. 29 (2020) 1269–1284. https://doi.org/10.1002/pro.3839.
[69] A. Chatzi, P. Manganas, K. Tokatlidis, Oxidative folding in the mitochondrial intermembrane space: A regulated process important for cell physiology and disease, Biochim. Biophys. Acta BBA - Mol. Cell Res. 1863 (2016) 1298–1306. https://doi.org/10.1016/j.bbamcr.2016.03.023.
[70] C.A. Goard, A.D. Schimmer, Mitochondrial matrix proteases as novel therapeutic targets in malignancy, Oncogene 33 (2014) 2690–2699. https://doi.org/10.1038/onc.2013.228.
[71] G. Twig, A. Elorza, A.J.A. Molina, H. Mohamed, J.D. Wikstrom, G. Walzer, L. Stiles, S.E. Haigh, S. Katz, G. Las, J. Alroy, M. Wu, B.F. Py, J. Yuan, J.T. Deeney, B.E. Corkey, O.S. Shirihai, Fission and selective fusion govern mitochondrial segregation and elimination by autophagy, EMBO J. 27 (2008) 433–446. https://doi.org/10.1038/sj.emboj.7601963.
[72] D.B. Zorov, I.A. Vorobjev, V.A. Popkov, V.A. Babenko, L.D. Zorova, I.B. Pevzner, D.N. Silachev, S.D. Zorov, N.V. Andrianova, E.Y. Plotnikov, Lessons from the Discovery of Mitochondrial Fragmentation (Fission): A Review and Update, Cells 8 (2019) 175. https://doi.org/10.3390/cells8020175.
[73] J.M. Quiles, Å.B. Gustafsson, The role of mitochondrial fission in cardiovascular health and disease, Nat. Rev. Cardiol. 19 (2022) 723–736. https://doi.org/10.1038/s41569-022-00703-y.
[74] E. Smirnova, L. Griparic, D.-L. Shurland, A.M. van der Bliek, Dynamin-related Protein Drp1 Is Required for Mitochondrial Division in Mammalian Cells, Mol. Biol. Cell 12 (2001) 2245–2256. https://doi.org/10.1091/mbc.12.8.2245.
[75] D.I. James, P.A. Parone, Y. Mattenberger, J.-C. Martinou, hFis1, a Novel Component of the Mammalian Mitochondrial Fission Machinery *, J. Biol. Chem. 278 (2003) 36373–36379. https://doi.org/10.1074/jbc.M303758200.
[76] Mff is an essential factor for mitochondrial recruitment of Drp1 during mitochondrial fission in mammalian cells | Journal of Cell Biology | Rockefeller University Press, (n.d.). https://rupress.org/jcb/article/191/6/1141/36220/Mff-is-an-essential-factor-for-mitochondrial (accessed March 31, 2025).

[77] R. Yu, S. Jin, U. Lendahl, M. Nistér, J. Zhao, Human Fis1 regulates mitochondrial dynamics through inhibition of the fusion machinery, EMBO J. 38 (2019) e99748. https://doi.org/10.15252/embj.201899748.
[78] N. Ishihara, Y. Eura, K. Mihara, Mitofusin 1 and 2 play distinct roles in mitochondrial fusion reactions via GTPase activity, J. Cell Sci. 117 (2004) 6535–6546. https://doi.org/10.1242/jcs.01565.
[79] S. Cipolat, O.M. de Brito, B. Dal Zilio, L. Scorrano, OPA1 requires mitofusin 1 to promote mitochondrial fusion, Proc. Natl. Acad. Sci. 101 (2004) 15927–15932. https://doi.org/10.1073/pnas.0407043101.
[80] N. Ishihara, Y. Fujita, T. Oka, K. Mihara, Regulation of mitochondrial morphology through proteolytic cleavage of OPA1, EMBO J. 25 (2006) 2966–2977. https://doi.org/10.1038/sj.emboj.7601184.
[81] T. Ban, T. Ishihara, H. Kohno, S. Saita, A. Ichimura, K. Maenaka, T. Oka, K. Mihara, N. Ishihara, Molecular basis of selective mitochondrial fusion by heterotypic action between OPA1 and cardiolipin, Nat. Cell Biol. 19 (2017) 856–863. https://doi.org/10.1038/ncb3560.
[82] Determinants and Functions of Mitochondrial Behavior | Annual Reviews, (n.d.). https://www.annualreviews.org/content/journals/10.1146/annurev-cellbio-101011-155756 (accessed March 31, 2025).
[83] P. Puigserver, Z. Wu, C.W. Park, R. Graves, M. Wright, B.M. Spiegelman, A Cold-Inducible Coactivator of Nuclear Receptors Linked to Adaptive Thermogenesis, Cell 92 (1998) 829–839. https://doi.org/10.1016/S0092-8674(00)81410-5.
[84] J. Lin, H. Wu, P.T. Tarr, C.-Y. Zhang, Z. Wu, O. Boss, L.F. Michael, P. Puigserver, E. Isotani, E.N. Olson, B.B. Lowell, R. Bassel-Duby, B.M. Spiegelman, Transcriptional co-activator PGC-1α drives the formation of slow-twitch muscle fibres, Nature 418 (2002) 797–801. https://doi.org/10.1038/nature00904.
[85] L. Leick, J.F.P. Wojtaszewski, S.T. Johansen, K. Kiilerich, G. Comes, Y. Hellsten, J. Hidalgo, H. Pilegaard, PGC-1α is not mandatory for exercise- and training-induced adaptive gene responses in mouse skeletal muscle, Am. J. Physiol.-Endocrinol. Metab. 294 (2008) E463–E474. https://doi.org/10.1152/ajpendo.00666.2007.
[86] J. Lin, P.-H. Wu, P.T. Tarr, K.S. Lindenberg, J. St-Pierre, C. Zhang, V.K. Mootha, S. Jäger, C.R. Vianna, R.M. Reznick, L. Cui, M. Manieri, M.X. Donovan, Z. Wu, M.P. Cooper, M.C. Fan, L.M. Rohas, A.M. Zavacki, S. Cinti, G.I. Shulman, B.B. Lowell, D. Krainc, B.M. Spiegelman, Defects in Adaptive Energy Metabolism with CNS-Linked Hyperactivity in PGC-1α Null Mice, Cell 119 (2004) 121–135. https://doi.org/10.1016/j.cell.2004.09.013.
[87] Z. Wu, P. Puigserver, U. Andersson, C. Zhang, G. Adelmant, V. Mootha, A. Troy, S. Cinti, B. Lowell, R.C. Scarpulla, B.M. Spiegelman, Mechanisms Controlling Mitochondrial Biogenesis and Respiration through the Thermogenic Coactivator PGC-1, Cell 98 (1999) 115–124. https://doi.org/10.1016/S0092-8674(00)80611-X.
[88] J.V. Virbasius, R.C. Scarpulla, Activation of the human mitochondrial transcription factor A gene by nuclear respiratory factors: a potential regulatory link between nuclear and mitochondrial gene expression in organelle biogenesis., Proc. Natl. Acad. Sci. 91 (1994) 1309–1313. https://doi.org/10.1073/pnas.91.4.1309.
[89] F.R. Jornayvaz, G.I. Shulman, Regulation of mitochondrial biogenesis, Essays Biochem. 47 (2010) 69–84. https://doi.org/10.1042/bse0470069.
[90] C. Ploumi, I. Daskalaki, N. Tavernarakis, Mitochondrial biogenesis and clearance: a balancing act, FEBS J. 284 (2017) 183–195. https://doi.org/10.1111/febs.13820.

[91] Y. Chen, D. Jiao, Y. Liu, X. Xu, Y. Wang, X. Luo, H. Saiyin, Y. Li, K. Gao, Y. Chen, S.-M. Zhao, L. Ma, C. Wang, FBXL4 mutations cause excessive mitophagy via BNIP3/BNIP3L accumulation leading to mitochondrial DNA depletion syndrome, Cell Death Differ. 30 (2023) 2351–2363. https://doi.org/10.1038/s41418-023-01205-1.
[92] H.M. Cho, J.R. Ryu, Y. Jo, T.W. Seo, Y.N. Choi, J.H. Kim, J.M. Chung, B. Cho, H.C. Kang, S.-W. Yu, S.J. Yoo, H. Kim, W. Sun, Drp1-Zip1 Interaction Regulates Mitochondrial Quality Surveillance System, Mol. Cell 73 (2019) 364-376.e8. https://doi.org/10.1016/j.molcel.2018.11.009.
[93] M. Frank, S. Duvezin-Caubet, S. Koob, A. Occhipinti, R. Jagasia, A. Petcherski, M.O. Ruonala, M. Priault, B. Salin, A.S. Reichert, Mitophagy is triggered by mild oxidative stress in a mitochondrial fission dependent manner, Biochim. Biophys. Acta BBA - Mol. Cell Res. 1823 (2012) 2297–2310. https://doi.org/10.1016/j.bbamcr.2012.08.007.
[94] M. Redza-Dutordoir, D.A. Averill-Bates, Interactions between reactive oxygen species and autophagy: Special issue: Death mechanisms in cellular homeostasis, Biochim. Biophys. Acta BBA - Mol. Cell Res. 1868 (2021) 119041. https://doi.org/10.1016/j.bbamcr.2021.119041.
[95] Y. Lu, Z. Li, S. Zhang, T. Zhang, Y. Liu, L. Zhang, Cellular mitophagy: Mechanism, roles in diseases and small molecule pharmacological regulation, Theranostics 13 (2023) 736–766. https://doi.org/10.7150/thno.79876.
[96] J.-M. Heo, A. Ordureau, J.A. Paulo, J. Rinehart, J.W. Harper, The PINK1-PARKIN Mitochondrial Ubiquitylation Pathway Drives a Program of OPTN/NDP52 Recruitment and TBK1 Activation to Promote Mitophagy, Mol. Cell 60 (2015) 7–20. https://doi.org/10.1016/j.molcel.2015.08.016.
[97] K. Palikaras, E. Lionaki, N. Tavernarakis, Mechanisms of mitophagy in cellular homeostasis, physiology and pathology, Nat. Cell Biol. 20 (2018) 1013–1022. https://doi.org/10.1038/s41556-018-0176-2.
[98] F. Haddad, F. Zaldivar, D.M. Cooper, G.R. Adams, IL-6-induced skeletal muscle atrophy, J. Appl. Physiol. 98 (2005) 911–917. https://doi.org/10.1152/japplphysiol.01026.2004.
[99] S.K. Powers, A.N. Kavazis, J.M. McClung, Oxidative stress and disuse muscle atrophy, J. Appl. Physiol. 102 (2007) 2389–2397. https://doi.org/10.1152/japplphysiol.01202.2006.
[100] M. Doucet, A.P. Russell, B. Léger, R. Debigaré, D.R. Joanisse, M.-A. Caron, P. LeBlanc, F. Maltais, Muscle Atrophy and Hypertrophy Signaling in Patients with Chronic Obstructive Pulmonary Disease, Am. J. Respir. Crit. Care Med. 176 (2007) 261–269. https://doi.org/10.1164/rccm.200605-704OC.
[101] S. Schiaffino, C. Mammucari, Regulation of skeletal muscle growth by the IGF1-Akt/PKB pathway: insights from genetic models, Skelet. Muscle 1 (2011) 4. https://doi.org/10.1186/2044-5040-1-4.
[102] A protein kinase B-dependent and rapamycin-sensitive pathway controls skeletal muscle growth but not fiber type specification, (n.d.). https://doi.org/10.1073/pnas.142166599.
[103] R. Sartori, G. Milan, M. Patron, C. Mammucari, B. Blaauw, R. Abraham, M. Sandri, Smad2 and 3 transcription factors control muscle mass in adulthood, Am. J. Physiol.-Cell Physiol. 296 (2009) C1248–C1257. https://doi.org/10.1152/ajpcell.00104.2009.
[104] A.C. McPherron, A.M. Lawler, S.-J. Lee, Regulation of skeletal muscle mass in mice by a new TGF-p superfamily member, Nature 387 (1997) 83–90. https://doi.org/10.1038/387083a0.
[105] K.R. Wagner, J.L. Fleckenstein, A.A. Amato, R.J. Barohn, K. Bushby, D.M. Escolar, K.M. Flanigan, A. Pestronk, R. Tawil, G.I. Wolfe, M. Eagle, J.M. Florence, W.M. King, S. Pandya, V. Straub, P. Juneau, K. Meyers, C. Csimma, T. Araujo, R. Allen, S.A. Parsons, J.M. Wozney, E.R.

LaVallie, J.R. Mendell, A phase I/IItrial of MYO-029 in adult subjects with muscular dystrophy, Ann. Neurol. 63 (2008) 561–571. https://doi.org/10.1002/ana.21338.
[106] S.B. Heymsfield, L.A. Coleman, R. Miller, D.S. Rooks, D. Laurent, O. Petricoul, J. Praestgaard, T. Swan, T. Wade, R.G. Perry, B.H. Goodpaster, R. Roubenoff, Effect of Bimagrumab vs Placebo on Body Fat Mass Among Adults With Type 2 Diabetes and Obesity: A Phase 2 Randomized Clinical Trial, JAMA Netw. Open 4 (2021) e2033457. https://doi.org/10.1001/jamanetworkopen.2020.33457.
[107] M. Kanbay, D. Siriopol, S. Copur, N.B. Hasbal, M. Güldan, K. Kalantar-Zadeh, T. Garfias-Veitl, S. von Haehling, Effect of Bimagrumab on body composition: a systematic review and meta-analysis, Aging Clin. Exp. Res. 36 (2024) 185. https://doi.org/10.1007/s40520-024-02825-4.
[108] K. Stefanakis, M. Kokkorakis, C.S. Mantzoros, The impact of weight loss on fat-free mass, muscle, bone and hematopoiesis health: Implications for emerging pharmacotherapies aiming at fat reduction and lean mass preservation, Metab. - Clin. Exp. 161 (2024). https://doi.org/10.1016/j.metabol.2024.156057.
[109] G.C. Minetti, Feige ,Jerome N., Bombard ,Florian, Heier ,Annabelle, Morvan ,Fredric, Nürnberg ,Bernd, Leiss ,Veronika, Birnbaumer ,Lutz, Glass ,David J., M. and Fornaro, Gαi2 Signaling Is Required for Skeletal Muscle Growth, Regeneration, and Satellite Cell Proliferation and Differentiation, Mol. Cell. Biol. 34 (2014) 619–630. https://doi.org/10.1128/MCB.00957-13.
[110] T.N. Stitt, D. Drujan, B.A. Clarke, F. Panaro, Y. Timofeyva, W.O. Kline, M. Gonzalez, G.D. Yancopoulos, D.J. Glass, The IGF-1/PI3K/Akt Pathway Prevents Expression of Muscle Atrophy-Induced Ubiquitin Ligases by Inhibiting FOXO Transcription Factors, Mol. Cell 14 (2004) 395–403. https://doi.org/10.1016/S1097-2765(04)00211-4.
[111] Y.-P. Li, Y. Chen, J. John, J. Moylan, B. Jin, D.L. Mann, M.B. Reid, TNF-α acts via p38 MAPK to stimulate expression of the ubiquitin ligase atrogin1/MAFbx in skeletal muscle, FASEB J. Off. Publ. Fed. Am. Soc. Exp. Biol. 19 (2005) 362–370. https://doi.org/10.1096/fj.04-2364com.
[112] R.W. Jackman, E.W. Cornwell, C.-L. Wu, S.C. Kandarian, Nuclear factor-κB signalling and transcriptional regulation in skeletal muscle atrophy, Exp. Physiol. 98 (2013) 19–24. https://doi.org/10.1113/expphysiol.2011.063321.
[113] G. Marazzi, D. Sassoon, FAPs are sensors for skeletal myofibre atrophy, Nat. Cell Biol. 20 (2018) 864–865. https://doi.org/10.1038/s41556-018-0149-5.
[114] J. Ye, Y. Zhang, J. Xu, Q. Zhang, D. Zhu, *FBXO40*, a gene encoding a novel muscle-specific F-box protein, is upregulated in denervation-related muscle atrophy, Gene 404 (2007) 53–60. https://doi.org/10.1016/j.gene.2007.08.020.
[115] A.J. Smuder, A.N. Kavazis, M.B. Hudson, W.B. Nelson, S.K. Powers, Oxidation enhances myofibrillar protein degradation via calpain and caspase-3, Free Radic. Biol. Med. 49 (2010) 1152–1160. https://doi.org/10.1016/j.freeradbiomed.2010.06.025.
[116] R.M. Murphy, Calpains, skeletal muscle function and exercise, Clin. Exp. Pharmacol. Physiol. 37 (2010) 385–391. https://doi.org/10.1111/j.1440-1681.2009.05310.x.
[117] J. Du, X. Wang, C. Miereles, J.L. Bailey, R. Debigare, B. Zheng, S.R. Price, W.E. Mitch, Activation of caspase-3 is an initial step triggering accelerated muscle proteolysis in catabolic conditions, J. Clin. Invest. 113 (2004) 115–123. https://doi.org/10.1172/JCI18330.
[118] F. Relaix, P.S. Zammit, Satellite cells are essential for skeletal muscle regeneration: the cell on the edge returns centre stage, Development 139 (2012) 2845–2856. https://doi.org/10.1242/dev.069088.
[119] T.H. Cheung, T.A. Rando, Molecular regulation of stem cell quiescence, Nat. Rev. Mol. Cell Biol. 14 (2013) 329–340. https://doi.org/10.1038/nrm3591.

[120] S. Fukada, The roles of muscle stem cells in muscle injury, atrophy and hypertrophy, J. Biochem. (Tokyo) 163 (2018) 353–358. https://doi.org/10.1093/jb/mvy019.
[121] D.A. Englund, K.A. Murach, C.M. Dungan, V.C. Figueiredo, I.J. Vechetti, E.E. Dupont-Versteegden, J.J. McCarthy, C.A. Peterson, Depletion of resident muscle stem cells negatively impacts running volume, physical function, and muscle fiber hypertrophy in response to lifelong physical activity, Am. J. Physiol.-Cell Physiol. 318 (2020) C1178–C1188. https://doi.org/10.1152/ajpcell.00090.2020.
[122] N.A. Dumont, C.F. Bentzinger, M.-C. Sincennes, M.A. Rudnicki, Satellite Cells and Skeletal Muscle Regeneration, in: Compr. Physiol., John Wiley & Sons, Ltd, 2015: pp. 1027–1059. https://doi.org/10.1002/cphy.c140068.
[123] P. Feige, C.E. Brun, M. Ritso, M.A. Rudnicki, Orienting Muscle Stem Cells for Regeneration in Homeostasis, Aging, and Disease, Cell Stem Cell 23 (2018) 653–664. https://doi.org/10.1016/j.stem.2018.10.006.
[124] A. de Morree, T.A. Rando, Regulation of adult stem cell quiescence and its functions in the maintenance of tissue integrity, Nat. Rev. Mol. Cell Biol. 24 (2023) 334–354. https://doi.org/10.1038/s41580-022-00568-6.
[125] D.P. Millay, J.R. O'Rourke, L.B. Sutherland, S. Bezprozvannaya, J.M. Shelton, R. Bassel-Duby, E.N. Olson, Myomaker is a membrane activator of myoblast fusion and muscle formation, Nature 499 (2013) 301–305. https://doi.org/10.1038/nature12343.
[126] O. Mashinchian, A. Pisconti, E. Le Moal, C.F. Bentzinger, Chapter Two - The Muscle Stem Cell Niche in Health and Disease, in: D. Sassoon (Ed.), Curr. Top. Dev. Biol., Academic Press, 2018: pp. 23–65. https://doi.org/10.1016/bs.ctdb.2017.08.003.
[127] P. Zhu, E.M. Pfrender, A.W.T. Steffeck, C.R. Reczek, Y. Zhou, A.V. Thakkar, N.R. Gupta, A. Kupai, A. Willbanks, R.L. Lieber, I. Roy, N.S. Chandel, C.B. Peek, Immunomodulatory role of the stem cell circadian clock in muscle repair, Sci. Adv. 11 (2025) eadq8538. https://doi.org/10.1126/sciadv.adq8538.
[128] N.A. Dumont, Y.X. Wang, J. von Maltzahn, A. Pasut, C.F. Bentzinger, C.E. Brun, M.A. Rudnicki, Dystrophin expression in muscle stem cells regulates their polarity and asymmetric division, Nat. Med. 21 (2015) 1455–1463. https://doi.org/10.1038/nm.3990.
[129] B. Evano, S. Khalilian, G.L. Carrou, G. Almouzni, S. Tajbakhsh, Dynamics of Asymmetric and Symmetric Divisions of Muscle Stem Cells In Vivo and on Artificial Niches, Cell Rep. 30 (2020) 3195-3206.e7. https://doi.org/10.1016/j.celrep.2020.01.097.
[130] H. Sies, R.J. Mailloux, U. Jakob, Fundamentals of redox regulation in biology, Nat. Rev. Mol. Cell Biol. 25 (2024) 701–719. https://doi.org/10.1038/s41580-024-00730-2.
[131] D.P. Jones, H. Sies, The Redox Code, Antioxid. Redox Signal. 23 (2015) 734–746. https://doi.org/10.1089/ars.2015.6247.
[132] C.T. Walsh, B.P. Tu, Y. Tang, Eight Kinetically Stable but Thermodynamically Activated Molecules that Power Cell Metabolism, Chem. Rev. 118 (2018) 1460–1494. https://doi.org/10.1021/acs.chemrev.7b00510.
[133] I. Vercellino, L.A. Sazanov, The assembly, regulation and function of the mitochondrial respiratory chain, Nat. Rev. Mol. Cell Biol. 23 (2022) 141–161. https://doi.org/10.1038/s41580-021-00415-0.
[134] N. Xie, L. Zhang, W. Gao, C. Huang, P.E. Huber, X. Zhou, C. Li, G. Shen, B. Zou, NAD+ metabolism: pathophysiologic mechanisms and therapeutic potential, Signal Transduct. Target. Ther. 5 (2020) 1–37. https://doi.org/10.1038/s41392-020-00311-7.

[135] C. Jacob, G.I. Giles, N.M. Giles, H. Sies, Sulfur and Selenium: The Role of Oxidation State in Protein Structure and Function, Angew. Chem. Int. Ed. 42 (2003) 4742–4758. https://doi.org/10.1002/anie.200300573.
[136] H. Sies, Oxidative stress: a concept in redox biology and medicine, Redox Biol. 4 (2015) 180–183. https://doi.org/10.1016/j.redox.2015.01.002.
[137] M.P. Murphy, H. Bayir, V. Belousov, C.J. Chang, K.J.A. Davies, M.J. Davies, T.P. Dick, T. Finkel, H.J. Forman, Y. Janssen-Heininger, D. Gems, V.E. Kagan, B. Kalyanaraman, N.-G. Larsson, G.L. Milne, T. Nyström, H.E. Poulsen, R. Radi, H. Van Remmen, P.T. Schumacker, P.J. Thornalley, S. Toyokuni, C.C. Winterbourn, H. Yin, B. Halliwell, Guidelines for measuring reactive oxygen species and oxidative damage in cells and in vivo, Nat. Metab. 4 (2022) 651–662. https://doi.org/10.1038/s42255-022-00591-z.
[138] R.G. Knowles, S. Moncada, Nitric oxide synthases in mammals, Biochem. J. 298 (1994) 249–258. https://doi.org/10.1042/bj2980249.
[139] R. Radi, Peroxynitrite, a Stealthy Biological Oxidant*, J. Biol. Chem. 288 (2013) 26464–26472. https://doi.org/10.1074/jbc.R113.472936.
[140] G. Barja, Mitochondrial Oxygen Radical Generation and Leak: Sites of Production in States 4 and 3, Organ Specificity, and Relation to Aging and Longevity, J. Bioenerg. Biomembr. 31 (1999) 347–366. https://doi.org/10.1023/A:1005427919188.
[141] M.P. Murphy, How mitochondria produce reactive oxygen species, Biochem. J. 417 (2008) 1–13. https://doi.org/10.1042/BJ20081386.
[142] J. St-Pierre, J.A. Buckingham, S.J. Roebuck, M.D. Brand, Topology of Superoxide Production from Different Sites in the Mitochondrial Electron Transport Chain*, J. Biol. Chem. 277 (2002) 44784–44790. https://doi.org/10.1074/jbc.M207217200.
[143] R.L.S. Goncalves, C.L. Quinlan, I.V. Perevoshchikova, M. Hey-Mogensen, M.D. Brand, Sites of Superoxide and Hydrogen Peroxide Production by Muscle Mitochondria Assessed *ex Vivo* under Conditions Mimicking Rest and Exercise*, J. Biol. Chem. 290 (2015) 209–227. https://doi.org/10.1074/jbc.M114.619072.
[144] J.F. Turrens, Mitochondrial formation of reactive oxygen species, J. Physiol. 552 (2003) 335–344. https://doi.org/10.1113/jphysiol.2003.049478.
[145] J.S. Stoolman, R.A. Grant, L.K. Billingham, T.A. Poor, S.E. Weinberg, M.C. Harding, Z. Lu, J. Miska, M. Szibor, G.S. Budinger, N.S. Chandel, Mitochondria complex III–generated superoxide is essential for IL-10 secretion in macrophages, Sci. Adv. 11 (2025) eadu4369. https://doi.org/10.1126/sciadv.adu4369.
[146] M.P. Murphy, E.T. Chouchani, Why succinate? Physiological regulation by a mitochondrial coenzyme Q sentinel, Nat. Chem. Biol. 18 (2022) 461–469. https://doi.org/10.1038/s41589-022-01004-8.
[147] A. Sorby-Adams, T.A. Prime, J.L. Miljkovic, H.A. Prag, T. Krieg, M.P. Murphy, A model of mitochondrial superoxide production during ischaemia-reperfusion injury for therapeutic development and mechanistic understanding, Redox Biol. 72 (2024) 103161. https://doi.org/10.1016/j.redox.2024.103161.
[148] C.E. CROSS, B. HALLIWELL, E.T. BORISH, W.A. PRYOR, B.N. AMES, R.L. SAUL, J.M. McCORD, D. HARMAN, Oxygen Radicals and Human Disease, Ann. Intern. Med. 107 (1987) 526–545. https://doi.org/10.7326/0003-4819-107-4-526.
[149] D.B. Zorov, C.R. Filburn, L.-O. Klotz, J.L. Zweier, S.J. Sollott, Reactive Oxygen Species (Ros-Induced) Ros Release: A New Phenomenon Accompanying Induction of the Mitochondrial

Permeability Transition in Cardiac Myocytes, J. Exp. Med. 192 (2000) 1001–1014. https://doi.org/10.1084/jem.192.7.1001.
[150] G. Hayashi, G. Cortopassi, Oxidative stress in inherited mitochondrial diseases, Free Radic. Biol. Med. 88 (2015) 10–17. https://doi.org/10.1016/j.freeradbiomed.2015.05.039.
[151] The NOX Family of ROS-Generating NADPH Oxidases: Physiology and Pathophysiology | Physiological Reviews | American Physiological Society, (n.d.). https://journals.physiology.org/doi/full/10.1152/physrev.00044.2005 (accessed April 1, 2025).
[152] Exercise-Induced Oxidative Stress: Cellular Mechanisms and Impact on Muscle Force Production | Physiological Reviews | American Physiological Society, (n.d.). https://journals.physiology.org/doi/full/10.1152/physrev.00031.2007 (accessed April 1, 2025).
[153] J.M. McCord, I. Fridovich, Superoxide Dismutases: You've Come a Long Way, Baby, Antioxid. Redox Signal. 20 (2014) 1548–1549. https://doi.org/10.1089/ars.2013.5547.
[154] J. VinÑa, M.-C. Gomez-Cabrera, A. Lloret, R. Marquez, J.B. Miñana, F.V. Pallardó, J. Sastre, Free Radicals in Exhaustive Physical Exercise: Mechanism of Production, and Protection by Antioxidants, IUBMB Life 50 (2000) 271–277. https://doi.org/10.1080/713803729.
[155] F. Derbre, B. Ferrando, M.C. Gomez-Cabrera, F. Sanchis-Gomar, V.E. Martinez-Bello, G. Olaso-Gonzalez, A. Diaz, A. Gratas-Delamarche, M. Cerda, J. Viña, Inhibition of Xanthine Oxidase by Allopurinol Prevents Skeletal Muscle Atrophy: Role of p38 MAPKinase and E3 Ubiquitin Ligases, PLOS ONE 7 (2012) e46668. https://doi.org/10.1371/journal.pone.0046668.
[156] J.D. Malhotra, R.J. Kaufman, Endoplasmic Reticulum Stress and Oxidative Stress: A Vicious Cycle or a Double-Edged Sword?, Antioxid. Redox Signal. 9 (2007) 2277–2294. https://doi.org/10.1089/ars.2007.1782.
[157] D. Nethery, D. Stofan, L. Callahan, A. DiMarco, G. Supinski, Formation of reactive oxygen species by the contracting diaphragm is PLA2dependent, J. Appl. Physiol. 87 (1999) 792–800. https://doi.org/10.1152/jappl.1999.87.2.792.
[158] E. Birben, U.M. Sahiner, C. Sackesen, S. Erzurum, O. Kalayci, Oxidative Stress and Antioxidant Defense, World Allergy Organ. J. 5 (2012) 9–19. https://doi.org/10.1097/WOX.0b013e3182439613.
[159] Exercise-Induced Oxidative Stress: Cellular Mechanisms and Impact on Muscle Force Production | Physiological Reviews | American Physiological Society, (n.d.). https://journals.physiology.org/doi/full/10.1152/physrev.00031.2007 (accessed April 1, 2025).
[160] T. Fukai, M. Ushio-Fukai, Superoxide Dismutases: Role in Redox Signaling, Vascular Function, and Diseases, Antioxid. Redox Signal. 15 (2011) 1583–1606. https://doi.org/10.1089/ars.2011.3999.
[161] G.K. Sakellariou, D. Pye, A. Vasilaki, L. Zibrik, J. Palomero, T. Kabayo, F. McArdle, H. Van Remmen, A. Richardson, J.G. Tidball, A. McArdle, M.J. Jackson, Role of superoxide–nitric oxide interactions in the accelerated age-related loss of muscle mass in mice lacking Cu,Zn superoxide dismutase, Aging Cell 10 (2011) 749–760. https://doi.org/10.1111/j.1474-9726.2011.00709.x.
[162] J. Vamecq, M. Cherkaoui-Malki, P. Andreoletti, N. Latruffe, The human peroxisome in health and disease: The story of an oddity becoming a vital organelle, Biochimie 98 (2014) 4–15. https://doi.org/10.1016/j.biochi.2013.09.019.
[163] M.J. Sullivan-Gunn, P.A. Lewandowski, Elevated hydrogen peroxide and decreased catalase and glutathione peroxidase protection are associated with aging sarcopenia, BMC Geriatr. 13 (2013) 104. https://doi.org/10.1186/1471-2318-13-104.
[164] Thioredoxins, Glutaredoxins, and Peroxiredoxins—Molecular Mechanisms and Health Significance: from Cofactors to Antioxidants to Redox Signaling | Antioxidants & Redox

Signaling, (n.d.). https://www.liebertpub.com/doi/full/10.1089/ars.2012.4599 (accessed April 1, 2025).
[165] S. Rohrbach, S. Gruenler, M. Teschner, J. Holtz, The thioredoxin system in aging muscle: key role of mitochondrial thioredoxin reductase in the protective effects of caloric restriction?, Am. J. Physiol.-Regul. Integr. Comp. Physiol. 291 (2006) R927–R935. https://doi.org/10.1152/ajpregu.00890.2005.
[166] J.M. May, C.E. Cobb, S. Mendiratta, K.E. Hill, R.F. Burk, Reduction of the Ascorbyl Free Radical to Ascorbate by Thioredoxin Reductase *, J. Biol. Chem. 273 (1998) 23039–23045. https://doi.org/10.1074/jbc.273.36.23039.
[167] Y. Matsushima, Nanri ,Hiroki, Nara ,Soichiro, Okufuji ,Tatsuya, Ohta ,Masanori, Hachisuka ,Kenji, M. and Ikeda, Hindlimb unloading decreases thioredoxin-related antioxidant proteins and increases thioredoxin-binding protein-2 in rat skeletal muscle, Free Radic. Res. 40 (2006) 715–722. https://doi.org/10.1080/10715760600580488.
[168] Y. Manabe, M. Takagi, M. Nakamura-Yamada, N. Goto-Inoue, M. Taoka, T. Isobe, N.L. Fujii, Redox proteins are constitutively secreted by skeletal muscle, J. Physiol. Sci. 64 (2014) 401–409. https://doi.org/10.1007/s12576-014-0334-7.
[169] O.W. Griffith, A. Meister, Glutathione: interorgan translocation, turnover, and metabolism., Proc. Natl. Acad. Sci. 76 (1979) 5606–5610. https://doi.org/10.1073/pnas.76.11.5606.
[170] L. Kennedy, J.K. Sandhu, M.-E. Harper, M. Cuperlovic-Culf, Role of Glutathione in Cancer: From Mechanisms to Therapies, Biomolecules 10 (2020) 1429. https://doi.org/10.3390/biom10101429.
[171] S. Baldelli, F. Ciccarone, D. Limongi, P. Checconi, A.T. Palamara, M.R. Ciriolo, Glutathione and Nitric Oxide: Key Team Players in Use and Disuse of Skeletal Muscle, Nutrients 11 (2019) 2318. https://doi.org/10.3390/nu11102318.
[172] C. Leeuwenburgh, J. Hollander, S. Leichtweis, M. Griffiths, M. Gore, L.L. Ji, Adaptations of glutathione antioxidant system to endurance training are tissue and muscle fiber specific, Am. J. Physiol.-Regul. Integr. Comp. Physiol. 272 (1997) R363–R369. https://doi.org/10.1152/ajpregu.1997.272.1.R363.
[173] E. Ardite, J.A. Barbera, J. Roca, J.C. Fernández-Checa, Glutathione Depletion Impairs Myogenic Differentiation of Murine Skeletal Muscle C2C12 Cells through Sustained NF-κB Activation, Am. J. Pathol. 165 (2004) 719–728. https://doi.org/10.1016/S0002-9440(10)63335-4.
[174] D.I. Benjamin, J.O. Brett, P. Both, J.S. Benjamin, H.L. Ishak, J. Kang, S. Kim, M. Chung, M. Arjona, C.W. Nutter, J.H. Tan, A.K. Krishnan, H. Dulay, S.M. Louie, A. de Morree, D.K. Nomura, T.A. Rando, Multiomics reveals glutathione metabolism as a driver of bimodality during stem cell aging, Cell Metab. 35 (2023) 472-486.e6. https://doi.org/10.1016/j.cmet.2023.02.001.
[175] N.S. Rajasekaran, S.B. Shelar, D.P. Jones, J.R. Hoidal, Reductive stress impairs myogenic differentiation, Redox Biol. 34 (2020) 101492. https://doi.org/10.1016/j.redox.2020.101492.
[176] T.P. Akerboom, M. Bilzer, H. Sies, The relationship of biliary glutathione disulfide efflux and intracellular glutathione disulfide content in perfused rat liver., J. Biol. Chem. 257 (1982) 4248–4252. https://doi.org/10.1016/S0021-9258(18)34713-6.
[177] H.J. Forman, H. Zhang, A. Rinna, Glutathione: Overview of its protective roles, measurement, and biosynthesis, Mol. Aspects Med. 30 (2009) 1–12. https://doi.org/10.1016/j.mam.2008.08.006.
[178] I. Leier, G. Jedlitschky, U. Buchholz, M. Center, S.P. Cole, R.G. Deeley, D. Keppler, ATP-dependent glutathione disulphide transport mediated by the MRP gene-encoded conjugate export pump., Biochem. J. 314 (1996) 433–437.
[179] S.C. Lu, Glutathione synthesis, Biochim. Biophys. Acta BBA - Gen. Subj. 1830 (2013) 3143–3153. https://doi.org/10.1016/j.bbagen.2012.09.008.

[180] G.F. Seelig, R.P. Simondsen, A. Meister, Reversible dissociation of gamma-glutamylcysteine synthetase into two subunits., J. Biol. Chem. 259 (1984) 9345–9347. https://doi.org/10.1016/S0021-9258(17)42703-7.
[181] C.S. Huang, M.E. Anderson, A. Meister, Amino acid sequence and function of the light subunit of rat kidney gamma-glutamylcysteine synthetase., J. Biol. Chem. 268 (1993) 20578–20583. https://doi.org/10.1016/S0021-9258(20)80764-9.
[182] B. Halliwell, J.M.C. Gutteridge, Antioxidant defences synthesized in vivo, in: B. Halliwell, J.M.C. Gutteridge (Eds.), Free Radic. Biol. Med., Oxford University Press, 2015: p. 0. https://doi.org/10.1093/acprof:oso/9780198717478.003.0003.
[183] The Incomplete Glutathione Puzzle: Just Guessing at Numbers and Figures? | Antioxidants & Redox Signaling, (n.d.). https://www.liebertpub.com/doi/full/10.1089/ars.2017.7123 (accessed April 1, 2025).
[184] M. Deponte, Glutathione catalysis and the reaction mechanisms of glutathione-dependent enzymes, Biochim. Biophys. Acta BBA - Gen. Subj. 1830 (2013) 3217–3266. https://doi.org/10.1016/j.bbagen.2012.09.018.
[185] K.C. Patra, N. Hay, The pentose phosphate pathway and cancer, Trends Biochem. Sci. 39 (2014) 347–354. https://doi.org/10.1016/j.tibs.2014.06.005.
[186] J.A. Ronchi, A. Francisco, L.A.C. Passos, T.R. Figueira, R.F. Castilho, The Contribution of Nicotinamide Nucleotide Transhydrogenase to Peroxide Detoxification Is Dependent on the Respiratory State and Counterbalanced by Other Sources of NADPH in Liver Mitochondria, J. Biol. Chem. 291 (2016) 20173–20187. https://doi.org/10.1074/jbc.M116.730473.
[187] C. Berndt, H. Alborzinia, V.S. Amen, S. Ayton, U. Barayeu, A. Bartelt, H. Bayir, C.M. Bebber, K. Birsoy, J.P. Böttcher, S. Brabletz, T. Brabletz, A.R. Brown, B. Brüne, G. Bulli, A. Bruneau, Q. Chen, G.M. DeNicola, T.P. Dick, A. Distéfano, S.J. Dixon, J.B. Engler, J. Esser-von Bieren, M. Fedorova, J.P. Friedmann Angeli, M.A. Friese, D.C. Fuhrmann, A.J. García-Sáez, K. Garbowicz, M. Götz, W. Gu, L. Hammerich, B. Hassannia, X. Jiang, A. Jeridi, Y.P. Kang, V.E. Kagan, D.B. Konrad, S. Kotschi, P. Lei, M. Le Tertre, S. Lev, D. Liang, A. Linkermann, C. Lohr, S. Lorenz, T. Luedde, A. Methner, B. Michalke, A.V. Milton, J. Min, E. Mishima, S. Müller, H. Motohashi, M.U. Muckenthaler, S. Murakami, J.A. Olzmann, G. Pagnussat, Z. Pan, T. Papagiannakopoulos, L. Pedrera Puentes, D.A. Pratt, B. Proneth, L. Ramsauer, R. Rodriguez, Y. Saito, F. Schmidt, C. Schmitt, A. Schulze, A. Schwab, A. Schwantes, M. Soula, B. Spitzlberger, B.R. Stockwell, L. Thewes, O. Thorn-Seshold, S. Toyokuni, W. Tonnus, A. Trumpp, P. Vandenabeele, T. Vanden Berghe, V. Venkataramani, F.C.E. Vogel, S. von Karstedt, F. Wang, F. Westermann, C. Wientjens, C. Wilhelm, M. Wölk, K. Wu, X. Yang, F. Yu, Y. Zou, M. Conrad, Ferroptosis in health and disease, Redox Biol. 75 (2024) 103211. https://doi.org/10.1016/j.redox.2024.103211.
[188] B.R. Stockwell, J.P.F. Angeli, H. Bayir, A.I. Bush, M. Conrad, S.J. Dixon, S. Fulda, S. Gascón, S.K. Hatzios, V.E. Kagan, K. Noel, X. Jiang, A. Linkermann, M.E. Murphy, M. Overholtzer, A. Oyagi, G.C. Pagnussat, J. Park, Q. Ran, C.S. Rosenfeld, K. Salnikow, D. Tang, F.M. Torti, S.V. Torti, S. Toyokuni, K.A. Woerpel, D.D. Zhang, Ferroptosis: A Regulated Cell Death Nexus Linking Metabolism, Redox Biology, and Disease, Cell 171 (2017) 273–285. https://doi.org/10.1016/j.cell.2017.09.021.
[189] E.V. Kalinina, N.N. Chernov, M.D. Novichkova, Role of glutathione, glutathione transferase, and glutaredoxin in regulation of redox-dependent processes, Biochem. Mosc. 79 (2014) 1562–1583. https://doi.org/10.1134/S0006297914130082.
[190] J.D. Hayes, D.J. and Pulford, The Glut athione S-Transferase Supergene Family: Regulation of GST and the Contribution of the lsoenzymes to Cancer Chemoprotection and Drug Resistance

Part II, Crit. Rev. Biochem. Mol. Biol. 30 (1995) 521–600. https://doi.org/10.3109/10409239509083492.
[191] L.G. Higgins, J.D. and Hayes, Mechanisms of induction of cytosolic and microsomal glutathione transferase (GST) genes by xenobiotics and pro-inflammatory agents, Drug Metab. Rev. 43 (2011) 92–137. https://doi.org/10.3109/03602532.2011.567391.
[192] I. Dalle-Donne, R. Rossi, G. Colombo, D. Giustarini, A. Milzani, Protein S-glutathionylation: a regulatory device from bacteria to humans, Trends Biochem. Sci. 34 (2009) 85–96. https://doi.org/10.1016/j.tibs.2008.11.002.
[193] M. Fratelli, H. Demol, M. Puype, S. Casagrande, I. Eberini, M. Salmona, V. Bonetto, M. Mengozzi, F. Duffieux, E. Miclet, A. Bachi, J. Vandekerckhove, E. Gianazza, P. Ghezzi, Identification by redox proteomics of glutathionylated proteins in oxidatively stressed human T lymphocytes, Proc. Natl. Acad. Sci. 99 (2002) 3505–3510. https://doi.org/10.1073/pnas.052592699.
[194] I.A. Cotgreave, R. Gerdes, I. Schuppe-Koistinen, C. Lind, [17] S-Glutathionylation of glyceraldehyde-3-phosphate dehydrogenase: Role of thiol oxidation and catalysis by glutaredoxin, in: H. Sies, L. Packer (Eds.), Methods Enzymol., Academic Press, 2002: pp. 175–182. https://doi.org/10.1016/S0076-6879(02)48636-3.
[195] T.R. Hurd, R. Requejo, A. Filipovska, S. Brown, T.A. Prime, A.J. Robinson, I.M. Fearnley, M.P. Murphy, Complex I within Oxidatively Stressed Bovine Heart Mitochondria Is Glutathionylated on Cys-531 and Cys-704 of the 75-kDa Subunit, J. Biol. Chem. 283 (2008) 24801–24815. https://doi.org/10.1074/jbc.M803432200.
[196] R.J. Mailloux, Protein S-glutathionylation reactions as a global inhibitor of cell metabolism for the desensitization of hydrogen peroxide signals, Redox Biol. 32 (2020) 101472. https://doi.org/10.1016/j.redox.2020.101472.
[197] D.E. Heppner, Y.M.W. Janssen-Heininger, A. van der Vliet, The role of sulfenic acids in cellular redox signaling: Reconciling chemical kinetics and molecular detection strategies, Arch. Biochem. Biophys. 616 (2017) 40–46. https://doi.org/10.1016/j.abb.2017.01.008.
[198] W. Dröge, Oxidative stress and ageing: is ageing a cysteine deficiency syndrome?, Philos. Trans. R. Soc. B Biol. Sci. 360 (2005) 2355–2372. https://doi.org/10.1098/rstb.2005.1770.
[199] S. Bannai, Exchange of cystine and glutamate across plasma membrane of human fibroblasts., J. Biol. Chem. 261 (1986) 2256–2263. https://doi.org/10.1016/S0021-9258(17)35926-4.
[200] M.H. Hanigan, W.A. Ricketts, Extracellular glutathione is a source of cysteine for cells that express gamma-glutamyl transpeptidase, Biochemistry 32 (1993) 6302–6306. https://doi.org/10.1021/bi00075a026.
[201] P.V.S. Oliveira, F.R.M. Laurindo, Implications of plasma thiol redox in disease, Clin. Sci. 132 (2018) 1257–1280. https://doi.org/10.1042/CS20180157.
[202] R.A. Blanco, T.R. Ziegler, B.A. Carlson, P.-Y. Cheng, Y. Park, G.A. Cotsonis, C.J. Accardi, D.P. Jones, Diurnal variation in glutathione and cysteine redox states in human plasma2, Am. J. Clin. Nutr. 86 (2007) 1016–1023. https://doi.org/10.1093/ajcn/86.4.1016.
[203] W.A. Al-Turk, S.J. Stohs, F.H. El-Rashidy, S. Othman, Changes in glutathione and its metabolizing enzymes in human erythrocytes and lymphocytes with age, J. Pharm. Pharmacol. 39 (1987) 13–16. https://doi.org/10.1111/j.2042-7158.1987.tb07154.x.
[204] P.S. Samiec, C. Drews-Botsch, E.W. Flagg, J.C. Kurtz, P. Sternberg, R.L. Reed, D.P. Jones, Glutathione in Human Plasma: Decline in Association with Aging, Age-Related Macular Degeneration, and Diabetes, Free Radic. Biol. Med. 24 (1998) 699–704. https://doi.org/10.1016/S0891-5849(97)00286-4.

[205] A.D. Dam, A.S. Mitchell, J.W.E. Rush, J. Quadrilatero, Elevated skeletal muscle apoptotic signaling following glutathione depletion, Apoptosis 17 (2012) 48–60. https://doi.org/10.1007/s10495-011-0654-5.
[206] I. Sinha-Hikim, A.P. Sinha-Hikim, M. Parveen, R. Shen, R. Goswami, P. Tran, A. Crum, K.C. Norris, Long-Term Supplementation With a Cystine-Based Antioxidant Delays Loss of Muscle Mass in Aging, J. Gerontol. Ser. A 68 (2013) 749–759. https://doi.org/10.1093/gerona/gls334.
[207] R.V. Sekhar, S.G. Patel, A.P. Guthikonda, M. Reid, A. Balasubramanyam, G.E. Taffet, F. Jahoor, Deficient synthesis of glutathione underlies oxidative stress in aging and can be corrected by dietary cysteine and glycine supplementation1234, Am. J. Clin. Nutr. 94 (2011) 847–853. https://doi.org/10.3945/ajcn.110.003483.
[208] A. Karelis, V. Messier, C. Suppère, P. Briand, R. Rabasa-Lhoret, Effect of cysteine-rich whey protein (Immunocal®) supplementation in combination with resistance training on muscle strength and lean body mass in non-frail elderly subjects: A randomized, double-blind controlled study, J. Nutr. Health Aging 19 (2015) 531–536. https://doi.org/10.1007/s12603-015-0442-y.
[209] E. Mosharov, M.R. Cranford, R. Banerjee, The Quantitatively Important Relationship between Homocysteine Metabolism and Glutathione Synthesis by the Transsulfuration Pathway and Its Regulation by Redox Changes, Biochemistry 39 (2000) 13005–13011. https://doi.org/10.1021/bi001088w.
[210] B.D. Paul, J.I. Sbodio, S.H. Snyder, Cysteine metabolism in neuronal redox homeostasis, Trends Pharmacol. Sci. 39 (2018) 513–524. https://doi.org/10.1016/j.tips.2018.02.007.
[211] J. Zhu, M. Berisa, S. Schwörer, W. Qin, J.R. Cross, C.B. Thompson, Transsulfuration Activity Can Support Cell Growth upon Extracellular Cysteine Limitation, Cell Metab. 30 (2019) 865-876.e5. https://doi.org/10.1016/j.cmet.2019.09.009.
[212] S. Pan, M. Fan, Z. Liu, X. Li, H. Wang, Serine, glycine and one-carbon metabolism in cancer (Review), Int. J. Oncol. 58 (2020) 158–170. https://doi.org/10.3892/ijo.2020.5158.
[213] O. Kabil, R. Banerjee, Enzymology of H2S Biogenesis, Decay and Signaling, Antioxid. Redox Signal. 20 (2014) 770–782. https://doi.org/10.1089/ars.2013.5339.
[214] N. Nagahara, T. Ito, H. Kitamura, T. Nishino, Tissue and subcellular distribution of mercaptopyruvate sulfurtransferase in the rat: confocal laser fluorescence and immunoelectron microscopic studies combined with biochemical analysis, Histochem. Cell Biol. 110 (1998) 243–250. https://doi.org/10.1007/s004180050286.
[215] K. Kaziród, M. Myszka, J. Dulak, A. Łoboda, Hydrogen sulfide as a therapeutic option for the treatment of Duchenne muscular dystrophy and other muscle-related diseases, Cell. Mol. Life Sci. 79 (2022) 608. https://doi.org/10.1007/s00018-022-04636-0.
[216] M. Myszka, O. Mucha, P. Podkalicka, U. Waśniowska, J. Dulak, A. Łoboda, Sodium hydrosulfide moderately alleviates the hallmark symptoms of Duchenne muscular dystrophy in *mdx* mice, Eur. J. Pharmacol. 955 (2023) 175928. https://doi.org/10.1016/j.ejphar.2023.175928.
[217] W. Bjørn-Yoshimoto, S.M. Underhill, The Importance of the Excitatory Amino Acid Transporter 3 (EAAT3), Neurochem. Int. 98 (2016) 4–18. https://doi.org/10.1016/j.neuint.2016.05.007.
[218] A.J. Scopelliti, R.M. Ryan, R.J. Vandenberg, Molecular Determinants for Functional Differences between Alanine-Serine-Cysteine Transporter 1 and Other Glutamate Transporter Family Members*, J. Biol. Chem. 288 (2013) 8250–8257. https://doi.org/10.1074/jbc.M112.441022.
[219] J. Lewerenz, S.J. Hewett, Y. Huang, M. Lambros, P.W. Gout, P.W. Kalivas, A. Massie, I. Smolders, A. Methner, M. Pergande, S.B. Smith, V. Ganapathy, P. Maher, The Cystine/Glutamate Antiporter System xc− in Health and Disease: From Molecular Mechanisms to Novel Therapeutic

Opportunities, Antioxid. Redox Signal. 18 (2013) 522–555. https://doi.org/10.1089/ars.2011.4391.
[220] S. Bannai, E. Kitamura, Transport interaction of L-cystine and L-glutamate in human diploid fibroblasts in culture., J. Biol. Chem. 255 (1980) 2372–2376. https://doi.org/10.1016/S0021-9258(19)85901-X.
[221] S. Bannai, Exchange of cystine and glutamate across plasma membrane of human fibroblasts., J. Biol. Chem. 261 (1986) 2256–2263. https://doi.org/10.1016/S0021-9258(17)35926-4.
[222] M. Makowske, H.N. Christensen, Contrasts in transport systems for anionic amino acids in hepatocytes and a hepatoma cell line HTC., J. Biol. Chem. 257 (1982) 5663–5670. https://doi.org/10.1016/S0021-9258(19)83829-2.
[223] S.A. Patel, B.A. Warren, J.F. Rhoderick, R.J. Bridges, Differentiation of substrate and non-substrate inhibitors of transport system *x*c−: an obligate exchanger of L-glutamate and L-cystine, Neuropharmacology 46 (2004) 273–284. https://doi.org/10.1016/j.neuropharm.2003.08.006.
[224] N. Jyotsana, K.T. Ta, K.E. DelGiorno, The Role of Cystine/Glutamate Antiporter SLC7A11/xCT in the Pathophysiology of Cancer, Front. Oncol. 12 (2022) 858462. https://doi.org/10.3389/fonc.2022.858462.
[225] H. Sato, M. Tamba, T. Ishii, S. Bannai, Cloning and Expression of a Plasma Membrane Cystine/Glutamate Exchange Transporter Composed of Two Distinct Proteins *, J. Biol. Chem. 274 (1999) 11455–11458. https://doi.org/10.1074/jbc.274.17.11455.
[226] F. Verrey, E.I. Closs, C.A. Wagner, M. Palacin, H. Endou, Y. Kanai, CATs and HATs: the SLC7 family of amino acid transporters, Pflüg. Arch. 447 (2004) 532–542. https://doi.org/10.1007/s00424-003-1086-z.
[227] E. Gasol, M. Jiménez-Vidal, J. Chillarón, A. Zorzano, M. Palacín, Membrane Topology of System Xc- Light Subunit Reveals a Re-entrant Loop with Substrate-restricted Accessibility *, J. Biol. Chem. 279 (2004) 31228–31236. https://doi.org/10.1074/jbc.M402428200.
[228] M. Bassi, E. Gasol, M. Manzoni, M. Pineda, M. Riboni, R. Martín, A. Zorzano, G. Borsani, M. Palacín, Identification and characterisation of human xCT that co-expresses, with 4F2 heavy chain, the amino acid transport activity system xc–, Pflüg. Arch. 442 (2001) 286–296. https://doi.org/10.1007/s004240100537.
[229] S. Chintala, W. Li, M.L. Lamoreux, S. Ito, K. Wakamatsu, E.V. Sviderskaya, D.C. Bennett, Y.-M. Park, W.A. Gahl, M. Huizing, R.A. Spritz, S. Ben, E.K. Novak, J. Tan, R.T. Swank, Slc7a11 gene controls production of pheomelanin pigment and proliferation of cultured cells, Proc. Natl. Acad. Sci. U. S. A. 102 (2005) 10964–10969. https://doi.org/10.1073/pnas.0502856102.
[230] M. Huizing, Y. Anikster, J.G. White, W.A. Gahl, Characterization of the Murine Gene Corresponding to Human Hermansky-Pudlak Syndrome Type 3: Exclusion of the *Subtle Gray* (*sut*) Locus, Mol. Genet. Metab. 74 (2001) 217–225. https://doi.org/10.1006/mgme.2001.3233.
[231] A. Takada, S. Bannai, Transport of cystine in isolated rat hepatocytes in primary culture., J. Biol. Chem. 259 (1984) 2441–2445. https://doi.org/10.1016/S0021-9258(17)43372-2.
[232] S. Bannai, H. Sato, T. Ishii, Y. Sugita, Induction of cystine transport activity in human fibroblasts by oxygen*, J. Biol. Chem. 264 (1989) 18480–18484. https://doi.org/10.1016/S0021-9258(18)51491-5.
[233] Y. Sakakura, H. Sato, A. Shiiya, M. Tamba, J. Sagara, M. Matsuda, N. Okamura, N. Makino, S. Bannai, Expression and function of cystine/glutamate transporter in neutrophils, J. Leukoc. Biol. 81 (2007) 974–982. https://doi.org/10.1189/jlb.0606385.
[234] T. Ishii, K. Itoh, S. Takahashi, H. Sato, T. Yanagawa, Y. Katoh, S. Bannai, M. Yamamoto, Transcription Factor Nrf2 Coordinately Regulates a Group of Oxidative Stress-inducible Genes

in Macrophages*, J. Biol. Chem. 275 (2000) 16023–16029. https://doi.org/10.1074/jbc.275.21.16023.
[235] H. Sato, S. Nomura, K. Maebara, K. Sato, M. Tamba, S. Bannai, Transcriptional control of cystine/glutamate transporter gene by amino acid deprivation, Biochem. Biophys. Res. Commun. 325 (2004) 109–116. https://doi.org/10.1016/j.bbrc.2004.10.009.
[236] H. Sato, K. Fujiwara, J. Sagara, S. Bannai, Induction of cystine transport activity in mouse peritoneal macrophages by bacterial lipopolysaccharide, Biochem. J. 310 (1995) 547–551. https://doi.org/10.1042/bj3100547.
[237] A.Y. Shih, T.H. Murphy, xCT Cystine Transporter Expression in HEK293 Cells: Pharmacology and Localization, Biochem. Biophys. Res. Commun. 282 (2001) 1132–1137. https://doi.org/10.1006/bbrc.2001.4703.
[238] H. Wang, M. Tamba, M. Kimata, K. Sakamoto, S. Bannai, H. Sato, Expression of the activity of cystine/glutamate exchange transporter, system xc−, by xCT and rBAT, Biochem. Biophys. Res. Commun. 305 (2003) 611–618. https://doi.org/10.1016/S0006-291X(03)00808-8.
[239] H. Sasaki, H. Sato, K. Kuriyama-Matsumura, K. Sato, K. Maebara, H. Wang, M. Tamba, K. Itoh, M. Yamamoto, S. Bannai, Electrophile Response Element-mediated Induction of the Cystine/Glutamate Exchange Transporter Gene Expression *, J. Biol. Chem. 277 (2002) 44765–44771. https://doi.org/10.1074/jbc.M208704200.
[240] K. Taguchi, H. Motohashi, M. Yamamoto, Molecular mechanisms of the Keap1–Nrf2 pathway in stress response and cancer evolution, Genes Cells 16 (2011) 123–140. https://doi.org/10.1111/j.1365-2443.2010.01473.x.
[241] K. Ameri, A.L. Harris, Activating transcription factor 4, Int. J. Biochem. Cell Biol. 40 (2008) 14–21. https://doi.org/10.1016/j.biocel.2007.01.020.
[242] M.A. Iqbal, M. Bilen, Y. Liu, V. Jabre, B.C. Fong, I. Chakroun, S. Paul, J. Chen, S. Wade, M. Kanaan, M.-E. Harper, M. Khacho, R.S. Slack, The integrated stress response promotes neural stem cell survival under conditions of mitochondrial dysfunction in neurodegeneration, Aging Cell 23 (2024) e14165. https://doi.org/10.1111/acel.14165.
[243] S. Liu, S. Liu, H. Jiang, Multifaceted roles of mitochondrial stress responses under ETC dysfunction – repair, destruction and pathogenesis, FEBS J. 289 (2022) 6994–7013. https://doi.org/10.1111/febs.16323.
[244] N.A. Khan, J. Nikkanen, S. Yatsuga, C. Jackson, L. Wang, S. Pradhan, R. Kivelä, A. Pessia, V. Velagapudi, A. Suomalainen, mTORC1 Regulates Mitochondrial Integrated Stress Response and Mitochondrial Myopathy Progression, Cell Metab. 26 (2017) 419-428.e5. https://doi.org/10.1016/j.cmet.2017.07.007.
[245] H.P. Harding, I. Novoa, Y. Zhang, H. Zeng, R. Wek, M. Schapira, D. Ron, Regulated Translation Initiation Controls Stress-Induced Gene Expression in Mammalian Cells, Mol. Cell 6 (2000) 1099–1108. https://doi.org/10.1016/S1097-2765(00)00108-8.
[246] D. Zhou, L.R. Palam, L. Jiang, J. Narasimhan, K.A. Staschke, R.C. Wek, Phosphorylation of eIF2 Directs ATF5 Translational Control in Response to Diverse Stress Conditions *, J. Biol. Chem. 283 (2008) 7064–7073. https://doi.org/10.1074/jbc.M708530200.
[247] M. Costa-Mattioli, P. Walter, The integrated stress response: From mechanism to disease, Science 368 (2020) eaat5314. https://doi.org/10.1126/science.aat5314.
[248] G. Sturm, K.R. Karan, A.S. Monzel, B. Santhanam, T. Taivassalo, C. Bris, S.A. Ware, M. Cross, A. Towheed, A. Higgins-Chen, M.J. McManus, A. Cardenas, J. Lin, E.S. Epel, S. Rahman, J. Vissing, B. Grassi, M. Levine, S. Horvath, R.G. Haller, G. Lenaers, D.C. Wallace, M.-P. St-Onge, S. Tavazoie, V. Procaccio, B.A. Kaufman, E.L. Seifert, M. Hirano, M. Picard, OxPhos defects

cause hypermetabolism and reduce lifespan in cells and in patients with mitochondrial diseases, Commun. Biol. 6 (2023) 1–22. https://doi.org/10.1038/s42003-022-04303-x.
[249] X.-X. Liu, X.-J. Li, B. Zhang, Y.-J. Liang, C.-X. Zhou, D.-X. Cao, M. He, G.-Q. Chen, J.-R. He, Q. Zhao, MicroRNA-26b is underexpressed in human breast cancer and induces cell apoptosis by targeting SLC7A11, FEBS Lett. 585 (2011) 1363–1367. https://doi.org/10.1016/j.febslet.2011.04.018.
[250] R.M. Drayton, E. Dudziec, S. Peter, S. Bertz, A. Hartmann, H.E. Bryant, J.WF. Catto, Reduced Expression of miRNA-27a Modulates Cisplatin Resistance in Bladder Cancer by Targeting the Cystine/Glutamate Exchanger SLC7A11, Clin. Cancer Res. 20 (2014) 1990–2000. https://doi.org/10.1158/1078-0432.CCR-13-2805.
[251] Y. Wu, X. Sun, B. Song, X. Qiu, J. Zhao, MiR-375/SLC7A11 axis regulates oral squamous cell carcinoma proliferation and invasion, Cancer Med. 6 (2017) 1686–1697. https://doi.org/10.1002/cam4.1110.
[252] J.C. Scheuermann, A.G. de Ayala Alonso, K. Oktaba, N. Ly-Hartig, R.K. McGinty, S. Fraterman, M. Wilm, T.W. Muir, J. Müller, Histone H2A deubiquitinase activity of the Polycomb repressive complex PR-DUB, Nature 465 (2010) 243–247. https://doi.org/10.1038/nature08966.
[253] M. Carbone, H. Yang, H.I. Pass, T. Krausz, J.R. Testa, G. Gaudino, BAP1 and cancer, Nat. Rev. Cancer 13 (2013) 153–159. https://doi.org/10.1038/nrc3459.
[254] CD44 Variant Regulates Redox Status in Cancer Cells by Stabilizing the xCT Subunit of System xc− and Thereby Promotes Tumor Growth: Cancer Cell, (n.d.). https://www.cell.com/cancer-cell/fulltext/S1535-6108(11)00050-X (accessed April 28, 2025).
[255] K. Tsuchihashi, S. Okazaki, M. Ohmura, M. Ishikawa, O. Sampetrean, N. Onishi, H. Wakimoto, M. Yoshikawa, R. Seishima, Y. Iwasaki, T. Morikawa, S. Abe, A. Takao, M. Shimizu, T. Masuko, M. Nagane, F.B. Furnari, T. Akiyama, M. Suematsu, E. Baba, K. Akashi, H. Saya, O. Nagano, The EGF Receptor Promotes the Malignant Potential of Glioma by Regulating Amino Acid Transport System xc(—), Cancer Res. 76 (2016) 2954–2963. https://doi.org/10.1158/0008-5472.CAN-15-2121.
[256] Y. Gu, C.P. Albuquerque, D. Braas, W. Zhang, G.R. Villa, J. Bi, S. Ikegami, K. Masui, B. Gini, H. Yang, T.C. Gahman, A.K. Shiau, T.F. Cloughesy, H.R. Christofk, H. Zhou, K.-L. Guan, P.S. Mischel, mTORC2 Regulates Amino Acid Metabolism in Cancer by Phosphorylation of the Cystine-Glutamate Antiporter xCT, Mol. Cell 67 (2017) 128-138.e7. https://doi.org/10.1016/j.molcel.2017.05.030.
[257] J. Zhang, I. Khvorostov, J.S. Hong, Y. Oktay, L. Vergnes, E. Nuebel, P.N. Wahjudi, K. Setoguchi, G. Wang, A. Do, H. Jung, J.M. McCaffery, I.J. Kurland, K. Reue, W.P. Lee, C.M. Koehler, M.A. Teitell, UCP2 regulates energy metabolism and differentiation potential of human pluripotent stem cells, EMBO J. 30 (2011) 4860–4873. https://doi.org/10.1038/emboj.2011.401.
[258] R. Wang, C.P. Dillon, L.Z. Shi, S. Milasta, R. Carter, D. Finkelstein, L.L. McCormick, P. Fitzgerald, H. Chi, J. Munger, D.R. Green, The Transcription Factor Myc Controls Metabolic Reprogramming upon T Lymphocyte Activation, Immunity 35 (2011) 871–882. https://doi.org/10.1016/j.immuni.2011.09.021.
[259] J. Zhang, E. Nuebel, G.Q. Daley, C.M. Koehler, M.A. Teitell, Metabolic Regulation in Pluripotent Stem Cells during Reprogramming and Self-Renewal, Cell Stem Cell 11 (2012) 589–595. https://doi.org/10.1016/j.stem.2012.10.005.
[260] A. Le, A.N. Lane, M. Hamaker, S. Bose, A. Gouw, J. Barbi, T. Tsukamoto, C.J. Rojas, B.S. Slusher, H. Zhang, L.J. Zimmerman, D.C. Liebler, R.J.C. Slebos, P.K. Lorkiewicz, R.M. Higashi, T.W.M. Fan, C.V. Dang, Glucose-Independent Glutamine Metabolism via TCA Cycling for

Proliferation and Survival in B Cells, Cell Metab. 15 (2012) 110–121. https://doi.org/10.1016/j.cmet.2011.12.009.
[261] M. Latil, P. Rocheteau, L. Châtre, S. Sanulli, S. Mémet, M. Ricchetti, S. Tajbakhsh, F. Chrétien, Skeletal muscle stem cells adopt a dormant cell state post mortem and retain regenerative capacity, Nat. Commun. 3 (2012) 903. https://doi.org/10.1038/ncomms1890.
[262] L. Machado, J.E. de Lima, O. Fabre, C. Proux, R. Legendre, A. Szegedi, H. Varet, L.R. Ingerslev, R. Barrès, F. Relaix, P. Mourikis, In Situ Fixation Redefines Quiescence and Early Activation of Skeletal Muscle Stem Cells, Cell Rep. 21 (2017) 1982–1993. https://doi.org/10.1016/j.celrep.2017.10.080.
[263] J.G. Ryall, S. Dell'Orso, A. Derfoul, A. Juan, H. Zare, X. Feng, D. Clermont, M. Koulnis, G. Gutierrez-Cruz, M. Fulco, V. Sartorelli, The NAD+-Dependent SIRT1 Deacetylase Translates a Metabolic Switch into Regulatory Epigenetics in Skeletal Muscle Stem Cells, Cell Stem Cell 16 (2015) 171–183. https://doi.org/10.1016/j.stem.2014.12.004.
[264] Distinct metabolic states govern skeletal muscle stem cell fates during prenatal and postnatal myogenesis | Journal of Cell Science | The Company of Biologists, (n.d.). https://journals.biologists.com/jcs/article/131/14/jcs212977/56828/Distinct-metabolic-states-govern-skeletal-muscle (accessed April 1, 2025).
[265] M. Cerletti, Y.C. Jang, L.W.S. Finley, M.C. Haigis, A.J. Wagers, Short-Term Calorie Restriction Enhances Skeletal Muscle Stem Cell Function, Cell Stem Cell 10 (2012) 515–519. https://doi.org/10.1016/j.stem.2012.04.002.
[266] H. Zhang, D. Ryu, Y. Wu, K. Gariani, X. Wang, P. Luan, D. D'Amico, E.R. Ropelle, M.P. Lutolf, R. Aebersold, K. Schoonjans, K.J. Menzies, J. Auwerx, NAD+ repletion improves mitochondrial and stem cell function and enhances life span in mice, Science 352 (2016) 1436–1443. https://doi.org/10.1126/science.aaf2693.
[267] K.E. Wellen, G. Hatzivassiliou, U.M. Sachdeva, T.V. Bui, J.R. Cross, C.B. Thompson, ATP-Citrate Lyase Links Cellular Metabolism to Histone Acetylation, Science 324 (2009) 1076–1080. https://doi.org/10.1126/science.1164097.
[268] N. Shyh-Chang, H.-H. Ng, The metabolic programming of stem cells, Genes Dev. 31 (2017) 336–346. https://doi.org/10.1101/gad.293167.116.
[269] A. L'honoré, P.-H. Commère, E. Negroni, G. Pallafacchina, B. Friguet, J. Drouin, M. Buckingham, D. Montarras, The role of Pitx2 and Pitx3 in muscle stem cells gives new insights into P38α MAP kinase and redox regulation of muscle regeneration, eLife 7 (n.d.) e32991. https://doi.org/10.7554/eLife.32991.
[270] M. Theret, L. Gsaier, B. Schaffer, G. Juban, S. Ben Larbi, M. Weiss-Gayet, L. Bultot, C. Collodet, M. Foretz, D. Desplanches, P. Sanz, Z. Zang, L. Yang, G. Vial, B. Viollet, K. Sakamoto, A. Brunet, B. Chazaud, R. Mounier, AMPKα1-LDH pathway regulates muscle stem cell self-renewal by controlling metabolic homeostasis, EMBO J. 36 (2017) 1946–1962. https://doi.org/10.15252/embj.201695273.
[271] M.G. Vander Heiden, L.C. Cantley, C.B. Thompson, Understanding the Warburg Effect: The Metabolic Requirements of Cell Proliferation, Science 324 (2009) 1029–1033. https://doi.org/10.1126/science.1160809.
[272] A. L'honoré, P.-H. Commère, J.-F. Ouimette, D. Montarras, J. Drouin, M. Buckingham, Redox Regulation by Pitx2 and Pitx3 Is Critical for Fetal Myogenesis, Dev. Cell 29 (2014) 392–405. https://doi.org/10.1016/j.devcel.2014.04.006.
[273] R. Buono, C. Vantaggiato, V. Pisa, E. Azzoni, M.T. Bassi, S. Brunelli, C. Sciorati, E. Clementi, Nitric Oxide Sustains Long-Term Skeletal Muscle Regeneration by Regulating Fate of Satellite

Cells Via Signaling Pathways Requiring Vangl2 and Cyclic GMP, Stem Cells 30 (2012) 197–209. https://doi.org/10.1002/stem.783.
[274] F.L. Grand, A.E. Jones, V. Seale, A. Scimè, M.A. Rudnicki, Wnt7a Activates the Planar Cell Polarity Pathway to Drive the Symmetric Expansion of Satellite Stem Cells, Cell Stem Cell 4 (2009) 535–547. https://doi.org/10.1016/j.stem.2009.03.013.
[275] S. Luo, C. Zhang, B. Zhang, C. Kim, Y. Qiu, Q. Du, L. Mei, W. Xiong, Regulation of heterochromatin remodelling and myogenin expression during muscle differentiation by FAK interaction with MBD2, EMBO J. 28 (2009) 2568–2582. https://doi.org/10.1038/emboj.2009.178.
[276] I.M. Conboy, T.A. Rando, The Regulation of Notch Signaling Controls Satellite Cell Activation and Cell Fate Determination in Postnatal Myogenesis, Dev. Cell 3 (2002) 397–409. https://doi.org/10.1016/S1534-5807(02)00254-X.
[277] N. Coant, Ben Mkaddem ,Sanae, Pedruzzi ,Eric, Guichard ,Cécile, Tréton ,Xavier, Ducroc ,Robert, Freund ,Jean-Noel, Cazals-Hatem ,Dominique, Bouhnik ,Yoram, Woerther ,Paul-Louis, Skurnik ,David, Grodet ,Alain, Fay ,Michèle, Biard ,Denis, Lesuffleur ,Thécla, Deffert ,Christine, Moreau ,Richard, Groyer ,André, Krause ,Karl-Heinz, Daniel ,Fanny, E. and Ogier-Denis, NADPH Oxidase 1 Modulates WNT and NOTCH1 Signaling To Control the Fate of Proliferative Progenitor Cells in the Colon, Mol. Cell. Biol. 30 (2010) 2636–2650. https://doi.org/10.1128/MCB.01194-09.
[278] Y. Funato, T. Michiue, M. Asashima, H. Miki, The thioredoxin-related redox-regulating protein nucleoredoxin inhibits Wnt–β-catenin signalling through Dishevelled, Nat. Cell Biol. 8 (2006) 501–508. https://doi.org/10.1038/ncb1405.
[279] A. Kipp, A. Banning, E.M. van Schothorst, C. Méplan, L. Schomburg, C. Evelo, S. Coort, S. Gaj, J. Keijer, J. Hesketh, R. Brigelius-Flohé, Four selenoproteins, protein biosynthesis, and Wnt signalling are particularly sensitive to limited selenium intake in mouse colon, Mol. Nutr. Food Res. 53 (2009) 1561–1572. https://doi.org/10.1002/mnfr.200900105.
[280] Y. Liu, A. He, J. Tang, A.M. Shah, G. Jia, G. Liu, G. Tian, X. Chen, J. Cai, B. Kang, H. Zhao, Selenium alleviates the negative effect of heat stress on myogenic differentiation of C2C12 cells with the response of selenogenome, J. Therm. Biol. 97 (2021) 102874. https://doi.org/10.1016/j.jtherbio.2021.102874.
[281] G. Pallafacchina, S. François, B. Regnault, B. Czarny, V. Dive, A. Cumano, D. Montarras, M. Buckingham, An adult tissue-specific stem cell in its niche: A gene profiling analysis of *in vivo* quiescent and activated muscle satellite cells, Stem Cell Res. 4 (2010) 77–91. https://doi.org/10.1016/j.scr.2009.10.003.
[282] R.H. Burdon, Superoxide and hydrogen peroxide in relation to mammalian cell proliferation, Free Radic. Biol. Med. 18 (1995) 775–794. https://doi.org/10.1016/0891-5849(94)00198-S.
[283] M. Mofarrahi, R.P. Brandes, A. Gorlach, J. Hanze, L.S. Terada, M.T. Quinn, D. Mayaki, B. Petrof, S.N.A. Hussain, Regulation of Proliferation of Skeletal Muscle Precursor Cells By NADPH Oxidase, Antioxid. Redox Signal. 10 (2008) 559–574. https://doi.org/10.1089/ars.2007.1792.
[284] K. Ohashi, Y. Nagata, E. Wada, P.S. Zammit, M. Shiozuka, R. Matsuda, Zinc promotes proliferation and activation of myogenic cells via the PI3K/Akt and ERK signaling cascade, Exp. Cell Res. 333 (2015) 228–237. https://doi.org/10.1016/j.yexcr.2015.03.003.
[285] S. Lee, H.S. Shin, P.K. Shireman, A. Vasilaki, H. Van Remmen, M.E. Csete, Glutathione-peroxidase-1 null muscle progenitor cells are globally defective, Free Radic. Biol. Med. 41 (2006) 1174–1184. https://doi.org/10.1016/j.freeradbiomed.2006.07.005.
[286] Altered in vitro Proliferation of Mouse SOD1-G93A Skeletal Muscle Satellite Cells | Neurodegenerative Diseases | Karger Publishers, (n.d.). https://karger.com/ndd/article-

abstract/11/3/153/205435/Altered-in-vitro-Proliferation-of-Mouse-SOD1-G93A?redirectedFrom=fulltext (accessed April 1, 2025).
[287] S.D. Sandiford, K.A. Kennedy, X. Xie, J.G. Pickering, S.S. Li, Dual Oxidase Maturation factor 1 (DUOXA1) overexpression increases reactive oxygen species production and inhibits murine muscle satellite cell differentiation, Cell Commun. Signal. 12 (2014) 5. https://doi.org/10.1186/1478-811X-12-5.
[288] M. Vezzoli, P. Castellani, G. Corna, A. Castiglioni, L. Bosurgi, A. Monno, S. Brunelli, A.A. Manfredi, A. Rubartelli, P. Rovere-Querini, High-Mobility Group Box 1 Release and Redox Regulation Accompany Regeneration and Remodeling of Skeletal Muscle, Antioxid. Redox Signal. 15 (2011) 2161–2174. https://doi.org/10.1089/ars.2010.3341.
[289] A. Montesano, L. Luzi, P. Senesi, N. Mazzocchi, I. Terruzzi, Resveratrol promotes myogenesis and hypertrophy in murine myoblasts, J. Transl. Med. 11 (2013) 310. https://doi.org/10.1186/1479-5876-11-310.
[290] Y.J. Piao, Y.H. Seo, F. Hong, J.H. Kim, Y.-J. Kim, M.H. Kang, B.S. Kim, S.A. Jo, I. Jo, D.-M. Jue, I. Kang, J. Ha, S.S. Kim, Nox 2 stimulates muscle differentiation via NF-κB/iNOS pathway, Free Radic. Biol. Med. 38 (2005) 989–1001. https://doi.org/10.1016/j.freeradbiomed.2004.11.011.
[291] S.B. Shelar, M. Narasimhan, G. Shanmugam, S.H. Litovsky, S.S. Gounder, G. Karan, C. Arulvasu, T.W. Kensler, J.R. Hoidal, V.M. Darley-Usmar, N.S. Rajasekaran, Disruption of nuclear factor (erythroid-derived-2)–like 2 antioxidant signaling: a mechanism for impaired activation of stem cells and delayed regeneration of skeletal muscle, FASEB J. 30 (2016) 1865–1879. https://doi.org/10.1096/fj.201500153.
[292] S. Lim, J.Y. Shin, A. Jo, J. K.r, M.N. Nguyen, T.G. Choi, J. Kim, J.-H. Park, Y.G. Eun, K.-S. Yoon, J. Ha, S.S. Kim, Carbonyl reductase 1 is an essential regulator of skeletal muscle differentiation and regeneration, Int. J. Biochem. Cell Biol. 45 (2013) 1784–1793. https://doi.org/10.1016/j.biocel.2013.05.025.
[293] G. Zaccagnini, F. Martelli, A. Magenta, C. Cencioni, P. Fasanaro, C. Nicoletti, P. Biglioli, P.G. Pelicci, M.C. Capogrossi, p66ShcA and Oxidative Stress Modulate Myogenic Differentiation and Skeletal Muscle Regeneration after Hind Limb Ischemia *, J. Biol. Chem. 282 (2007) 31453–31459. https://doi.org/10.1074/jbc.M702511200.
[294] Mitochondrial H2O2 generated from electron transport chain complex I stimulates muscle differentiation | Cell Research, (n.d.). https://www.nature.com/articles/cr201155 (accessed April 1, 2025).
[295] E.P. Hoffman, R.H. Brown, L.M. Kunkel, Dystrophin: The protein product of the duchenne muscular dystrophy locus, Cell 51 (1987) 919–928. https://doi.org/10.1016/0092-8674(87)90579-4.
[296] D.G. Allen, N.P. Whitehead, S.C. Froehner, Absence of Dystrophin Disrupts Skeletal Muscle Signaling: Roles of Ca2+, Reactive Oxygen Species, and Nitric Oxide in the Development of Muscular Dystrophy, Physiol. Rev. 96 (2016) 253–305. https://doi.org/10.1152/physrev.00007.2015.
[297] C.A. Bellissimo, M.C. Garibotti, C.G.R. Perry, Mitochondrial stress responses in Duchenne muscular dystrophy: metabolic dysfunction or adaptive reprogramming?, Am. J. Physiol.-Cell Physiol. 323 (2022) C718–C730. https://doi.org/10.1152/ajpcell.00249.2022.
[298] G. Bulfield, W.G. Siller, P.A. Wight, K.J. Moore, X chromosome-linked muscular dystrophy (mdx) in the mouse., Proc. Natl. Acad. Sci. 81 (1984) 1189–1192. https://doi.org/10.1073/pnas.81.4.1189.

[299] T.A. Rando, M.-H. Disatnik, Y. Yu, A. Franco, Muscle cells from *mdx* mice have an increased susceptibility to oxidative stress, Neuromuscul. Disord. 8 (1998) 14–21. https://doi.org/10.1016/S0960-8966(97)00124-7.
[300] Bmi1 enhances skeletal muscle regeneration through MT1-mediated oxidative stress protection in a mouse model of dystrophinopathy | Journal of Experimental Medicine | Rockefeller University Press, (n.d.). https://rupress.org/jem/article/211/13/2617/41462/Bmi1-enhances-skeletal-muscle-regeneration-through (accessed April 1, 2025).
[301] Isobaric Tagging-Based Quantification for Proteomic Analysis: A Comparative Study of Spared and Affected Muscles from mdx Mice at the Early Phase of Dystrophy | PLOS One, (n.d.). https://journals.plos.org/plosone/article?id=10.1371/journal.pone.0065831 (accessed April 1, 2025).
[302] N.P. Whitehead, C. Pham, O.L. Gervasio, D.G. Allen, N-Acetylcysteine ameliorates skeletal muscle pathophysiology in mdx mice, J. Physiol. 586 (2008) 2003–2014. https://doi.org/10.1113/jphysiol.2007.148338.
[303] M. Segatto, R. Szokoll, R. Fittipaldi, C. Bottino, L. Nevi, K. Mamchaoui, P. Filippakopoulos, G. Caretti, BETs inhibition attenuates oxidative stress and preserves muscle integrity in Duchenne muscular dystrophy, Nat. Commun. 11 (2020) 6108. https://doi.org/10.1038/s41467-020-19839-x.
[304] R. Renjini, N. Gayathri, A. Nalini, M.M. Srinivas Bharath, Oxidative Damage in Muscular Dystrophy Correlates with the Severity of the Pathology: Role of Glutathione Metabolism, Neurochem. Res. 37 (2012) 885–898. https://doi.org/10.1007/s11064-011-0683-z.
[305] L.Z.-H. Zhou, A.P. Johnson, T.A. Rando, NFκB and AP-1 mediate transcriptional responses to oxidative stress in skeletal muscle cells, Free Radic. Biol. Med. 31 (2001) 1405–1416. https://doi.org/10.1016/S0891-5849(01)00719-5.
[306] A. Michelucci, C. Liang, F. Protasi, R.T. Dirksen, Altered Ca2+ Handling and Oxidative Stress Underlie Mitochondrial Damage and Skeletal Muscle Dysfunction in Aging and Disease, Metabolites 11 (2021) 424. https://doi.org/10.3390/metabo11070424.
[307] R.A. DeFronzo, E. Jacot, E. Jequier, E. Maeder, J. Wahren, J.P. Felber, The Effect of Insulin on the Disposal of Intravenous Glucose: Results from Indirect Calorimetry and Hepatic and Femoral Venous Catheterization, Diabetes 30 (1981) 1000–1007. https://doi.org/10.2337/diab.30.12.1000.
[308] R.A. DeFronzo, D. Tripathy, Skeletal Muscle Insulin Resistance Is the Primary Defect in Type 2 Diabetes, Diabetes Care 32 (2009) S157–S163. https://doi.org/10.2337/dc09-S302.
[309] M. Brownlee, Biochemistry and molecular cell biology of diabetic complications, Nature 414 (2001) 813–820. https://doi.org/10.1038/414813a.
[310] N. Houstis, E.D. Rosen, E.S. Lander, Reactive oxygen species have a causal role in multiple forms of insulin resistance, Nature 440 (2006) 944–948. https://doi.org/10.1038/nature04634.
[311] C. Bonnard, A. Durand, S. Peyrol, E. Chanseaume, M.-A. Chauvin, B. Morio, H. Vidal, J. Rieusset, Mitochondrial dysfunction results from oxidative stress in the skeletal muscle of diet-induced insulin-resistant mice, J. Clin. Invest. 118 (2008) 789–800. https://doi.org/10.1172/JCI32601.
[312] J. Szendroedi, A.I. Schmid, M. Meyerspeer, C. Cervin, M. Kacerovsky, G. Smekal, S. Gräser-Lang, L. Groop, M. Roden, Impaired Mitochondrial Function and Insulin Resistance of Skeletal Muscle in Mitochondrial Diabetes, Diabetes Care 32 (2009) 677–679. https://doi.org/10.2337/dc08-2078.
[313] C.K. Maurya, D. Arha, A.K. Rai, S. Kant Kumar, J. Pandey, D.R. Avisetti, S.V. Kalivendi, A. Klip, A.K. Tamrakar, NOD2 activation induces oxidative stress contributing to mitochondrial

dysfunction and insulin resistance in skeletal muscle cells, Free Radic. Biol. Med. 89 (2015) 158–169. https://doi.org/10.1016/j.freeradbiomed.2015.07.154.
[314] O.M. Palacios, J.J. Carmona, S. Michan, K.Y. Chen, Y. Manabe, J.L.W. III, L.J. Goodyear, Q. Tong, Diet and exercise signals regulate SIRT3 and activate AMPK and PGC-1α in skeletal muscle, Aging 1 (2009) 771–783. https://doi.org/10.18632/aging.100075.
[315] E. Jing, B. Emanuelli, M.D. Hirschey, J. Boucher, K.Y. Lee, D. Lombard, E.M. Verdin, C.R. Kahn, Sirtuin-3 (Sirt3) regulates skeletal muscle metabolism and insulin signaling via altered mitochondrial oxidation and reactive oxygen species production, Proc. Natl. Acad. Sci. 108 (2011) 14608–14613. https://doi.org/10.1073/pnas.1111308108.
[316] X. Kong, R. Wang, Y. Xue, X. Liu, H. Zhang, Y. Chen, F. Fang, Y. Chang, Sirtuin 3, a New Target of PGC-1α, Plays an Important Role in the Suppression of ROS and Mitochondrial Biogenesis, PLOS ONE 5 (2010) e11707. https://doi.org/10.1371/journal.pone.0011707.
[317] L. Yang, J. Zhang, W. Xing, X. Zhang, J. Xu, H. Zhang, L. Chen, X. Ning, G. Ji, J. Li, Q. Zhao, F. Gao, SIRT3 Deficiency Induces Endothelial Insulin Resistance and Blunts Endothelial-Dependent Vasorelaxation in Mice and Human with Obesity, Sci. Rep. 6 (2016) 23366. https://doi.org/10.1038/srep23366.
[318] Y.-C. Lai, D.M. Tabima, J.J. Dube, K.S. Hughan, R.R. Vanderpool, D.A. Goncharov, C.M. St. Croix, A. Garcia-Ocaña, E.A. Goncharova, S.P. Tofovic, A.L. Mora, M.T. Gladwin, SIRT3–AMP-Activated Protein Kinase Activation by Nitrite and Metformin Improves Hyperglycemia and Normalizes Pulmonary Hypertension Associated With Heart Failure With Preserved Ejection Fraction, Circulation 133 (2016) 717–731. https://doi.org/10.1161/CIRCULATIONAHA.115.018935.
[319] Y. Wei, J.R. Sowers, R. Nistala, H. Gong, G.M.-E. Uptergrove, S.E. Clark, E.M. Morris, N. Szary, C. Manrique, C.S. Stump, Angiotensin II-induced NADPH Oxidase Activation Impairs Insulin Signaling in Skeletal Muscle Cells *, J. Biol. Chem. 281 (2006) 35137–35146. https://doi.org/10.1074/jbc.M601320200.
[320] A. Espinosa, C. Campos, A. Díaz Vegas, J. Galgani Fuentes, N.M. Juretic Díaz, C. Osorio Fuentealba, J.L. Bucarey, G. Tapia, R. Valenzuela, A.E. Contreras Ferrat, P. Llanos Vidal, E. Jaimovich Pérez, Insulin-Dependent H2O2 Production Is Higher in Muscle Fibers of Mice Fed with a High-Fat Diet, (2013). https://doi.org/10.3390/ijms140815740.
[321] Y. Ohta, S. Kinugawa, S. Matsushima, T. Ono, M.A. Sobirin, N. Inoue, T. Yokota, K. Hirabayashi, H. Tsutsui, Oxidative stress impairs insulin signal in skeletal muscle and causes insulin resistance in postinfarct heart failure, Am. J. Physiol.-Heart Circ. Physiol. 300 (2011) H1637–H1644. https://doi.org/10.1152/ajpheart.01185.2009.
[322] A. Bravard, C. Bonnard, A. Durand, M.-A. Chauvin, R. Favier, H. Vidal, J. Rieusset, Inhibition of xanthine oxidase reduces hyperglycemia-induced oxidative stress and improves mitochondrial alterations in skeletal muscle of diabetic mice, Am. J. Physiol.-Endocrinol. Metab. 300 (2011) E581–E591. https://doi.org/10.1152/ajpendo.00455.2010.
[323] C.T. MORIYA, H. SATOH, H. WATADA, Febuxostat Improves Insulin Resistance in the Skeletal Muscle In Vitro and In Vivo, Diabetes 67 (2018) 1927-P. https://doi.org/10.2337/db18-1927-P.
[324] K. Loh, H. Deng, A. Fukushima, X. Cai, B. Boivin, S. Galic, C. Bruce, B.J. Shields, B. Skiba, L.M. Ooms, N. Stepto, B. Wu, C.A. Mitchell, N.K. Tonks, M.J. Watt, M.A. Febbraio, P.J. Crack, S. Andrikopoulos, T. Tiganis, Reactive oxygen species enhance insulin sensitivity, Cell Metab. 10 (2009) 260–272. https://doi.org/10.1016/j.cmet.2009.08.009.
[325] S.E. Alway, M.J. Myers, J.S. Mohamed, Regulation of Satellite Cell Function in Sarcopenia, Front. Aging Neurosci. 6 (2014). https://doi.org/10.3389/fnagi.2014.00246.

[326] S.C.Y. Yu, K.S.F. Khow, A.D. Jadczak, R. Visvanathan, Clinical Screening Tools for Sarcopenia and Its Management, Curr. Gerontol. Geriatr. Res. 2016 (2016) 5978523. https://doi.org/10.1155/2016/5978523.
[327] J. Bauer, J.E. Morley, A.M.W.J. Schols, L. Ferrucci, A.J. Cruz-Jentoft, E. Dent, V.E. Baracos, J.A. Crawford, W. Doehner, S.B. Heymsfield, A. Jatoi, K. Kalantar-Zadeh, M. Lainscak, F. Landi, A. Laviano, M. Mancuso, M. Muscaritoli, C.M. Prado, F. Strasser, S. von Haehling, A.J.S. Coats, S.D. Anker, Sarcopenia: A Time for Action. An SCWD Position Paper, J. Cachexia Sarcopenia Muscle 10 (2019) 956–961. https://doi.org/10.1002/jcsm.12483.
[328] A.A. Sayer, A. Cruz-Jentoft, Sarcopenia definition, diagnosis and treatment: consensus is growing, Age Ageing 51 (2022) afac220. https://doi.org/10.1093/ageing/afac220.
[329] R. Vettor, G. Milan, C. Franzin, M. Sanna, P. De Coppi, R. Rizzuto, G. Federspil, The origin of intermuscular adipose tissue and its pathophysiological implications, Am. J. Physiol.-Endocrinol. Metab. 297 (2009) E987–E998. https://doi.org/10.1152/ajpendo.00229.2009.
[330] C.K. Daw, J.W. Starnes, T.P. White, Muscle atrophy and hypoplasia with aging: impact of training and food restriction, J. Appl. Physiol. 64 (1988) 2428–2432. https://doi.org/10.1152/jappl.1988.64.6.2428.
[331] E. Marty, Y. Liu, A. Samuel, O. Or, J. Lane, A review of sarcopenia: Enhancing awareness of an increasingly prevalent disease, Bone 105 (2017) 276–286. https://doi.org/10.1016/j.bone.2017.09.008.
[332] F. Bellanti, A.D. Romano, A. Lo Buglio, V. Castriotta, G. Guglielmi, A. Greco, G. Serviddio, G. Vendemiale, Oxidative stress is increased in sarcopenia and associated with cardiovascular disease risk in sarcopenic obesity, Maturitas 109 (2018) 6–12. https://doi.org/10.1016/j.maturitas.2017.12.002.
[333] H.M. Blau, B.D. Cosgrove, A.T.V. Ho, The central role of muscle stem cells in regenerative failure with aging, Nat. Med. 21 (2015) 854–862. https://doi.org/10.1038/nm.3918.
[334] A.E. Almada, A.J. Wagers, Molecular circuitry of stem cell fate in skeletal muscle regeneration, ageing and disease, Nat. Rev. Mol. Cell Biol. 17 (2016) 267–279. https://doi.org/10.1038/nrm.2016.7.
[335] M. Lavasani, A.R. Robinson, A. Lu, M. Song, J.M. Feduska, B. Ahani, J.S. Tilstra, C.H. Feldman, P.D. Robbins, L.J. Niedernhofer, J. Huard, Muscle-derived stem/progenitor cell dysfunction limits healthspan and lifespan in a murine progeria model, Nat. Commun. 3 (2012) 608. https://doi.org/10.1038/ncomms1611.
[336] M.J. Jackson, Interactions Between Reactive Oxygen Species Generated by Contractile Activity and Aging in Skeletal Muscle?, Antioxid. Redox Signal. 19 (2013) 804–812. https://doi.org/10.1089/ars.2013.5383.
[337] S. Fulle, S. Di Donna, C. Puglielli, T. Pietrangelo, S. Beccafico, R. Bellomo, F. Protasi, G. Fanò, Age-dependent imbalance of the antioxidative system in human satellite cells, Exp. Gerontol. 40 (2005) 189–197. https://doi.org/10.1016/j.exger.2004.11.006.
[338] A.S. Brack, M.J. Conboy, S. Roy, M. Lee, C.J. Kuo, C. Keller, T.A. Rando, Increased Wnt Signaling During Aging Alters Muscle Stem Cell Fate and Increases Fibrosis, Science 317 (2007) 807–810. https://doi.org/10.1126/science.1144090.
[339] J.D. Bernet, J.D. Doles, J.K. Hall, K. Kelly-Tanaka, T.A. Carter, B.B. Olwin, P38 MAPK signaling underlies a cell autonomous loss of stem cell self-renewal in aged skeletal muscle, Nat. Med. 20 (2014) 265–271. https://doi.org/10.1038/nm.3465.

[340] M.T. Tierney, T. Aydogdu, D. Sala, B. Malecova, S. Gatto, P.L. Puri, L. Latella, A. Sacco, STAT3 signaling controls satellite cell expansion and skeletal muscle repair, Nat. Med. 20 (2014) 1182–1186. https://doi.org/10.1038/nm.3656.
[341] M. Narita, Quality and quantity control of proteins in senescence, Aging 2 (2010) 311–314.
[342] E. Marzetti, S.E. Wohlgemuth, H.A. Lees, H.-Y. Chung, S. Giovannini, C. Leeuwenburgh, Age-related activation of mitochondrial caspase-independent apoptotic signaling in rat gastrocnemius muscle, Mech. Ageing Dev. 129 (2008) 542–549. https://doi.org/10.1016/j.mad.2008.05.005.

CHAPTER 2: .

Cystine/Glutamate Antiporter xCT Controls Skeletal Muscle Glutathione Redox, Bioenergetics and Differentiation

Michel N. Kanaan*[1,2,3], Chantal A. Pileggi*[1,2] Charbel Y. Karam[1,2], Luke S. Kennedy[1,2], Claire Fong-McMaster[1,2], Miroslava Cuperlovic-Culf[1,2,4] and Mary-Ellen Harper[1,2]

[1] Department of Biochemistry, Microbiology and Immunology, Faculty of Medicine, University of Ottawa, 451 Smyth Road, Ottawa, ON, Canada, K1H 8M5

[2] Ottawa Institute of Systems Biology, University of Ottawa, ON, Canada, K1H 8M5

[3] Dr. Eric Poulin Centre for Neuromuscular Disease (CNMD), University of Ottawa, ON, Canada, K1H 8M5

[4] National Research Council of Canada, Digital Technologies Research Centre, 1200 Montreal Road, Ottawa, ON, Canada, K1A 0R6

*Co-first authors

Declarations of interest: None

Correspondence: Dr. ME Harper

Phone: 613-562-5800 ext. 8458

Email: mharper@uottawa.ca

Running title: xCT controls skeletal muscle redox, bioenergetics, and regeneration

2.1 STATEMENT OF MANUSCRIPT STATUS AND CONTRIBUTIONS

2.1.1 Statement of Manuscript Status

The manuscript “Cystine/Glutamate Antiporter xCT Controls Skeletal Muscle Glutathione Redox, Bioenergetics and Differentiation” has been accepted for publication in the journal *Redox Biology*. PMID: 38815331

Redox Biology, May 2024, In Press. https://doi: 10.1016/j.redox.2024.103213

2.1.2Acknowledgements

The authors would like to thank Jian Xuan for expert assistance in the care and maintenance of the mouse colonies and overall assistance in the laboratory., as well as Nikita Larionov, Dr. Mireille Khacho, Dr. William Chen, Dr. Derek Hall, Marie Esper, and Dr. Michael A. Rudnicki for sharing protocols. The authors acknowledge the Brain and Mind Research Institute at the University of Ottawa (uOBMRI), the Louise Pelletier Histology Core facility (RRID: SCR_021737) and the Cell Biology and Image Acquisition Core (RRID: SCR_021845) at the University of Ottawa.

2.1.3 Author Contributions

Conceptualization: MK, CAP, MEH

Data curation: MK, CAP, LK, MCC, MEH

Formal analysis: MK, CAP, CK, LK, MCC, CFM

Funding acquisition: MEH

Investigation: MK, CAP CK, LK

Methodology: MK, CAP, CK, LK, CFM, MCC, MEH

Supervision: MCC, MEH

Writing - original draft: MK, CAP, CK, LK, MEH

Writing - review & editing: ML, CAP, CK, LK, CFM, MCC, MEH

2.1.4 Funding

This work was supported by a grant from the Canadian Institutes of Health Research (CIHR), FDN-143278 (to MEH).

2.1.5 Conflict of Interests

The authors declare that they have no conflicts of interest with the contents of this article.

2.2 Abstract

Cysteine, the rate-controlling amino acid in cellular glutathione synthesis is imported as cystine, by the cystine/glutamate antiporter, xCT, and subsequently reduced to cysteine. As glutathione redox is important in muscle regeneration in aging, we hypothesized that xCT exerts upstream control over skeletal muscle glutathione redox, metabolism and regeneration. Bioinformatic analyses of publicly available datasets revealed that expression levels of xCT and GSH-related genes are inversely correlated with myogenic differentiation genes. Muscle satellite cells (MuSCs) isolated from Slc7a11$^{sut/sut}$ mice, which harbour a mutation in the Slc7a11 gene encoding xCT, required media supplementation with 2-mercaptoethanol to support cell proliferation but not myotube differentiation, despite persistently lower GSH. Slc7a11$^{sut/sut}$ primary myotubes were larger compared to WT myotubes, and also exhibited higher glucose uptake and cellular oxidative capacities. Immunostaining of myogenic markers (Pax7, MyoD, and myogenin) in cardiotoxin-damaged tibialis anterior muscle fibres revealed greater MuSC activation and commitment to differentiation in Slc7a11$^{sut/sut}$ muscle compared to WT mice, culminating in larger myofiber cross-sectional areas at 21 days post-injury. Slc7a11$^{sut/sut}$ mice subjected to a 5-week exercise training protocol demonstrated enhanced insulin tolerance compared to WT mice, but blunted muscle mitochondrial biogenesis and respiration in response to exercise training. Our results demonstrate that the absence of xCT inhibits cell proliferation but promotes myotube differentiation by regulating cellular metabolism and glutathione redox. Altogether, these results support the notion that myogenesis is a redox-regulated process and may help inform novel therapeutic approaches for muscle wasting and dysfunction in aging and disease.

Keywords: redox, glutathione, mitochondria, oxidative phosphorylation, glycolysis, myogenesis

2.3 Introduction

Adult skeletal muscle demonstrates remarkable plasticity and regenerative capacity in response to various intrinsic and extrinsic stimuli, such as those associated with exercise and injury [1]. Muscle stem cells, also known as muscle satellite cells (MuSCs), facilitate postnatal skeletal muscle growth, repair, and regeneration [1,2]. MuSCs cells reside in a quiescent state (G0 phase) beneath the basal lamina of postmitotic multinucleated myofibers and rely predominately on mitochondrial oxidative phosphorylation (OXPHOS) to support their metabolic activity. In response to myogenic stimuli, activated MuSCs re-enter the cell cycle to generate a pool of rapidly proliferating myoblasts that exit the cell cycle and either return to quiescence for renewal or enter a terminal G0 phase, and thereby commit to differentiation. Committed myoblasts irreversibly progress through a tightly regulated differentiation program involving the sequential expression of myogenic regulatory factors (MRFs) remodelling that orchestrate myoblast fusion and formation of multinucleated myotubes [3,4].

Substantial bioenergetic remodelling occurs during myogenesis, resulting in changes in cellular redox status that controls the process by activating the expression of MRFs. Specifically, activated MuSCs undergo metabolic transitions, away from OXPHOS and towards glycolysis, which increases the intracellular NADH/NAD+ ratio, and promotes the expression of MyoD and Pax7 via histone acetylation [5–7]. The commitment of myoblasts to differentiation involves the transition from glycolysis back to mitochondrial OXPHOS, which is accompanied by changes in cellular redox status and progressive increases in reactive oxygen species (ROS) generated by mitochondria and NADPH oxidases [4,8]. Low levels of ROS are key messengers involved in activating transcription factors and redox-dependent cellular signalling pathways that mediate multiple steps of myogenesis, such as self-renewal of the quiescent MuSC pool, cell cycle re-entry, myoblast proliferation, and terminal differentiation (reviewed in [9]), [3,4,8,10–13].

Glutathione (GSH) has well-recognized roles in maintaining cellular redox and iron homeostasis by minimizing oxidative stress and damage [14]. Impaired GSH redox has been associated with impaired muscle regeneration and age-dependent dysfunction of MuSCs [15]. Cysteine is an amino acid that supports cellular redox homeostasis and is the rate controlling substrate for GSH synthesis. In the blood, cysteine exists predominantly in its oxidized dimer form, cystine; however, in the cytoplasm cystine is rapidly reduced to two molecules of cysteine by NADPH-dependent reactions involving GSH or thioredoxin reductase 1 (TRR1) [16]. The transport of cystine into cells occurs exclusively through the cystine/glutamate antiporter, also called system Xc^-, which exchanges intracellular glutamate for extracellular cystine in a 1:1 ratio [17]. System Xc^- is a heteromeric amino acid transporter (HAT) composed of a transmembrane light chain subunit, xCT (encoded by the gene, *SLC7A11*), which is linked by a disulfide bridge to the chaperone protein, 4F2 heavy chain subunit (4F2hc/*SLC3A2*) [17–20]. The catalytic xCT subunit determines the substrate specificity, whereas the 4F2hc subunit facilitates plasma membrane localization [17].

The nuclear factor erythroid 2-related factor 2 (NRF2) is a redox-sensitive transcription factor for *SLC7A11* that plays a key role in regulating MuSC GSH redox in response to oxidative stress [17]. High glutathione concentrations are critical to maintain the highly metabolic SC pool, which is constantly exposed to high levels of ROS [15]. ROS can also impair myotube differentiation through sustained NF-κB activation [21]. However, ROS and GSH redox-dependent reactions (*e.g.*, protein glutathionylation) play key roles in initiating and regulating myogenesis. Indeed, myoblasts cultured in media supplemented with N-acetyl-cysteine (NAC) or GSH-ethyl ester exhibit impaired myotube differentiation due to reductive stress [22]. As xCT plays a critical role in maintaining skeletal muscle glutathione redox, the aim of this project was to determine the role of xCT during myogenic

differentiation. We hypothesized that xCT may play opposing roles in the proliferation and differentiation of myocytes.

2.4 Experimental Procedures

2.4.1 Bioinformatic Analysis of C2C12 Transcriptomics Differentiation Profiles

Publicly available published C2C12 transcriptomics datasets that include pre- and post-differentiation timepoints were identified for analyses of *Slc7a11* expression during cell differentiation. Ten selected transcriptomics datasets were obtained from the GEO database (https://www.ncbi.nlm.nih.gov/geo/) using the Bioconductor [23] GEOquery library (version 2.66) [24] in R* (version 4.2.2) [25] and include GSE989 [26], GSE84158 [27], GSE4694 [28], GSE46492 [29], GSE16992 [30], GSE148294 [31], GSE126370 [32], GSE11415 [33], GSE110957 [34], GSE108503 [35].

Prior to analysis all entries that were not assigned a gene symbol or identifier or that had over 30% missing values were removed from the transcriptomics datasets. Gene expression values in each replicate were scaled relative to the time point of myoblast differentiation in each dataset and log2 transformed. For consistency across different experimental designs in each selected dataset, time points before differentiation (*e.g.,* t = -24 hours or -48 hours) were omitted from further analysis. Additionally, any timepoints present in less than two datasets (GSE16992, t = 144 hours) were also omitted. As well, time points in certain datasets were set to relative scale according to experimental design such that 0 timepoints correspond to the initiation of differentiation (>80% confluency) and all other timepoints were adjusted accordingly (GSE989 and GSE4694, differentiation was initiated at t = -24 hours, thus all timepoints were shifted forward 24 hours) for equivalent comparisons across datasets. Plots of expression values show the mean with 95% confidence intervals and were produced using the seaborn package (version 0.12.2) [36] in Python (version 3.8.18) [37]. When multiple probes are annotated to a single gene in microarray data, mean expression values were calculated for each probe.

2.4.2 Correlation Analysis

Correlations of gene expression values in the GSE11415 dataset were calculated as distance correlations using the "distance_correlation" function in Python's statsmodels package (version 0.14.0, [38]). Correlations were calculated using z-score normalized expression values from all replicates, with significant correlations defined as values with p-values < 0.003 according to the two-sided Student's t-test [39] using the Student's cumulative distribution function (calculated through t.cdf function in SciPy (version 1.10.1) [40]. As per Monti *et al*. [39], the sign of the correlations was determined based on corresponding Pearson correlation values (using SciPy's pearsonr function).

2.4.3 Hierarchical Clustering

Transcriptomics data from the GSE11415 datasets were clustered using cosine distances with average linkages using Scipy's "spatial.distance.pdist" and "cluster.hierarchy" functions, respectively. Nearest genes were selected based on the cluster linkages distance, with an inter-cluster distance less than 0.98. Prior to clustering, gene expression values were z-score normalized and all replicate values were included in clustering.

2.4.4 Enrichment Analysis

Functional enrichments of significantly correlated genes were determined using ShinyGO (version 0.77) [41] and default parameters (FDR < 0.05, top 20 pathways, minimum 10 and max 2000 pathway genes). Results were downloaded and plotted in Python using seaborn, with enrichments for negatively correlated genes assigned a negative fold enrichment value.

2.4.5 Animals

All mouse experiments were performed following the principles and guidelines of the Canadian Council of Animal Care and the Animal Care Committee at the University of Ottawa. C3H/HeSnJ wild type (WT) mice and background-matched $Slc7a11^{sut/sut}$ ($xCT^{-/-}$) mice were a kind gift from Dr. Sandra Hewett

(Syracuse University). Mice were housed under standard conditions with controlled temperature (22-23°C), humidity (30-60%), and 12/12 h light-dark cycles (07:00–19:00 light). Mice had *ad libitum* access to water and a standard diet (18% protein and 6% fat; 2018 Teklad Global Diet, Madison, WI).

2.4.6 Measurements of Body Composition, Food Intake, Volitional Activity, and Indirect Calorimetry

Body composition was measured between 08:00-10:00 using a nuclear magnetic resonance imaging whole-body composition analyzer (EchoMRI-700, Echo Medical Systems, Houston, TX). A 12-chamber comprehensive lab animal monitoring system (CLAMS, Columbus Instruments, Columbus, OH) was used to measure volitional activity, food intake, volume of O_2 consumption (VO_2), volume of CO_2 production (VCO_2), and respiratory exchange ratio (RER). Eight mice per genotype were individually housed in CLAMS chambers and acclimated for 24–48 h at thermoneutrality (28°C) with *ad libitum* access to standard chow prior to data collection during normal light-dark phase cycles (07:00–19:00). The average of 48 hours of indirect calorimetry measurements (2 light or 2 dark cycles) were used for quantification for each mouse.

2.4.7 Oral Glucose Tolerance Test and Intraperitoneal Insulin Tolerance Test

Oral glucose tolerance tests (OGTT) and intraperitoneal insulin tolerance tests (ITT) were conducted in mice after a 6 h fast pre- and post-5-week exercise training. For the OGTT, 2 mg glucose/g body weight was administered through oral gavage. Saphenous blood was collected at 0-, 15-, 30-, and 60-min, and 120-min post-gavage for glucose determinations (One Touch Basic; LifeScan, Burnaby, BC). For ITT, mice were intraperitoneally injected with insulin (Humalog Rapid Acting; Eli Lilly, Indianapolis, IL) at 0.75m U/g BW. Blood glucose levels were measured at 0-, 15-, 30-, and 60-min, and 120-min following the insulin injection.

2.4.8 Exercise Training Protocol

Mice, aged 5 weeks, underwent a 5-week exercise training program on a treadmill (Exer 3/6; Columbus Instruments, Columbus, OH) as described previously [42]. During the first week of training program mice were acclimated, training duration was increased gradually from 10 min on D1 to 50 min on D5, and the training intensity gradually increased by 1 m/min every 2 min, starting with a speed of 8 m/min to reach a maximum of 14 m/min. In subsequent weeks, mice were trained on the treadmill at 14 m/min, 1 h/day, 5 d/wk.

2.4.9 Muscle Injury Protocol

Subcutaneous injections of buprenorphine (0.1 mg/kg) were administered 30 min prior to cardiotoxin treatment. Mice were anesthetized with isoflurane, hindlimbs were disinfected with ethanol and the left tibialis anterior (TA) muscles were injected with 50 µl of 10 µM cardiotoxin (L8102, Latoxan). Tissue was collected at D4, D7 and D21 post-injury.

2.4.10 C2C12 Cell Culture

C2C12 murine myoblasts (CRL-1772, ATCC, Manassas, VA) were cultured in 25 mM glucose DMEM supplemented with 10% bovine growth serum (HyClone) and 1% antibiotic-antimycotic. When myoblasts were approximately 90% confluent, differentiation was induced for 6 days using 5.5 mM-glucose DMEM, supplemented with 2% horse serum and 1% antibiotic-antimycotic. During differentiation, the medium was replaced every 48 h. Cells were collected at different stages, specifically when myoblasts reached > 80% confluence and following 3 and 6 days of differentiation (D3 and D6). D3, and D6 of differentiation.

2.4.11 Mouse Primary Muscle Cell Isolation and Culture

Hindlimb skeletal muscles were rapidly dissected and cleaned from fat and connective tissue and placed in sterile PBS supplemented with 1% antibiotic-antimycotic. The tissue was then washed twice with PBS

and treated with 1 mg/ml Dispase II (Sigma) and 1 mg/ml Collagenase B (Sigma). Tissue was minced with a sterile razor blade and subsequently incubated at 37°C for 30 min, with mixing every 5 min. The homogenate was then centrifuged at 500 g for 5 min and pellets were resuspended and transferred to dishes coated with Matrigel (Corning) containing DMEM (25 mM glucose) containing 20% fetal bovine serum, 10% horse serum, 2.5 ng/ml β-FGF (Sigma), 1x non-essential amino acids (11140050, Gibco), and 1% antibiotic-antimycotic. Primary cell enrichment was achieved by employing the differential adhesion process to remove fibroblast populations [43]. Throughout proliferation and during the first 24 h of differentiation, the medium was supplemented with 50 μM of 2-mercaptoethanol. Differentiation was induced using either high or low glucose DMEM (5.5 mM or 25 mM glucose, respectively) supplemented with 2% horse serum and 1% antibiotic-antimycotic. Media supplementation with 2-mercaptoethanol was removed during the last 24 h of proliferation for myoblasts and during differentiation, and media was replaced every 48 h.

2.4.12 Immunostaining of Primary Muscle Cells

Cells cultured in Matrigel-coated dishes were harvested 24 h after plating (myoblasts), 24 h after differentiation. 100,000 cells (in 100 μl) were loaded into a double Cytofunnel (Thermo Fisher Scientific) set on a double Cytoslide (Thermo Fisher Scientific) and centrifuged at 500 rpm for 5 min at room temperature using a cytocentrifuge (Epredia™ Cytospin™ 4). Cells were fixed with 4% paraformaldehyde (PFA, Sigma) for 3 min and quenched with 100 mM glycine (Biobasic) for 5 min at room temperature. Cells were washed 3 times with 1x PBS before staining. Cells were permeabilized for 10 min in PBS containing 0.2% Triton-X (Sigma), blocked in 5% goat serum (Sigma), 2% BSA-PBS for 30 min, and incubated for 2 h with Pax7 (1:2, DSHB, Pax7) at room temperature. The following day, sections were washed three times with 1 x PBS and subsequently incubated in species-specific fluorescent secondary antibodies diluted in 1x PBS containing 4,6-diamidino-2-phenylindole (DAPI).

Cells were washed in PBS, and then incubated for 1 h with the secondary antibody (Alexa Fluor 568 Goat anti-Mouse IgG1 (1:2000, A-21124, Thermo Fischer Scientific) diluted in 1x PBS containing DAPI at RT. To assess the S-phase entry, cells were incubated with 1 μM of 5-ethynyl-2'-deoxyuridine (EdU, Lumiprobe) for 24 h prior to harvesting. A 30-min incubation with the labeling mix [0.1 μM Sulfo-Cyanine5 azide dye (Lumiprobe), 2 mM copper (II) sulfate pentahydrate (Sigma), and 20 mg/ml of L-ascorbic acid (Sigma) were applied before blocking.

For differentiation assessment, cells were cultured in 24-well plates and differentiated for the following intervals: 1 day, 2 days, and 4 days. At each time point cells were fixed with 4% PFA (Sigma) for 15 min after 3 washes in PBS. Cells were permeabilized for 15 min in PBS containing 0.5% Triton-X and incubated with myosin (1:50, DSHB, MYH1E) overnight at 4°C. Cells were washed in PBS and then incubated for 1 h with species-specific secondary antibodies diluted in 1 x PBS containing DAPI at RT. Wells were filled with PBS and cells were imaged at 10x on a Zeiss AxioObserver Z1 fluorescent microscope equipped with an AxioCam MRm CCD camera.

2.4.13 GSH and GSSG Measurements

GSH and GSSG levels were measured by high-performance liquid chromatography (HPLC; Agilent 1100 series), as previously described [44]. Cells were cultured in 100 mm dishes with the indicated conditions, collected with trypsin then washed twice with ice-cold PBS. Cells were lysed on ice for 20 min in 1:1 homogenization buffer [125 mM sucrose, 1.5 mM EDTA, 5 mM Tris, 0.5% trifluoroacetic acid (TFA) and 0.5% meta-phosphoric acid (MPA) in 50% mobile phase (10% HPLC grade methanol, 0.09% TFA – 0.2μm filtered)]. Homogenates were centrifuged at 14,000 g for 20 min at 4°C, and the supernatant of each sample was subsequently collected for analysis. An Agilent HPLC system equipped with a Pursuit C18 column (150 ×4.6 mm, 5 μm; Agilent) with a flow rate of 1 ml/min was used to detect GSH and GSSG using the Agilent UV-visible wavelength detector at 215 nm. Standard solutions of GSH

(G4251, Sigma) and GSSG (G4501, Sigma) were used to determine the retention times. Absolute amounts of GSH and GSSG were determined by integrating the area under the respective peaks using a chromatogram, and values were calculated from standard curves. All values were normalized to protein amount in each well determined by a BCA assay (Pierce™ BCA Protein Assay; 23225, Thermo Fisher).

2.4.14 Extracellular Flux Determinations of Cellular Bioenergetics

Extracellular flux analyses were conducted using the Seahorse XFe96 Analyzer (Agilent) to measure oxygen consumption rates (OCR) and extracellular acidification rates (ECAR). Cells were plated at 20,000 cells/well in high-glucose DMEM media. After 24h, differentiation was induced for 7 days using a low-glucose DMEM medium with constant media changes (48h). Following resting respiration measurements, myotubes were treated with consecutive injections of oligomycin (2 μg/mL), FCCP (2.4 μM), and combined antimycin A (5.5 μM)/ rotenone (7.7 μM). To calculate resting and leak-dependent and maximal rates, non-mitochondrial OCR given after antimycin A and rotenone injections was subtracted from the resting measurements and those after oligomycin and FCCP injections, respectively. ATP-linked OCR was measured by calculating the difference between resting and leak respiration. Lastly, reserve capacity assessed by subtracting resting OCR from the maximal OCR, reflects the respiratory flexibility of myotubes under certain conditions. Maximal ECAR was determined following the injection of monensin (20 μM). The glycolytic reserve value was calculated by subtracting the resting rates from the maximal rates. All values were normalized to protein concentration (Pierce BCA protein assay) and analyzed with the Seahorse Wave software (version 2.4.3; Agilent) and Excel (Microsoft) software.

2.4.15 In situ Determinations of Oxygen Consumption in Cultured Primary Cells during Proliferation and Differentiation

Wild-type and Slc7a11$^{sut/sut}$ primary muscle cells were cultured in a regular 96-well plate at 40,000 cells/well for assessments using the Resipher system (Lucid Scientific). Cellular OCR was measured throughout proliferation and differentiation of the primary muscle cells either in a high-glucose or a low-glucose differentiation medium. For protein quantification, primary cells were cultured in the same conditions in parallel plates and analyzed at D1, D4, and D7 post-differentiation.

2.4.16 Glucose Uptake in Primary Muscle Cells

Cells were cultured in a 96-well white/clear bottom plate (Corning) at 40000 cells/well. Cells were differentiated for 4-5 d in a low-glucose or high-glucose differentiation medium. On the day of the assay (Glucose Uptake Cell-Based Assay Kit, 600470, Cayman), cells were starved from serum for 3 h. Then for the last 30 min before the assay, cells were incubated with 200 µg/ml of (2-(N-(7-Nitrobenz-2-oxa-1,3-diazol-4-yl) amino)-2-Deoxyglucose (2-NBDG) with either 5.5 mM or 25 mM of glucose. Then, cells were washed and centrifuged according to the manufacturer's protocol, and cellular 2-NBDG was detected at 485/535 nm using a BioTek Synergy H1 Multi-Mode Plate Reader (BioTek Instruments, Winooski, VT).

2.4.17. Cell Death and Growth Assays

For assessing cell death and growth, the IncuCyteZOOM live cell imaging system from Essen BioScience was used. Cells were seeded onto 96-well plates (10^4 cells/well) and treated with 250 nM of the Incucyte Cytotox green dye (4633, Sartorius) with and without 50 µM of 2ME. Cells were imaged for 48 h using a 10× objective. Three to four images per well were captured every hour, and there were 4 technical replicates for each condition. Cell confluence was measured by phase contrast microscope

and cell death was assessed by Incucyte Cytotox dye. IncuCyteZOOM2018A software was used for automated confluence and Incucyte^{+} cell measurements.

2.4.18 High-resolution Respirometry of ex vivo Muscle

As previously described [45], TA myofibers were permeabilized with 50 µg/ml saponin (Sigma) and oxygen consumption was measured in an Oxygraph-2k (Oroboros, Austria). To evaluate adenylate-free leak respiration and complex I-driven respiration, malate (2 mM), pyruvate (5 mM), glutamate (10 mM), adenosine diphosphate, and Mg2+ (5 mM) were added. The maximum oxidative phosphorylation capacity (for Complex I and II) was assessed by adding succinate (10 mM) and ADP (5 mM). To evaluate leak-linked respiration, oligomycin (2.5 µM) was added. The maximal respiratory capacity was measured by adding carbonyl cyanide p-trifluoro-methoxyphenyl hydrazone (FCCP) with 1uM incremental additions until a plateau was observed. Antimycin A (2.5 µM) was then added to determine non-mitochondrial oxygen consumption. Finally, to assess maximal complex IV activity, N, N′, N′-Tetramethyl-p-phenylenediamine (TMPD) (0.5 mM), ascorbate (2 mM), and sodium azide (100 mM) were added.

2.4.19 Muscle Tissue Immunohistochemistry

To assess regenerative capacity, freshly isolated TA muscles were fixed with 2% formaldehyde for 30 min, incubated in 5% sucrose for 2 h, and transferred to 20% sucrose for 48 h. Muscles were subsequently embedded in O.C.T. (4583, Tissue-Tek), and stored at -80ºC for later analysis. Transverse 14 µm cryosections were permeabilized for 10 min at room temperature in 1x PBS containing 0.1% Triton X-100 and 0.1M glycine. Blocking was for 1 h at room temperature in 1x PBS containing 1:40 mouse-on-mouse (MOM) blocking reagent (VectorLabs), 5% goat serum, and 2% BSA. Sections were incubated with primary antibodies at 4°C overnight using primary antibodies against Pax7 (1:2, Pax7, DSHB), Myogenin (1:2, F5D, DSHB), and MyoD1 (1:500, ab133627, Abcam). The following day, sections were

washed three times with 1 x PBS and subsequently incubated in species-specific fluorescent secondary antibodies diluted in 1x PBS containing (DAPI) for 2 h at RT. Sections were mounted in ProLong Gold antifade reagent (P36934, Invitrogen) and imaged at 20x on a Zeiss AxioObserver Z1 fluorescent microscope equipped with an AxioCam MRm CCD camera. For fiber typing, samples were imaged at 10x using an EVOS FL Auto 2 microscope (Thermo Fisher) and the primary antibodies were as follows: type I fibres (1:100, BA-F8, DSHB), type IIa fibres (1:100, SC-71, DSHB), type IIb fibres (1:25, BF-F3, DSHB), and dystrophin (1:10, MANDYS1(3B7), DSHB). Alexa Fluor-conjugated secondary antibodies were used at 1:500 concentration. Immunofluorescent images were analyzed in Imaris 10.1 (Oxford Instruments) and QuPath 0.5.0 to quantify the expression levels of myogenic markers by nuclear colocalization, and for fiber typing analyses.

2.4.20 Muscle Cross-sectional Area Determinations

To measure the cross-sectional area (CSA) of myofibers, transverse 14 µm cryosections were stained with hematoxylin and eosin (H&E). Samples were imaged at 20x using an EVOS FL Auto 2 microscope (Thermo Fisher) and analyzed using Cellpose [46] and ImageJ.

2.4.21 Protein Extraction

Cells or tissues were homogenized in 1x RIPA buffer (EMD Millipore, 20-188) supplemented with a protease inhibitor cocktail (P8340, Sigma) and phosphatase inhibitor cocktail (78420, Thermo Fischer Scientific). Protein concentration was measured using a BCA assay as per the manufacturer's instructions, and samples were stored at −80°C until further use.

2.4.22 Western Blot Analyses

Samples were prepared in 1 x Laemmli buffer containing 100 mM DTT, run on SDS-PAGE, and transferred to nitrocellulose or PVDF (Bio-Rad) membranes. Samples for anti-glutathione blots were prepared and run under non-reducing conditions (no DTT or 2ME) to preserve the protein

glutathionylation (PSSG) and prevent any changes in free GSH and GSSG during sample preparation and analysis. Membranes were blocked for 1 h using 5% BSA in Tris-buffered saline containing 0.1% Tween-20 (TBST) at room temperature (RT). Membranes were incubated in primary antibodies (1:1000 unless otherwise stated) overnight at 4°C against: ATF4 (11815-S, Cell Signaling), glutathione (101-A, Virogen), GPx1 (ab22604, Abcam), GPx4 (ab16800, Abcam), myogenin (F5D, Developmental Studies Hybridoma Bank (DSHB), 0.5 µg/ml), myosin (MF20, DSHB, 0.5 µg/ml), phospho-NF-κB p65 (Ser536) (3033, Cell Signalling), total NF-κB p65 (8242, Cell Signalling), OXPHOS proteins (ab110413, Abcam), SOD1 (sc-11407, Santa Cruz), SOD2 (sc-30080, Santa Cruz), xCT (ab175186, Abcam). For loading control the following primary antibodies were used, β-Actin (4967, Cell Signalling, 1:5000), GAPDH (60004-1-Ig, Protein Tech, 1:10,000), α-tubulin (11224-1-AP, Protein tech), Vinculin (ab129002, Abcam, 1:5000). Membranes were incubated in Immobilon chemiluminescent horseradish peroxidase-conjugated substrate (Millipore) and protein bands were visualized using the ChemiDoc™ MP Imaging System (Bio-Rad). Densitometry band analyses were performed using ImageJ software, and the abundance of target proteins are presented normalized to vinculin, GAPDH, or β-actin.

2.4.23 Enzymatic Activity Analyses

Enzymatic activities were performed in enriched mitochondrial fractions for complex I and muscle tissue homogenate for citrate synthase (CS) and lactate dehydrogenase (LDH), as previously described [47,48]. The change in the rate of absorbance and pathlength were measured using a BioTek Synergy Mx Microplate Reader (BioTek Instruments). Enzyme activities were calculated using the extinction coefficients of 13.6 $mM^{-1}cm^{-1}$ for CS, and 6.22 $mM^{-1}cm^{-1}$ for LDH and complex I, and values are expressed per mg of protein.

2.4.24 Statistics

Unless otherwise mentioned, all data are shown as means ± standard error of the mean (SEM). Statistical analyses were conducted using Prism (GraphPad, La Jolla, CA). Statistical significance of C2C12 time course experiments was determined using a one-way repeated measures (RM) ANOVA with Tukey post hoc tests. For time course experiments on WT vs. Slc7a11$^{sut/sut}$ primary cells undergoing differentiation, a two-way RM ANOVA was used with time as a repeated factor and genotype as a between-subjects factor. Two-tailed Student's t-tests were used to determine statistical significance for WT vs. Slc7a11$^{sut/sut}$ in cardiotoxin-induced muscle injury experiments. To assess the effect of the exercise intervention, a two-way ANOVA with exercise and genotype as factors was used with Tukey post hoc tests. P-values < 0.05 were considered statistically significant.

2.5 Results

2.5.1 xCT controls GSH Redox during Myogenic Proliferation

To investigate the role of xCT during myogenic differentiation, we leveraged publicly available transcriptomic datasets on Gene Expression Omnibus (GEO) to compare the expression of *Slc7a11* at selected timepoints of C2C12 myocyte differentiation. As expected, expression level of myosin heavy chain 1 (*Myh1)*, a marker of myogenic differentiation, increased with differentiation time, whereas *Slc7a11* expression decreased during differentiation, as demonstrated by lower expression relative to myoblast levels (**Figure 2.1A**). We subsequently compared the signed distance correlations between *Slc7a11* and genes also changing across differentiation on the GSE11415 dataset [33,39,49], which contains the greatest number of samples within the timeframe of interest (12 h to 8 d). The expression of Slc*7a11* was strongly correlated with ~1900 genes, of which 1516 genes positively correlated with *Slc7a11* and 398 genes negatively correlated with *Slc7a11* throughout differentiation. Of the 1900 significantly correlated genes, hierarchical clustering identified 732 (632 positively and 92 negatively correlated) genes also cluster with *Slc7a11*, based on HCL (see **Methods**). Genes that positively correlated with *Slc7a11* included cyclin D kinases (*Cdk5*, *Cdk10*, *Cdk12*), and glutathione enzymes (*Gsta1*, *Gsto1*, *Gsto2*, *Mgst2, Gpx4*). In contrast, the ubiquitin E3 ligases *Skp1* and *Prpf19* that specifically targets cell-cycle regulatory proteins for degradation during cell cycle exit was also negatively correlated with *Slc7a11* during C2C12 differentiation [50,51].

We next analyzed the functions of the genes tightly correlated with *Slc7a11* during differentiation. KEGG pathway analysis revealed that *Slc7a11* positively correlated with genes enriched in ribosome and autophagy pathways, whereas *Slc7a11* negatively correlated with genes involved in FoxO, MAPK, and PI3K-Akt signalling (**Figure 2.1B**). Gene ontology (GO) biological processes terms were enriched for metabolic processes such as peptide and RNA metabolism, mitochondrial organization, and translation

as strong correlation partners (**Supplemental Figure 2.1A**). Negatively correlated genes were found to be enriched in terms for apoptosis and cell death (also observed to a lesser extent in positively correlated genes), and predominantly in RNA metabolism, processing, and splicing via the spliceosome, which is similarly enriched in the KEGG enrichment analysis as highly enriched pathways.

To build upon the *in-silico* data, we quantified xCT protein expression in C2C12 myoblasts following 3 and 6 days of differentiation into myotubes. As expected, markers of differentiation, myogenin and myosin increased during differentiation, as evidenced by higher expression in day 3 and day 6 myotubes (D3, D6, respectively) compared to myoblasts **(Figure 2.1C**). In line with gene expression data, xCT protein levels progressively decreased with differentiation, with a drastic 82% decrease in D6 myotubes vs. myoblasts (**Figure 2.1D**). The downregulation of xCT transcript and protein expression during C2C12 myogenic progression was accompanied by increased levels of protein glutathionylation (PSSG) during myogenic differentiation (**Figure 2.1E**). Consistent with previous metabolomic analyses [52],cellular concentrations of glutathione increased during myogenic progression, resulting in ~2.9-fold higher GSSG, and ~1.8-fold higher total glutathione (GSH+2*GSSG) in D6 myotubes vs. myoblasts (**Figure 2.1F**). While the concentration of GSH slightly increased during myogenic progression, the drastic increase in GSSG culminated in lower GSH:GSSG ratios. Immunoblot analysis of the key enzymes involved in GSH biosynthesis revealed similar levels of glutamate-cysteine ligase (GCLc) and GSH synthetase (GSS) (**Supplementary Figure 2.1B**), indicating that GSH biosynthesis is maintained during myogenesis, but GSH undergoes a redox shift towards an oxidized state.

Superoxide dismutase 2 (SOD2) expression is induced during myogenesis [13], and reduces superoxide ($O_2^{\cdot -}$) into hydrogen peroxide (H_2O_2), a critical signaling molecule involved in myogenesis [13].Consistent with these findings, SOD2, but not SOD1, increased during differentiation (**Figure**

2.1G). The expression of glutathione peroxidase 1 (GPx1) and GPx4 decreased during myogenesis (**Figure 2.1H**).

To assess any corresponding changes in cellular metabolism we conducted extracellular flux analyses on proliferating myoblasts, and at D3 and D6 of differentiation. Quantification of the oxygen consumption rate (OCR) and extracellular acidification rate (ECAR) in myoblasts and myotubes confirmed previous reports of increased oxidative and decreased glycolytic metabolic capacity during differentiation into myotubes (**Figure 2.1I**). Interestingly, the spare respiratory capacity negatively correlated with the GSH:GSSG ratio across differentiation time (Pearson r=-0.69, R^2=0.50, **Supplementary Figure 2.1C**), indicating that myotubes with lower glutathione redox have a greater capacity to respond to high energetic demands.

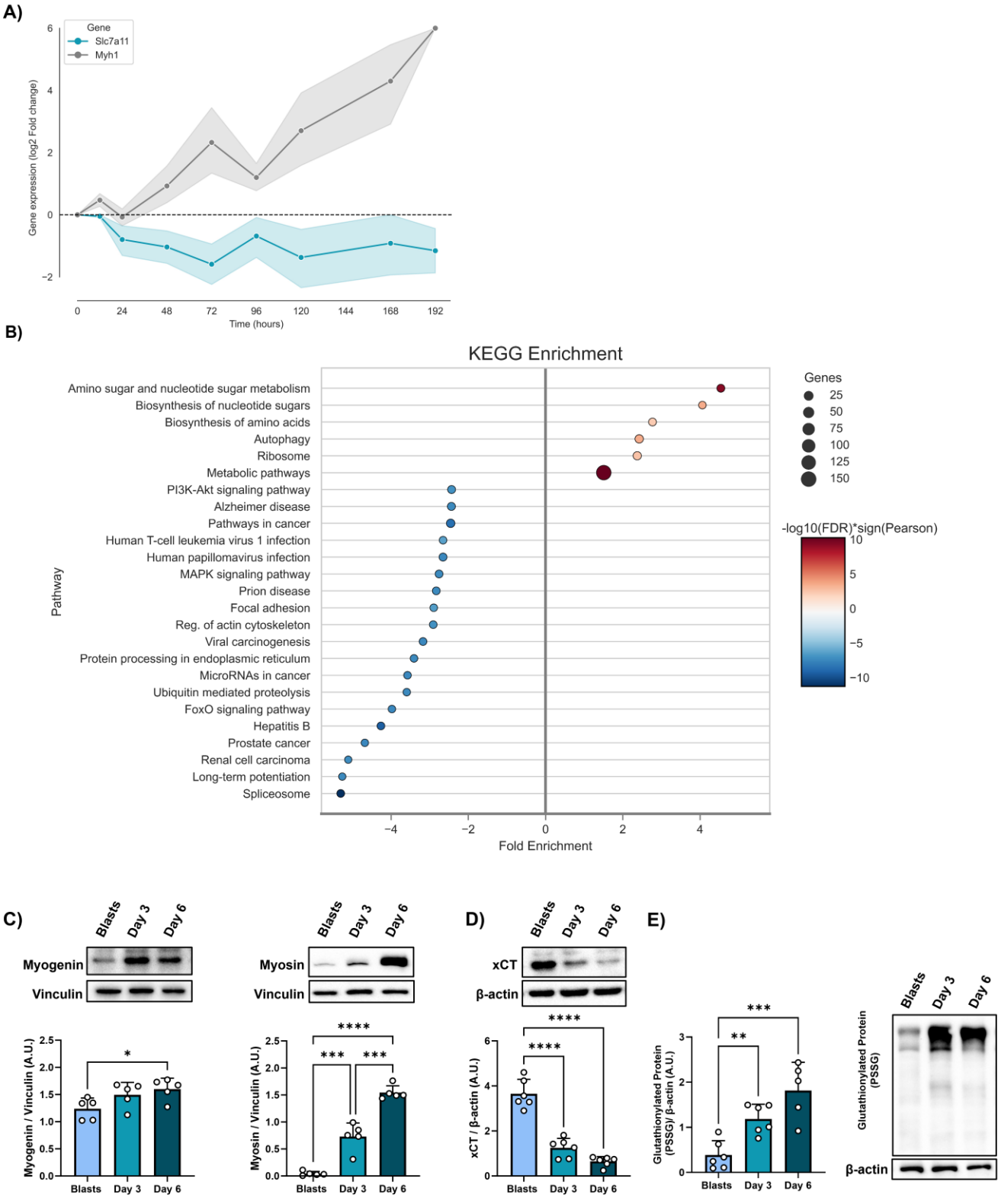
A)
Gene
Slc7a11
Myh1
Gene expression (log2 Fold change)
Time (hours)
B)
KEGG Enrichment
Amino sugar and nucleotide sugar metabolism
Biosynthesis of nucleotide sugars
Biosynthesis of amino acids
Autophagy
Ribosome
Metabolic pathways
PI3K-Akt signaling pathway
Alzheimer disease
Pathways in cancer
Human T-cell leukemia virus 1 infection
Human papillomavirus infection
MAPK signaling pathway
Prion disease
Focal adhesion
Reg. of actin cytoskeleton
Viral carcinogenesis
Protein processing in endoplasmic reticulum
MicroRNAs in cancer
Ubiquitin mediated proteolysis
FoxO signaling pathway
Hepatitis B
Prostate cancer
Renal cell carcinoma
Long-term potentiation
Spliceosome
Pathway
Fold Enrichment
Genes
-log10(FDR)*sign(Pearson)
C)
Blasts
Day 3
Day 6
Myogenin
Vinculin
Myogenin / Vinculin (A.U.)
Myosin
Myosin / Vinculin (A.U.)
D)
xCT
β-actin
xCT / β-actin (A.U.)
E)
Glutathionylated Protein (PSSG) β-actin (A.U.)
Glutathionylated Protein (PSSG)

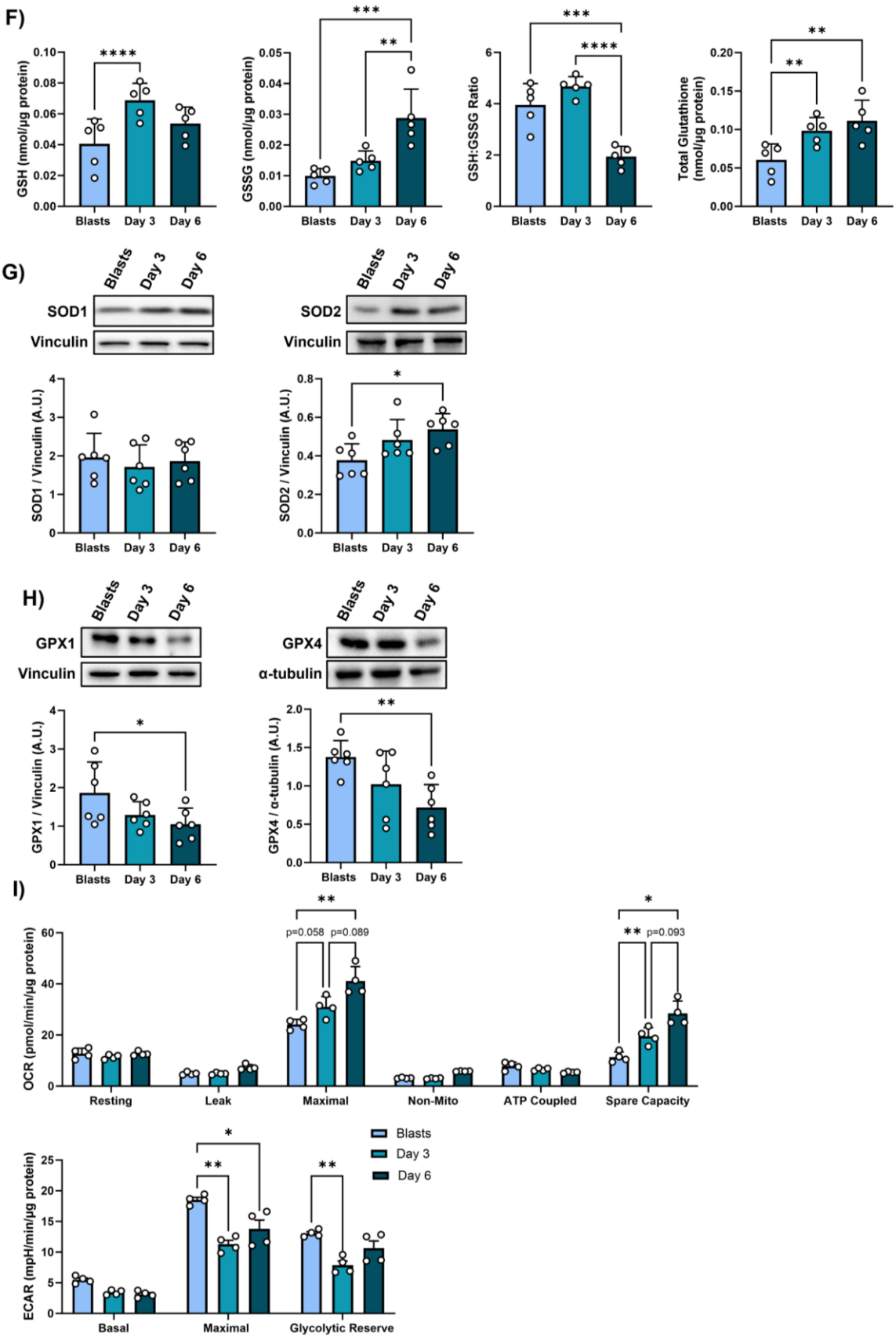
F)
GSH (nmol/µg protein)
GSSG (nmol/µg protein)
GSH:GSSG Ratio
Total Glutathione (nmol/µg protein)
Blasts
Day 3
Day 6
G)
SOD1
SOD2
Vinculin
SOD1 / Vinculin (A.U.)
SOD2 / Vinculin (A.U.)
H)
GPX1
GPX4
α-tubulin
GPX1 / Vinculin (A.U.)
GPX4 / α-tubulin (A.U.)
I)
OCR (pmol/min/µg protein)
p=0.058
p=0.089
p=0.093
Resting
Leak
Maximal
Non-Mito
ATP Coupled
Spare Capacity
ECAR (mpH/min/µg protein)
Basal
Maximal
Glycolytic Reserve

Figure 2.1. xCT Controls GSH Redox During Myogenic Proliferation
(A) Slc7a11 and Myh1 expression across differentiation time points in C2C12 transcriptomic datasets (represented as mean expression values with 95% CI bands highlighted). **(B)** Enriched KEGG pathways in positively (red) and negatively (blue) correlated genes with Slc7a11 throughout C2C12 differentiation. **(C-E)** C2C12 myoblasts and myotubes differentiated for 3 or 6 days (D3 and D6) were immunoblotted for **(C)** differentiation markers (myogenin and myosin), **(D)** xCT, and **(E)** post-translational glutathionylation. **F)** Reduced glutathione (GSH), oxidized glutathione (GSSG), total glutathione (GSH+2*GSSG), and the GSH: GSSG ratio in myoblasts and D3 and D6 myotubes. **(G-H)** C2C12 myoblasts and D3 and D6 myotubes were immunoblotted for **(G)** SOD1 and SOD2, **(H)** GPx1 and GPx4. **(I)** Oxygen consumption rate (OCR) and extracellular acidification rates (ECAR) in C2C12 myoblasts and D3 and D6 myotubes. The statistical significance of the differences between groups was determined using a one-way RM ANOVA with post hoc Tukey HSD test. Results are presented as mean ± SEM, *p < 0.05, **p < 0.01, ***p < 0.001, ****p < 0.0001, n = 4-6.

2.5.2 Absence of Functional xCT Inhibits Proliferation but Potentiates Myogenesis

To examine the potential physiological implications of xCT in skeletal muscle, we studied subtle gray ($Slc7a11^{sut/sut}$) mice, which are naturally null for xCT, and genetic background-matched controls (C3H/HeSnJ). Specifically, $Slc7a11^{sut/sut}$ mice harbor a spontaneous recessive mutation in *Slc7a11* that results in the truncation of xCT at the C terminus [53,54]. Analyses of mouse body composition characteristics revealed that the $Slc7a11^{sut/sut}$ mice had lower body fat mass and percent body fat compared to WT controls, despite similar body weights (**Table 2.1**). The reduced fat mass in the $Slc7a11^{sut/sut}$ mice was also reflected as an increase in the proportion of lean body mass compared to WT mice (**Table 2.1**). Continuous automated monitoring of physiologic parameters revealed that *ad libitum* food intake, metabolic rates (VO_2), and respiratory exchange ratios (RER; VCO_2/VO_2) were similar between genotypes.

	WT	Slc7a11$^{sut/sut}$
n	8	8
Body Weight (g)	20.06 ± 0.82	20.80 ± 0.88
Fat Mass (g)	1.44 ± 0.15	1.02 ± 0.07*
Lean Mass (g)	16.37 ± 0.67	17.50 ± 0.76
Body Fat %	7.10 ± 0.57	4.89 ± 0.24*
Body Lean Mass %	81.62 ± 0.47	84.09 ± 0.41*
Food Intake (g/day)	4.14 ± 0.24	4.18 ± 0.30
VO_2 (mL/hr/kg lean body mass) **Light** **Dark**	 4.70 ± 0.15 5.46 ± 0.18	 4.43 ± 0.20 5.33 ± 0.30
Respiratory exchange ratio (RER) **Light** **Dark**	 0.94 ± 0.01 0.96 ± 0.01	 0.94 ± 0.01 0.97 ± 0.01

Table 2.1. Metabolic Phenotyping of WT and Slc7a11$^{sut/sut}$

To examine the impact of xCT deficiency on myogenic capacity, we next isolated primary MuSCs from Slc7a11$^{sut/sut}$ and WT mice. MuSCs isolated from Slc7a11$^{sut/sut}$ muscle were unable to proliferate without supplementing the culture medium with 2-mercaptoethanol (2ME; 50μM), consistent with observations in melanocytes isolated from Slc7a11$^{sut/sut}$ mice [53]. Supplementation with a reducing agent converts extracellular cystine to cysteine, which can then be transported into cells via the Na(+)-dependent amino acid transporters, System A (alanine-preferring) and alanine-serine-cysteine (ASC) transporter [55]. While 2ME supplementation was necessary for myoblast proliferation, we found that it is not necessary during the differentiation of Slc7a11$^{sut/sut}$ primary myotubes, indicating the importance of xCT in maintaining cell redox during cell proliferation over differentiation stages (**Figure 2.2A**).

Supporting the established role of xCT in cell proliferation, analyses of primary myoblasts immunostained for markers involved in cell proliferation revealed there was a lower proportion of Pax7^{+}EdU^{+} cells in Slc7a11$^{sut/sut}$ compared to WT primary myoblasts prior to differentiation (**Figure 2.2B**). Following 24 h of differentiation, the proportion of Pax7^{+}EdU^{+} WT myoblasts rapidly decreased to levels similar to Slc7a11$^{sut/sut}$ myoblasts. To assess if Slc7a11$^{sut/sut}$ myoblasts were undergoing differentiation, cells were fixed and stained with sarcomeric myosin to visualize myotube structure. Quantification of myotube area revealed that primary Slc7a11$^{sut/sut}$ cells had a greater area at day 2 of differentiation compared to WT myotubes (**Figure 2.2C**), suggesting a more rapid differentiation. At day 4 of differentiation, myotube area was similar between WT and Slc7a11$^{sut/sut}$ myotubes. Immunoblotting of myogenic markers, myogenin and myosin, showed no difference between groups throughout differentiation (**Supplementary Figure 2.2A**). We next quantified protein expression levels of key redox-sensitive factors involved in the control of myogenesis. The expression of activating transcription factor 4 (ATF4), a stress-inducible transcription factor for xCT [56], was upregulated in the Slc7a11$^{sut/sut}$ myoblasts prior to differentiation (**Figure 2.2D**). In contrast, the ratio of phospho-NF-κB/total NF-κB, a

redox-sensitive transcription factor for SOD2 [13,57], tended to decrease in Slc7a11$^{sut/sut}$ myotubes at D4 (**Supplementary Figure 2.2B**). The expression levels of the antioxidant enzymes SOD2 and GPx4 were elevated in Slc7a11$^{sut/sut}$ at day 2 of differentiation (**Figure 2.2E and 2.2F**), whereas SOD1 expression did not change between genotypes.

Cultured myoblasts require at least 5 mM glucose during differentiation to maintain high intracellular NADH/NAD^{+} and support MyoD activation in the progression of myogenesis [58]. However, high glucose (*e.g.,* 25 mM) can promote adipogenic conversion of muscle-derived SCs [59]. Therefore, we conducted glutathione and metabolic measurements of cells under both standard experimental conditions which use relatively high glucose (25 mM) and physiological levels of glucose (5.5 mM). Intracellular levels of reduced GSH and total glutathione were lower in Slc7a11$^{sut/sut}$ myotubes compared to WT under both high (**Supplementary Figure 2.2C)** and low glucose conditions (**Figure 2.2G**), indicating that Slc7a11$^{sut/sut}$ myotubes maintain lower GSH levels throughout differentiation. However, only Slc7a11$^{sut/sut}$ myotubes differentiated in high glucose exhibited a lower GSH:GSSG ratio than WT (**Supplementary Figure 2.2C**).

Continuous real-time measurements of resting cellular respiration throughout 7 days of differentiation revealed that Slc7a11$^{sut/sut}$ myoblasts had lower oxygen consumption rates (OCRs) compared to WT myoblasts during early myogenesis (*i.e.,* D0 and D1). At D2 of differentiation, Slc7a11$^{sut/sut}$ and WT myotubes cultured in differentiation medium containing 25 mM glucose had similar OCRs (**Supplementary Figure 2.2D**). In contrast, Slc7a11$^{sut/sut}$ myotubes cultured in differentiation medium containing 5.5 mM glucose demonstrated remarkably higher OCRs through myogenesis at D3 compared to WT myotubes (**Figure 2.2H**).

Extracellular flux bioenergetic profiling of myotubes cultured for 4 days failed to recapitulate the increase in resting OCR observed in Slc7a11$^{sut/sut}$ myotubes cultured in low glucose (**Figure 2.2I**).

Likewise, resting OCRs were similar in Slc7a11$^{sut/sut}$ and WT myotubes cultured in high glucose (**Supplementary Figure 2.2E**). Despite this, maximal respiration capacity was higher in Slc7a11$^{sut/sut}$ myotubes regardless of media glucose concentration and was associated with a 29% and 46% increased spare respiratory capacity in Slc7a11$^{sut/sut}$ myotubes cultured in low and high glucose conditions, respectively (**Figure 2.2I, Supplementary Figure 2.2E** respectively). Similar to the data from C2C12 myotubes, spare respiratory capacity tended to negatively correlate with the GSH:GSSG ratio in myotubes cultured in high glucose conditions (Pearson r=-0.66, R^2= 0.43, p= 0.076, **Supplementary Figure 2.2F**), indicating that the lower glutathione redox in Slc7a11$^{sut/sut}$ myotubes improves their capacity to respond to high energetic demands. No correlation was observed when primary myotubes were cultured under low glucose conditions (Pearson r=-0.45, R^2=0.20, p=0.27, data not shown). Analysis of extracellular acidification rates (ECAR), a proxy measure of glycolysis, revealed no difference in basal and maximal respiration in both glucose conditions (**Supplementary Figure 2.2G-H**). However, the glycolytic reserve was higher in Slc7a11$^{sut/sut}$ myotubes cultured in high glucose conditions (**Supplementary Figure 2.2G**), indicating a greater ability of Slc7a11$^{sut/sut}$ myotubes to respond to energetic demands. Evaluation of glucose uptake using 2-NBDG revealed that Slc7a11$^{sut/sut}$ myotubes cultured in low glucose differentiation media had greater glucose uptake compared to WT myotubes (**Figure 2.2J**), whereas glucose uptake rates were similar between WT and Slc7a11$^{sut/sut}$ myotubes cultured in high glucose differentiation media (**Supplementary Figure 2.2I**).

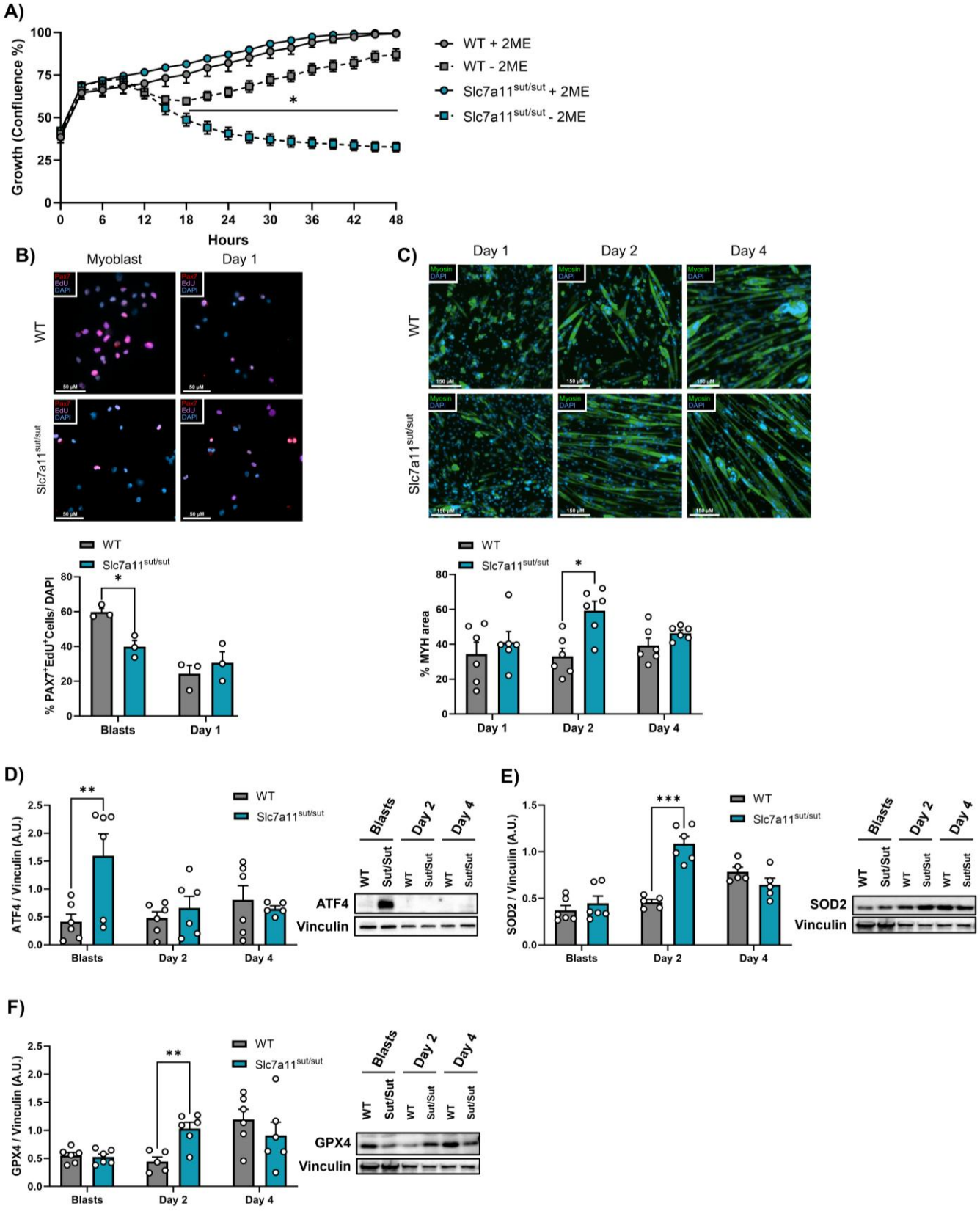
A)
Growth (Confluence %)
Hours
WT + 2ME
WT - 2ME
Slc7a11sut/sut + 2ME
Slc7a11sut/sut - 2ME
B)
Myoblast
Day 1
WT
Slc7a11sut/sut
% PAX7+EdU+Cells/ DAPI
Blasts
Day 1
C)
Day 1
Day 2
Day 4
% MYH area
D)
ATF4 / Vinculin (A.U.)
ATF4
Vinculin
E)
SOD2 / Vinculin (A.U.)
SOD2
F)
GPX4 / Vinculin (A.U.)
GPX4

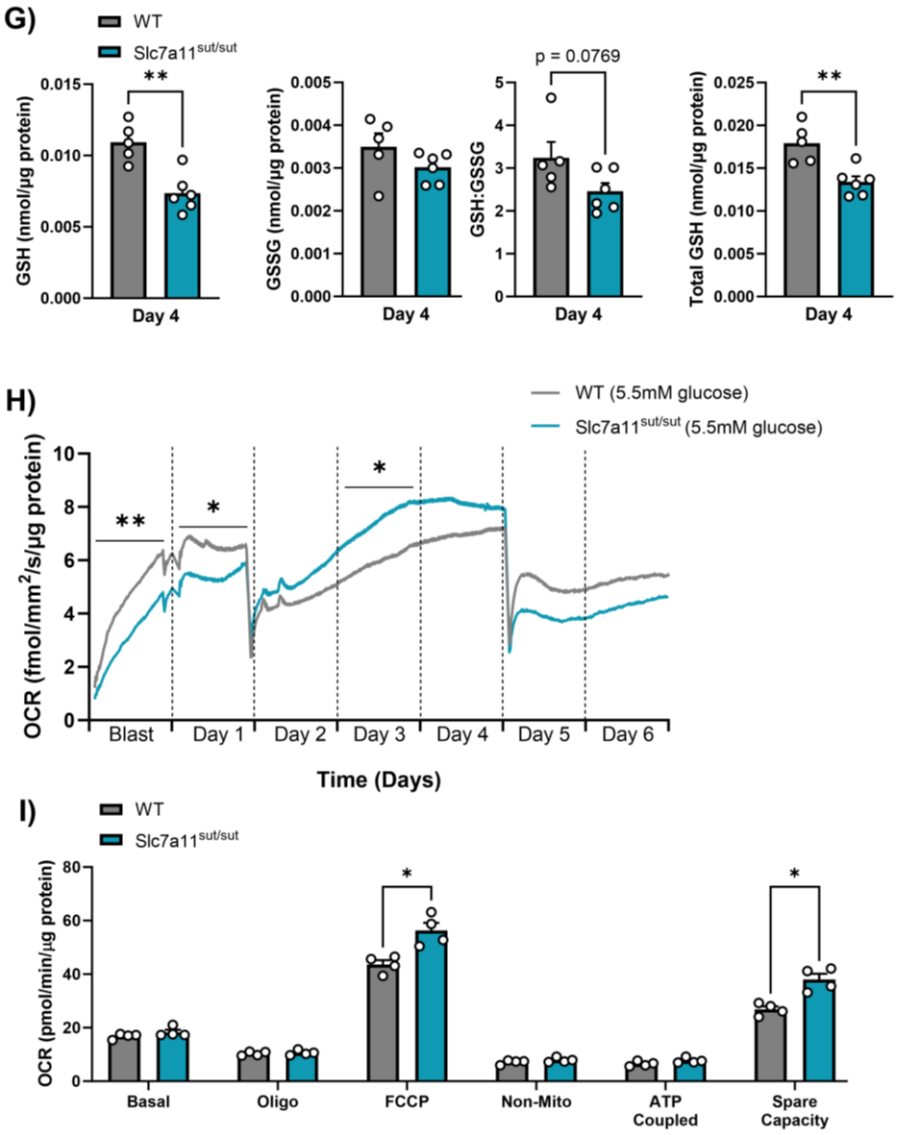
G)
WT
Slc7a11sut/sut
GSH (nmol/µg protein)
GSSG (nmol/µg protein)
GSH:GSSG
p = 0.0769
Total GSH (nmol/µg protein)
Day 4
H)
WT (5.5mM glucose)
Slc7a11sut/sut (5.5mM glucose)
OCR (fmol/mm2/s/µg protein)
Blast
Day 1
Day 2
Day 3
Day 4
Day 5
Day 6
Time (Days)
I)
OCR (pmol/min/µg protein)
Basal
Oligo
FCCP
Non-Mito
ATP Coupled
Spare Capacity
J)
2NBDG Uptake/ µg protein

Figure 2.2. Absence of Functional xCT Inhibits Proliferation but Potentiates Myogenesis
Primary MuSCs were isolated from Slc7a11$^{sut/sut}$ and WT muscle. Myotubes were differentiated under normal physiological glucose concentrations (5.5 mM glucose). **(A)** Real-time measurement of primary myoblasts confluence using an Incucyte® live cell imager. Two-way ANOVA with Tukey post-hoc tests. **(B)** Immunofluorescence analyses of Pax7 (red), EdU+ (purple), and DAPI (blue) in proliferating myoblasts and myotubes at day 1 of differentiation, scale bar = 50 μm, n = 3. **(C)** Immunofluorescence analyses of myosin (green) and DAPI (blue) in differentiating myotubes at days 1, 2, and 4 of differentiation. The myosin-positive area as a percent of the total area analyzed is plotted, scale bar = 150 μm, n = 6. **(D-F)** Immunoblot of primary myoblasts and myotubes at day 2 and day 4 of differentiation against **(D)** ATF4, **(E)** SOD2, and **(F)** GPx4, two-way RM ANOVA with post hoc Tukey HSD tests (B-F). **(G)** Reduced glutathione (GSH), oxidized glutathione (GSSG), total glutathione (GSH+2*GSSG), and the GSH: GSSG ratio in primary myotubes differentiated for 4 days, two-tailed Student's t-tests, n = 5-6. **(H)** Continuous oxygen consumption rates (OCRs) were measured using a RESIPHER real-time cell analyzer throughout myotube differentiation (day 1 to day 7), two-tailed Student's t-tests, n = 4. **(I)** OCR measured in myotubes using a Seahorse analyzer differentiated for 4 days, one-way RM ANOVA with post hoc Tukey HSD tests, n = 4. **(J)** Glucose uptake rate measured as the rate of increase in (2-(N-(7-nitrobenz-2-oxa-1,3-diazol-4-yl) amino)-2-deoxyglucose (2-NBDG) fluorescence intensity in primary myotubes differentiated for 4 days, two-tailed student's t-test, n = 3. Results are presented as mean ± SEM, *p < 0.05, **p < 0.01, ***p < 0.001, ****p < 0.001.

2.5.3 In vivo Evidence of Enhanced Myogenesis in the Absence of xCT Function

To determine if xCT contributes to skeletal muscle regenerative capacity *in vivo*, we induced injury with cardiotoxin injections in the TA muscle in Slc7a11$^{sut/sut}$ and WT mice. Prior to injury, Slc7a11$^{sut/sut}$ and WT mice had similar muscle cross-sectional areas (**Supplementary Figure 2.3A**). Four days after cardiotoxin-induced muscle injury, immunofluorescent analyses of myogenic markers revealed that Slc7a11$^{sut/sut}$ muscle had similar levels of Pax7^{+} cells, but higher levels of both MyoD^{+} and MyoG^{+} cells compared to injured WT muscle, indicating greater MuSC activation and commitment to myogenesis (**Figure 2.3A and Supplementary Figure 2.3B**). At 7 days post-injury, Slc7a11$^{sut/sut}$ muscle had a lower proportion Pax7^{+} cells than injured WT muscle, but the proportion of MyoD^{+} cells remained higher in Slc7a11$^{sut/sut}$ (**Figure 2.3B and Supplementary Figure 2.3C**).

Regeneration efficiency, as determined by the cross-sectional area (CSA) of mature myofibers at 21 days post-injury, revealed that Slc7a11$^{sut/sut}$ myofibers were larger in cross-sectional area compared to WT muscle (**Figure 2.3C**). Stratification of the frequency distribution in CSA of regenerating fibers revealed that Slc7a11$^{sut/sut}$ muscle had a lower proportion of small fibers (<1000 μm^2) compared to WT muscle (**Figure 2.3C**), consistent with enhanced regenerative capacity in Slc7a11$^{sut/sut}$ muscle. To assess the cellular basis of the increased regeneration efficiency in Slc7a11$^{sut/sut}$ muscle, we sought to determine regenerating muscle fiber type and myofiber CSA at 21 days post-injury. Immunohistochemical analysis of the uninjured muscle revealed that Slc7a11$^{sut/sut}$ had a lower proportion of type IIa fibers (mixed fast oxidative/glycolytic) compared to WT muscle (**Figure 2.3D**), but the proportions of types IIb and IIx (fast, glycolytic) were similar between genotypes **(Figure 2.3D**). In injured muscle, the proportion of type IIa muscle fibres was similar between Slc7a11$^{sut/sut}$ and WT, despite a ~40% increase in comparison to uninjured Slc7a11$^{sut/sut}$ which did not reach statistical significance (p=0.084) (**Figure 2.3D**). Taken together, the greater number of activated and committed MuSCs at days 4 and 7 post-injury and the

increased CSA of mature myofibers at day 21 post-injury in Slc7a11$^{sut/sut}$ muscle is consistent with improved muscle regeneration in Slc7a11$^{sut/sut}$ mice.

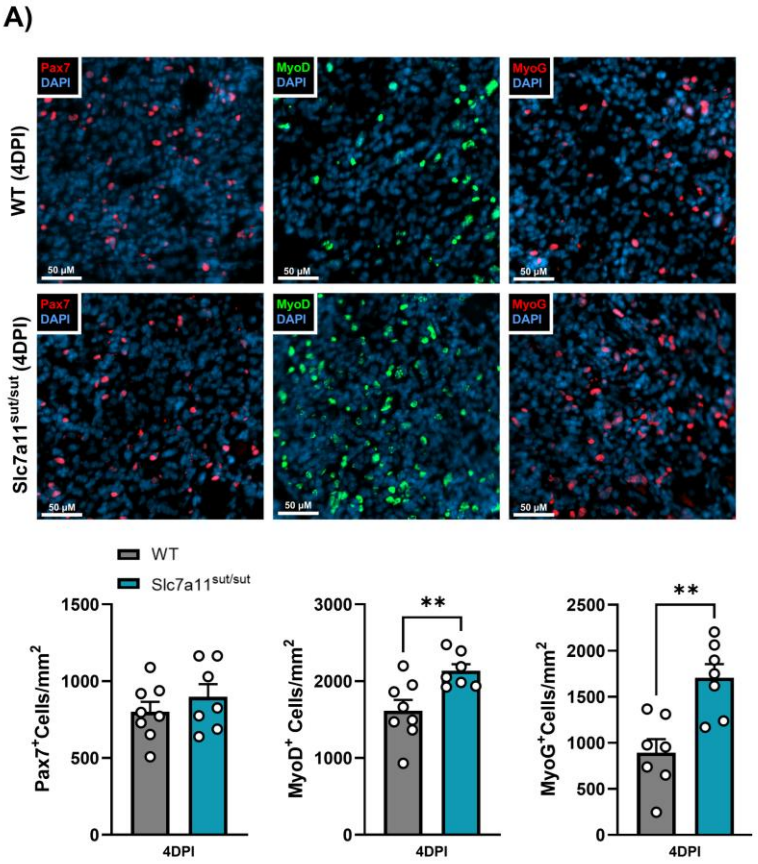
A)
Pax7
DAPI
MyoD
DAPI
MyoG
DAPI
WT (4DPI)
Slc7a11sut/sut (4DPI)
50 µM
WT
Slc7a11sut/sut
Pax7+Cells/mm2
MyoD+ Cells/mm2
MyoG+Cells/mm2
**
4DPI

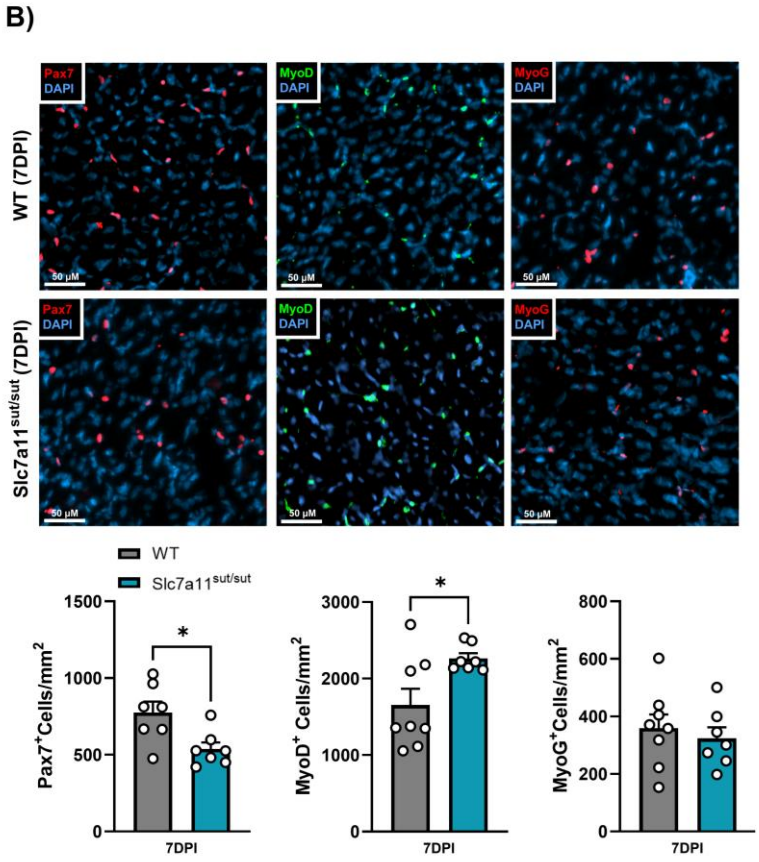
B)
Pax7
DAPI
MyoD
DAPI
MyoG
DAPI
WT (7DPI)
Slc7a11sut/sut (7DPI)
50 µM
WT
Slc7a11sut/sut
Pax7+Cells/mm2
MyoD+ Cells/mm2
MyoG+Cells/mm2
*
7DPI

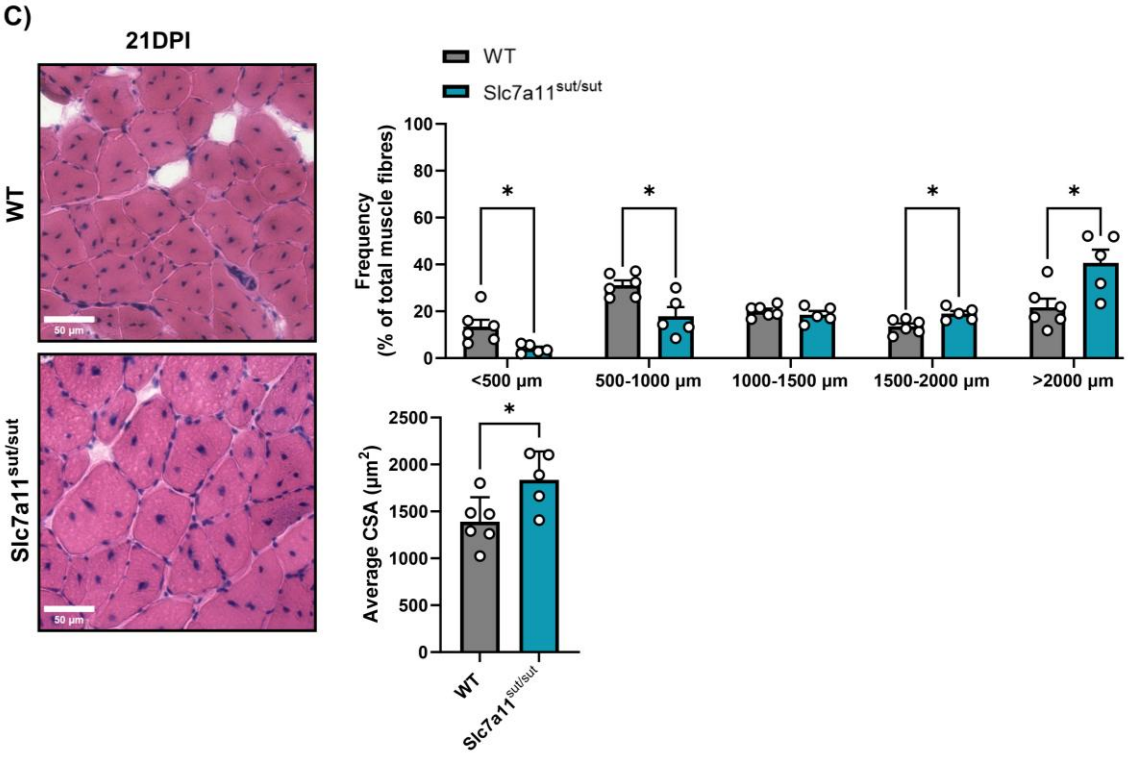
C)
21DPI
WT
Slc7a11sut/sut
50 µm
WT
Slc7a11sut/sut
Frequency (% of total muscle fibres)
100
80
60
40
20
0
*
*
*
*
<500 µm
500-1000 µm
1000-1500 µm
1500-2000 µm
>2000 µm
Average CSA (µm2)
2500
2000
1500
1000
500
0
*
WT
Slc7a11sut/sut

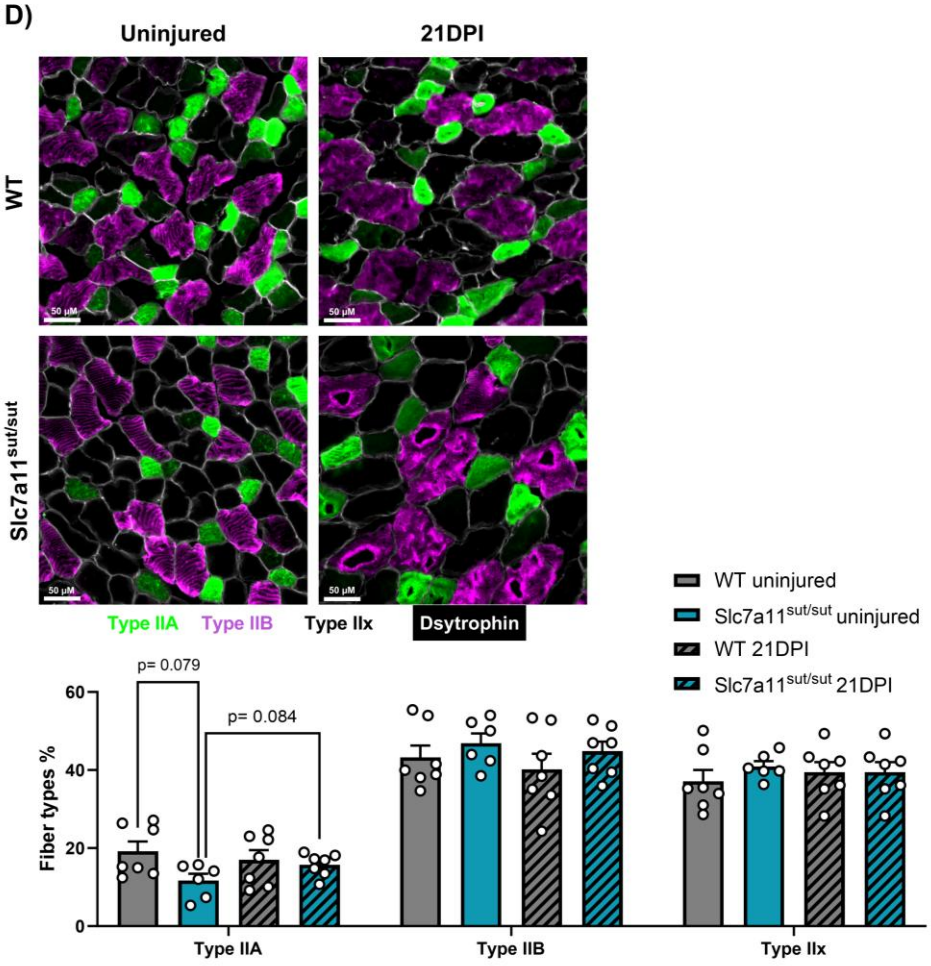
D)
Uninjured
21DPI
WT
Slc7a11sut/sut
50 µM
Type IIA
Type IIB
Type IIx
Dsytrophin
WT uninjured
Slc7a11sut/sut uninjured
WT 21DPI
Slc7a11sut/sut 21DPI
p= 0.079
p= 0.084
Fiber types %
60
40
20
0
Type IIA
Type IIB
Type IIx

Figure 2.3. Absence of xCT Enhances myogenesis Following Cardiotoxin-induced Muscle Injury
Immunofluorescence analyses of myogenic markers (Pax7, MyoD, and MyoG) and DAPI (blue) in *Tibialis anterior* (TA) muscle sections **(A)** at day 4 and **(B)** at day 7 post-cardiotoxin-induced injury. Scale bar = 50 µm. Two-tailed Student's t-tests, n =7-8. DPI=days post-injury. **(C)** Hematoxylin and eosin (H&E) staining of muscle sections from TA muscles after 21 days of cardiotoxin injection (21DPI). Frequency distribution of myofiber cross-sectional area (CSA) and average myofiber CSA are plotted. Scale bar = 50 µm. Two-tailed Student's t-tests, n = 5-6. **(D)** Fiber types in uninjured and 21 DPI injured TA muscle sections showing MYH type IIA (green), MYH type IIB (purple), MYH type IIx (unstained), and dystrophin (white), scale bar = 50 µm. Two-way ANOVA with post hoc Tukey HSD test, n = 5-8. Results are presented as mean ± SEM, *$p < 0.05$, **$p < 0.01$, ***$p < 0.001$, ****$p < 0.0001$.

2.5.4 Increased Insulin Sensitivity and Impaired Muscle Mitochondrial Energetics Response to Exercise Training in xCT deficient Mice

To assess the *in vivo* metabolic implications of xCT deficiency in mice we next examined response to a 5-week exercise training protocol in Slc7a11$^{sut/sut}$ and WT mice (**Figure 2.4A**). First, we examined the impact of the xCT mutation on whole-body glucose tolerance and insulin sensitivity, hypothesizing greater insulin sensitivity in Slc7a11$^{sut/sut}$ mice, given our findings from cultured muscle cells. WT and Slc7a11$^{sut/sut}$ mice exhibited comparable glucose tolerance (**Supplementary Figure 2.4A**). However, Slc7a11$^{sut/sut}$ mice demonstrated greater glucose disposal in response to an insulin tolerance test (ITT) before the exercise intervention, an effect that was even more pronounced after exercise training (**Figure 2.4B**). Exercise training increased soleus mass when normalized to body weight in Slc7a11$^{sut/sut}$ mice only, but not the weights of the gastrocnemius or TA (**Supplementary Figure 2.4B)**.

High-resolution respirometry (HRR) conducted on permeabilized TA fibers revealed similar respiratory rates between non-exercised WT and Slc7a11$^{sut/sut}$ mice. In contrast, exercise training increased complex I and complex I + II- driven oxidative phosphorylation (CI OXPHOS, CI+CII OXPHOS, respectively) and maximal mitochondrial respiration in WT TA muscle, but not in Slc7a11$^{sut/sut}$ mice (**Figure 2.4C**). The enhanced respiratory capacity in WT but not Slc7a11$^{sut/sut}$ muscle was associated with a strong trend for lower CI OXPHOS and CI+CII OXPHOS in exercised Slc7a11$^{sut/sut}$ muscle compared to exercised WT muscle (**Figure 2.4C**). To test if this trend for decreased complex I function was attributable to intrinsic dysfunction or decreased NADH availability, we next quantified the maximal catalytic oxidation of NADH by complex I in isolated skeletal muscle mitochondria. Similar to our observations in permeabilized muscle fibres, complex I-specific activity was similar between groups in non-exercised mice, but increased after exercise training in mitochondria isolated from WT but not Slc7a11$^{sut/sut}$ muscle (**Figure 2.4D**). Protein levels of key electron transport chain subunits were comparable between non-exercised and exercised WT and Slc7a11$^{sut/sut}$ mice (**Supplementary Figure 2.4C**), suggesting that

differences were not due to complex-specific defects. However, the tendency of lower respiratory capacity in Slc7a11$^{sut/sut}$ muscle after exercise may be attributable to an unanticipated decrease in mitochondrial density, as citrate synthase (CS) activity, a marker of mitochondrial content was lower in exercised Slc7a11$^{sut/sut}$ TA muscle compared to non-exercised Slc7a11$^{sut/sut}$ mice (**Figure 2.4E**).

Given the absence of training-induced increases in OXPHOS in Slc7a11$^{sut/sut}$ mice, we quantified LDH activity as a proxy measure of muscle glycolytic capacity. LDH activity was higher in WT muscle than Slc7a11$^{sut/sut}$ muscle in non-exercised mice. However, the exercise intervention induced a pronounced increase in LDH activity in Slc7a11$^{sut/sut}$ muscle (**Figure 2.4F**). Interestingly, levels of GSH and GSSG in the TA muscle remained similar across all groups, indicating compensatory mechanisms developed by Slc7a11$^{sut/sut}$ mice (**Supplementary Figure 2.4D**).

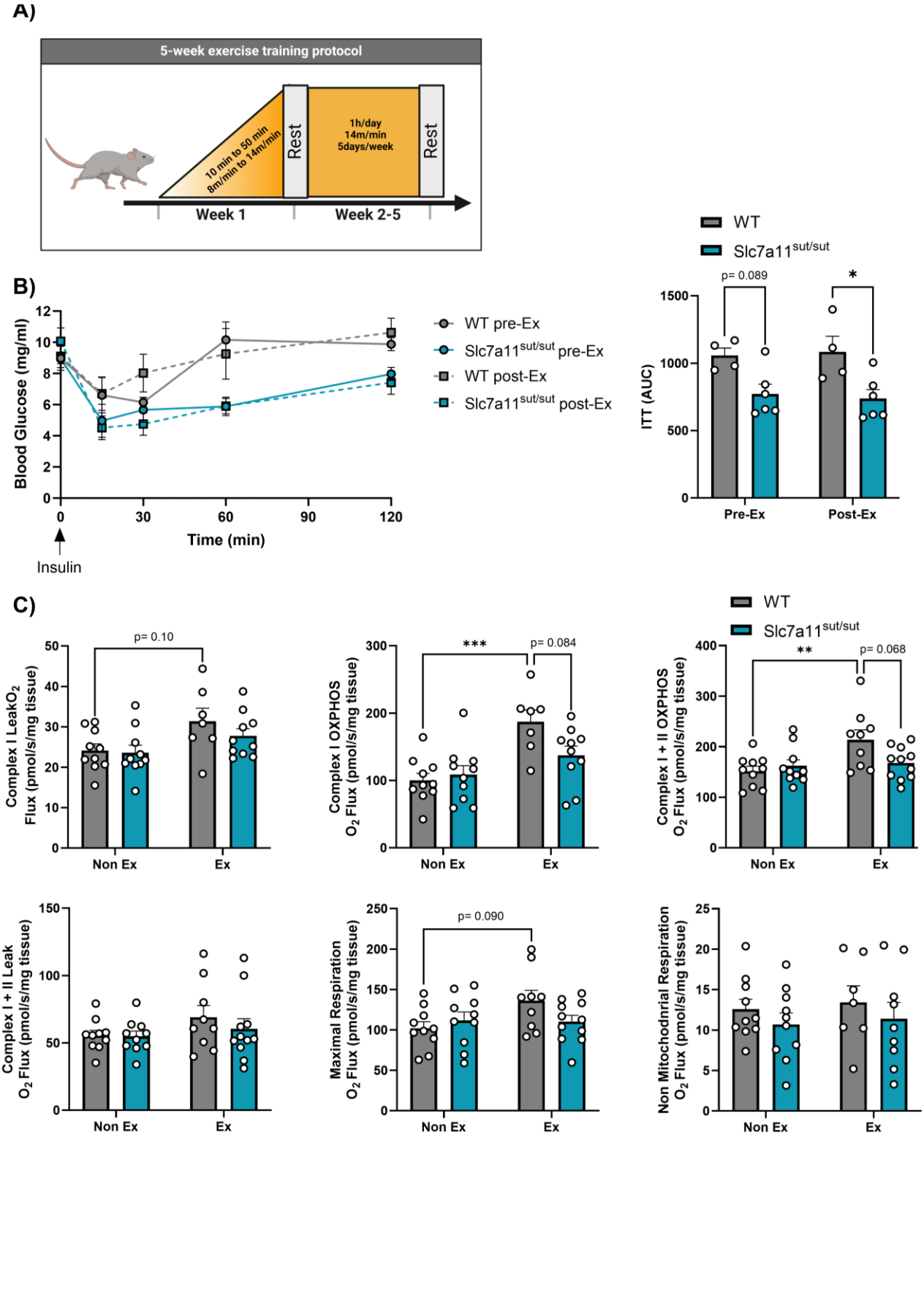
A)
5-week exercise training protocol
10 min to 50 min
8m/min to 14m/min
Rest
1h/day
14m/min
5days/week
Rest
Week 1
Week 2-5
B)
Blood Glucose (mg/ml)
Time (min)
Insulin
WT pre-Ex
Slc7a11sut/sut pre-Ex
WT post-Ex
Slc7a11sut/sut post-Ex
WT
Slc7a11sut/sut
p= 0.089
*
ITT (AUC)
Pre-Ex
Post-Ex
C)
WT
Slc7a11sut/sut
Complex I LeakO2 Flux (pmol/s/mg tissue)
p= 0.10
Complex I OXPHOS O2 Flux (pmol/s/mg tissue)
***
p= 0.084
Complex I + II OXPHOS O2 Flux (pmol/s/mg tissue)
**
p= 0.068
Complex I + II Leak O2 Flux (pmol/s/mg tissue)
Maximal Respiration O2 Flux (pmol/s/mg tissue)
p= 0.090
Non Mitochodnrial Respiration O2 Flux (pmol/s/mg tissue)
Non Ex
Ex

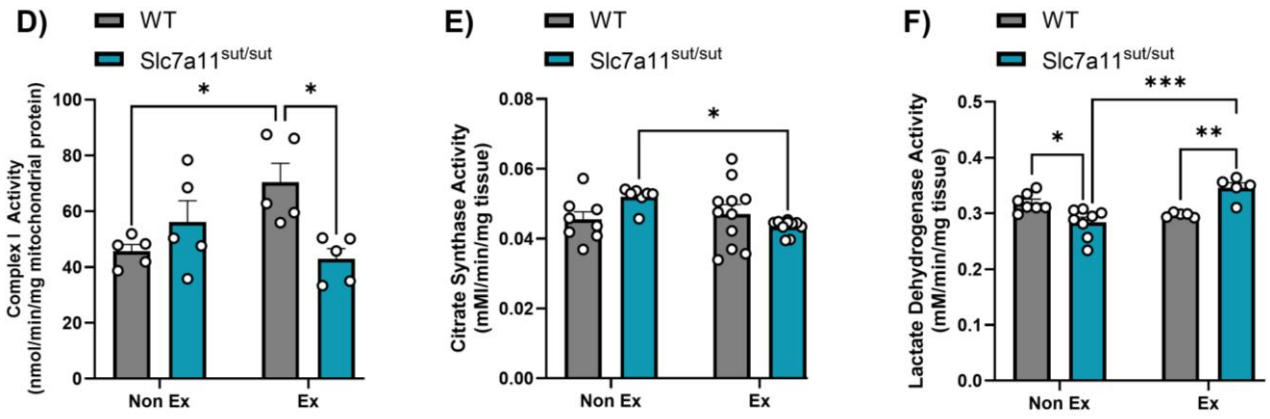

Figure 2.4. Increased Insulin Sensitivity and Impaired Muscle Mitochondrial Energetics in Response to Exercise Training in Slc7a11$^{sut/sut}$ mice

(A) Overall design schematic for the 5-week mice exercise training intervention. **(B)** Insulin sensitivity test (ITT) showing blood glucose levels in response to insulin at different time points (0, 15 min, 30 min, 60 min, 120 min) in pre-exercised (pre-Ex) and post- exercised (post-Ex) WT and Slc7a11$^{sut/sut}$ mice, n = 4-6. **(C)** High-resolution respiratory flux per mg of saponin-permeabilized TA muscle of non-exercised (Non-Ex) and exercised (Ex) WT and Slc7a11$^{sut/sut}$ mice, n =7-11. **(D-E)** Enzyme activities in TA of non-exercised and exercised mice WT and Slc7a11$^{sut/sut}$ mice of **(D)** Complex I, **(E)** Citrate synthase and **(F)** lactate dehydrogenase.

The statistical significance of the differences between groups was determined by two-way ANOVA with post hoc Tukey HSD test. Results are presented as mean ± SEM, *p < 0.05, **p < 0.01, ***p < 0.001, ****p < 0.0001. n = 8-11.

2.6 Discussion

Cellular redox and metabolic remodeling are essential for maintaining skeletal muscle health and regeneration during times of physiological stress such as exercise and injury [9,60]. Here, we demonstrate that xCT plays a crucial role in maintaining the pool of MuSCs by supporting myoblast proliferation, whereas xCT expression is rapidly downregulated during muscle cell differentiation. Moreover, our results from Slc7a11$^{sut/sut}$ muscle and primary myocytes indicate that the absence of xCT leads to enhanced muscle cell differentiation and tissue regeneration while altering cellular metabolism.

Myoblast proliferation requires high levels of GSH to maintain cellular redox homeostasis

MuSC activation and cell cycle progression is mediated by an intrinsic metabolic redox cycle that requires high levels of GSH to maintain cellular redox homeostasis, participate in thiol–disulfide exchange reactions during cell proliferation, and regulate numerous redox-controlled transcription factors [57,61–64]. The initial transition of G0 to G1 requires cell-type-specific, redox-dependent signaling pathways to induce transcription of cell cycle genes, including CDKs. GSH is recruited from the cytoplasm into the nucleus during the G1 phase to participate in redox reactions and mitigate oxidative DNA damage during active replication and division [65,66]. High concentrations of H_2O_2 can permanently induce cell cycle arrest [67], and depleting GSH in cultured cells inhibits the G1/S transition [68]. Primary melanocytes isolated from Slc7a11$^{sut/sut}$ mice have ~20-30% lower rates of cystine import and decreased intracellular GSH levels than cells isolated from WT controls [53], suggesting that the senescence we observed in isolated Slc7a11$^{sut/sut}$ MuSCs cultured in media without a reducing agent may be attributable to limited intracellular cysteine availability to support the increased demands for *de novo* GSH synthesis [16]. Similarly, the lower Pax7^{+}EdU^{+} number of myoblasts we observed in Slc7a11$^{sut/sut}$ MuSCs supports the idea that xCT is critical in supporting high GSH demands during cell proliferation.

Perturbed GSH metabolism contributes to lower viability and slower cell cycle re-entry of muscle MuSCs and is associated with SC dysfunction during aging [15].

GSSG acts as a redox-sensitive switch to promote myotube differentiation

When proliferating myoblasts reach confluence, the cell cycle is repressed and GSH is redistributed between the nucleus and the cytoplasm [65], which alleviates the high demand for GSH. The rapid downregulation of xCT during differentiation that we observed in both our computational and time course analyses of C2C12 myoblasts suggests that cysteine availability to support glutathione metabolism is dramatically lower during differentiation. Commitment to differentiation is accompanied by increases in mitochondrial density and complex-I generated ROS [13,69–71]. Elevations in ROS during myogenesis activate NF-κB to induce SOD2 expression to catalyse the conversion of superoxide ($O_2^{\cdot-}$) into H_2O_2 [13,72,73], and we observed a trend for elevated SOD2 expression during early differentiation in $Slc7a11^{sut/sut}$ myotubes. Subsequently, increasing activity of GPxs reduce H_2O_2 to H_2O, resulting in elevated GSSG levels. Both H_2O_2 and GSSG are key signaling molecules that can reversibly oxidize protein thiol residues that act as a redox-sensitive "switches" to control cellular processes, including differentiation [74–77]. Specifically, increases in H_2O_2 and GSSG can stimulate important steps in initiating muscle differentiation, including MAPK and NF-κB signaling, as well as activating protein 1 (AP-1) assembly of heterodimers that are composed of Jun, Fos, ATF and MAF proteins [78,79]. Our enrichment analysis revealed that *Slc7a11* is negatively correlated with genes involved in MAPK, PI3K-AKT, and FoxO signalling pathways, which are also involved in triggering myogenesis through the exit of myoblasts from the cell cycle for terminal differentiation, which altogether supports opposing roles for xCT in proliferation vs. differentiation.

Upregulation of the NRF2-ATF4 axis mediates myotube stress response

Evidence supports the notion that redox reactions are particularly important in coordinating muscle regenerative processes following acute muscle injury. During the early stages of myotoxin-induced injury, rapid MuSC proliferation is required to provide a sufficient pool of myogenic progenitors. The decreased number of PAX7+ cells in Slc7a11$^{sut/sut}$ injured muscle at 7 DPI indicates that the pool of myogenic progenitors is depleted. This diminishing pool of myogenic progenitors is likely attributable to impaired cell proliferation as well as a more rapid myogenic commitment, as evidenced by increases in MyoD/MyoG during early regeneration, and greater TA cross-sectional area in regenerated muscle. During myogenesis, increases in MAPK, PI3K-AKT, and NF-κB signaling induce NRF2, a critical regulator of the antioxidant response [80]. Subsequently, NRF2 can bind to antioxidant response element (ARE) sequences in the promoter region of >250 target genes [80], including those involved in GSH synthesis and ATF4, a member of the AP-1 complex [81]. While ablation of NRF2 has been shown to exacerbate exercise-induced oxidative stress and impair muscle regenerative capacity [82], increased NRF2 activation via sulforaphane has also been shown to impair myogenesis by inhibiting basal ROS signaling and promoting reductive stress [22]. The NRF2-ATF4 axis is particularly important in response to various stress conditions, such as amino acid starvation, as ATF4 regulates serine biosynthesis and activates the pentose phosphate pathway to support GSH and NADPH production [83,84]. In skeletal muscle endothelial cells, restricting sulfur amino acids increases glycolysis and glucose uptake while inhibiting OXPHOS in an ATF4-dependent manner [85]. Thus, our observations of higher ATF4 expression in Slc7a11$^{sut/sut}$ myoblasts may reflect a compensatory mechanism to support GSH production. Moreover, the increased glucose uptake and glycolytic capacity are in line with the upregulation of the NRF2-ATF4 stress response. Furthermore, primary myotubes from Slc7a11$^{sut/sut}$ mice demonstrated higher respiration rates compared to WT, which may be due to increased intracellular glutamate availability to support TCA cycle metabolism [32].

Impaired mitochondrial adaptations to exercise training

Exercise training elicits beneficial adaptations in skeletal muscle mitochondrial capacity by enhancing mitochondrial biogenesis and respiratory function [86–88]. The lack of improvements in mitochondrial capacity in Slc7a11$^{sut/sut}$ muscle following exercise training combined with increased LDH activity, suggest a potential shift towards glycolysis, which is altogether consistent with the conclusion that Slc7a11$^{sut/sut}$ mice have an impaired ability to respond to prolonged physiological stressors. Mitochondria and NADPH oxidases generate ROS during aerobic exercise, which are necessary to stimulate mitochondrial biogenesis and strengthen endogenous antioxidant defense systems. Therefore, it is plausible that the repeated exercise training sessions generated excessive oxidative stress, rendering impaired bioenergetic responses typically observed in response to exercise training. Alternatively, post-translational modifications to complex I subunits, such as protein glutathionylation and acetylation, can reversibly modify complex I activity, a mechanism proposed to regulate ROS formation [89,90]. Of note, decreases NAD^+ availability and increases in NADH can promote cellular senescence in stem cells due to lower NAD^+ availability to support NAD^+-dependent enzymes (e.g. sirtuins) and is associated with lower mitochondrial quality and biogenesis [91–93]. Thus, while the observed complex I dysfunction may not be related to the immediate availability of NADH for oxidation, decreases in NAD^+ may contribute to the impaired myoblast proliferation and exercise bioenergetic adaptation phenotype in the Slc7a11$^{sut/sut}$ mice [6].

The Slc7a11$^{sut/sut}$ mice exhibited overall a mild phenotype, with moderately lower fat mass and enhanced glucose disposal. Similar to our results, *Slc7a11* knockout mice (xCT$^{-/-}$) were found to have increased glucose disposal despite lower insulin secretion attributed to mild ER stress in beta cells [94]. As insulin can also promote myogenesis, the enhanced insulin response observed in Slc7a11$^{sut/sut}$ mice may be an important factor in the greater myogenesis observed in these mice. Studies in aged mice have revealed

that Slc7a11$^{sut/sut}$ mice have increased lifespans and delayed priming of the innate immune system, despite high plasma cystine concentrations and an increased cystine/cysteine ratio [95]. However, deficiency in xCT has no apparent effect on age-related loss of muscle mass and strength [95]. The overall mild phenotype observed in Slc7a11$^{sut/sut}$ mice suggests that *de novo* cysteine synthesis via an alternative metabolic pathway, such as reverse transsulfuration of methionine to cysteine [96], can compensate for the limited cystine uptake *in vivo*. However, the capacity of cysteine synthesis via transsulfuration when extracellular cystine uptake is compromised is dependent upon CBS expression [97].

In conclusion, our results reveal contrasting roles for xCT in the proliferation and differentiation of MuSCs. Specifically, we demonstrate that xCT is required to support the high demand for GSH during MuSC proliferation and self-renewal. However, during myotube differentiation, our findings show that xCT expression is rapidly downregulated as the cellular environment switches to a more oxidized phenotype to facilitate myogenic progression, which is dependent upon redox-sensitive signalling. Moreover, the absence of xCT enhances myogenic differentiation and muscle regeneration. The enhanced insulin-stimulated glucose uptake in xCT-mutant mice pre and post-5-week exercise training, and blunted muscle mitochondrial synthesis and respiration in response to training highlight the importance of maintaining cellular redox homeostasis for integrated metabolic adaptations in muscle. Taken together, these results highlight the role of cellular redox homeostasis in myogenic differentiation and may have significant implications in developing novel interventions to improve redox homeostasis in muscle dystrophies, chronic metabolic disorders, and age-related muscle loss.

2.7. References

[1] N.A. Dumont, C.F. Bentzinger, M.C. Sincennes, M.A. Rudnicki, Satellite Cells and Skeletal Muscle Regeneration, Compr Physiol 5 (2015) 1027–1059. https://doi.org/10.1002/CPHY.C140068.

[2] H. Yin, F. Price, M.A. Rudnicki, Satellite Cells and the Muscle Stem Cell Niche, Physiol Rev 93 (2013) 23. https://doi.org/10.1152/PHYSREV.00043.2011.

[3] J. Sin, A.M. Andres, D.J.R. Taylo R, T. Weston, Y. Hiraumi, A. Stotland, B.J. Kim, C. Huang, K.S. Doran, R.A. Gottlieb, Mitophagy is required for mitochondrial biogenesis and myogenic differentiation of C2C12 myoblasts, Autophagy 12 (2016) 369–380. https://doi.org/10.1080/15548627.2015.1115172.

[4] A.H.V. Remels, R.C.J. Langen, P. Schrauwen, G. Schaart, A.M.W.J. Schols, H.R. Gosker, Regulation of mitochondrial biogenesis during myogenesis, Mol Cell Endocrinol 315 (2010) 113–120. https://doi.org/10.1016/J.MCE.2009.09.029.

[5] M.C. Sincennes, C.E. Brun, A.Y.T. Lin, T. Rosembert, D. Datzkiw, J. Saber, H. Ming, Y. ichi Kawabe, M.A. Rudnicki, Acetylation of PAX7 controls muscle stem cell self-renewal and differentiation potential in mice, Nature Communications 2021 12:1 12 (2021) 1–15. https://doi.org/10.1038/s41467-021-23577-z.

[6] J.G. Ryall, S. Dell'Orso, A. Derfoul, A. Juan, H. Zare, X. Feng, D. Clermont, M. Koulnis, G. Gutierrez-Cruz, M. Fulco, V. Sartorelli, The NAD+-Dependent SIRT1 Deacetylase Translates a Metabolic Switch into Regulatory Epigenetics in Skeletal Muscle Stem Cells, Cell Stem Cell 16 (2015) 171–183. https://doi.org/10.1016/J.STEM.2014.12.004.

[7] A. L'honoré, P.H. Commère, J.F. Ouimette, D. Montarras, J. Drouin, M. Buckingham, Redox Regulation by Pitx2 and Pitx3 Is Critical for Fetal Myogenesis, Dev Cell 29 (2014) 392–405. https://doi.org/10.1016/J.DEVCEL.2014.04.006.

[8] Y.J. Piao, Y.H. Seo, F. Hong, J.H. Kim, Y.J. Kim, M.H. Kang, B.S. Kim, S.A. Jo, I. Jo, D.M. Jue, I. Kang, J. Ha, S.S. Kim, Nox 2 stimulates muscle differentiation via NF-kappaB/iNOS pathway, Free Radic Biol Med 38 (2005) 989–1001. https://doi.org/10.1016/J.FREERADBIOMED.2004.11.011.

[9] E. Le Moal, V. Pialoux, G. Juban, C. Groussard, H. Zouhal, B. Chazaud, R. Mounier, Redox Control of Skeletal Muscle Regeneration, Antioxid Redox Signal 27 (2017) 276. https://doi.org/10.1089/ARS.2016.6782.

[10] W.C. Burhans, N.H. Heintz, The cell cycle is a redox cycle: linking phase-specific targets to cell fate, Free Radic Biol Med 47 (2009) 1282–1293. https://doi.org/10.1016/J.FREERADBIOMED.2009.05.026.

[11] D. Malinska, A.P. Kudin, M. Bejtka, W.S. Kunz, Changes in mitochondrial reactive oxygen species synthesis during differentiation of skeletal muscle cells, Mitochondrion 12 (2012) 144–148. https://doi.org/10.1016/J.MITO.2011.06.015.

[12] P. Fortini, C. Ferretti, E. Iorio, M. Cagnin, L. Garribba, D. Pietraforte, M. Falchi, B. Pascucci, S. Baccarini, F. Morani, S. Phadngam, G. De Luca, C. Isidoro, E. Dogliotti, The fine tuning of metabolism, autophagy and differentiation during in vitro myogenesis, Cell Death & Disease 2016 7:3 7 (2016) e2168–e2168. https://doi.org/10.1038/cddis.2016.50.

[13] S. Lee, E. Tak, J. Lee, M. Rashid, M.P. Murphy, J. Ha, S.S. Kim, Mitochondrial H2O2 generated from electron transport chain complex I stimulates muscle differentiation, Cell Research 2011 21:5 21 (2011) 817–834. https://doi.org/10.1038/cr.2011.55.

[14] S.M. Beer, E.R. Taylor, S.E. Brown, C.C. Dahm, N.J. Costa, M.J. Runswick, M.P. Murphy, Glutaredoxin 2 catalyzes the reversible oxidation and glutathionylation of mitochondrial membrane thiol proteins: implications for mitochondrial redox regulation and antioxidant DEFENSE, J Biol Chem 279 (2004) 47939–47951. https://doi.org/10.1074/JBC.M408011200.
[15] D.I. Benjamin, J.O. Brett, P. Both, J.S. Benjamin, H.L. Ishak, J. Kang, S. Kim, M. Chung, M. Arjona, C.W. Nutter, J.H. Tan, A.K. Krishnan, H. Dulay, S.M. Louie, A. de Morree, D.K. Nomura, T.A. Rando, Multiomics reveals glutathione metabolism as a driver of bimodality during stem cell aging, Cell Metab 35 (2023) 472-486.e6. https://doi.org/10.1016/J.CMET.2023.02.001.
[16] X. Liu, Y. Zhang, L. Zhuang, K. Olszewski, B. Gan, NADPH debt drives redox bankruptcy: SLC7A11/xCT-mediated cystine uptake as a double-edged sword in cellular redox regulation, Genes Dis 8 (2021) 731. https://doi.org/10.1016/J.GENDIS.2020.11.010.
[17] J. Lewerenz, S.J. Hewett, Y. Huang, M. Lambros, P.W. Gout, P.W. Kalivas, A. Massie, I. Smolders, A. Methner, M. Pergande, S.B. Smith, V. Ganapathy, P. Maher, The cystine/glutamate antiporter system xc- in health and disease: From molecular mechanisms to novel therapeutic opportunities, Antioxid Redox Signal 18 (2013) 522–555. https://doi.org/10.1089/ARS.2011.4391
[18] H. Sato, M. Tamba, T. Ishii, S. Bannai, Cloning and expression of a plasma membrane cystine/glutamate exchange transporter composed of two distinct proteins, Journal of Biological Chemistry 274 (1999) 11455–11458. https://doi.org/10.1074/jbc.274.17.11455.
[19] D. Fotiadis, Y. Kanai, M. Palacín, The SLC3 and SLC7 families of amino acid transporters, Mol Aspects Med 34 (2013) 139–158. https://doi.org/10.1016/J.MAM.2012.10.007.
[20] F. Verrey, E.I. Closs, C.A. Wagner, M. Palacin, H. Endou, Y. Kanai, CATs and HATs: The SLC7 family of amino acid transporters, Pflugers Arch 447 (2004) 532–542. https://doi.org/10.1007/S00424-003-1086-Z
[21] E. Ardite, J.A. Barbera, J. Roca, J.C. Fernández-Checa, Glutathione depletion impairs myogenic differentiation of murine skeletal muscle C2C12 cells through sustained NF-kappaB activation, Am J Pathol 165 (2004) 719–728. https://doi.org/10.1016/S0002-9440(10)63335-4.
[22] N.S. Rajasekaran, S.B. Shelar, D.P. Jones, J.R. Hoidal, Reductive stress impairs myogenic differentiation, Redox Biol 34 (2020). https://doi.org/10.1016/J.REDOX.2020.101492.
[23] W. Huber, V.J. Carey, R. Gentleman, S. Anders, M. Carlson, B.S. Carvalho, H.C. Bravo, S. Davis, L. Gatto, T. Girke, R. Gottardo, F. Hahne, K.D. Hansen, R.A. Irizarry, M. Lawrence, M.I. Love, J. MaCdonald, V. Obenchain, A.K. Oleš, H. Pagès, A. Reyes, P. Shannon, G.K. Smyth, D. Tenenbaum, L. Waldron, M. Morgan, Orchestrating high-throughput genomic analysis with Bioconductor, Nature Methods 2015 12:2 12 (2015) 115–121. https://doi.org/10.1038/nmeth.3252.
[24] D. Sean, P.S. Meltzer, GEOquery: a bridge between the Gene Expression Omnibus (GEO) and BioConductor, Bioinformatics 23 (2007) 1846–1847. https://doi.org/10.1093/BIOINFORMATICS/BTM254.
[25] R Core Team, https://www.R-project.org, R: A Language and Environment for Statistical Computing. R Foundation for Statistical Computing, Vienna, Austria. (2021).
[26] K.K. Tomczak, V.D. Marinescu, M.F. Ramoni, D. Sanoudou, F. Montanaro, M. Han, L.M. Kunkel, I.S. Kohane, A.H. Beggs, Expression profiling and identification of novel genes involved in myogenic differentiation, FASEB J 18 (2004) 403–405. https://doi.org/10.1096/FJ.03-0568FJE.
[27] M.D. Doynova, J.F. Markworth, D. Cameron-Smith, M.H. Vickers, J.M. O'Sullivan, Linkages between changes in the 3D organization of the genome and transcription during myotube differentiation in vitro, Skelet Muscle 7 (2017). https://doi.org/10.1186/S13395-017-0122-1.

[28] I.H.B. Chen, M. Huber, T. Guan, A. Bubeck, L. Gerace, Nuclear envelope transmembrane proteins (NETs) that are up-regulated during myogenesis, BMC Cell Biol 7 (2006). https://doi.org/10.1186/1471-2121-7-38.
[29] M.A. Arya, A.K. Tai, E.C. Wooten, C.D. Parkin, E. Kudryavtseva, G.S. Huggins, Notch pathway activation contributes to inhibition of C2C12 myoblast differentiation by ethanol, PLoS One 8 (2013). https://doi.org/10.1371/JOURNAL.PONE.0071632.
[30] S. Rajan, H.C.P. Dang, H. Djambazian, H. Zuzan, Y. Fedyshyn, T. Ketela, J. Moffat, T.J. Hudson, R. Sladek, Analysis of early C2C12 myogenesis identifies stably and differentially expressed transcriptional regulators whose knock-down inhibits myoblast differentiation, Physiol Genomics 44 (2012) 183–197. https://doi.org/10.1152/PHYSIOLGENOMICS.00093.2011.
[31] X. Zhu, B. Lan, X. Yi, C. He, L. Dang, X. Zhou, Y. Lu, Y. Sun, Z. Liu, X. Bai, K. Zhang, B. Li, M.J. Li, Y. Chen, L. Zhang, HRP2-DPF3a-BAF complex coordinates histone modification and chromatin remodeling to regulate myogenic gene transcription, Nucleic Acids Res 48 (2020) 6563–6582. https://doi.org/10.1093/NAR/GKAA441.
[32] T. Zhang, X. Guan, U.L. Choi, Q. Dong, M.M.T. Lam, J. Zeng, J. Xiong, X. Wang, T.C.W. Poon, H. Zhang, X. Zhang, H. Wang, R. Xie, B. Zhu, G. Li, Phosphorylation of TET2 by AMPK is indispensable in myogenic differentiation, Epigenetics Chromatin 12 (2019). https://doi.org/10.1186/S13072-019-0281-X.
[33] Q. Ma, G.-W. Chirn, J.D. Szustakowski, A. Bakhtiarova, P.A. Kosinski, D. Kemp, N. Nirmala, Uncovering mechanisms of transcriptional regulations by systematic mining of cis regulatory elements with gene expression profiles, BioData Min 1 (2008). https://doi.org/10.1186/1756-0381-1-4.
[34] I. Castiglioni, R. Caccia, J.M. Garcia-Manteiga, G. Ferri, G. Caretti, I. Molineris, K. Nishioka, D. Gabellini, The Trithorax protein Ash1L promotes myoblast fusion by activating Cdon expression, Nat Commun 9 (2018). https://doi.org/10.1038/S41467-018-07313-8.
[35] A. Predeus, O.A. Ivanova, N. V Khromova, A.M. Kiselev, D.E. Polev, N.A. Smolina, A.A. Kostareva, R.I. Dmitrieva, P62Pathway analysis of RNA-sequencing of various stages of myodifferentiaion identifies conditions favoring type i and type II fibers, and highlights increased efficiency of combined differentiation, Cardiovasc Res 114 (2018) S16–S16. https://doi.org/10.1093/CVR/CVY060.027.
[36] M.L. Waskom, seaborn: statistical data visualization, J Open Source Softw 6 (2021) 3021. https://doi.org/10.21105/JOSS.03021.
[37] G. Van Rossum, F.L. Drake, Python 3 Reference Manual; CreateSpace, Scotts Valley, CA (2009) 242. https://www.python.org/ (accessed February 6, 2024).
[38] S. Seabold, J. Perktold, Statsmodels: Econometric and Statistical Modeling with Python, SciPy (2010) 92–96. https://doi.org/10.25080/MAJORA-92BF1922-011.
[39] F. Monti, D. Stewart, A. Surendra, I. Alecu, T. Nguyen-Tran, S.A.L. Bennett, M. Cuperlovic-Culf, Signed Distance Correlation (SiDCo): an online implementation of distance correlation and partial distance correlation for data-driven network analysis, Bioinformatics 39 (2023). https://doi.org/10.1093/BIOINFORMATICS/BTAD210.
[40] P. Virtanen, R. Gommers, T.E. Oliphant, M. Haberland, T. Reddy, D. Cournapeau, E. Burovski, P. Peterson, W. Weckesser, J. Bright, S.J. van der Walt, M. Brett, J. Wilson, K.J. Millman, N. Mayorov, A.R.J. Nelson, E. Jones, R. Kern, E. Larson, C.J. Carey, İ. Polat, Y. Feng, E.W. Moore, J. VanderPlas, D. Laxalde, J. Perktold, R. Cimrman, I. Henriksen, E.A. Quintero, C.R. Harris, A.M. Archibald, A.H. Ribeiro, F. Pedregosa, P. van Mulbregt, A. Vijaykumar, A. Pietro Bardelli, A. Rothberg, A. Hilboll, A. Kloeckner, A. Scopatz, A. Lee, A. Rokem, C.N. Woods, C. Fulton, C.

Masson, C. Häggström, C. Fitzgerald, D.A. Nicholson, D.R. Hagen, D. V. Pasechnik, E. Olivetti, E. Martin, E. Wieser, F. Silva, F. Lenders, F. Wilhelm, G. Young, G.A. Price, G.L. Ingold, G.E. Allen, G.R. Lee, H. Audren, I. Probst, J.P. Dietrich, J. Silterra, J.T. Webber, J. Slavič, J. Nothman, J. Buchner, J. Kulick, J.L. Schönberger, J.V. de Miranda Cardoso, J. Reimer, J. Harrington, J.L.C. Rodríguez, J. Nunez-Iglesias, J. Kuczynski, K. Tritz, M. Thoma, M. Newville, M. Kümmerer, M. Bolingbroke, M. Tartre, M. Pak, N.J. Smith, N. Nowaczyk, N. Shebanov, O. Pavlyk, P.A. Brodtkorb, P. Lee, R.T. McGibbon, R. Feldbauer, S. Lewis, S. Tygier, S. Sievert, S. Vigna, S. Peterson, S. More, T. Pudlik, T. Oshima, T.J. Pingel, T.P. Robitaille, T. Spura, T.R. Jones, T. Cera, T. Leslie, T. Zito, T. Krauss, U. Upadhyay, Y.O. Halchenko, Y. Vázquez-Baeza, SciPy 1.0: fundamental algorithms for scientific computing in Python, Nature Methods 2020 17:3 17 (2020) 261–272. https://doi.org/10.1038/s41592-019-0686-2.

[41] S.X. Ge, D. Jung, D. Jung, R. Yao, ShinyGO: a graphical gene-set enrichment tool for animals and plants, Bioinformatics 36 (2020) 2628–2629. https://doi.org/10.1093/BIOINFORMATICS/BTZ931.

[42] C. Aguer, O. Fiehn, E.L. Seifert, V. Bézaire, J.K. Meissen, A. Daniels, K. Scott, J.-M. Renaud, M. Padilla, D.R. Bickel, M. Dysart, S.H. Adams, M.-E. Harper, Muscle uncoupling protein 3 overexpression mimics endurance training and reduces circulating biomarkers of incomplete β-oxidation, The FASEB Journal 27 (2013) 4213–4225. https://doi.org/10.1096/fj.13-234302.

[43] A. Shahini, K. Vydiam, D. Choudhury, N. Rajabian, T. Nguyen, P. Lei, S.T. Andreadis, Efficient and high yield isolation of myoblasts from skeletal muscle, Stem Cell Res 30 (2018) 122–129. https://doi.org/10.1016/J.SCR.2018.05.017.

[44] A. Liaghati, C.A. Pileggi, G. Parmar, D.A. Patten, N. Hadzimustafic, A. Cuillerier, K.J. Menzies, Y. Burelle, M.-E. Harper, Grx2 regulates skeletal muscle mitochondrial structure and autophagy, Front Physiol 12 (2021) 604210. https://doi.org/10.3389/fphys.2021.604210

[45] D. Pesta, E. Gnaiger, High-resolution respirometry: OXPHOS protocols for human cells and permeabilized fibers from small biopsies of human muscle, Mitochondrial Bioenergetics: Methods and Protocols (2012) 25–58. https://doi.org/10.1007/978-1-61779-382-0_3

[46] C. Stringer, T. Wang, M. Michaelos, M. Pachitariu, Cellpose: a generalist algorithm for cellular segmentation, Nature Methods 2020 18:1 18 (2020) 100–106. https://doi.org/10.1038/s41592-020-01018-x.

[47] C.A. Pileggi, C.P. Hedges, S.A. Segovia, J.F. Markworth, B.R. Durainayagam, C. Gray, X.D. Zhang, M.P.G. Barnett, M.H. Vickers, A.J.R. Hickey, C.M. Reynolds, D. Cameron-Smith, Maternal high fat diet alters skeletal muscle mitochondrial catalytic activity in adult male rat offspring, Front Physiol 7 (2016). https://doi.org/10.3389/fphys.2016.00546.

[48] M. Spinazzi, A. Casarin, V. Pertegato, L. Salviati, C. Angelini, Assessment of mitochondrial respiratory chain enzymatic activities on tissues and cultured cells, Nat Protoc 7 (2012) 1235–1246. https://doi.org/10.1038/nprot.2012.058

[49] G.J. Székely, M.L. Rizzo, N.K. Bakirov, Measuring and testing dependence by correlation of distances, Ann Stat 35 (2007) 2769–2794. https://doi.org/10.1214/009053607000000505.

[50] S. Ruijtenberg, S. Van Den Heuvel, G1/S Inhibitors and the SWI/SNF Complex Control Cell-Cycle Exit during Muscle Differentiation, Cell 162 (2015) 300–313. https://doi.org/10.1016/J.CELL.2015.06.013.

[51] K. Yano, R.U. Takahashi, Y. Yamamoto, S. Kan, H. Sakagami, H. Tahara, B. Shiotani, J. Abe, T. Shidooka, Y. Sudo, PRPF19 regulates p53-dependent cellular senescence by modulating alternative splicing of MDM4 mRNA, Journal of Biological Chemistry 297 (2021) 100882. https://doi.org/10.1016/j.jbc.2021.100882.

[52] A. Kumar, Y. Kumar, J.K. Sevak, S. Kumar, N. Kumar, S.D. Gopinath, Metabolomic analysis of primary human skeletal muscle cells during myogenic progression, Sci Rep 10 (2020) 11824. https://doi.org/10.1038/s41598-020-68796-4.
[53] S. Chintala, W. Li, M.L. Lamoreux, S. Ito, K. Wakamatsu, E. V. Sviderskaya, D.C. Bennett, Y.M. Park, W.A. Gahl, M. Huizing, R.A. Spritz, S. Ben, E.K. Novak, J. Tan, R.T. Swank, Slc7a11 gene controls production of pheomelanin pigment and proliferation of cultured cells, Proc Natl Acad Sci U S A 102 (2005) 10964–10969. https://doi.org/10.1073/PNAS.0502856102.
[54] R.T. Swank, M. Reddington, E.K. Novak, Inherited prolonged bleeding time and platelet storage pool deficiency in the subtle gray (sut) mouse., Lab Anim Sci 46 (1996) 56–60.
[55] T. Ishii, G.E. Mann, Redox status in mammalian cells and stem cells during culture in vitro: Critical roles of Nrf2 and cystine transporter activity in the maintenance of redox balance, Redox Biol 2 (2014) 786–794. https://doi.org/10.1016/J.REDOX.2014.04.008.
[56] H. Sato, S. Nomura, K. Maebara, K. Sato, M. Tamba, S. Bannai, Transcriptional control of cystine/glutamate transporter gene by amino acid deprivation, Biochem Biophys Res Commun 325 (2004) 109–116. https://doi.org/10.1016/J.BBRC.2004.10.009.
[57] D. Galter, S. Mihm, W. Dröge, Distinct effects of glutathione disulphide on the nuclear transcription factors κB and the activator protein-1, Eur J Biochem 221 (1994) 639–648. https://doi.org/10.1111/J.1432-1033.1994.TB18776.X.
[58] M. Fulco, Y. Cen, P. Zhao, E.P. Hoffman, M.W. McBurney, A.A. Sauve, V. Sartorelli, Glucose Restriction Inhibits Skeletal Myoblast Differentiation by Activating SIRT1 through AMPK-Mediated Regulation of Nampt, Dev Cell 14 (2008) 661. https://doi.org/10.1016/J.DEVCEL.2008.02.004.
[59] P. Aguiari, S. Leo, B. Zavan, V. Vindigni, A. Rimessi, K. Bianchi, C. Franzin, R. Cortivo, M. Rossato, R. Vettor, G. Abatangelo, T. Pozzan, P. Pinton, R. Rizzuto, High glucose induces adipogenic differentiation of muscle-derived stem cells, Proc Natl Acad Sci U S A 105 (2008) 1226–1231. https://doi.org/10.1073/PNAS.0711402105
[60] R. Belli, A. Bonato, L. De Angelis, S. Mirabilii, M.R. Ricciardi, A. Tafuri, A. Molfino, M. Leigheb, P. Costelli, M. Caruso, M. Muscaritoli, E. Ferraro, Metabolic reprogramming promotes myogenesis during aging, Front Physiol 10 (2019) 442450. https://doi.org/10.3389/FPHYS.2019.00897
[61] F. V. Pallardó, J. Markovic, J.L. García, J. Viña, Role of nuclear glutathione as a key regulator of cell proliferation, Mol Aspects Med 30 (2009) 77–85. https://doi.org/10.1016/J.MAM.2009.01.001.
[62] R. Brigelius-Flohé, Glutathione peroxidases and redox-regulated transcription factors, Biol Chem 387 (2006) 1329–1335. https://doi.org/10.1515/BC.2006.166.
[63] Y. Sun, L.W. Oberley, Redox regulation of transcriptional activators, Free Radic Biol Med 21 (1996) 335–348. https://doi.org/10.1016/0891-5849(96)00109-8.
[64] C.K. Sen, L. Packer, Antioxidant and redox regulation of gene transcription, The FASEB Journal 10 (1996) 709–720. https://doi.org/10.1096/FASEBJ.10.7.8635688.
[65] J. Markovic, C. Borrás, Á. Ortega, J. Sastre, J. Viña, F. V. Pallardó, Glutathione is recruited into the nucleus in early phases of cell proliferation, Journal of Biological Chemistry 282 (2007) 20416–20424. https://doi.org/10.1074/jbc.M609582200.
[66] M. Poot, H. Teubert, P.S. Rabinovitch, T.J. Kavanagh, De novo synthesis of glutathione is required for both entry into and progression through the cell cycle, J Cell Physiol 163 (1995) 555–560. https://doi.org/10.1002/JCP.1041630316.

[67] K.J.A. Davies, The broad spectrum of responses to oxidants in proliferating cells: a new paradigm for oxidative stress, IUBMB Life 48 (1999) 41–47. https://doi.org/10.1080/713803463.
[68] J.P. Messina, D.A. Lawrence, Cell cycle progression of glutathione-depleted human peripheral blood mononuclear cells is inhibited at S phase., The Journal of Immunology 143 (1989) 1974–1981. https://doi.org/10.4049/JIMMUNOL.143.6.1974.
[69] C.S. Kraft, C.M.R. LeMoine, C.N. Lyons, D. Michaud, C.R. Mueller, C.D. Moyes, Control of mitochondrial biogenesis during myogenesis, Am J Physiol Cell Physiol 290 (2006). https://doi.org/10.1152/AJPCELL.00463.2005.
[70] E. Barbieri, M. Battistelli, L. Casadei, L. Vallorani, G. Piccoli, M. Guescini, A.M. Gioacchini, E. Polidori, S. Zeppa, P. Ceccaroli, L. Stocchi, V. Stocchi, E. Falcieri, Morphofunctional and Biochemical Approaches for Studying Mitochondrial Changes during Myoblasts Differentiation, J Aging Res 2011 (2011). https://doi.org/10.4061/2011/845379.
[71] V.E. Jahnke, O. Sabido, D. Freyssenet, Control of mitochondrial biogenesis, ROS level, and cytosolic Ca2+ concentration during the cell cycle and the onset of differentiation in L6E9 myoblasts, Am J Physiol Cell Physiol 296 (2009). https://doi.org/10.1152/AJPCELL.00377.2008.
[72] J. Hollander, R. Fiebig, M. Gore, T. Ookawara, H. Ohno, L. Ji, Superoxide dismutase gene expression is activated by a single bout of exercise in rat skeletal muscle, Pflugers Arch 442 (2001) 426–434. https://doi.org/10.1007/S004240100539.
[73] L.Z.H. Zhou, A.P. Johnson, T.A. Rando, NFκB and AP-1 mediate transcriptional responses to oxidative stress in skeletal muscle cells, Free Radic Biol Med 31 (2001) 1405–1416. https://doi.org/10.1016/S0891-5849(01)00719-5.
[74] C.R. Reczek, N.S. Chandel, ROS-dependent signal transduction, Curr Opin Cell Biol 33 (2015) 8–13. https://doi.org/10.1016/J.CEB.2014.09.010.
[75] K.M. Holmström, T. Finkel, Cellular mechanisms and physiological consequences of redox-dependent signalling, Nature Reviews Molecular Cell Biology 2014 15:6 15 (2014) 411–421. https://doi.org/10.1038/nrm3801.
[76] J.H. Limón-Pacheco, N.A. Hernández, M.L. Fanjul-Moles, M.E. Gonsebatt, Glutathione depletion activates mitogen-activated protein kinase (MAPK) pathways that display organ-specific responses and brain protection in mice, Free Radic Biol Med 43 (2007) 1335–1347. https://doi.org/ 10.1016/j.freeradbiomed.2007.06.028.
[77] D.J. Templeton, M.S. Aye, J. Rady, F. Xu, J. V. Cross, Purification of Reversibly Oxidized Proteins (PROP) Reveals a Redox Switch Controlling p38 MAP Kinase Activity, PLoS One 5 (2010) e15012. https://doi.org/ 10.1371/journal.pone.0015012.
[78] L. De Angelis, J. Zhao, J.J. Andreucci, E.N. Olson, G. Cossu, J.C. McDermott, Regulation of vertebrate myotome development by the p38 MAP kinase-MEF2 signaling pathway, Dev Biol 283 (2005) 171–179. https://doi.org/10.1016/J.YDBIO.2005.04.009.
[79] A. Cuenda, P. Cohen, Stress-activated protein kinase-2/p38 and a rapamycin-sensitive pathway are required for C2C12 myogenesis, J Biol Chem 274 (1999) 4341–4346. https://doi.org/10.1074/JBC.274.7.4341.
[80] C. Tonelli, I.I.C. Chio, D.A. Tuveson, Transcriptional Regulation by Nrf2, Antioxid Redox Signal 29 (2018) 1727–1745. https://doi.org/10.1089/ARS.2017.7342.
[81] Q. Ma, Role of Nrf2 in Oxidative Stress and Toxicity, Annu Rev Pharmacol Toxicol 53 (2013) 401. https://doi.org/10.1146/annurev-pharmtox-011112-140320.
[82] M. Narasimhan, J. Hong, N. Atieno, V.R. Muthusamy, C.J. Davidson, N. Abu-Rmaileh, R.S. Richardson, A. V. Gomes, J.R. Hoidal, N.S. Rajasekaran, Nrf2 deficiency promotes apoptosis and

impairs PAX7/MyoD expression in aging skeletal muscle cells, Free Radic Biol Med 71 (2014) 402–414. https://doi.org/10.1016/J.FREERADBIOMED.2014.02.023.
[83] C.M. Adams, S.M. Ebert, M.C. Dyle, Role of ATF4 in skeletal muscle atrophy, Curr Opin Clin Nutr Metab Care 20 (2017) 164–168. https://doi.org/10.1097/MCO.0000000000000362.
[84] K. Pakos-Zebrucka, I. Koryga, K. Mnich, M. Ljujic, A. Samali, A.M. Gorman, The integrated stress response, EMBO Rep 17 (2016) 1374–1395. https://doi.org/10.15252/EMBR.201642195.
[85] A. Longchamp, T. Mirabella, A. Arduini, M.R. MacArthur, A. Das, J.H. Treviño-Villarreal, C. Hine, I. Ben-Sahra, N.H. Knudsen, L.E. Brace, J. Reynolds, P. Mejia, M. Tao, G. Sharma, R. Wang, J.M. Corpataux, J.A. Haefliger, K.H. Ahn, C.H. Lee, B.D. Manning, D.A. Sinclair, C.S. Chen, C.K. Ozaki, J.R. Mitchell, Amino Acid Restriction Triggers Angiogenesis via GCN2/ATF4 Regulation of VEGF and H2S Production, Cell 173 (2018) 117-129.e14. https://doi.org/10.1016/J.CELL.2018.03.001.
[86] J.O. Holloszy, Biochemical adaptations in muscle. Effects of exercise on mitochondrial oxygen uptake and respiratory enzyme activity in skeletal muscle, J Biol Chem 242 (1967) 2278–2282. https://doi.org/10.1016/S0021-9258(18)96046-1
[87] B. Egan, J.R. Zierath, Exercise metabolism and the molecular regulation of skeletal muscle adaptation, Cell Metab 17 (2013) 162–184. https://doi.org/10.1016/j.cmet.2012.12.012
[88] H. Pilegaard, B. Saltin, P.D. Neufer, Exercise induces transient transcriptional activation of the PGC-1α gene in human skeletal muscle, J Physiol 546 (2003) 851–858. https://doi.org/10.1113/jphysiol.2002.034850
[89] T.R. Hurd, R. Requejo, A. Filipovska, S. Brown, T.A. Prime, A.J. Robinson, I.M. Fearnley, M.P. Murphy, Complex I within Oxidatively Stressed Bovine Heart Mitochondria Is Glutathionylated on Cys-531 and Cys-704 of the 75-kDa Subunit potential role of CYS residues in decreasing oxidative damage, Journal of Biological Chemistry 283 (2008) 24801–24815. https://doi.org/10.1074/jbc.M803432200
[90] E.R. Taylor, F. Hurrell, R.J. Shannon, T.-K. Lin, J. Hirst, M.P. Murphy, Reversible glutathionylation of complex I increases mitochondrial superoxide formation, Journal of Biological Chemistry 278 (2003) 19603–19610. https://doi.org/ 10.1074/jbc.M209359200
[91] X. Ji, M. Zheng, T. Yu, J. Kang, T. Fan, B. Xu, NAD+-Consuming Enzymes in Stem Cell Homeostasis, Oxid Med Cell Longev 2023 (2023). https://doi.org/10.1155/2023/4985726.
[92] H. Zhang, D. Ryu, Y. Wu, K. Gariani, X. Wang, P. Luan, D. D'Amico, E.R. Ropelle, M.P. Lutolf, R. Aebersold, K. Schoonjans, K.J. Menzies, J. Auwerx, NAD+ repletion improves mitochondrial and stem cell function and enhances life span in mice, Science 352 (2016) 1436–1443. https://doi.org/10.1126/SCIENCE.AAF2693.
[93] X. Yuan, Y. Liu, B.M. Bijonowski, A.C. Tsai, Q. Fu, T.M. Logan, T. Ma, Y. Li, NAD+/NADH redox alterations reconfigure metabolism and rejuvenate senescent human mesenchymal stem cells in vitro, Communications Biology 2020 3:1 3 (2020) 1–15. https://doi.org/10.1038/s42003-020-01514-y.
[94] A. de Baat, D.T. Meier, L. Rachid, A. Fontana, M. Böni-Schnetzler, M.Y. Donath, Cystine/glutamate antiporter System xc- deficiency impairs insulin secretion in mice, Diabetologia 66 (2023) 2062–2074. https://doi.org/10.1007/S00125-023-05993-6.
[95] L. Verbruggen, G. Ates, O. Lara, J. De Munck, A. Villers, L. De Pauw, S. Ottestad-Hansen, S. Kobayashi, P. Beckers, P. Janssen, H. Sato, Y. Zhou, E. Hermans, R. Njemini, L. Arckens, N.C. Danbolt, D. De Bundel, J.L. Aerts, K. Barbé, B. Guillaume, L. Ris, E. Bentea, A. Massie, Lifespan extension with preservation of hippocampal function in aged system xc−-deficient male mice,

Molecular Psychiatry 2022 27:4 27 (2022) 2355–2368. https://doi.org/10.1038/s41380-022-01470-5.
[96] C.D. Bindu Paul, T.H. Solomon Snyder, J.I. Sbodio, S.H. Snyder, B.D. Paul, Regulators of the transsulfuration pathway, Br J Pharmacol 176 (2019) 583–593. https://doi.org/10.1111/BPH.14446.
[97] J. Zhu, M. Berisa, S. Schwörer, W. Qin, J.R. Cross, C.B. Thompson, Transsulfuration Activity Can Support Cell Growth upon Extracellular Cysteine Limitation, Cell Metab 30 (2019) 865-876.e5. https://doi.org/10.1016/J.CMET.2019.09.009.

2.8 Supplementary Figures

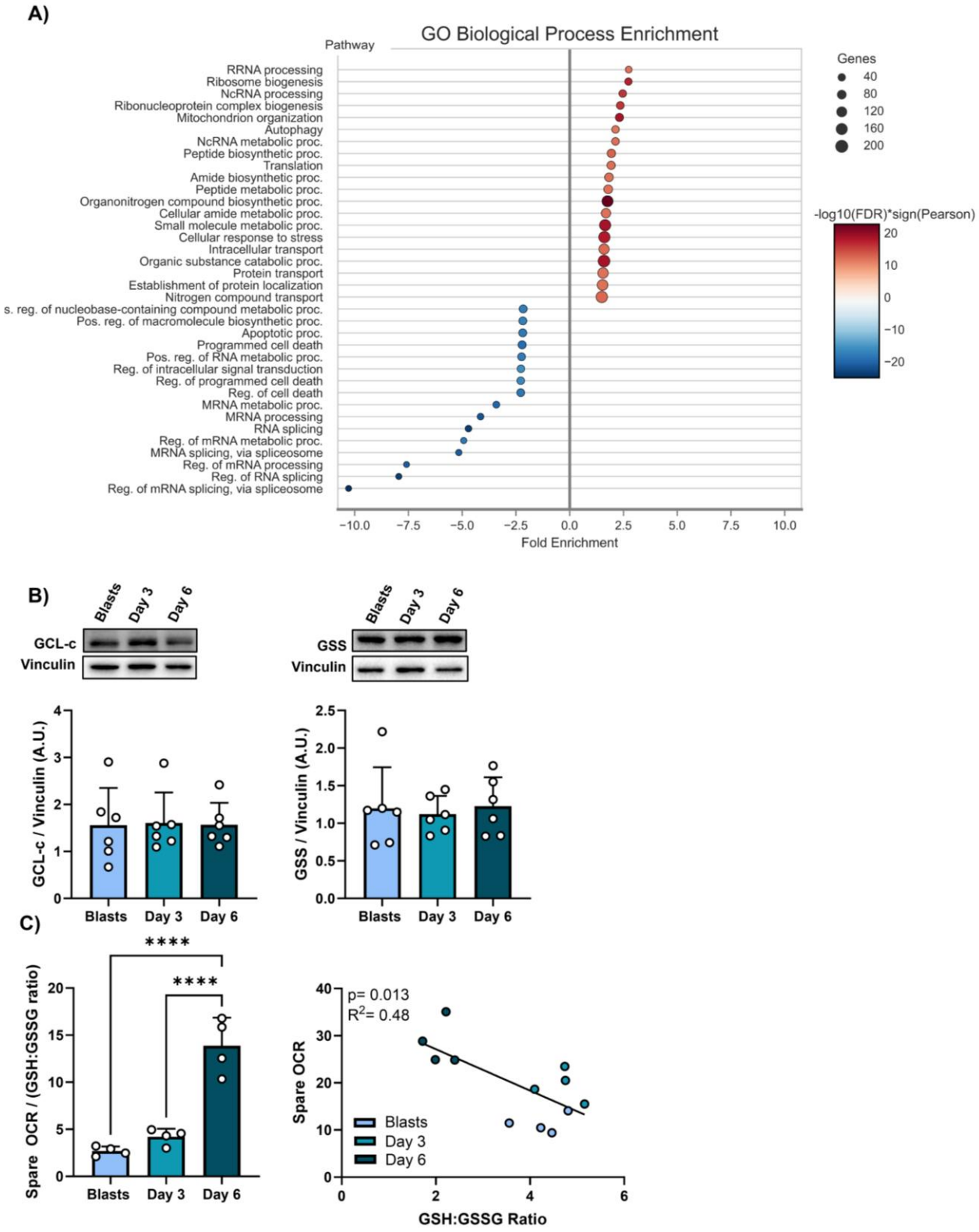

Supplementary Figure 2.1.
(A) Enrichment analysis results for positively (red) and negatively (blue) correlated genes with Slc7a11 throughout C2C12 differentiation in Gene ontology terms for biological processes**. (B)** Immunoblot analysis of the key enzymes involved in GSH biosynthesis revealed similar levels of glutamate-cysteine ligase (GCLc) and GSH synthetase (GSS) in C2C12 myoblasts, and following D3 and D6 of differentiation, one-way RM ANOVA with Tukey HSD, n=6. **(C)** Correlation analysis between GSH:GSSG ratio and spare respiratory capacity throughout C2C12 differentiation.

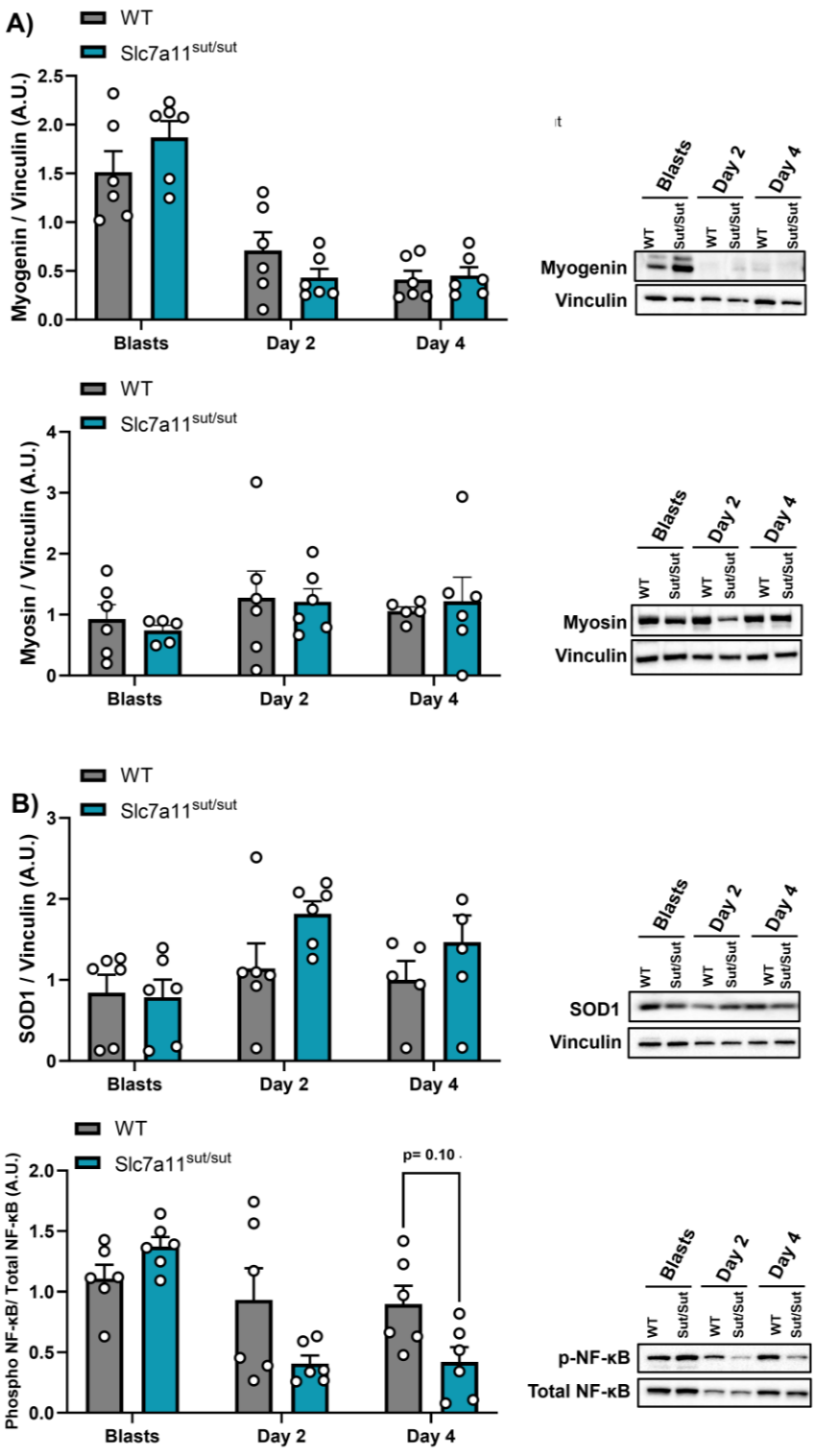
A)
WT
Slc7a11sut/sut
Myogenin / Vinculin (A.U.)
2.5
2.0
1.5
1.0
0.5
0.0
Blasts
Day 2
Day 4
Blasts
Day 2
Day 4
WT
Sut/Sut
Myogenin
Vinculin
WT
Slc7a11sut/sut
Myosin / Vinculin (A.U.)
4
3
2
1
0
Blasts
Day 2
Day 4
Myosin
Vinculin
B)
WT
Slc7a11sut/sut
SOD1 / Vinculin (A.U.)
3
2
1
0
SOD1
Vinculin
WT
Slc7a11sut/sut
p= 0.10
Phospho NF-κB/ Total NF-κB (A.U.)
2.0
1.5
1.0
0.5
0.0
p-NF-κB
Total NF-κB

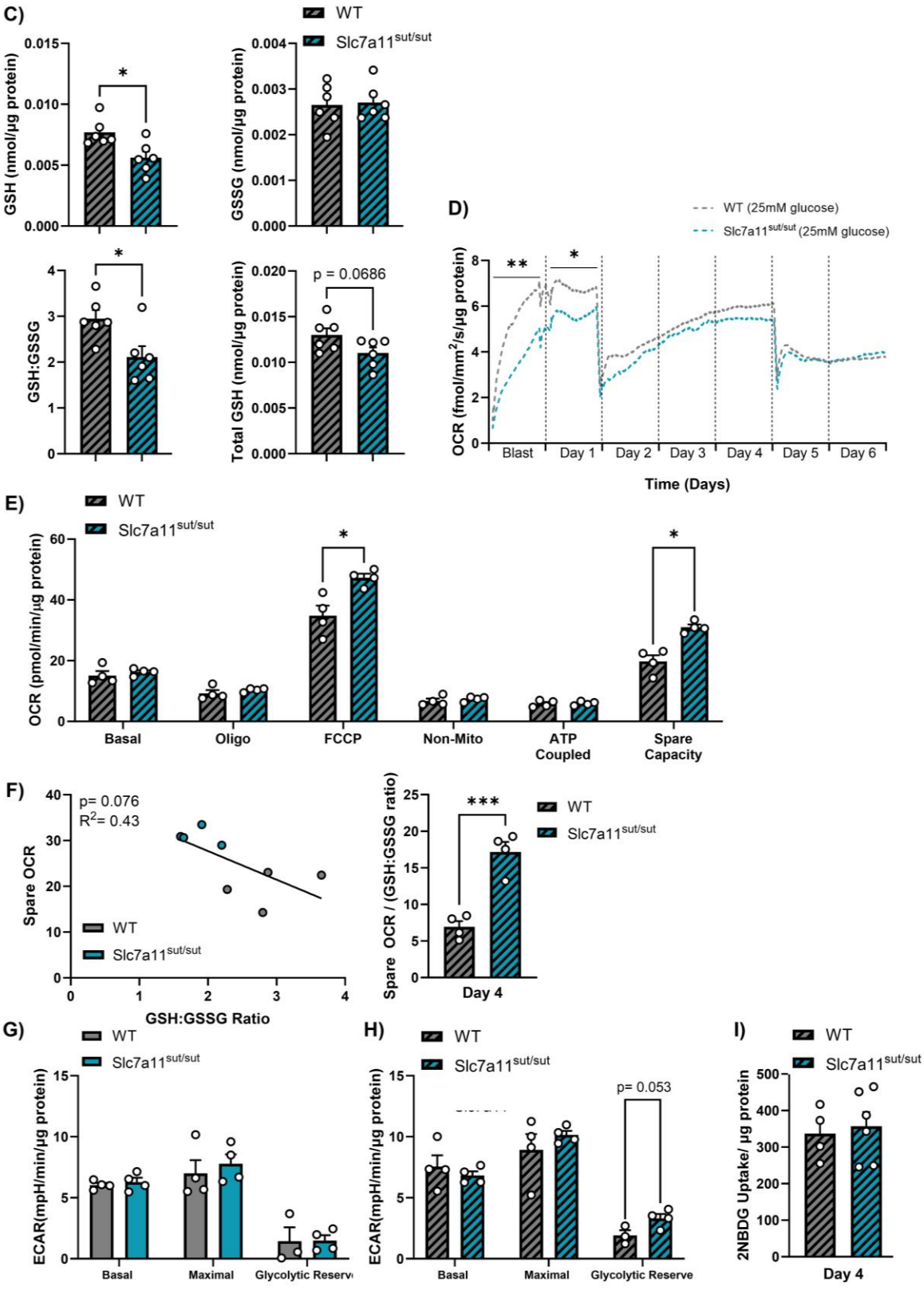
C)
WT
Slc7a11sut/sut
GSH (nmol/µg protein)
GSSG (nmol/µg protein)
GSH:GSSG
Total GSH (nmol/µg protein)
p = 0.0686
D)
WT (25mM glucose)
Slc7a11sut/sut (25mM glucose)
OCR (fmol/mm2/s/µg protein)
Blast
Day 1
Day 2
Day 3
Day 4
Day 5
Day 6
Time (Days)
E)
WT
Slc7a11sut/sut
OCR (pmol/min/µg protein)
Basal
Oligo
FCCP
Non-Mito
ATP Coupled
Spare Capacity
F)
p= 0.076
R2= 0.43
Spare OCR
GSH:GSSG Ratio
Spare OCR / (GSH:GSSG ratio)
Day 4
G)
ECAR(mpH/min/µg protein)
Basal
Maximal
Glycolytic Reserve
H)
p= 0.053
I)
2NBDG Uptake/ µg protein
Day 4

Supplementary Figure 2.2.
(A) Immunoblot of myogenin and myosin in primary myoblasts and myotubes differentiated for 2 and 4 days in normal physiological glucose concentrations (5.5 mM), n = 5-6. **(B)** Immunoblot of SOD1 and phospho-NF-κB/total NF-κB in primary myoblasts and myotubes differentiated for 2 and 4 days in normal physiological glucose concentrations (5.5 mM), n = 5-6. **(C)** Total reduced GSH, total oxidized GSH (GSSG), GSH: GSSG ratio, and total glutathione in primary myotubes differentiated for 4 days in high glucose concentrations (25 mM), n = 5-6. **(D)** Continuous oxygen consumption rates (OCRs) were measured using a RESIPHER real-time cell analyzer throughout myotube differentiation in cells cultured in high glucose media (day 1 to day 7), n = 4. **(E)** OCR measured using a Seahorse analyzer in myotubes differentiated for 4 days in high glucose conditions (25 mM), n = 4. **(F)** Correlation analysis between GSH:GSSG ratio and spare respiratory capacity in myotubes differentiated for 4 days in high glucose media. **(G)** Extracellular acidification rates (ECAR) in myotubes differentiated for 4 days in normal physiological glucose concentrations (5.5 mM), n = 4. (**H**) Extracellular acidification rates (ECAR) in myotubes differentiated for 4 days in high glucose concentrations (25 mM), n = 4. **(I)** Glucose uptake rate measured as the rate of increase in (2-(N-(7-Nitrobenz-2-oxa-1,3-diazol-4-yl) amino)-2-Deoxyglucose (2-NBDG) fluorescence intensity in myotubes differentiated for 4 days in high glucose concentrations (25 mM), n = 3. Results are presented as mean ± SEM, *p < 0.05, **p < 0.01, ***p < 0.001, ****p < 0.0001.

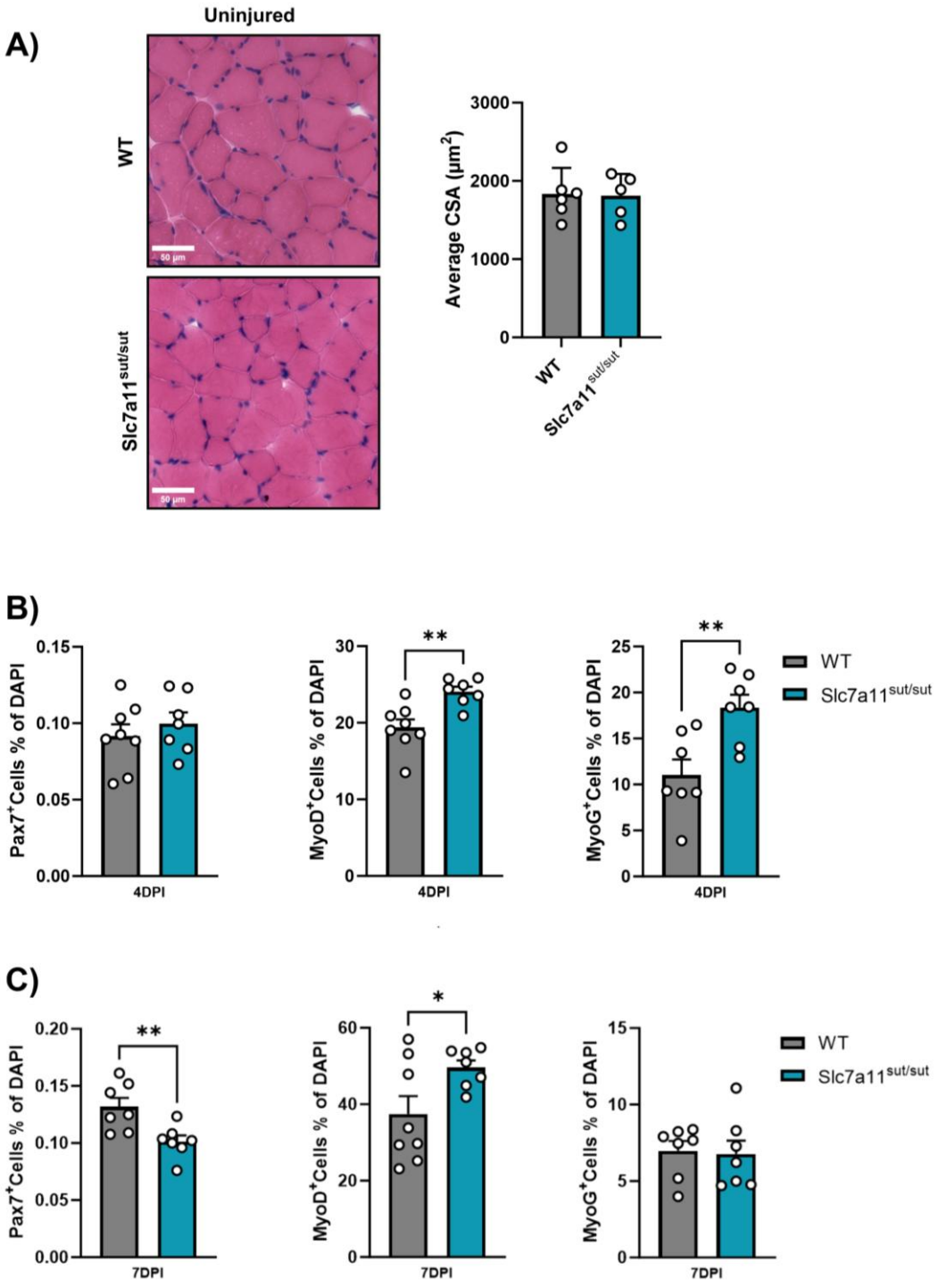

Supplementary Figure 2.3.
(A) Hematoxylin and eosin (H&E) staining of muscle sections and average myofiber cross sectional area in uninjured TA muscles. Scale bar = 50 µm. Two-tailed Student's t-tests, n = 5-6. **(B-C)** The proportion of DAPI colocalized with myogenic markers (Pax7, MyoD, and MyoG) in *Tibialis anterior* (TA) muscle sections **(B)** at day 4 and **(C)** at day 7 post-cardiotoxin-induced injury. Two-tailed Student's t-tests, n =7-8. DPI=days post injury.

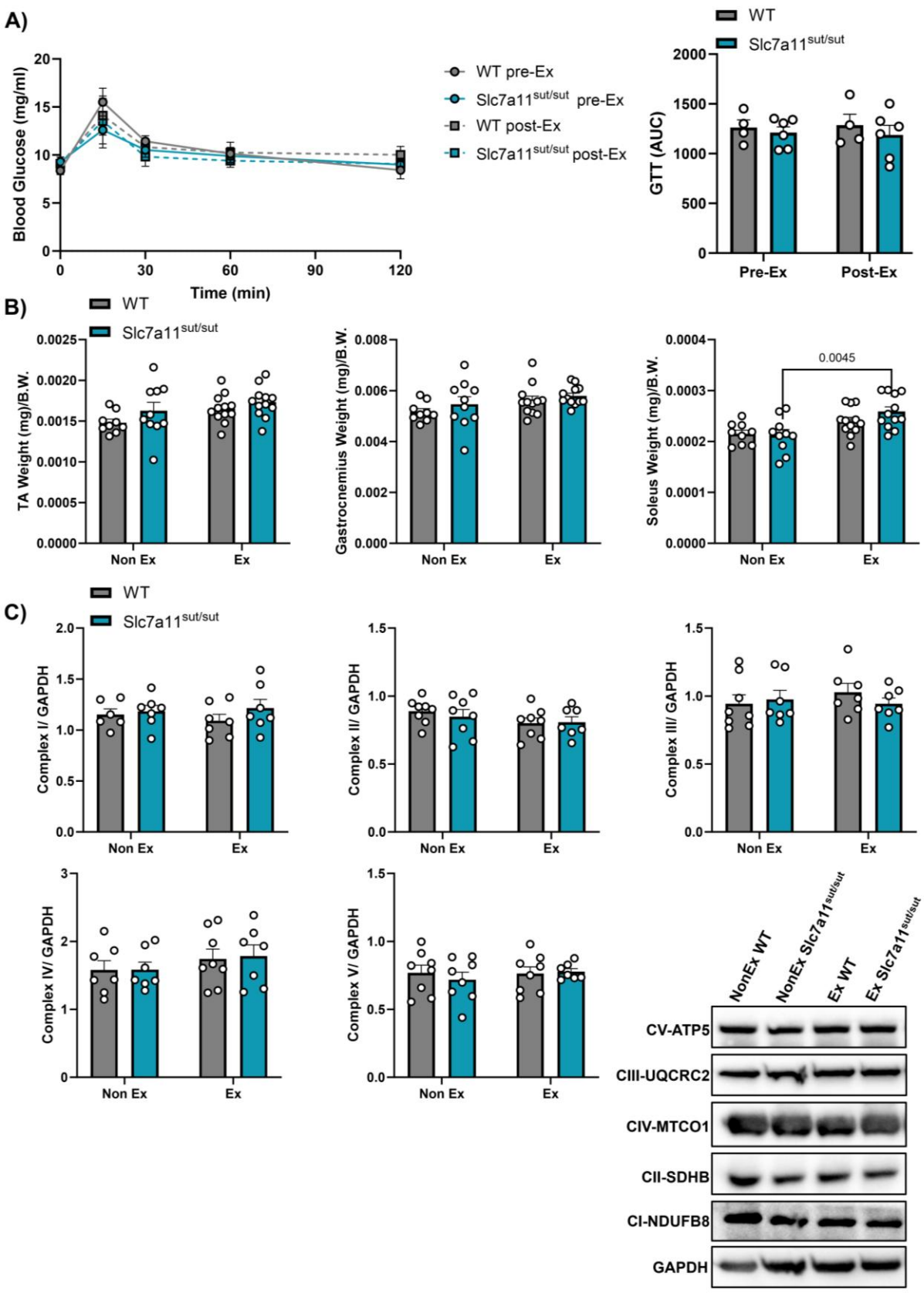
A)
Blood Glucose (mg/ml)
Time (min)
WT pre-Ex
Slc7a11sut/sut pre-Ex
WT post-Ex
Slc7a11sut/sut post-Ex
WT
Slc7a11sut/sut
GTT (AUC)
Pre-Ex
Post-Ex
B)
TA Weight (mg)/B.W.
Gastrocnemius Weight (mg)/B.W.
Soleus Weight (mg)/B.W.
0.0045
Non Ex
Ex
C)
Complex I/ GAPDH
Complex II/ GAPDH
Complex III/ GAPDH
Complex IV/ GAPDH
Complex V/ GAPDH
NonEx WT
NonEx Slc7a11sut/sut
Ex WT
Ex Slc7a11sut/sut
CV-ATP5
CIII-UQCRC2
CIV-MTCO1
CII-SDHB
CI-NDUFB8
GAPDH

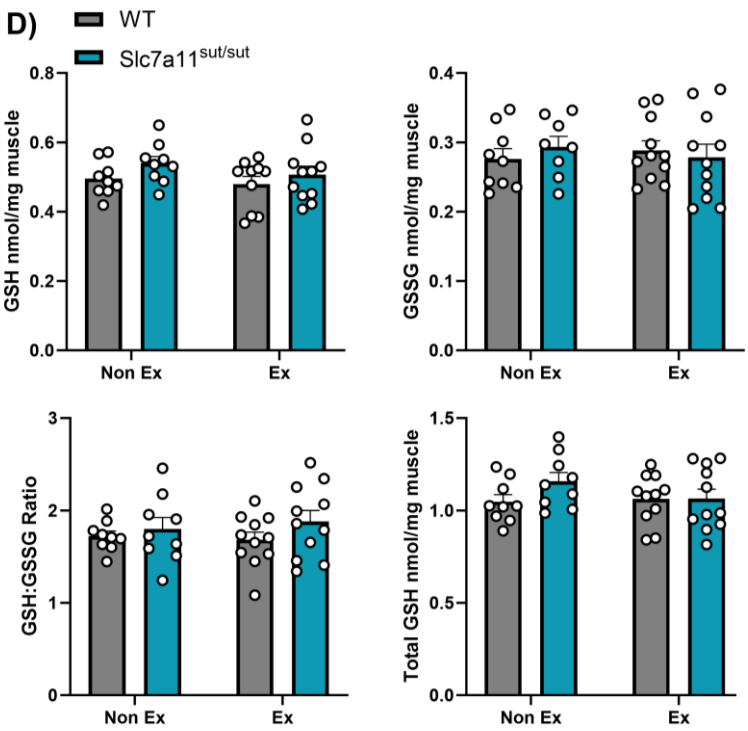

Supplementary Figure 2.4.
(A) An oral glucose tolerance test (GTT) demonstrated that blood glucose levels were similar between pre- and post-exercised WT and Slc7a11sut/sut mice, n = 4-6. **(B)** Weight of the TA, gastrocnemius, and soleus muscle normalized to mice body weight (BW), collected from non-exercised (Non-Ex) and exercised (Ex) WT and Slc7a11sut/sut mice, n = 10-12. **(C)** Immunoblot of different mitochondrial complexes in the TA muscle of non-exercised (Non-Ex) and exercised (Ex) WT and Slc7a11sut/sut mice, n = 6-8. **(D)** Total reduced GSH, total oxidized GSH (GSSG), GSH: GSSG ratio, and total glutathione in the TA muscle of non-exercised (Non-Ex) and exercised (Ex) WT and Slc7a11sut/sut mice, n = 8-11. Results are presented as mean ± SEM, *p < 0.05, **p < 0.01.

CHAPTER 3:

Impaired xCT-mediated cystine uptake drives serine and proline metabolic reprogramming and mitochondrial fission in skeletal muscle cells

Michel N. Kanaan*[1,2], Charbel Y. Karam*[1,2], Luke S. Kennedy[1,2], Chantal A. Pileggi[1,2], Miroslava Cuperlovic-Culf[1,2,3], and Mary-Ellen Harper[1,2]

[1] Department of Biochemistry, Microbiology and Immunology, Faculty of Medicine, University of Ottawa, 451 Smyth Road, Ottawa, ON, Canada, K1H 8M5

[2] Ottawa Institute of Systems Biology, University of Ottawa, ON, Canada, K1H 8M5

[3] National Research Council of Canada, Digital Technologies Research Centre, 1200 Montreal Road, Ottawa, ON, Canada, K1A 0R6

*Co-first authors

Conflicts of interest: None

Correspondence: Dr. ME Harper

Phone: 613-562-5800 ext. 8458

Email: mharper@uottawa.ca

Running title: xCT-mediated metabolic reprogramming and mitochondrial fission in skeletal muscle cells

3.1 STATEMENT OF MANUSCRIPT STATUS AND CONTRIBUTIONS

3.1.1 Statement of Manuscript Status

The manuscript “Impaired xCT-mediated cystine uptake drives serine and proline metabolic reprogramming and mitochondrial fission in skeletal muscle cells” has been submitted for publication in the journal *Redox Biology* on March 10, 2025.

3.1.2Acknowledgements

This research is funded through a grant from the Natural Sciences and Engineering Research Council (NSERC) of Canada (RGPIN-2020-04468). The authors would like to thank Dr. Sandra Hewett (Syracuse University) who provided C3H/HeSnJ wild-type (WT) mice along with background-matched Slc7a11$^{sut/sut}$ (xCT$^{-/-}$) mice. The authors gratefully acknowledge the University of Ottawa Metabolomics Core facility, the Louise Pelletier Histology Core facility (RRID: SCR_021737), the Cell Biology and Image Acquisition Core (RRID: SCR_021845), and the University of Ottawa Animal Care and Veterinary Service. MK is a recipient of the Scholarship in Translational Research (STaR) award from the Éric Poulin Centre for Neuromuscular Disease (CNMD). CK is the recipient of a Canada Graduate Scholarship – Master’s (CGS-M) from the Canadian Institute of Health Research (CIHR).

3.1.3 Author Contributions

Conceptualization: MK, CYK, MEH

Data curation: MK, CYK, LK, CAP, MCC, MEH

Formal analysis: MK, CYK, LK, CAP, MCC

Funding acquisition: MEH

Investigation: MK, CYK, LK

Methodology: MK, CYK, LK, CAP, MCC, MEH

Supervision: MCC, MEH

Roles/Writing - original draft: MK, CYK, LK, CAP, MEH

Writing - review & editing: MK, CYK, LK, CAP, MCC, MEH

3.1.4 Funding

This work was supported by a grant from the Natural Sciences and Engineering Research Council (NSERC) of Canada (RGPIN-2020-04468 to MEH).

3.1.5 Conflict of Interests

The authors declare that they have no conflicts of interest with the contents of this article.

3.2 Abstract

Muscle satellite cell (MuSC) proliferation is tightly regulated by redox homeostasis and nutrient availability, which are often disrupted in muscular pathologies. Beyond its role in maintaining cellular redox homeostasis, this study identified a key metabolic role for cystine/glutamate antiporter xCT in proliferating MuSCs. We investigated the impact of impaired xCT-mediated cystine import in Slc7a11$^{sut/sut}$ MuSCs isolated from mice that harbor a mutation in the *SLC7A11* gene, which encodes xCT. We used complementary approaches to study how disrupted cystine import affects glutathione (GSH) redox, cellular bioenergetics, mitochondrial dynamics, and metabolism. Oxygen consumption rates of Slc7a11$^{sut/sut}$ MuSCs were lower, indicative of compromised mitochondrial oxidative capacity. This was accompanied by a fragmented mitochondrial network associated with redox-sensitive DRP1 oligomerization, but no changes in the protein levels of key mitochondrial dynamics regulatory factors. Metabolomic profiling revealed a distinct metabolic signature in Slc7a11$^{sut/sut}$ MuSCs, manifested by major differences in BCAAs, pyrimidines, cysteine, methionine, and GSH. Despite lower overall bioenergetic flux, stable-isotope tracing analyses (SITA) showed that xCT deficiency increased glucose uptake, channeling glucose-derived carbons into *de novo* serine biosynthesis to fuel cysteine production via the transsulfuration pathway, partially compensating for disrupted GSH redox. Furthermore, xCT deficiency triggered upregulated pyrroline-5-carboxylate synthase (P5CS)-mediated proline reductive biosynthesis. By directing glutamate into proline synthesis, MuSCs apparently downregulate oxidative phosphorylation (OXPHOS) and regulate intracellular glutamate levels in response to impaired cystine/glutamate antiporter function. Our findings highlight the roles of xCT in regulating redox balance and metabolic reprogramming in proliferating MuSCs, providing insights that may inform therapeutic strategies for muscular and redox-related pathologies.

Keywords: Slc7a11, cystine/glutamate antiporter, system Xc−, metabolic reprogramming, cysteine, proline, mitochondria, oxidative phosphorylation, glycolysis, transsulfuration pathway, skeletal muscle, myopathy.

3.3 Introduction

Cysteine, a thiol-containing amino acid, is imported into cells via alanine-serine-cysteine transporters (ASCTs) and excitatory amino acid transporters (EAATs) [1]. In the extracellular space, cysteine predominantly exists in its oxidized form, cystine, which is imported into cells exclusively via system Xc− (xCT), in exchange for intracellular glutamate. xCT is a plasma membrane cystine/glutamate antiporter and comprises a heavy chain (4F2hc/SLC3A2), essential for membrane insertion, and a light chain (xCT/SLC7A11), which determines substrate specificity and transport activity [2–4]. As cysteine is the rate-controlling precursor for the biosynthesis of glutathione (GSH), xCT-mediated cellular uptake of cystine has well-established roles in lowering the levels of reactive oxygen species (ROS), maintaining intracellular redox homeostasis, and increasing cellular resistance to apoptosis [5,6].

Skeletal muscle possesses remarkable regenerative capacity due to a designated population of adult stem cells known as muscle satellite cells (MuSCs) [7,8]. In response to injury or exercise, quiescent MuSCs are activated and enter a proliferative phase to generate a pool of myoblasts dedicated to repairing muscle tissue while others commit to self-renewal ensuring the maintenance of the quiescent MuSC pool [9]. Failure to maintain the quiescent MuSC pool is linked to aging, muscular dystrophies, and metabolic diseases [10,11]. The initiation of MuSC proliferation requires substantial metabolic reprogramming involving a shift from mitochondrial oxidative phosphorylation (OXPHOS) to glycolysis usually ascribed to the high demands for rapid ATP production [12,13]. This metabolic shift during MuSCs proliferation also involves increased amino acid uptake to support biosynthetic requirements for rapid cell growth [14,15]. Mammalian cells have high rates of cyst(e)ine uptake and glutamate excretion during proliferation, implicating an important role for xCT in the control of these processes [14].

We previously demonstrated in Slc7a11$^{sut/sut}$ mice that the absence of xCT was associated with greater MuSC activation *in vivo* following cardiotoxin muscle damage and greater commitment to muscle

differentiation [16]. An important question emerging from this work was, how does impaired cystine import and glutamate efflux impact metabolic pathways, redox and mitochondrial dynamics in MuSCs? Here, we leveraged metabolomic profiling, stable isotope tracer analysis (SITA), metabolite transport and oxidation analyses, cell imaging and bioinformatic approaches in muscle cells *in vitro.* Findings show that xCT deficiency or its chemical inhibition in muscle cells promotes metabolic reprogramming, shifting glycolytic intermediates toward serine, cysteine, and proline biosynthesis in an attempt to compensate for disrupted cysteine and GSH metabolism and to restore GSH redox at the expense of oxidative metabolism. These metabolic perturbations are accompanied by impaired mitochondrial oxidative capacity, DRP1-mediated mitochondrial fragmentation, and elevated oxidative stress related to insufficient cyst(e)ine availability for GSH biosynthesis.

3.4 Experimental Procedures

3.4.1. Animals

All mouse experiments were conducted according to the principles and guidelines set by the Canadian Council on Animal Care and were approved by the Animal Care Committee at the University of Ottawa. Experiments were conducted using primary muscle cells isolated from male and female C3H/HeSnJ wild-type (WT) mice and background-matched Slc7a11$^{sut/sut}$ (xCT$^{-/-}$) mice. No sex dimorphism was observed in any outcome measured. Mice were housed under standard conditions, maintaining a controlled temperature of 22-23°C, humidity levels of 30-60%, and a 12 h light/dark cycle (lights on from 07:00 to 19:00). Mice were given free access to water and fed a standard diet containing 18% protein and 6% fat (2018 Teklad Global Diet).

3.4.2. Mouse Primary Muscle Cell isolation and Culture

Skeletal muscles of the hindlimb were rapidly dissected and cleaned from fat and connective tissue. Muscle tissues were washed with PBS supplemented with 1% antibiotic-antimycotic. Tissues were then treated with an enzymatic cocktail containing 1 mg/ml Dispase II and 1 mg/ml Collagenase B (Sigma-Aldrich) and chopped with a sterile razor blade. The homogenate was incubated at 37°C for 30 min and vortexed every 5 min during the incubation. The homogenate was then centrifuged at 500 g for 5 min and pellets were resuspended and transferred into Matrigel-coated containing DMEM (25 mM glucose) supplemented with 20% fetal bovine serum, 10% horse serum, 2.5 ng/ml β-FGF (Sigma-Aldrich), 1x non-essential amino acids (11140050, Gibco), and 1% antibiotic-antimycotic. Fibroblast populations were eliminated by the differential adhesion method, and primary muscle cell enrichment was achieved [17]. Primary MuSCs were cultured for 48 h. During the initial 24 h period, the cell culture medium was supplemented with 50 μM of 2-mercaptoethanol (2ME), which was essential for early Slc7a11$^{sut/sut}$

MuSCs survival as previously reported [16]. 2ME was removed for the remaining 24 h, except for the Slc7a11$^{sut/sut}$ + 2ME condition, which was retained as a rescue treatment.

3.4.3. Immunostaining of Primary Muscle Cells

To conduct mitochondrial morphological analyses, cells were cultured in 8-well glass slide plates (Millipore) coated with Matrigel (Corning). Cells from different conditions were rapidly washed with warm PBS and then fixed with 4% PFA (Sigma-Aldrich) for 15 min. After fixation, cells were washed twice with PBS and incubated for 2 h at room temperature (RT) in PBS containing 1% BSA, 0.2% Triton-X (Sigma-Aldrich), and anti-TOMM20 (1:500, 11802, Protein Tech). Cells were washed twice with PBS and incubated for 1 h at RT in PBS containing 1% BSA and a secondary antibody (Alexa Fluor 488 goat anti-rabbit IgG (H+L), 1:500, A-11008, Thermo Fisher Scientific). After 2 washes, cells were incubated for 5 min at RT with 4,6-diamidino-2-phenylindole (DAPI, 1:1000, Sigma-Aldrich). The polypropylene wells were lifted off the slide before mounting the cells in ProLong Gold antifade reagent (Invitrogen). Cells were imaged using a confocal microscope Zeiss LSM880 equipped with AiryScan FAST technology 63X/1.4 oil objective. Mitochondrial morphological analyses were performed using Mitochondria Analyzer, a three-dimensional mitochondrial analysis pipeline in ImageJ/Fiji, as previously described [18].

3.4.5. Cystine and Glucose Uptake in Primary Muscle Cells

Primary MuSCs were plated at 10,000 cells per well in Matrigel-coated 96-well white/clear bottom plates. Cystine uptake was measured using a cystine uptake assay kit (UP05, Dojindo), while glucose uptake was measured using a cell-based assay kit (600470, Cayman) following manufacturers' instructions. Briefly, for cystine uptake, cells were deprived of cystine for 30 min, then incubated with the cystine analog, selenocystine at 37°C for 30 min. Cells were then incubated with fluorescein O, O'-diacrylate, and (tris(2-carboxyethyl) phosphine for 30 min. For glucose uptake, cells were deprived of

serum for 3 h before the assay. During the last hour, cells were starved of glucose for 30 min, then incubated with 200 µg/ml of 2-(N-(7-nitrobenz-2-oxa-1,3-diazol-4-yl) amino)-2-deoxyglucose (2-NBDG) for 30 min. Cystine and glucose uptake rates were determined by measuring fluorescence intensity at 490/535 nm and 485/535 nm, respectively, using a BioTek Synergy H1 Multi-Mode Plate Reader (BioTek Instruments).

3.4.6. GSH and GSSG Measurements

Primary MuSCs for each indicated condition were grown in 100 mm Petri dishes, harvested with trypsin, and then washed with ice-cold PBS. A 1:1 homogenization buffer [125 mM sucrose, 1.5 mM EDTA, 5 mM Tris, 0.5% trifluoroacetic acid (TFA), and 0.5% meta-phosphoric acid (MPA) in 50% mobile phase (10% HPLC grade methanol, 0.09% TFA – 0.2µm filtered)] was used to homogenize the cells for 20 min on ice. Cell lysates were centrifuged at 14,000 g for 20 min at 4°C, and supernatants were used for measurements. To quantify GSH and GSSG levels, an HPLC 1100 Series system (Agilent) equipped with a Pursuit C18 column (150×4.6 mm, 5 µm; Agilent) was employed with a 1 ml/min flow rate using a UV-visible wavelength detector at 215 nm (Agilent), as previously described [19]. Data were analyzed using the OpenLab CDS 2.8 software and values were normalized to cellular protein levels using a bicinchoninic acid (BCA) assay (Pierce BCA Protein Assay, 23225, Thermo Fisher Scientific).

3.4.7. Cellular Bioenergetics

A Seahorse XFe96 Analyzer (Agilent) was used to assess oxygen consumption rates (OCR) and extracellular acidification rates (ECAR) in primary MuSCs plated at 10,000 cells/well. Mitochondrial stress tests assessed cellular resting respiration before and following four consecutive injections: oligomycin (2 µg/mL), FCCP (2.4 µM), combined antimycin A (5.5 µM) / rotenone (7.7 µM), and monensin (20 µM). This allowed determinations of resting, leak-dependent, and maximal rates of oxygen consumption. These rates were corrected for non-mitochondrial OCR, measured as antimycin

A/rotenone-independent respiration. ATP-linked OCR was calculated as the difference between resting and leak respiration, and reserve capacity was determined by subtracting resting OCR from maximal OCR. The injection of monensin at the end of the injection cycle allowed the measurement of maximal ECAR, which is a proxy measure of the glycolytic capacity of cells [20]. Beyond resting levels of glycolytic rates, glycolytic reserve was determined by subtracting resting rates from the maximal rates in the presence of monensin.

For the glycolysis stress test, cells were washed and incubated in a glucose-free medium. After measuring resting ECAR, cells were treated with consecutive injections of glucose (10 nM), oligomycin (2 µg/mL), and 2-deoxyglucose (2DG, 50 mM). Following glucose and oligomycin injections, glycolysis and glycolytic capacity were determined, respectively. The glycolytic reserve was measured as the difference between glycolysis and glycolytic capacity.

3.4.8. Citrate Synthase Activity

Maximal citrate synthase activity as a measure of mitochondrial content was determined in protein samples in the presence of DTNB as previously described [16]. The change in the rate of absorbance at 412 nm and pathlength was measured using a BioTek Synergy Mx Microplate Reader (BioTek Instruments). The extinction coefficient of 13.6 $mM^{-1}cm^{-1}$ was used. Values are expressed per µg cellular protein.

3.4.9. Cellular Protein Levels

To measure cellular protein content, RIPA buffer (Millipore) supplemented with a protease inhibitor cocktail (P8340, Sigma-Aldrich) and phosphatase inhibitor cocktail (78420, Thermo Fisher Scientific) was used during cell homogenization. A BCA assay was used to measure protein concentrations, as per the manufacturer's protocol. Protein samples were kept at −80°C for later use.

3.4.10. Western Blot Analyses

Protein samples were prepared in 1 x Laemmli buffer containing 100 mM DTT. Samples were separated on SDS-PAGE and then transferred onto PVDF (Bio-Rad) or nitrocellulose membranes. For glutathionylation, MFN1/2 oligomerization, and DRP1 oligomerization immunoblots, samples were prepared in 1 x Laemmli without DTT. Membranes were blocked with 5% BSA in Tris-buffered saline containing 0.1% Tween-20 (TBST) for 1 h at RT. Primary antibody incubations were overnight at 4°C. The following antibodies were purchased from Abcam: xCT (1:2000, ab175186), GPX1 (1:2000, ab22604), GPX4 (1:2000, ab16800), Grx2 (1:1000, ab191292), NRF2 (1:1000, ab31163), Total OXPHOS (1:1000, ab110413), and MFN1/2 (1:5000, ab57602). Antibodies from Santa Cruz were: GCL-c (1:1000, sc-390811), and GSS (1:1000, sc-365863). Antibodies from Protein Tech were: GCL-m (1:1000, 14241-1), OPA1 (1:2000, 27733-1), BCAT2 (1:2000, 16417-1), PHGDH (1:2000, 14719-1), PSAT1 (1:5000, 10501-1), PSPH (1:2000, 14513-1), CBS (1:2000, 14787-1), CTH (1:2000, 12217-1), GS (1:2000, 11037-2), GLS1 (1:2000, 12855-1), GLS2 (1:2000, 20171-1), GLUD1 (1:5000, 14299-1), P5CS (1:2000, 17719-1), PYCR1 (1:1000, 13108-1), PYCR2 (1:1000, 55060-1), ALDH4A1 (P5CDH) (1:1000, 11604-1), and PRODH (1:2000, 22980-1).

Additional antibodies included: Glutathione (1:1000, 101-A, Virogen), DRP1 (1:2000, 611113, BD Biosciences), and ATF4 (1:1000, 11815-S, Cell Signalling). Primary antibodies used against loading controls were: GAPDH (1:10000, 60004-1-Ig, Proteintech), and Vinculin (1:5000, ab129002, Abcam). A ChemiDoc™ MP Imaging System (Bio-Rad) was used to visualize protein bands and ImageJ software was employed to conduct protein band densitometry. The abundance of all target proteins is presented as normalized to the indicated loading control.

3.4.11. Mitochondrial H_2O_2 Emission

Mitochondrial H_2O_2 release was measured in cells using the fluorescent probe Amplex Red (ex/em: 563/587) using a Hitachi F2500 spectrophotometer as previously described [21]. Briefly, 1.5 million cells were incubated in 600 µL of buffer Z (in mM: 110 K-MES, 35 KCl, 1 EGTA, 5 K_2HPO_4, 3 $MgCl_2{\cdot}6H_2O$, and 0.5 mg/mL BSA, pH 7.3 at 4°C) in a 1 cm quartz cuvette with magnetic stirring at 37°C supplemented with 1.2 U/mL horseradish peroxidase, and 20 µM Amplex Red. Cells were permeabilized with 2 µg/µL digitonin. After baseline readings, the following were added sequentially: 2.5-5 mM malate-glutamate, 5 mM succinate, 10 mM ADP, and 8 µM antimycin-A. Values are reported as arbitrary fluorescence units.

3.4.12. Metabolomic Stable Isotope Tracer Analysis (SITA) and LC-MS

Stable isotope tracing was performed as previously described [22]. Briefly, cells were seeded in 60 mm dishes to achieve ~75% confluency for 24 h. DMEM was then replaced with equivalent media without 2ME, FBS, and HS, supplemented with 20% dialyzed FBS for 24 h. Then, an equivalent labelled medium with 25 mM [U-^{13}C]-glucose (CLM-1396-1, Cambridge Isotope Laboratories Inc) was added for the indicated time points. Cells were washed three times with ice-cold 150 mM ammonium formate solution, quenched in 230 µL ice-cold LC/MS grade 1:1 methanol:water solution, and vortexed for 10 s, before adding 220 µL acetonitrile. The collected cells were then homogenized using a bead mill homogenizer at 4°C for two rounds of 60 s at 30 Hz (Fisherbrand Bead Mill 24 Homogenizer). Homogenates were incubated with a 2:1 dichloromethane:water solution on ice for 10 min then centrifuged at 1,500 g for 10 min at 1°C. Water-soluble metabolites were collected from the upper phase, dried using a refrigerated CentriVap Vacuum Concentrator at −4°C (LabConco Corporation), and stored at -80°C before LC-MS analyses. Control samples that were not incubated with [U-^{13}C]-glucose were included in all tracer experiments.

Samples were randomized and re-suspended with 75% acetonitrile, cleared by centrifugation, and run in negative ESI on a 6545B Q-TOF mass spectrometer (Agilent) equipped with a 1290 Infinity II ultra-high-performance LC (Agilent) using hydrophilic interaction chromatography (HILIC-Z). Continuous internal mass calibration was executed using signals from purine [12,000 full width at half maximum (FWHM) resolution] and hexakis (1H, 1H, 3H-tetrafluoropropoxy) phosphazine (24,000 FWHM resolution). HILIC separation was obtained using the Poroshell 120 HILIC-Z column (2.1; 100 mm, 2.7 mm; Agilent) and the corresponding guard column. The chromatographic conditions and mass spectrometry acquisition parameters are described elsewhere [23]. The binary solvent system consisted of 10 mM ammonium acetate (pH 9) in water (solvent A) and 100 mM ammonium acetate in 85% acetonitrile (solvent B), both having 0.1% medronic acid. The gradient for separation started at 96% B for 1.5 min, then decreased from 96% to 65% B for 6.5 min followed by a 2 min hold at 65% B, and 7 min of re-equilibration to 96% B. This took the total run time to 17 min at a 0.25 mL/min flow rate. The injection volume was 10 µL, and the column temperature was maintained at 35°C.

Mass spectrometry detection was performed in negative ESI full scan mode with a mass range of 50 to 1000 m/z. The mass spectrometer source conditions consisted of a capillary voltage of 3000 V. Drying and sheath gas temperatures were set to 200 and 300°C and flow rates to 10 and 12 L/min, respectively. Nebulizer pressure was set to 40 psi and the fragmentor voltage was 175 V. Data were acquired in centroid mode at the rate of 3 spectra per second in the extended dynamic range mode (2 GHz). A target list of metabolites was created using “MassHunter Pathways to PCDL” software (Agilent). Metabolite retention times were provided from an in-house database.

3.4.13. Metabolomic Profiling

Samples were collected and run using LC-MS as mentioned in the SITA protocol but without tracer. All values were normalized to the protein content of parallel plates. Data were analyzed using Python

(Python Software Foundation. Python Language Reference, version 3.8.18. Available at www.python.org) and R (version 4.2.2.) [24]. All figures were produced using the matplotlib [25] and ggplot2 [26] libraries. Unless stated otherwise, statistical tests were performed through their respective Scipy method [27]. All data and code for these analyses are available in our GitHub repository: https://github.com/lkenn012/xCT_metabolomics

3.4.14. Analysis of Metabolomic Profiling Data

Hierarchical clustering and several statistical methods were applied after pre-processing the data from sample groups. Three different feature selection methods were employed for differential metabolite determination including Welch's t-test; orthogonal partial least squares discriminant analysis (OPLS-DA); and significance analysis of microarrays (SAM). Missing values were imputed according to a limit of detection imputation defined as ⅕ of the minimum value per metabolite feature. Following this, abundance values were $\log_{10}$-transformed and z-score normalized. Z-score normalized values were used for all statistical analyses except for significance testing by Welch's t-test, where the raw values including missing values were used.

For OPLS-DA, the "ropls" R package (version 1.30.0) [28] was used with 7-fold cross-validation for computing predictive performance (Q^2) and 20 permutation tests for computing significance. Important metabolites for sample group separation were determined based on the peak predictive performance of OPLS-DA models using increasingly stringent VIP score thresholds (using the formulation defined as $\boldsymbol{Vip_{4,pred}}$ by Galindo-Prieto, Eriksson, and Trygg [29]) of metabolite features, as suggested by Anderson and Bro [30]. For SAM tests, significantly different metabolites between WT and Slc7a11$^{sut/sut}$ samples were carried out using the "samr" R package (version 3.0) with 100 permutation tests (nperms=100) [31].

Enrichment plots for metabolite clusters were generated using the Metaboanalyst web server [32] via over-representation analysis, using all identified metabolites in the dataset as background (excluding non-specific metabolites such as total hexoses). Agglomerative hierarchical clustering linkages were determined according to the Ward algorithm applied to Euclidean distances (maximum cluster distance of 4) for Slc7a11$^{sut/sut}$ and WT unlabelled metabolomics data. Robinson-Fould metrics were computed using the ETE3 Python library [33] (ete3 version 3.1.3); these metrics estimate the conservation between two clustering dendrograms based on the proportion of shared linkages between metabolites.

3.4.15. Statistics

Unless otherwise mentioned, all data are shown as a mean ± standard error of the mean (SEM). Statistical analyses were conducted using Prism (GraphPad, La Jolla, CA). A two-tailed Student's t-test was used to determine statistical significance between WT vs. Slc7a11sut/sut. The statistical significance of primary MuSCs experiments with 3 different conditions (WT, Slc7a11sut/sut, and Slc7a11sut/sut + 2ME) was determined using one-way ANOVA with Tukey post hoc tests. P-values < 0.05 were considered statistically significant.

3.5 Results

3.5.1. xCT Controls GSH Levels and Redox in Proliferating Muscle Cells

Our first objective was to determine how xCT-mediated cystine import influences cellular GSH metabolism in proliferating MuSCs. To this end, we utilized primary muscle cells isolated from Slc7a11$^{sut/sut}$ mice and WT controls. Slc7a11$^{sut/sut}$ mice have a recessive mutation in the *Slc7a11* gene, resulting in the truncation of the xCT protein at the C terminus [34,35]. Slc7a11$^{sut/sut}$ MuSCs were cultured in media supplemented with β-mercaptoethanol (2ME) to support cell viability during proliferation [16]. 2ME was removed 24 hours before experimental analyses to allow analyses of the impact of xCT deficiency on metabolism, given that 2ME reduces extracellular cystine to cysteine, which can be transported into cells via Na (+)-dependent amino acid transporters, thereby masking the impact of xCT on cellular functions. We first measured cystine uptake levels to validate our cell model and approach. As expected, cystine uptake was lower (52%) in Slc7a11$^{sut/sut}$ MuSCs than in WT (**Figure 3.1A).** A similar decrease of cystine uptake was observed in WT MuSCs treated with the xCT inhibitor, erastin (10μM) (**Figure 3.1A**). In line with impaired cystine uptake, HPLC analyses revealed lower intracellular levels of GSH, GSH:GSSG, and total GSH, but higher GSSG in Slc7a11$^{sut/sut}$ MuSCs compared to WT MuSCs (**Figure 3.1B**). However, treating Slc7a11$^{sut/sut}$ MuSCs with 2ME effectively increased GSH, GSH:GSSG, and total GSH to levels higher than those in WT MuSCs (**Figure 3.1B**). Furthermore, immunoblotting analysis revealed that Slc7a11$^{sut/sut}$ MuSCs have a trend for decreased protein glutathionylation levels compared to WT (**Figure 3.1C**). These findings indicate that the xCT mutation impairs cystine influx and intracellular glutathione redox.

To evaluate the impact of xCT deficiency on mechanisms of GSH biosynthesis we measured the protein levels of key enzymes involved in this process. Immunoblotting analyses demonstrated similar levels of glutamate-cysteine ligase catalytic subunit (GCL-c) in both groups, but lower levels of the regulatory

glutamate-cysteine ligase modifier subunit (GCL-m) in Slc7a11$^{sut/sut}$ MuSCs compared to WT (**Figure 3.1D**) [36]. Interestingly, protein levels of GSH synthetase (GSS), which catalyzes the last step of GSH biosynthesis by adding glycine, were higher in Slc7a11$^{sut/sut}$ MuSCs (**Figure 3.1D**), in a failed attempt to compensate for decreased cyst(e)ine availability for GSH biosynthesis. These findings are consistent with the idea that the decrease in intracellular GSH in Slc7a11$^{sut/sut}$ MuSCs results from impaired GSH synthesis due to lower GCL-m protein levels and limited cysteine availability.

To assess if the perturbed cellular GSH redox influenced the susceptibility of Slc7a11$^{sut/sut}$ MuSCs to oxidative stress, we quantified H_2O_2 production. H_2O_2 production was higher in Slc7a11$^{sut/sut}$ MuSCs than in WT across different mitochondrial respiratory states (**Figure 3.1E**). Despite increased H_2O_2 production, there were similar protein levels of GSH peroxidase 1 (GPX1), GSH peroxidase 4 (GPX4), and NRF2 between WT and Slc7a11$^{sut/sut}$ MuSCs (**Figure 3.1F and G, Supplementary Figure 3.1A**). These findings suggest that the increase in H_2O_2 levels was not attributable to lower protein levels of GSH-dependent antioxidant enzymes; instead, it may result from limited GSH availability.

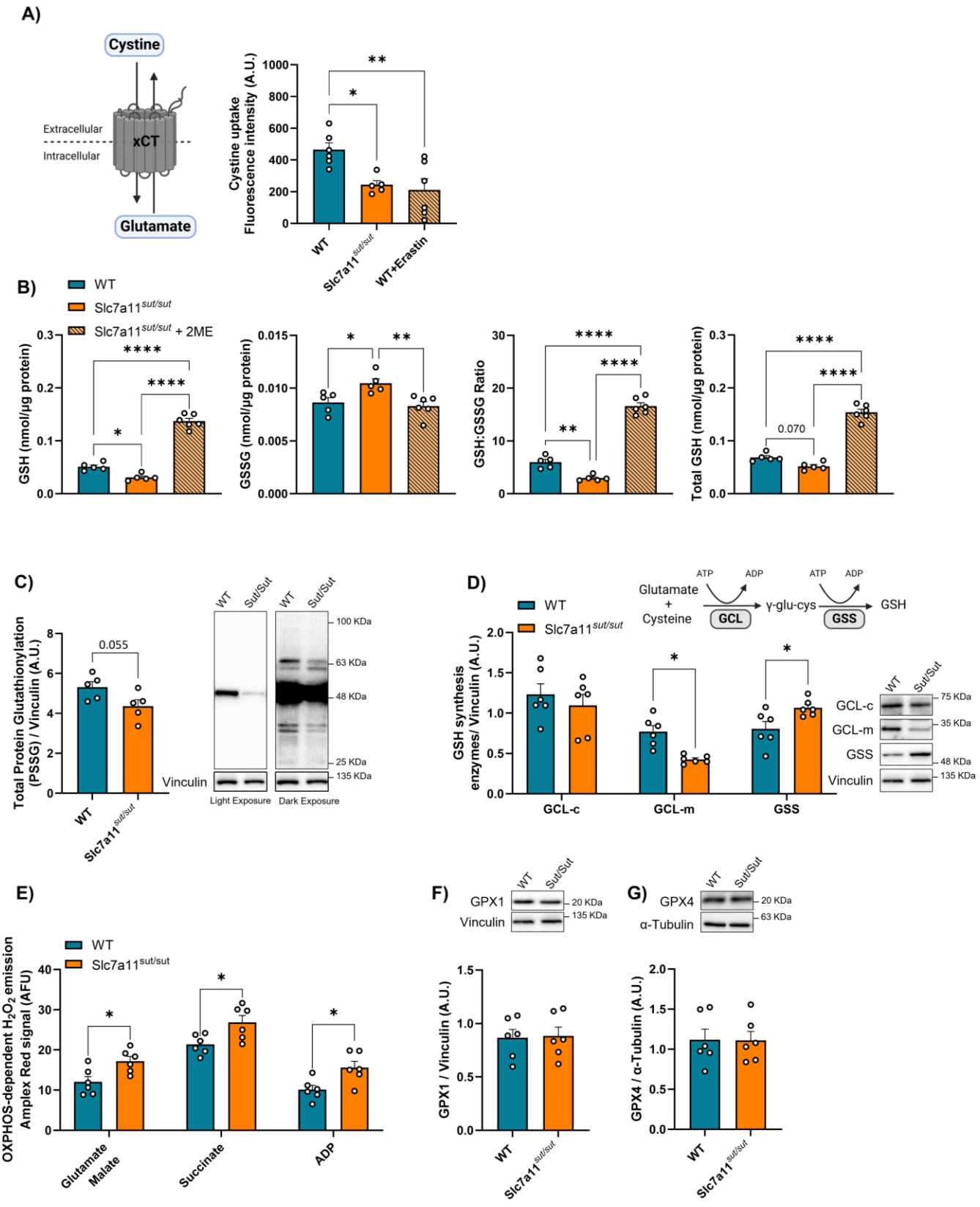
A)
Cystine
Extracellular
Intracellular
xCT
Glutamate
Cystine uptake Fluorescence intensity (A.U.)
WT
Slc7a11sut/sut
WT+Erastin
B)
WT
Slc7a11sut/sut
Slc7a11sut/sut + 2ME
GSH (nmol/µg protein)
GSSG (nmol/µg protein)
GSH:GSSG Ratio
Total GSH (nmol/µg protein)
0.070
C)
Total Protein Glutathionylation (PSSG) / Vinculin (A.U.)
0.055
Vinculin
Light Exposure
Dark Exposure
100 KDa
63 KDa
48 KDa
25 KDa
135 KDa
D)
GSH synthesis enzymes/ Vinculin (A.U.)
Glutamate + Cysteine
ATP
ADP
GCL
γ-glu-cys
GSS
GSH
GCL-c
GCL-m
GSS
75 KDa
35 KDa
48 KDa
135 KDa
E)
OXPHOS-dependent H2O2 emission Amplex Red signal (AFU)
Glutamate Malate
Succinate
ADP
F)
GPX1
Vinculin
20 KDa
135 KDa
GPX1 / Vinculin (A.U.)
G)
GPX4
α-Tubulin
20 KDa
63 KDa
GPX4 / α-Tubulin (A.U.)

Figure 3.1. xCT Controls GSH Levels and Redox in Proliferating Muscle Cells
(A) Rate of cystine uptake measured using the fluorescent probe fluorescein O, O'-diacrylate in WT, Slc7a11$^{sut/sut}$, and WT + erastin MuSCs. **(B)** Reduced glutathione (GSH), oxidized glutathione (GSSG), GSH:GSSG ratio, and total glutathione (GSH + (2 x GSSG)) measured by HPLC in WT, Slc7a11$^{sut/sut}$, and Slc7a11$^{sut/sut}$ + 2ME. **(C-D)** Immunoblots of WT and Slc7a11$^{sut/sut}$ MuSCs against **(C)** post-translational glutathionylation, and **(D)** GSH synthesis enzymes, glutamate-cysteine ligase (GCL) catalytic (GCL-c) and modifier (GCL-m) subunits, and GSH synthetase (GSS). **(E)** Mitochondrial H_2O_2 emissions in digitonin permeabilized WT and Slc7a11$^{sut/sut}$ MuSCs. **(F-G)** Immunoblots of WT and Slc7a11$^{sut/sut}$ MuSCs against **(F)** GPX1, and **(G)** GPX4. Comparisons between groups were determined using a one-way ANOVA with post hoc Tukey HSD test, n = 5-6 (A-B); two-tailed Student's t-test, n = 5-6 (C-G). Results are presented as mean ± SEM, *p < 0.05, **p < 0.01, ***p < 0.001, ****p < 0.0001.

3.5.2. Impaired cellular bioenergetics accompanied by fragmented mitochondrial structure in Slc7a11$^{sut/sut}$ MuSCs

Given that cellular GSH redox is known to be important in maintaining mitochondrial energy homeostasis, we performed Seahorse XF analyses to assess mitochondrial respiration and glycolytic flux in WT and Slc7a11$^{sut/sut}$ MuSCs [37,38]. Slc7a11$^{sut/sut}$ MuSCs displayed overall lower oxidative capacity with a 42 % decrease in resting, a 33% decrease in leak, and a 50% decrease in maximal oxygen consumption rates (OCR) compared to WT MuSCs (**Figure 3.2A and B)**. Quantification of extracellular acidification rates (ECAR), a proxy measure of glycolysis, revealed that Slc7a11$^{sut/sut}$ MuSCs display a trend for a decrease in resting and maximal ECAR rates compared to WT MuSCs (**Figure 3.2C and D**). When forcing the cells to use glycolysis by inhibiting OXPHOS, the Slc7a11$^{sut/sut}$ MuSCs exhibited an impaired ability to upregulate glycolysis (**Supplementary Figure 3.2A and B**). However, when using the Mookerjee method [39] to evaluate absolute ATP levels from glycolysis and OXPHOS under different metabolic states, it was clear that Slc7a11$^{sut/sut}$ MuSCs were more dependent on glycolytic than OXPHOS for ATP production. Specifically, there was a higher proportion of ATP derived from glycolysis in Slc7a11$^{sut/sut}$ MuSCs during resting and maximal respiration (**Figure 3.2E and F**). In line with these findings, glucose uptake was higher in Slc7a11$^{sut/sut}$ than in WT MuSCs, further confirming the greater dependence on glycolysis in xCT-deficient cells (**Figure 3.2G**).

To determine whether the diminished OXPHOS capacity observed in Slc7a11$^{sut/sut}$ MuSCs resulted from decreased mitochondrial content, we measured citrate synthase activity and the protein levels of key OXPHOS proteins. Findings showed that citrate synthase activity and protein levels of OXPHOS complexes I, II, and IV were lower in Slc7a11$^{sut/sut}$ compared to WT MuSCs (**Figure 3.2H, Supplementary Figure 3.2C**), indicative of decreased mitochondrial content in Slc7a11$^{sut/sut}$ compared to WT MuSCs.

GSH redox and oxidative stress are critical in regulating mitochondrial dynamics [40]. Specifically, high GSSG levels promote mitochondrial hyperfusion [40,41], and oxidative stress is associated with increased fission [42]. Given our observations of elevated GSSG levels and H_2O_2 emissions in Slc7a11$^{sut/sut}$ MuSCs, we were curious as to whether the xCT deficiency would cause hyperfusion, increased fission, or no change in the mitochondrial network. Quantitative analysis of TOMM20-stained MuSCs revealed that the mitochondrial network was more fragmented in Slc7a11$^{sut/sut}$ MuSCs compared to WT MuSCs, as indicated by the lower total branch length per mitochondrion and lower number of branches per mitochondrion (**Figure 3.2I, J, and K**). The fragmented mitochondrial reticulum observed in Slc7a11$^{sut/sut}$ MuSCs was not attributed to differences in protein levels of the large GTPase proteins that maintain mitochondrial fusion and fission, including optic atrophy 1 (OPA1), mitofusins 1 and 2 (MFN1/2). Moreover, dynamin-related protein-1 (DRP1) protein levels were comparable between Slc7a11$^{sut/sut}$ MuSCs and WT (**Supplementary Figure 3.2D**). As GSH redox also plays a role in determining MFN1/2 oligomerization which drives mitochondrial fusion by regulating disulfide modifications in the mitochondrial membrane [41,43], we then performed immunoblots under non-reducing conditions to preserve disulfide bonds and found that Slc7a11$^{sut/sut}$ MuSCs had less MFN1/2 oligomers (between 160 and 250 kDa, **Supplementary Figure 3.2E**) compared to WT MuSCs, but displayed higher DRP1 oligomerization than WT MuSCs (**Supplementary Figure 3.2F**). In summary, xCT deficiency results in a fragmented mitochondrial network in MuSCs associated with lower MFN1/2 oligomers and higher DRP1 oligomerization, which may contribute to impaired mitochondrial oxidative capacity.

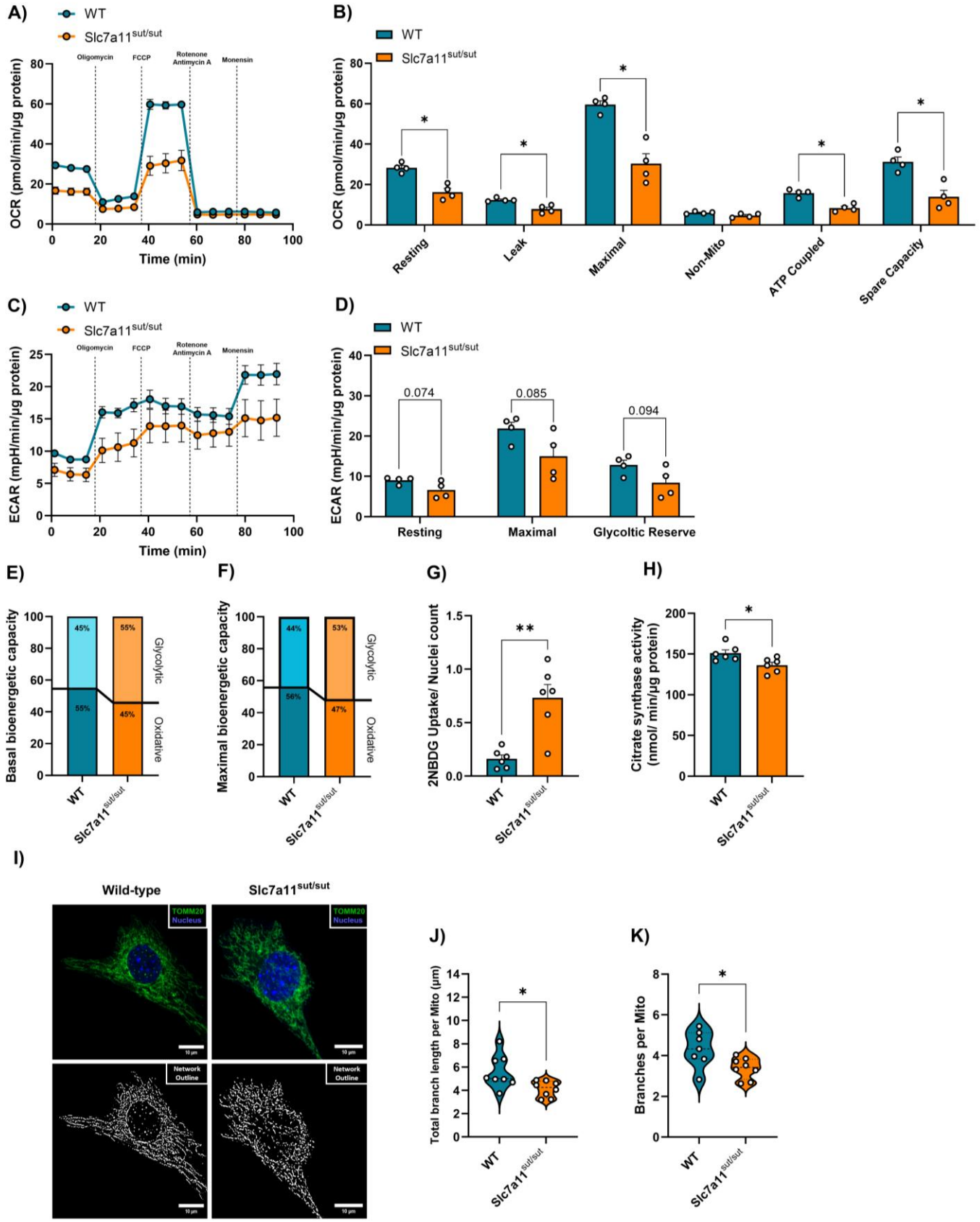
A)
WT
Slc7a11sut/sut
Oligomycin
FCCP
Rotenone Antimycin A
Monensin
OCR (pmol/min/µg protein)
Time (min)
B)
WT
Slc7a11sut/sut
OCR (pmol/min/µg protein)
Resting
Leak
Maximal
Non-Mito
ATP Coupled
Spare Capacity
C)
WT
Slc7a11sut/sut
Oligomycin
FCCP
Rotenone Antimycin A
Monensin
ECAR (mpH/min/µg protein)
Time (min)
D)
WT
Slc7a11sut/sut
ECAR (mpH/min/µg protein)
0.074
0.085
0.094
Resting
Maximal
Glycoltic Reserve
E)
Basal bioenergetic capacity
45%
55%
55%
45%
Glycolytic
Oxidative
WT
Slc7a11sut/sut
F)
Maximal bioenergetic capacity
44%
56%
53%
47%
Glycolytic
Oxidative
WT
Slc7a11sut/sut
G)
2NBDG Uptake/ Nuclei count
WT
Slc7a11sut/sut
H)
Citrate synthase activity (nmol/ min/µg protein)
WT
Slc7a11sut/sut
I)
Wild-type
Slc7a11sut/sut
TOMM20
Nucleus
Network Outline
J)
Total branch length per Mito (µm)
WT
Slc7a11sut/sut
K)
Branches per Mito
WT
Slc7a11sut/sut

Figure 3.2. Impaired cellular bioenergetics accompanied by fragmented mitochondrial structure in Slc7a11$^{sut/sut}$ MuSCs

(A-B) Oxygen consumption rates (OCR) and **(C-D)** extracellular acidification rates (ECAR) measured in primary WT and Slc7a11$^{sut/sut}$ MuSCs. The contributions of OXPHOS and glycolysis to ATP production were calculated following the Mookerjee *et al*., 2017 method for **(E)** Basal and **(F)** Maximal bioenergetic capacities in WT and Slc7a11$^{sut/sut}$ MuSCs. **(G)** Glucose uptake quantified using 2-NBDG in WT and Slc7a11$^{sut/sut}$ primary MuSCs. **(H)** Citrate synthase enzyme activity in WT and Slc7a11$^{sut/sut}$ MuSCs. **(I)** Immunofluorescence staining of TOMM20 (green) and DAPI (blue), scale bar = 10 μm. Thresholded TOMM20 signals are shown in white. **(J-K)** Quantitative morphometric analyses of TOMM20-staining examining **(J)** total branch length per mitochondria (μm), and **(K)** number of branches per mitochondria. Each data point represents a region of interest (ROI) containing 2 to 3 mitochondria. 2 ROI were imaged and analyzed for each sample, n = 4. The statistical significance of the differences between groups was determined using a two-tailed Student's t-test, n = 4 (A-F, J-K); n = 6 (G-H). Results are presented as mean ± SEM, *p < 0.05, **p < 0.01, ***p < 0.001, ****p < 0.0001.

3.5.3. Metabolomic Profiling Analysis Reveals Distinct Phenotypes Including Differences in Branched Chain Amino Acids, Cysteine, Methionine, and Proline in Slc7a11$^{sut/sut}$ MuSCs

To elucidate the specific metabolic pathways impacted by impaired xCT function, we analyzed the global metabolite profiles in WT and Slc7a11$^{sut/sut}$ MuSCs under steady-state conditions using ion-pairing (LC-MS). We applied three different feature selection methods to the 107 detected metabolites to characterize the metabolic phenotypes (Welch's t-test $p<0.05$; OPLS-DA; and SAM), which consistently identified 27 metabolites that differed in abundance between Slc7a11$^{sut/sut}$ and WT MuSCs (**Figure 3.3A, B, Table 3.1, and Supplementary Figure 3.3A, B and C**). Slc7a11$^{sut/sut}$ MuSCs had lower levels of GSH, 4,5-dihydroorotate, uracil, dihydrouracil, and orotic acid, but higher levels of several amino acids compared to WT MuSCs, including proline, methionine, glycine, glutamine, and branched-chain amino acids (BCAAs, valine, leucine, and isoleucine) (**Figure 3. 3A and Table 3.1**). Hierarchical clustering showed well-distinguished metabolic clusters between Slc7a11$^{sut/sut}$ and WT MuSCs, with a normalized Robinson-Foulds (RF) distance of 0.914 (where RF=1 no common clustering in dendrograms, see Experimental Procedures) [44]. The 27 identified metabolites differing in abundance were dispersed across several clusters in the WT samples (clusters 1, 2, and 3), but largely showed related behavior and grouped in a single cluster (cluster 3) in Slc7a11$^{sut/sut}$ MuSCs. While clusters 6 and 7 in WT samples are largely consistent with Slc7a11$^{sut/sut}$ clusters 5 and 6, differences in the clustering of many other metabolites further indicate an overall metabolic reprogramming (**Supplementary Figure 3.3D**).

Metabolite set enrichment analyses of the 27 differing metabolites further highlighted major differences between Slc7a11$^{sut/sut}$ and WT MuSCs in the metabolism of BCAAs, pyrimidines, cysteine, methionine, and GSH (**Figure 3.3C**). BCAAs are catabolized by branched-chain amino acid transaminases (BCATs), which exist in two isoforms: the cytosolic and redox-sensitive BCAT1, and mitochondrial BCAT2, which is the predominant isoform in skeletal muscle [45,46]. The increased abundance of valine, leucine, and

isoleucine (**Figure 3.3D**) could be related to decreased BCAA catabolism, as protein levels of branched-chain amino acid transaminase 2 (BCAT2), was lower in Slc7a11$^{sut/sut}$ MuSCs (**Figure 3.3E**). As anticipated, metabolites involved in endogenous cysteine biosynthesis, such as serine and methionine, were more abundant in Slc7a11$^{sut/sut}$ MuSCs (**Figure 3.3F**). Importantly, key metabolites related to proline biosynthesis and urea cycle (glutamine, ornithine, and proline) were also among the most elevated metabolites in Slc7a11$^{sut/sut}$ MuSCs compared to WT (**Figure 3.3G**).

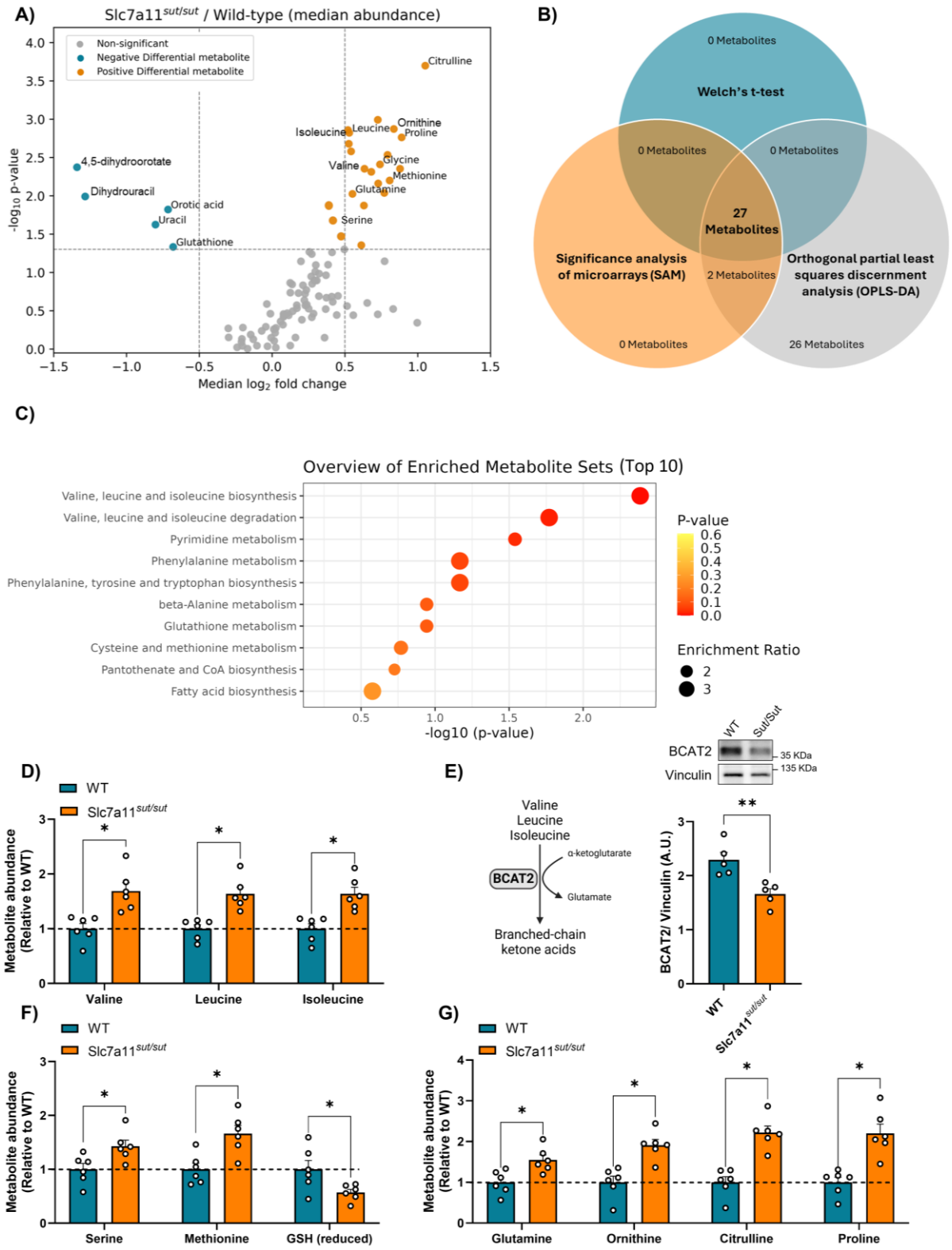
A)
Slc7a11sut/sut / Wild-type (median abundance)
Non-significant
Negative Differential metabolite
Positive Differential metabolite
Citrulline
Isoleucine
Leucine
Ornithine
Proline
Valine
Glycine
Methionine
Glutamine
4,5-dihydroorotate
Dihydrouracil
Orotic acid
Uracil
Glutathione
Serine
-log10 p-value
Median log2 fold change
B)
0 Metabolites
Welch's t-test
0 Metabolites
0 Metabolites
27 Metabolites
Significance analysis of microarrays (SAM)
2 Metabolites
Orthogonal partial least squares discernment analysis (OPLS-DA)
0 Metabolites
26 Metabolites
C)
Overview of Enriched Metabolite Sets (Top 10)
Valine, leucine and isoleucine biosynthesis
Valine, leucine and isoleucine degradation
Pyrimidine metabolism
Phenylalanine metabolism
Phenylalanine, tyrosine and tryptophan biosynthesis
beta-Alanine metabolism
Glutathione metabolism
Cysteine and methionine metabolism
Pantothenate and CoA biosynthesis
Fatty acid biosynthesis
-log10 (p-value)
P-value
Enrichment Ratio
D)
WT
Slc7a11sut/sut
Metabolite abundance (Relative to WT)
Valine
Leucine
Isoleucine
E)
Valine
Leucine
Isoleucine
α-ketoglutarate
BCAT2
Glutamate
Branched-chain ketone acids
WT
Sut/Sut
BCAT2
Vinculin
35 KDa
135 KDa
BCAT2/ Vinculin (A.U.)
WT
Slc7a11sut/sut
F)
WT
Slc7a11sut/sut
Metabolite abundance (Relative to WT)
Serine
Methionine
GSH (reduced)
G)
WT
Slc7a11sut/sut
Metabolite abundance (Relative to WT)
Glutamine
Ornithine
Citrulline
Proline

Figure 3.3. Metabolomic Profiling Analysis Reveals Distinct Phenotypes Including Differences in Branched Chain Amino Acids, Cysteine, Methionine, and Proline in Slc7a11$^{sut/sut}$ MuSCs
(A) Volcano plot of metabolite profiles. **(B)** Metabolites differing in abundance between WT and Slc7a11$^{sut/sut}$ MuSCs were determined by Welch's t-test, OPLS-DA, and SAM. **(C)** KEGG metabolite set enrichment analysis (top 10, p-value < 0.30) of metabolic pathways altered in Slc7a11$^{sut/sut}$ MuSCs. **(D)** Abundance of branched-chain amino acid metabolites valine, leucine, and isoleucine (relative to WT) **(E)** Immunoblot of branched-chain amino acid transaminase 2 (BCAT2) in WT and Slc7a11$^{sut/sut}$ MuSCs. **(F-G)** Abundance of serine, methionine, GSH (reduced), glutamine, ornithine, citrulline, and proline (relative to WT). Comparisons between groups were determined using a two-tailed Student's t-test, n = 6 (D-G). Results are presented as mean ± SEM, *p < 0.05, **p < 0.01.

Metabolite	**WT**	**Slc7a11$^{sut/sut}$**	**log2 FC**	**t-test p-value**	**SAM**	**OPLS-DA**
Citrulline	14922	33139	1.05198	0.00020	0.02486	1.60270
Tryptophan	55109	94749	0.72614	0.00102	0.02486	1.71256
Ornithine	13565	25924	0.83596	0.00134	0.02486	1.39675
Phenylalanine	30191	48760	0.52096	0.00139	0.02486	1.72568
Leucine	19273	31582	0.52991	0.00151	0.02486	1.73038
Proline	349393	769361	0.88983	0.00173	0.02486	1.66877
Isoleucine	16476	26944	0.52684	0.00210	0.02486	1.65313
Tyrosine	17564	27135	0.54251	0.00263	0.02486	1.64029
Ethyl pyruvate	53655	85704	0.79305	0.00293	0.02486	1.58940
Glycine	17762	30089	0.74111	0.00390	0.02486	1.61603
4,5-dihydroorotate	86398	37895	-1.33959	0.00425	0.02486	1.63022
Uridine	30710	50472	0.87892	0.00444	0.02486	1.54333
Valine	8513	14383	0.63449	0.00444	0.02486	1.60971
Threonine	144251	240015	0.68138	0.00487	0.02486	1.54312
Methionine	158338	263288	0.80749	0.00632	0.02486	1.55373
Histidine	41111	71955	0.72868	0.00691	0.02486	1.56655
Histamine	12046	19978	0.77063	0.00919	0.02486	1.56147
Glutamine	330381	511514	0.55201	0.00945	0.03072	1.47808
Dihydrouracil	31715	12634	-1.28365	0.01022	0.02486	1.68672
Asparagine	48528	68521	0.38894	0.01325	0.03947	1.46708

Lysine	7731	13708	0.63061	0.01340	0.03397	1.17329
Orotic acid	35192	20464	-0.71437	0.01510	0.03408	1.27957
Serine	111068	158695	0.41710	0.02090	0.04093	1.36111
Uracil	65576	37279	-0.80083	0.02378	0.03072	1.43802
Malonic acid	14312	20449	0.47252	0.03366	0.04492	1.28729
2-Acetamido-2-Deoxy-D-Glucopyranose	5053	7244	0.61275	0.04414	0.04255	1.25646
Glutathione (reduced)	169737	96518	-0.67949	0.04648	0.03743	1.26352

Table 3.1. List of significantly different metabolites between WT and Slc7a11$^{sut/sut}$ MuSCs.
Rows in grey indicate a higher abundance of metabolite in WT compared to Slc7a11$^{sut/sut}$ MuSCs.

3.5.4. xCT Deficiency Upregulates Glucose Uptake and Promotes Cellular de novo Serine Synthesis

Given the evidence of greater reliance on glycolysis for ATP production in Slc7a11$^{sut/sut}$ MuSCs, we next performed stable isotope tracing analysis (SITA) of [U-^{13}C]-glucose to elucidate alterations in flux through specific metabolic pathways. After testing various incubation times following standard practices, a 12-hour incubation with ^{13}C-labelled glucose proved optimal for most metabolic pathways of interest (**Supplementary Figure 3.4A**) [47]. The integration of ^{13}C into the glycolytic metabolites 3-phosphoglycerate (3PG) and 2-phosphoglycerate (2PG) was similar between Slc7a11$^{sut/sut}$ and WT MuSCs (**Figure 3.4A, B and C**). Glucose-derived pyruvate is the major end-product of glycolysis, which can subsequently be converted to acetyl-CoA by pyruvate dehydrogenase (PDH) to enter the TCA cycle or can contribute to TCA cycle anaplerosis via pyruvate carboxylase (PC) production of oxaloacetate. The Slc7a11$^{sut/sut}$ MuSCs displayed elevated amounts of pyruvate m+3 and lactate m+3 compared to WT (**Figures 3.4D and E**) indicating that pyruvate accumulates instead of entering the TCA cycle. Indeed, the calculated citrate m+2 / pyruvate m+3 and citrate m+3 / pyruvate m+3 ratios, proxy measures for PDH- and PC-dependent labelling respectively [48], were lower in the Slc7a11$^{sut/sut}$ MuSCs (**Figures 3.4F and G**). Moreover, Slc7a11$^{sut/sut}$ MuSCs had a lower carbon labelling to TCA cycle metabolites (**Figure 3.4H and Supplementary Figure 3.4B)**, further supporting the conclusion that there is an impaired utilization of glucose-derived carbons in the TCA cycle by Slc7a11$^{sut/sut}$ MuSCs.

Glucose also serves as a precursor for *de novo* serine synthesis by converting glycolysis-derived 3PG to 3-phosphohydroxypyruvate in a reaction catalyzed by phosphoglycerate dehydrogenase (PHGDH) [49]. *De novo* serine synthesis is upregulated during times of amino acid starvation, as serine is a major donor to the carbon pool for one-carbon (1C) metabolism, linking the folate and methionine cycles with the transsulfuration pathway to support amino acid metabolism, redox homeostasis, nucleotide biosynthesis, and methylation reactions [50]. Serine 1C metabolism also plays a key role in GSH biosynthesis via

endogenous cysteine and glycine biosynthesis [51] (**Figure 3.4I**). Thus, we hypothesized that the Slc7a11$^{sut/sut}$ MuSCs would have an increased reliance on glycolytic metabolism to support *de novo* synthesis of serine as a compensatory mechanism to restore GSH redox. Consistent with our hypothesis, Slc7a11$^{sut/sut}$ MuSCs had higher serine m+3 levels (from glycolysis-derived 3PG) compared to WT [52], indicating an increased serine biosynthesis from glycolysis (**Figure 3.4J).** Moreover, protein levels of key enzymes involved in *de novo* serine synthesis (PSAT1 and PSPH) were higher in Slc7a11$^{sut/sut}$ MuSCs compared to WT MuSCs (**Figure 3.4K**). Notably, WT and Slc7a11$^{sut/sut}$ MuSCs had similar m+2 labelling to glycine, suggesting that glucose-derived serine is preferentially shunted towards the transsulfuration pathway for cysteine biosynthesis **(Supplementary Figure 3.4C**). Indeed, while expression of cystathionine β-synthase (CBS), which catalyzes the conversion of serine and homocysteine to cystathionine, was comparable between genotypes, the protein level of cystathionine γ-lyase (CTH), which converts cystathionine to cysteine, was higher in the Slc7a11$^{sut/sut}$ MuSCs (**Figure 3.4L**). The levels of GSH m+2 (derived from glycine m+2 or glutamate m+2 incorporation), and GSH m+4 (derived from the incorporation of both glycine m+2 and glutamate m+2) were lower in Slc7a11$^{sut/sut}$ MuSCs (**Figure 3.4M**). Conversely, the level of GSH m+3 (derived from cysteine m+3 incorporation) was not different between genotypes, suggesting that transsulfuration pathway activity in Slc7a11$^{sut/sut}$ MuSCs resulted in GSH biosynthesis (**Figure 3.4M**). Lastly, we measured protein levels of activating transcription factor 4 (ATF4), a key regulator of serine biosynthesis and cellular response to amino acid starvation [53]. In line with upregulated serine biosynthesis and transsulfuration pathway activity, immunoblots showed increased ATF4 in Slc7a11$^{sut/sut}$ MuSCs (**Supplementary Figure 3.4D**).

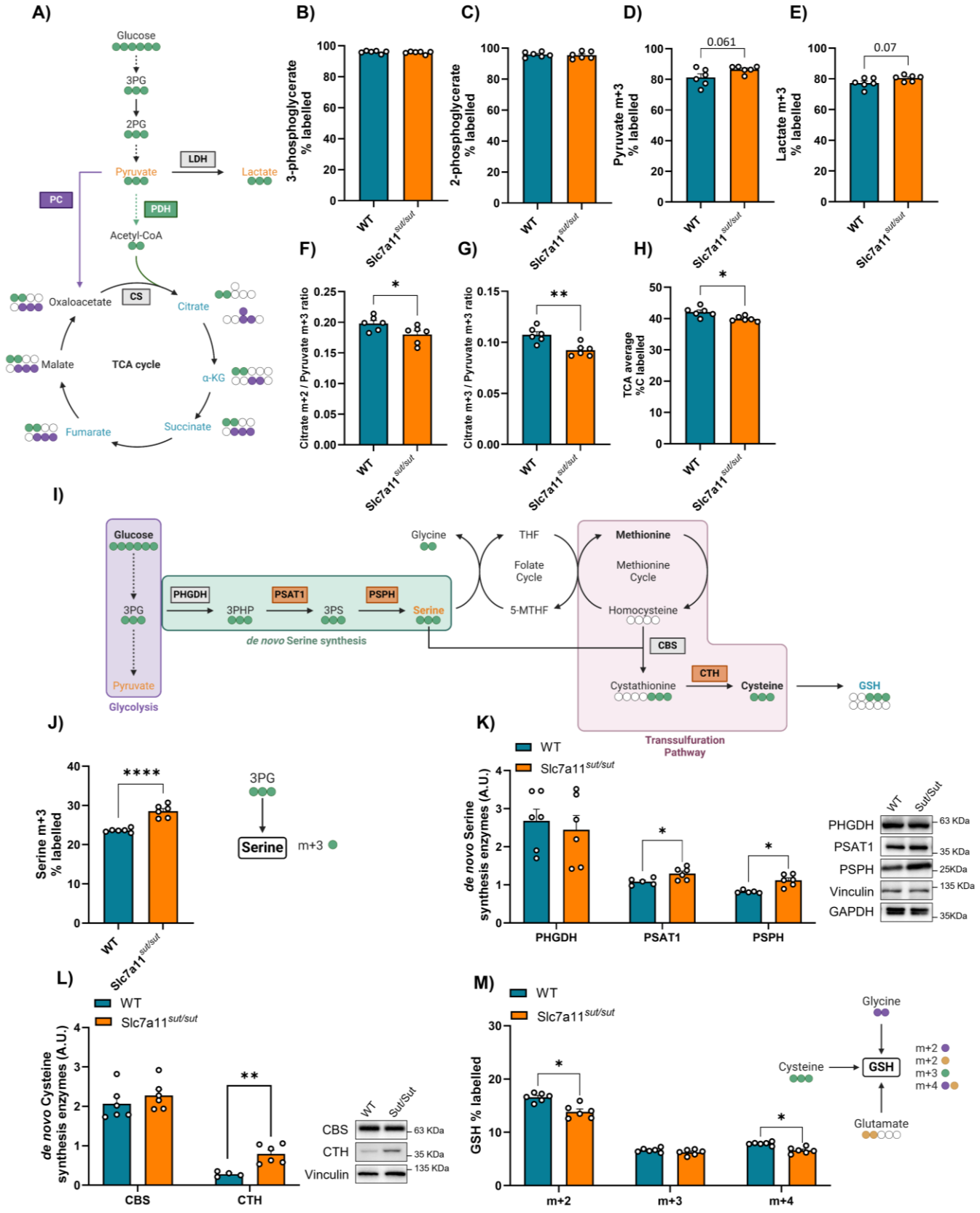
A)
Glucose
3PG
2PG
Pyruvate
LDH
Lactate
PC
PDH
Acetyl-CoA
Oxaloacetate
CS
Citrate
Malate
TCA cycle
α-KG
Fumarate
Succinate
B)
3-phosphoglycerate % labelled
C)
2-phosphoglycerate % labelled
D)
Pyruvate m+3 % labelled
0.061
E)
Lactate m+3 % labelled
0.07
F)
Citrate m+2 / Pyruvate m+3 ratio
G)
Citrate m+3 / Pyruvate m+3 ratio
H)
TCA average %C labelled
WT
Slc7a11sut/sut
I)
Glucose
3PG
Pyruvate
Glycolysis
PHGDH
3PHP
PSAT1
3PS
PSPH
Serine
de novo Serine synthesis
Glycine
THF
Folate Cycle
5-MTHF
Methionine
Methionine Cycle
Homocysteine
CBS
CTH
Cystathionine
Cysteine
GSH
Transsulfuration Pathway
J)
Serine m+3 % labelled
3PG
Serine
m+3
K)
WT
Slc7a11sut/sut
de novo Serine synthesis enzymes (A.U.)
PHGDH
PSAT1
PSPH
Sut/Sut
63 KDa
35 KDa
25KDa
Vinculin
135 KDa
GAPDH
35KDa
L)
de novo Cysteine synthesis enzymes (A.U.)
CBS
CTH
M)
GSH % labelled
Glycine
Cysteine
GSH
Glutamate
m+2
m+2
m+3
m+4
m+2
m+3
m+4

Figure 3.4. xCT Deficiency Upregulates Glucose Uptake and Promotes Cellular *de novo* Serine Synthesis

(A) Stable isotope tracing diagram for [U-^{13}C]-Glucose through glycolysis and TCA cycle via pyruvate dehydrogenase (PDH, green) and pyruvate carboxylase (PC, purple). Labelled metabolites are coloured orange (higher in Slc7a11$^{sut/sut}$ MuSCs), blue (lower in Slc7a11$^{sut/sut}$ MuSCs), and black (similar between Slc7a11$^{sut/sut}$ and WT MuSCs). **(B-E)** [U-^{13}C]-Glucose labelling (12 hrs) of labelled glycolytic intermediate metabolites 3-phosphoglycerate, labelled 2-phosphoglycerate, pyruvate m+3, and lactate m+3, in WT and Slc7a11$^{sut/sut}$ MuSCs. **(F-G)** Citrate m+2 / pyruvate m+3 and citrate m+3 / pyruvate m+3 ratios of [U-^{13}C]-glucose labelling (12 hrs) as proxies of PDH and PC, respectively. **(H)** Relative proportion of labelled TCA cycle intermediates (citrate, α-ketoglutarate, succinate, fumarate, and malate) derived from [U-^{13}C]-glucose precursor. **(I)** [U-^{13}C]-glucose labelling through the *de novo* serine synthesis pathway, and cysteine biosynthesis via the transsulfuration pathway. Enzymes and labelled metabolites are coloured orange (higher in Slc7a11$^{sut/sut}$ MuSCs), blue (lower in Slc7a11$^{sut/sut}$ MuSCs), and black (similar between Slc7a11$^{sut/sut}$ and WT MuSCs). **(J)** [U-^{13}C]-glucose labelling (12 hrs) of serine m+2 (from gluconeogenesis) and serine m+3 (from glycolysis) expressed as percentage of total respective metabolite levels. **(K-L)** Immunoblot of **(K)** *de novo* serine synthesis (PHGDH, PSAT1, and PSPH), and **(L)** *de novo* cysteine synthesis (CBS and CTH) enzymes. **(M)** [U-^{13}C]-glucose labelling (12 hrs) of GSH m+2 (from [U-^{13}C]-glucose-derived glycine or glutamate), GSH m+3 (from [U-^{13}C]-glucose-derived cysteine), and GSH m+4 (from [U-^{13}C]-glucose derived glycine and glutamate). The statistical significance of the differences between groups was determined using a two-tailed Student's t-test, n = 6. Results are presented as mean ± SEM, *p < 0.05, **p < 0.01, ***p < 0.001, ****p < 0.0001.

3.5.5. Increased Proline Biosynthesis in the Absence of Functional xCT

Proline was among the most significantly increased metabolites in Slc7a11$^{sut/sut}$ MuSCs compared to WT. Proline biosynthesis involves the intermediate, pyrroline-5-carboxylate (P5C), which is produced from glutamate by P5C synthase (P5CS) and subsequently converted to proline by P5C reductase (PYCR)[54] (**Figure 3.5A**). While the ^{13}C-labelled glucose labelling to TCA cycle related metabolites, αKG and glutamate were lower in Slc7a11$^{sut/sut}$ MuSCs (**Figure 3.5B and C**), increased levels of proline were revealed by the metabolomic profiling and the stable isotope approaches (**Figure 3.5D and Figure 3.3G**). These results suggest an increased relative efflux of carbons from the TCA cycle toward proline biosynthesis via the glutamate-P5C-proline axis in Slc7a11$^{sut/sut}$ MuSCs. This is further supported by higher protein levels of P5CS and higher levels of urea cycle intermediates including ornithine and citrulline (**Figure 3.5E and Figure 3.3G**). However, the protein levels of enzymes involved in the last step of proline biosynthesis, pyrroline-5-carboxylate reductases 1 and 2 (PYCR1 and PYCR2), were comparable between both genotypes (**Figure 3.5E**). Levels of proline dehydrogenase (PRODH) and pyrroline-5-carboxylate dehydrogenase (P5CDH), which are enzymes responsible for the degradation of proline and P5C, respectively, were comparable between the two groups (**Figure 3.5F**).

Proline and glutamine metabolism are closely interconnected through glutamate and its derivative P5C [55]. Therefore, we immunoblotted for various enzymes that mediate the interconversion of glutamine and glutamate such as glutamine synthase (GS) and glutaminase (GLS) [56]. The levels of GS, which catalyzes glutamine biosynthesis from glutamate, were lower in Slc7a11$^{sut/sut}$ MuSCs (**Figure 3.5G**). There were similar GLS1 and GLS2 protein levels in WT and Slc7a11$^{sut/sut}$ MuSCs (**Figure 3.5G**), supporting the conclusion that glutamine degradation into glutamate was comparable between groups. Thus, glutamine accumulation in Slc7a11$^{sut/sut}$ MuSCs, does not appear to be related to impaired glutaminolysis. Glutamate can also be converted to α-ketoglutarate (α-KG) to enter the TCA cycle in a

reaction catalyzed by glutamate dehydrogenase (GLUD1) [56]. Despite lower ^{13}C-labelled flux of metabolites into the TCA cycle in Slc7a11$^{sut/sut}$ MuSCs, GLUD1 protein levels were not different between groups (**Figure 3.5G**). Altogether, these findings are consistent with the conclusion that glutamate in xCT-deficient MuSCs primarily serves as a precursor for proline biosynthesis rather than an anaplerotic substrate for the TCA cycle.

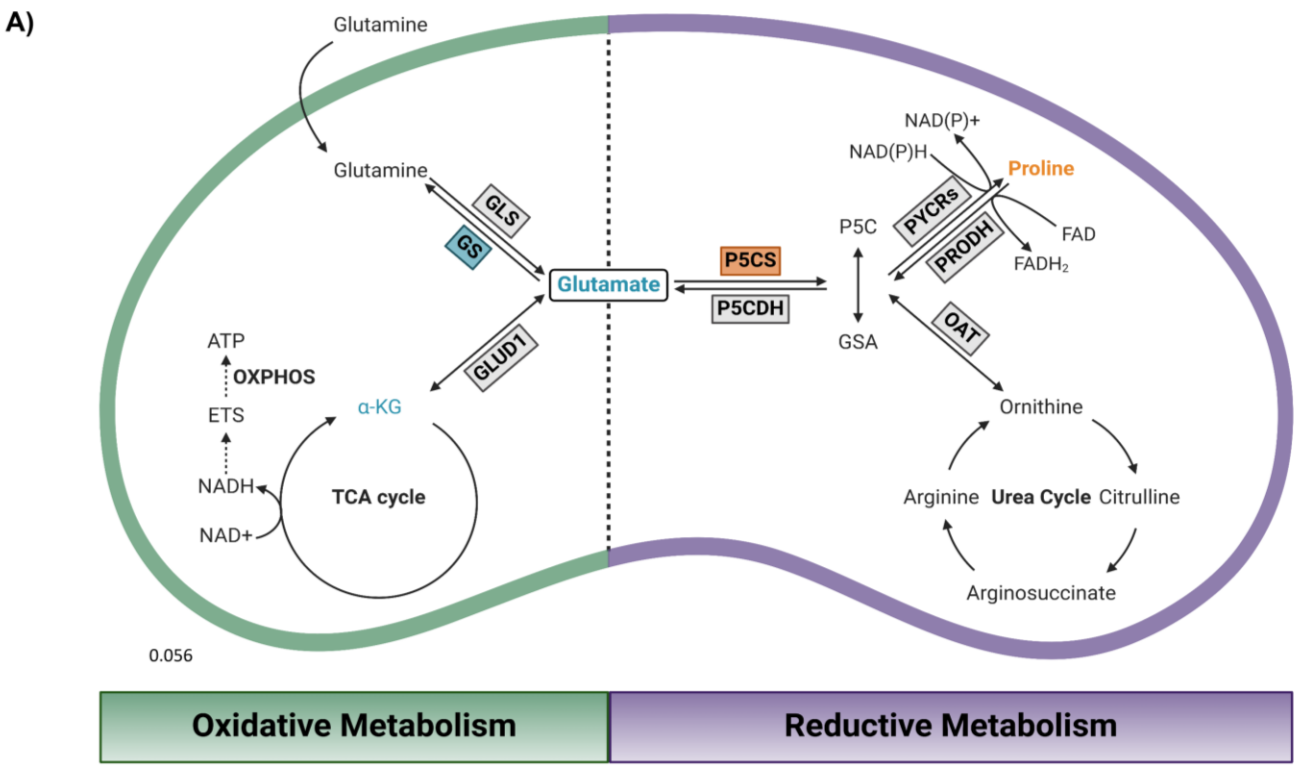
A)
Glutamine
Glutamine
GLS
GS
Glutamate
P5CS
P5CDH
NAD(P)+
NAD(P)H
Proline
PYCRs
PRODH
FAD
FADH2
P5C
GSA
OAT
GLUD1
ATP
OXPHOS
ETS
α-KG
NADH
NAD+
TCA cycle
Ornithine
Arginine
Urea Cycle
Citrulline
Arginosuccinate
0.056
Oxidative Metabolism
Reductive Metabolism

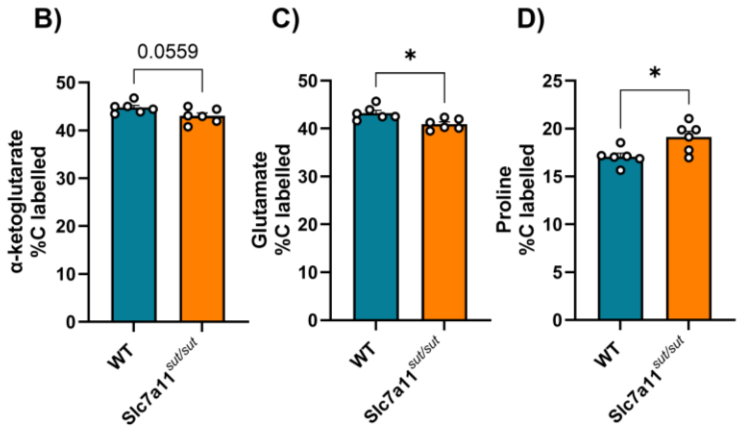
B)
0.0559
α-ketoglutarate %C labelled
WT
Slc7a11sut/sut
C)
*
Glutamate %C labelled
WT
Slc7a11sut/sut
D)
*
Proline %C labelled
WT
Slc7a11sut/sut

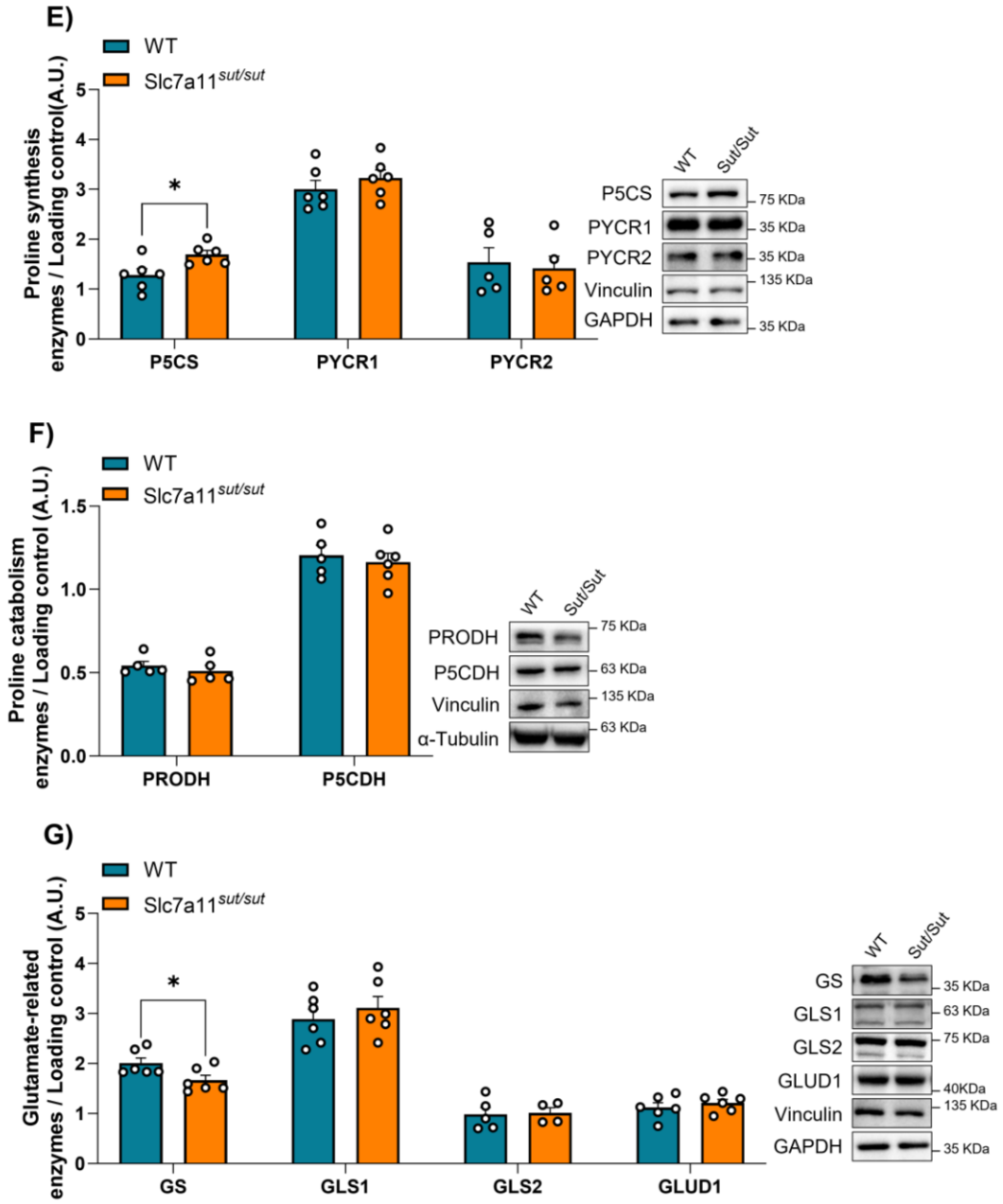

Figure 3.5. Increased Proline Biosynthesis in the Absence of Functional xCT

(A) Diagram showing glutamate oxidative and reductive metabolism. Enzymes and labelled metabolites are colored orange (higher in Slc7a11$^{sut/sut}$ MuSCs), blue (lower in Slc7a11$^{sut/sut}$ MuSCs), and black (similar between Slc7a11$^{sut/sut}$ and WT MuSCs). **(B-D)** [U-^{13}C]-glucose labelling (12 hrs) of α-ketoglutarate, glutamate, and proline. **(E-G)** Immunoblots of **(E)** proline synthesis (P5CS, PYCR1, and PYCR2), **(F)** proline catabolism (PRODH and P5CDH), and **(G)** glutamate synthesis (GS, GLS1, GLS2, and GLUD1) enzymes. The statistical significance of the differences between groups was determined using a two-tailed Student's t-test, n = 6. Results are presented as mean ± SEM, *$p < 0.05$.

3.6. Discussion

In response to impaired nutrient uptake, cells attempt to compensate and adapt, sometimes effectively, and other times inadequately, leading to cellular dysfunction. Here we have examined the impact of impairments in the plasma membrane amino transporter xCT, which is responsible for cellular cystine uptake and glutamate efflux. We previously showed that xCT deficiency *in vivo* in mice disrupts muscle GSH redox but enhances their MuSC activation and myogenic differentiation following cardiotoxin-induced muscle injury [16]. Here, using metabolomic, bioenergetic, imaging, and molecular approaches *in vitro* we demonstrate that xCT deficiency or chemical inhibition leads to impaired cystine import, resulting in disrupted GSH redox balance. This perturbed GSH redox is associated with compromised mitochondrial structure and function, characterized by mitochondrial fragmentation and a greater reliance on glycolytic metabolism to produce ATP. Extensive metabolomic analyses then revealed that xCT deficiency induces broad metabolic reprogramming as evidenced by upregulated *de novo* cysteine and serine synthesis, and elevated proline biosynthesis. Despite the metabolic reprogramming elicited by xCT dysfunction, redox dysfunction persists and is accompanied by impairments in cellular energetics and mitochondrial dynamics.

It is well recognized that cellular levels of cysteine can be derived from GSH degradation, protein catabolism, and methionine metabolism; however, dietary cystine uptake remains the primary source of cellular cysteine [57]. In plasma, approximately 65% of cysteine is bound to proteins via S-cysteinylation, 30% circulates as cystine, and only 5% exists as free reduced cysteine [58]. While reduced cysteine enters cells through non-specific transporters such as ASCTs and EAATs, cystine, the predominant form in circulation, is exclusively imported via the cystine/glutamate antiporter xCT [59,60]. Our findings of decreased intracellular levels of cysteine and GSH in Slc7a11$^{sut/sut}$ MuSCs further highlight the importance of xCT in regulating cysteine and GSH metabolism. Beyond serving as

a rate-limiting precursor for GSH synthesis, cysteine plays a central role in metabolism through its degradation, generating H_2S and other organic intermediates that contribute to carbon metabolism and serve as substrates for the TCA cycle [58]. The importance of H_2S in muscle metabolism was recently highlighted by Sprenger *et al*. [61]. Additionally, cysteine can be catabolized via cysteine dioxygenase, further influencing cellular metabolic pathways [62]. Cysteine plays another metabolic role through GSH redox, influencing mitochondrial remodeling in response to variable bioenergetic needs [37]. Moreover, mitochondrial cysteine is essential for preserving mitochondrial integrity by supporting the synthesis of ETC proteins and iron-sulfur clusters as reported in non-small cell lung cancer [63]. Thus, the overall aim of this work was to examine the impact of impaired or inhibited xCT activity on metabolic pathways, cellular bioenergetics, and mitochondrial morphology in MuSCs.

When mitochondrial health is disrupted, cells can initiate a stress response to promote recovery. To buffer cellular metabolism, dysfunctional mitochondria induce a reparative pathway that shifts energy metabolism to glycolysis in an ATF4-dependent manner [38]. We found that Slc7a11$^{sut/sut}$ MuSCs display lower bioenergetic flux overall, but a higher proportional glucose uptake and a greater reliance on glycolytic metabolism to produce ATP. In addition to greater reliance on glycolysis, higher ATF4 protein levels in Slc7a11$^{sut/sut}$ MuSCs are consistent with previous findings in mitochondrial myopathy mouse models where ATF4-mediated response shifts cellular oxidative metabolism to favor glycolysis [64]. These findings suggest that xCT deficiency in MuSCs leads to an adaptive metabolic response, causing increased reliance on glycolysis and other metabolic alterations that are discussed in subsequent sections.

To support cell resilience, mitochondrial morphology can change in response to various cellular stressors including oxidative stress, nutrient deprivation, and hypoxia [65]. Cellular mitochondrial networks continuously undergo remodeling to regulate metabolism and coordinate complex signaling pathways involved in cell pluripotency, proliferation, differentiation, and senescence [66–69]. For example,

mitochondrial hyperfusion can occur as an acute stress response to preserve mitochondrial oxidative capacities and protect against apoptosis [70]. However, when stress conditions are prolonged or exceed the intracellular antioxidant capacities, mitochondrial fission is triggered to eliminate damaged mitochondria and to maintain mitochondrial homeostasis [66,71,72]. Mitochondrial redox and more specifically, GSH redox, are key regulators of mitochondrial dynamics, and multiple proteins that interact with fusion/fission proteins such as CDK5, Parkin, PKA/AKAP1, and ROMO1 contain redox-sensitive residues [37,73]. While we initially hypothesized that the high GSSG observed in $Slc7a11^{sut/sut}$ MuSCs would promote mitochondrial hyperfusion and MFN1/2 oligomerization, mitochondria in $Slc7a11^{sut/sut}$ MuSCs were more fragmented with an upregulation of DRP1 oligomerization. These findings align with observations in C2C12 myoblasts, where H_2O_2-induced oxidative stress triggers DRP1-mediated mitochondrial fragmentation, leading to a loss of mitochondrial membrane potential and decreased cellular respiration [74]. Others found that DRP1-mediated fission is tightly regulated by redox signaling, where oxidative stress induces oxidation of the Cys^{644} residue in DRP1, initiating DRP1 GTPase oligomerization and activity [75,76]. Hong *et al*. showed that DRP1-mediated mitochondrial fission is essential for MuSC activation, supporting the quiescence-to-proliferation transition [77]. Conversely, excessive mitochondrial fission is associated with cellular senescence [74,78–81]. Thus, xCT deficiency and subsequent disruption of GSH redox in MuSCs induce mitochondrial fragmentation at least in part by promoting DRP1 redox-driven oligomerization.

xCT has been extensively studied in the brain due to the role of glutamate as a key excitatory neurotransmitter [82,83]. Glutamate is also a crucial metabolite in muscle as it participates in numerous metabolic pathways [84]. In $Slc7a11^{sut/sut}$ MuSCs, we observed altered amino acid metabolism, including a pronounced enrichment in BCAA metabolism. These findings are consistent with observations in cancer cells, which adapt their amino acid metabolism to regulate intracellular glutamate levels by

suppressing its biosynthesis or enhancing its utilization [85]. BCAAs are oxidized in skeletal muscle by BCATs, converting them into branched-chain α-keto acids through the reversible transfer of an amino group to α-KG, resulting in glutamate production [86]. Our findings revealed that Slc7a11$^{sut/sut}$ MuSCs suppress glutamate biosynthesis from BCAAs, as evidenced by lower protein levels of BCAT2. Another potential source of glutamate is through GLS, which catalyzes glutamine degradation into glutamate [87]; however, we did not observe any changes in GLS protein in Slc7a11$^{sut/sut}$ MuSCs. Thus, our findings are consistent with the conclusion that glutamine degradation is not a factor here, though it is important to note that protein levels alone do not reflect the enzymatic activity of those proteins. However, our metabolomics data did reveal an accumulation of glutamine in Slc7a11$^{sut/sut}$ MuSCs, consistent with lower glutamine catabolism. In line with our findings, Muir *et al*. showed that extracellular cystine and xCT expression are critical for facilitating glutamine metabolism in cancer cells [85]. It is also important to note that protein levels of GS were lower in Slc7a11$^{sut/sut}$ MuSCs, which may prevent glutamine accumulation, a phenomenon also observed in C2C12 cells [88].

Beyond its well-established role in supporting cellular redox via the xCT-GSH axis, xCT is increasingly recognized for its crucial role in adapting to the altered metabolic demands of proliferating cancer cells. Specifically, high xCT activity in cancer cell lines can promote glucose dependency and glutamine utilization to support rapid growth and survival under nutrient-stress conditions [89–93]. Therapeutically, erastin-mediated xCT inhibition mitigates tumor cell proliferation by inducing ferroptosis, an iron-dependent mechanism of cell death that is driven by lipid peroxidation [94]. Despite extensive literature highlighting the importance of xCT in cancer cell survival and metabolism, its role in controlling metabolic pathways in muscle cells remains largely unexplored [95]. Interestingly, we observed distinct metabolic clustering between WT and Slc7a11$^{sut/sut}$ MuSCs, with xCT deficiency driving metabolites to converge to a specialized metabolic cluster. Similar metabolic convergences have

been observed in mutant SOD1 ALS mice with hypermetabolism, reflecting decreased metabolic flexibility as an adaptive mechanism to cellular stress [96]. Our findings highlight the critical role of xCT in reshaping amino acid metabolism and driving metabolic reprogramming in MuSCs.

As a reparative metabolic response to mitochondrial stress, cells upregulate glycolysis, directing glucose-derived carbons into *de novo* serine biosynthesis. This process fuels one-carbon metabolism including the folate and methionine cycles, thereby supporting *de novo* cysteine biosynthesis via reverse transsulfuration [51]. Our findings showed increased *de novo* serine biosynthesis in Slc7a11$^{sut/sut}$ MuSCs as evidenced by higher m+3 serine labelling and higher protein levels of PSAT1 and PSPH. Additionally, we found that Slc7a11$^{sut/sut}$ MuSCs actively used the transsulfuration pathway to produce cysteine endogenously, as indicated by higher CTH protein levels and comparable m+3 GSH labelling between groups. These observations align with results in tumor cells cultured in cystine-depleted media, where cysteine deprivation resulted in increased CBS and CTH protein levels in an ATF4-dependent manner to sustain cell proliferation and GSH biosynthesis [97]. It is well known that enhanced flux through the transsulfuration pathway produces hydrogen sulfide (H_2S), which, at low concentrations, can promote mitochondrial biogenesis and enhance mitochondrial bioenergetics in a sulfide quinone reductase (SQR)-dependent manner [98,99]. However, at high concentrations, H_2S can inhibit complex IV, decrease cell proliferation, and shift metabolism towards reductive carboxylation, further linking redox stress to mitochondrial dysfunction [100,101]. Nonetheless, the work of Sprenger *et al.* very recently showed the importance of ergothionine in the control of muscle mitochondrial metabolism and exercise performance through the activation of the H_2S-producing enzyme 3-mercaptopyruvate sulfurtransferase (MPST) [61]. MPST produces pyruvate and H_2S in mitochondria to support mitochondrial respiration [98,102]. Therefore, increased reliance on the transsulfuration pathway for *de novo* cysteine synthesis may also contribute to impaired mitochondrial respiration in Slc7a11$^{sut/sut}$ MuSCs.

Glutamate, the most abundant intracellular amino acid, can serve as a key precursor for TCA cycle anaplerosis through α-KG. Additionally, glutamate can support proline biosynthesis via its conversion to P5C [103]. Our findings of lower mitochondrial respiration and impaired glycolytic flux into the TCA cycle in Slc7a11$^{sut/sut}$ MuSCs suggest that glutamate is not being oxidized through the TCA cycle but instead redirected toward reductive proline biosynthesis. Indeed, we found higher proline abundance and increased protein levels of P5CS in Slc7a11$^{sut/sut}$ MuSCs. Our findings are consistent with increased glutamate flux toward proline biosynthesis observed in neurons treated with the psychostimulant methamphetamine, where proline biosynthesis serves as a protective mechanism to mitigate glutamate accumulation [104]. However, this is an energetically costly process with glycolysis serving as the primary energy source for this process [105,106]. In this context, proline biosynthesis provides an essential supply of NAD^+ crucial for sustaining efficient glycolysis, a key hallmark of the reparative metabolic response to mitochondrial stress [107,108]. Thus, proline biosynthesis may offer a bioenergetic advantage for Slc7a11$^{sut/sut}$ MuSCs, supporting their metabolic dependence on glycolysis to maintain intracellular glutamate homeostasis.

The proline cycle (i.e., the interconversion of proline and P5C) plays a key role in maintaining cellular redox homeostasis. We found that Slc7a11$^{sut/sut}$ MuSCs favor proline synthesis over degradation by increasing P5CS protein levels, while PRODH protein levels remain comparable between groups. This observation is consistent with the fact that proline catabolism, catalyzed by PRODH, generates ROS by transferring electrons to FAD and converting oxygen into superoxide, while proline biosynthesis is a reductive process that mitigates ROS production and promotes cell survival by preventing apoptosis [109,110]. When cells are exposed to nutrient deprivation or oxidizing agents, P5CS is upregulated and diffusely localized within mitochondria, where it forms oligomerized filament-like structures [109]. Through proline cycle and the mitochondrially localized P5CS, mitochondria can be hubs for competing

metabolic pathways such as OXPHOS and reductive proline biosynthesis [107]. Ryu *et al*. demonstrated that P5CS, along with mitochondrial fusion/fission, regulate the balance between OXPHOS and reductive proline biosynthesis by creating distinct mitochondrial subpopulations: one enriched in ATP synthase for OXPHOS, and another enriched in P5CS which prioritizes reductive biosynthesis by suppressing TCA cycle activity and glutamate oxidation [111]. Similarly, our findings of enhanced P5CS-mediated proline biosynthesis accompanied by increased DRP1 oligomerization in Slc7a11$^{sut/sut}$ MuSCs suggest that Slc7a11$^{sut/sut}$ MuSCs may employ proline reductive biosynthesis to suppress oxidative metabolism and counteract elevated H_2O_2 levels. Altogether, proline metabolism emerges as a crucial adaptive mechanism in xCT-deficient cells, enabling MuSCs to balance between oxidative and reductive pathways.

In conclusion, our research demonstrates that xCT-mediated cystine import regulates GSH redox and promotes *de novo* serine, cysteine, and proline synthesis in proliferating muscle cells. In many muscular dystrophies and metabolic diseases, MuSC health is compromised due to disrupted redox and metabolic homeostasis [112–116]. Therefore, a deeper understanding of the metabolic role of xCT in muscle cells provides valuable insights into the crosstalk between cellular redox regulation and metabolic homeostasis. Our findings not only enhance our understanding of the fundamental mechanisms governing xCT function but also highlight cyst(e)ine metabolism as a therapeutic target to restore disrupted redox balance and metabolic homeostasis often associated with muscle-related diseases and pathologies.

3.7. References

[1] S.K. Adla, H. Virtanen, T. Thongsodsaeng, K.M. Huttunen, Amino acid transporters in neurological disorders and neuroprotective effects of cysteine derivatives, Neurochem. Int. 177 (2024) 105771. https://doi.org/10.1016/j.neuint.2024.105771.

[2] D. Fotiadis, Y. Kanai, M. Palacín, The SLC3 and SLC7 families of amino acid transporters, Mol. Aspects Med. 34 (2013) 139–158. https://doi.org/10.1016/j.mam.2012.10.007.

[3] H. Sato, M. Tamba, T. Ishii, S. Bannai, Cloning and Expression of a Plasma Membrane Cystine/Glutamate Exchange Transporter Composed of Two Distinct Proteins *, J. Biol. Chem. 274 (1999) 11455–11458. https://doi.org/10.1074/jbc.274.17.11455.

[4] J. Lewerenz, S.J. Hewett, Y. Huang, M. Lambros, P.W. Gout, P.W. Kalivas, A. Massie, I. Smolders, A. Methner, M. Pergande, S.B. Smith, V. Ganapathy, P. Maher, The Cystine/Glutamate Antiporter System xc− in Health and Disease: From Molecular Mechanisms to Novel Therapeutic Opportunities, Antioxid. Redox Signal. 18 (2013) 522–555. https://doi.org/10.1089/ars.2011.4391.

[5] M.H. Stipanuk, J.E. Dominy, J.-I. Lee, R.M. Coloso, Mammalian Cysteine Metabolism: New Insights into Regulation of Cysteine Metabolism12, J. Nutr. 136 (2006) 1652S-1659S. https://doi.org/10.1093/jn/136.6.1652S.

[6] Y.P. Kang, A. Mockabee-Macias, C. Jiang, A. Falzone, N. Prieto-Farigua, E. Stone, I.S. Harris, G.M. DeNicola, Non-canonical Glutamate-Cysteine Ligase Activity Protects against Ferroptosis, Cell Metab. 33 (2021) 174-189.e7. https://doi.org/10.1016/j.cmet.2020.12.007.

[7] A.S. Brack, T.A. Rando, Tissue-Specific Stem Cells: Lessons from the Skeletal Muscle Satellite Cell, Cell Stem Cell 10 (2012) 504–514. https://doi.org/10.1016/j.stem.2012.04.001.

[8] F. Relaix, M. Bencze, M.J. Borok, A. Der Vartanian, F. Gattazzo, D. Mademtzoglou, S. Perez-Diaz, A. Prola, P.C. Reyes-Fernandez, A. Rotini, Taglietti, Perspectives on skeletal muscle stem cells, Nat. Commun. 12 (2021) 1–11. https://doi.org/10.1038/s41467-020-20760-6.

[9] H. Yin, F. Price, M.A. Rudnicki, Satellite Cells and the Muscle Stem Cell Niche, Physiol. Rev. 93 (2013) 23–67. https://doi.org/10.1152/physrev.00043.2011.

[10] P. Sousa-Victor, L. García-Prat, P. Muñoz-Cánoves, Control of satellite cell function in muscle regeneration and its disruption in ageing, Nat. Rev. Mol. Cell Biol. 23 (2022) 204–226. https://doi.org/10.1038/s41580-021-00421-2.

[11] J.J. Dowling, C.C. Weihl, M.J. Spencer, Molecular and cellular basis of genetically inherited skeletal muscle disorders, Nat. Rev. Mol. Cell Biol. 22 (2021) 713–732. https://doi.org/10.1038/s41580-021-00389-z.

[12] J.G. Ryall, S. Dell'Orso, A. Derfoul, A. Juan, H. Zare, X. Feng, D. Clermont, M. Koulnis, G. Gutierrez-Cruz, M. Fulco, V. Sartorelli, The NAD+-Dependent SIRT1 Deacetylase Translates a Metabolic Switch into Regulatory Epigenetics in Skeletal Muscle Stem Cells, Cell Stem Cell 16 (2015) 171–183. https://doi.org/10.1016/j.stem.2014.12.004.

[13] F. Pala, D. Di Girolamo, S. Mella, S. Yennek, L. Chatre, M. Ricchetti, S. Tajbakhsh, Distinct metabolic states govern skeletal muscle stem cell fates during prenatal and postnatal myogenesis, J. Cell Sci. 131 (2018) jcs212977. https://doi.org/10.1242/jcs.212977.

[14] A.M. Hosios, V.C. Hecht, L.V. Danai, M.O. Johnson, J.C. Rathmell, M.L. Steinhauser, S.R. Manalis, M.G. Vander Heiden, Amino Acids Rather than Glucose Account for the Majority of Cell Mass in Proliferating Mammalian Cells, Dev. Cell 36 (2016) 540–549. https://doi.org/10.1016/j.devcel.2016.02.012.

[15] T. Huang, J. Zhou, B. Wang, X. Wang, W. Xiao, M. Yang, Y. Liu, Q. Wang, Y. Xiang, X. Lan, Integrated Amino Acids and Transcriptome Analysis Reveals Arginine Transporter SLC7A2 Is a Novel Regulator of Myogenic Differentiation, Int. J. Mol. Sci. 25 (2023) 95. https://doi.org/10.3390/ijms25010095.
[16] M.N. Kanaan, C.A. Pileggi, C.Y. Karam, L.S. Kennedy, C. Fong-McMaster, M. Cuperlovic-Culf, M.-E. Harper, Cystine/glutamate antiporter xCT controls skeletal muscle glutathione redox, bioenergetics and differentiation, Redox Biol. 73 (2024) 103213. https://doi.org/10.1016/j.redox.2024.103213.
[17] A. Shahini, K. Vydiam, D. Choudhury, N. Rajabian, T. Nguyen, P. Lei, S.T. Andreadis, Efficient and high yield isolation of myoblasts from skeletal muscle, Stem Cell Res. 30 (2018) 122–129. https://doi.org/10.1016/j.scr.2018.05.017.
[18] A. Chaudhry, R. Shi, D.S. Luciani, A pipeline for multidimensional confocal analysis of mitochondrial morphology, function, and dynamics in pancreatic β-cells, Am. J. Physiol.-Endocrinol. Metab. 318 (2020) E87–E101. https://doi.org/10.1152/ajpendo.00457.2019.
[19] A. Liaghati, C.A. Pileggi, G. Parmar, D.A. Patten, N. Hadzimustafic, A. Cuillerier, K.J. Menzies, Y. Burelle, M.-E. Harper, Grx2 Regulates Skeletal Muscle Mitochondrial Structure and Autophagy, Front. Physiol. 12 (2021). https://doi.org/10.3389/fphys.2021.604210.
[20] S.A. Mookerjee, D.G. Nicholls, M.D. Brand, Determining Maximum Glycolytic Capacity Using Extracellular Flux Measurements, PLoS ONE 11 (2016) e0152016. https://doi.org/10.1371/journal.pone.0152016.
[21] R. Godin, F. Daussin, S. Matecki, T. Li, B.J. Petrof, Y. Burelle, Peroxisome proliferator-activated receptor γ coactivator 1-α gene transfer restores mitochondrial biomass and improves mitochondrial calcium handling in post-necrotic mdx mouse skeletal muscle, J. Physiol. 590 (2012) 5487–5502. https://doi.org/10.1113/jphysiol.2012.240390.
[22] S. McGuirk, Y. Audet-Delage, M.G. Annis, Y. Xue, M. Vernier, K. Zhao, C. St-Louis, L. Minarrieta, D.A. Patten, G. Morin, C.M. Greenwood, V. Giguère, S. Huang, P.M. Siegel, J. St-Pierre, Resistance to different anthracycline chemotherapeutics elicits distinct and actionable primary metabolic dependencies in breast cancer, eLife 10 (2021) e65150. https://doi.org/10.7554/eLife.65150.
[23] C. Menzies, S. Naz, D. Patten, T. Alquier, B.M. Bennett, B. Lacoste, Distinct Basal Metabolism in Three Mouse Models of Neurodevelopmental Disorders, eNeuro 8 (2021). https://doi.org/10.1523/ENEURO.0292-20.2021.
[24] R Core team, R: A Language and Environment for Statistical Computing, R Foundation for Statistical Computing, Vienna, Austria, (2021). https://www.r-project.org/.
[25] J.D. Hunter, Matplotlib: A 2D Graphics Environment, Comput. Sci. Eng. 9 (2007) 90–95. https://doi.org/10.1109/MCSE.2007.55.
[26] H. Wickham, ggplot2, Springer International Publishing, Cham, 2016. https://doi.org/10.1007/978-3-319-24277-4.
[27] P. Virtanen, R. Gommers, T.E. Oliphant, M. Haberland, T. Reddy, D. Cournapeau, E. Burovski, P. Peterson, W. Weckesser, J. Bright, S.J. van der Walt, M. Brett, J. Wilson, K.J. Millman, N. Mayorov, A.R.J. Nelson, E. Jones, R. Kern, E. Larson, C.J. Carey, İ. Polat, Y. Feng, E.W. Moore, J. VanderPlas, D. Laxalde, J. Perktold, R. Cimrman, I. Henriksen, E.A. Quintero, C.R. Harris, A.M. Archibald, A.H. Ribeiro, F. Pedregosa, P. van Mulbregt, SciPy 1.0: fundamental algorithms for scientific computing in Python, Nat. Methods 17 (2020) 261–272. https://doi.org/10.1038/s41592-019-0686-2.

[28] E.A. Thévenot, A. Roux, Y. Xu, E. Ezan, C. Junot, Analysis of the Human Adult Urinary Metabolome Variations with Age, Body Mass Index, and Gender by Implementing a Comprehensive Workflow for Univariate and OPLS Statistical Analyses, J. Proteome Res. 14 (2015) 3322–3335. https://doi.org/10.1021/acs.jproteome.5b00354.
[29] B. Galindo-Prieto, L. Eriksson, J. Trygg, Variable influence on projection (VIP) for orthogonal projections to latent structures (OPLS), J. Chemom. 28 (2014) 623–632. https://doi.org/10.1002/cem.2627.
[30] C.M. Andersen, R. Bro, Variable selection in regression—a tutorial, J. Chemom. 24 (2010) 728–737. https://doi.org/10.1002/cem.1360.
[31] R. Tibshirani, Michael J. Seo, G. Chu, Balasubramanian Narasimhan, Jun Li, samr: SAM: Significance Analysis of Microarrays, (2005) 3.0. https://doi.org/10.32614/CRAN.package.samr.
[32] Z. Pang, L. Xu, C. Viau, Y. Lu, R. Salavati, N. Basu, J. Xia, MetaboAnalystR 4.0: a unified LC-MS workflow for global metabolomics, Nat. Commun. 15 (2024) 3675. https://doi.org/10.1038/s41467-024-48009-6.
[33] J. Huerta-Cepas, F. Serra, P. Bork, ETE 3: Reconstruction, Analysis, and Visualization of Phylogenomic Data, Mol. Biol. Evol. 33 (2016) 1635–1638. https://doi.org/10.1093/molbev/msw046.
[34] S. Chintala, W. Li, M.L. Lamoreux, S. Ito, K. Wakamatsu, E.V. Sviderskaya, D.C. Bennett, Y.-M. Park, W.A. Gahl, M. Huizing, R.A. Spritz, S. Ben, E.K. Novak, J. Tan, R.T. Swank, Slc7a11 gene controls production of pheomelanin pigment and proliferation of cultured cells, Proc. Natl. Acad. Sci. U. S. A. 102 (2005) 10964–10969. https://doi.org/10.1073/pnas.0502856102.
[35] R.T. Swank, M. Reddington, E.K. Novak, Inherited prolonged bleeding time and platelet storage pool deficiency in the subtle gray (sut) mouse, Lab. Anim. Sci. 46 (1996) 56–60.
[36] M. Föller, I.S. Harris, A. Elia, R. John, F. Lang, T.J. Kavanagh, T.W. Mak, Functional significance of glutamate–cysteine ligase modifier for erythrocyte survival in vitro and in vivo, Cell Death Differ. 20 (2013) 1350–1358. https://doi.org/10.1038/cdd.2013.70.
[37] P.H.G.M. Willems, R. Rossignol, C.E.J. Dieteren, M.P. Murphy, W.J.H. Koopman, Redox Homeostasis and Mitochondrial Dynamics, Cell Metab. 22 (2015) 207–218. https://doi.org/10.1016/j.cmet.2015.06.006.
[38] A. Suomalainen, J. Nunnari, Mitochondria at the crossroads of health and disease, Cell 187 (2024) 2601–2627. https://doi.org/10.1016/j.cell.2024.04.037.
[39] S.A. Mookerjee, A.A. Gerencser, D.G. Nicholls, M.D. Brand, Quantifying intracellular rates of glycolytic and oxidative ATP production and consumption using extracellular flux measurements, J. Biol. Chem. 292 (2017) 7189–7207. https://doi.org/10.1074/jbc.M116.774471.
[40] T. Shutt, M. Geoffrion, R. Milne, H.M. McBride, The intracellular redox state is a core determinant of mitochondrial fusion, EMBO Rep. 13 (2012) 909–915. https://doi.org/10.1038/embor.2012.128.
[41] O. Thaher, C. Wolf, P.N. Dey, A. Pouya, V. Wüllner, S. Tenzer, A. Methner, The thiol switch C684 in Mitofusin-2 mediates redox-induced alterations of mitochondrial shape and respiration, Neurochem. Int. 117 (2018) 167–173. https://doi.org/10.1016/j.neuint.2017.05.009.
[42] Y. Zhou, D. Long, Y. Zhao, S. Li, Y. Liang, L. Wan, J. Zhang, F. Xue, L. Feng, Oxidative stress-mediated mitochondrial fission promotes hepatic stellate cell activation via stimulating oxidative phosphorylation, Cell Death Dis. 13 (2022) 1–15. https://doi.org/10.1038/s41419-022-05088-x.
[43] S. Mattie, J. Riemer, J.G. Wideman, H.M. McBride, A new mitofusin topology places the redox-regulated C terminus in the mitochondrial intermembrane space, J. Cell Biol. 217 (2018) 507–515. https://doi.org/10.1083/jcb.201611194.

[44] D.F. Robinson, L.R. Foulds, Comparison of phylogenetic trees, Math. Biosci. 53 (1981) 131–147. https://doi.org/10.1016/0025-5564(81)90043-2.
[45] L. Francois, P. Boskovic, J. Knerr, W. He, G. Sigismondo, C. Schwan, T.H. More, M. Schlotter, M.E. Conway, J. Krijgsveld, K. Hiller, R. Grosse, P. Lichter, B. Radlwimmer, BCAT1 redox function maintains mitotic fidelity, Cell Rep. 41 (2022) 111524. https://doi.org/10.1016/j.celrep.2022.111524.
[46] G. Mann, S. Mora, G. Madu, O.A.J. Adegoke, Branched-chain Amino Acids: Catabolism in Skeletal Muscle and Implications for Muscle and Whole-body Metabolism, Front. Physiol. 12 (2021). https://doi.org/10.3389/fphys.2021.702826.
[47] J.M. Buescher, M.R. Antoniewicz, L.G. Boros, S.C. Burgess, H. Brunengraber, C.B. Clish, R.J. DeBerardinis, O. Feron, C. Frezza, B. Ghesquiere, E. Gottlieb, K. Hiller, R.G. Jones, J.J. Kamphorst, R.G. Kibbey, A.C. Kimmelman, J.W. Locasale, S.Y. Lunt, O.D. Maddocks, C. Malloy, C.M. Metallo, E.J. Meuillet, J. Munger, K. Nöh, J.D. Rabinowitz, M. Ralser, U. Sauer, G. Stephanopoulos, J. St-Pierre, D.A. Tennant, C. Wittmann, M.G. Vander Heiden, A. Vazquez, K. Vousden, J.D. Young, N. Zamboni, S.-M. Fendt, A roadmap for interpreting 13C metabolite labeling patterns from cells, Curr. Opin. Biotechnol. 34 (2015) 189–201. https://doi.org/10.1016/j.copbio.2015.02.003.
[48] P. Pachnis, Z. Wu, B. Faubert, A. Tasdogan, W. Gu, S. Shelton, A. Solmonson, A.D. Rao, A.K. Kaushik, T.J. Rogers, J.M. Ubellacker, C.A. LaVigne, C. Yang, B. Ko, V. Ramesh, J. Sudderth, L.G. Zacharias, M.S. Martin-Sandoval, D. Do, T.P. Mathews, Z. Zhao, P. Mishra, S.J. Morrison, R.J. DeBerardinis, In vivo isotope tracing reveals a requirement for the electron transport chain in glucose and glutamine metabolism by tumors, Sci. Adv. 8 (2022) eabn9550. https://doi.org/10.1126/sciadv.abn9550.
[49] A.C. Newman, O.D.K. Maddocks, One-carbon metabolism in cancer, Br. J. Cancer 116 (2017) 1499–1504. https://doi.org/10.1038/bjc.2017.118.
[50] B.J. Gheller, J.E. Blum, E.W. Lim, M.K. Handzlik, E.H. Hannah Fong, A.C. Ko, S. Khanna, M.E. Gheller, E.L. Bender, M.S. Alexander, P.J. Stover, M.S. Field, B.D. Cosgrove, C.M. Metallo, A.E. Thalacker-Mercer, Extracellular serine and glycine are required for mouse and human skeletal muscle stem and progenitor cell function, Mol. Metab. 43 (2021) 101106. https://doi.org/10.1016/j.molmet.2020.101106.
[51] J. Zhu, M. Berisa, S. Schwörer, W. Qin, J.R. Cross, C.B. Thompson, Transsulfuration Activity Can Support Cell Growth upon Extracellular Cysteine Limitation, Cell Metab. 30 (2019) 865-876.e5. https://doi.org/10.1016/j.cmet.2019.09.009.
[52] R. Zhang, B. Chen, L. Lin, H. Zhang, T. Luan, 13C isotope-based metabolic flux analysis revealing cellular landscape of glucose metabolism in human liver cells exposed to perfluorooctanoic acid, Sci. Total Environ. 770 (2021) 145329. https://doi.org/10.1016/j.scitotenv.2021.145329.
[53] M. Tajan, M. Hennequart, E.C. Cheung, F. Zani, A.K. Hock, N. Legrave, O.D.K. Maddocks, R.A. Ridgway, D. Athineos, A. Suárez-Bonnet, R.L. Ludwig, L. Novellasdemunt, N. Angelis, V.S.W. Li, G. Vlachogiannis, N. Valeri, N. Mainolfi, V. Suri, A. Friedman, M. Manfredi, K. Blyth, O.J. Sansom, K.H. Vousden, Serine synthesis pathway inhibition cooperates with dietary serine and glycine limitation for cancer therapy, Nat. Commun. 12 (2021) 366. https://doi.org/10.1038/s41467-020-20223-y.
[54] D.H. Tran, R. Kesavan, H. Rion, M.H. Soflaee, A. Solmonson, D. Bezwada, H.S. Vu, F. Cai, J.A. Phillips, R.J. DeBerardinis, G. Hoxhaj, Mitochondrial NADP+ is essential for proline biosynthesis during cell growth, Nat. Metab. 3 (2021) 571–585. https://doi.org/10.1038/s42255-021-00374-y.

[55] L. Burke, I. Guterman, R. Palacios Gallego, R.G. Britton, D. Burschowsky, C. Tufarelli, A. Rufini, The Janus-like role of proline metabolism in cancer, Cell Death Discov. 6 (2020) 1–17. https://doi.org/10.1038/s41420-020-00341-8.
[56] H.C. Yoo, Y.C. Yu, Y. Sung, J.M. Han, Glutamine reliance in cell metabolism, Exp. Mol. Med. 52 (2020) 1496–1516. https://doi.org/10.1038/s12276-020-00504-8.
[57] Y.-M. Go, D.P. Jones, Cysteine/cystine redox signaling in cardiovascular disease, Free Radic. Biol. Med. 50 (2011) 495–509. https://doi.org/10.1016/j.freeradbiomed.2010.11.029.
[58] V.D.B. Bonifácio, S.A. Pereira, J. Serpa, J.B. Vicente, Cysteine metabolic circuitries: druggable targets in cancer, Br. J. Cancer 124 (2021) 862–879. https://doi.org/10.1038/s41416-020-01156-1.
[59] M.G. Bianchi, R. Franchi-Gazzola, L. Reia, M. Allegri, J. Uggeri, M. Chiu, R. Sala, O. Bussolati, Valproic acid induces the glutamate transporter excitatory amino acid transporter-3 in human oligodendroglioma cells, Neuroscience 227 (2012) 260–270. https://doi.org/10.1016/j.neuroscience.2012.09.055.
[60] W. Zhang, D. Trachootham, J. Liu, G. Chen, H. Pelicano, C. Garcia-Prieto, W. Lu, J.A. Burger, C.M. Croce, W. Plunkett, M.J. Keating, P. Huang, Stromal control of cystine metabolism promotes cancer cell survival in chronic lymphocytic leukaemia, Nat. Cell Biol. 14 (2012) 276–286. https://doi.org/10.1038/ncb2432.
[61] H.-G. Sprenger, M.J. Mittenbühler, Y. Sun, J.G. Van Vranken, S. Schindler, A. Jayaraj, S.A. Khetarpal, A.L. Smythers, A. Vargas-Castillo, A.M. Puszynska, J.B. Spinelli, A. Armani, T. Kunchok, B. Ryback, H.-S. Seo, K. Song, L. Sebastian, C. O'Young, C. Braithwaite, S. Dhe-Paganon, N. Burger, E.L. Mills, S.P. Gygi, J.A. Paulo, H. Arthanari, E.T. Chouchani, D.M. Sabatini, B.M. Spiegelman, Ergothioneine controls mitochondrial function and exercise performance via direct activation of MPST, Cell Metab. (2025). https://doi.org/10.1016/j.cmet.2025.01.024.
[62] J.E. Dominy, J. Hwang, M.H. Stipanuk, Overexpression of cysteine dioxygenase reduces intracellular cysteine and glutathione pools in HepG2/C3A cells, Am. J. Physiol.-Endocrinol. Metab. 293 (2007) E62–E69. https://doi.org/10.1152/ajpendo.00053.2007.
[63] N.P. Ward, S.J. Yoon, T. Flynn, A.M. Sherwood, M.A. Olley, J. Madej, G.M. DeNicola, Mitochondrial respiratory function is preserved under cysteine starvation via glutathione catabolism in NSCLC, Nat. Commun. 15 (2024) 4244. https://doi.org/10.1038/s41467-024-48695-2.
[64] S. Forsström, C.B. Jackson, C.J. Carroll, M. Kuronen, E. Pirinen, S. Pradhan, A. Marmyleva, M. Auranen, I.-M. Kleine, N.A. Khan, A. Roivainen, P. Marjamäki, H. Liljenbäck, L. Wang, B.J. Battersby, U. Richter, V. Velagapudi, J. Nikkanen, L. Euro, A. Suomalainen, Fibroblast Growth Factor 21 Drives Dynamics of Local and Systemic Stress Responses in Mitochondrial Myopathy with mtDNA Deletions, Cell Metab. 30 (2019) 1040-1054.e7. https://doi.org/10.1016/j.cmet.2019.08.019.
[65] C.A. Galloway, H. Lee, Y. Yoon, Mitochondrial morphology – Emerging role in bioenergetics, Free Radic. Biol. Med. 53 (2012) 10.1016/j.freeradbiomed.2012.09.035. https://doi.org/10.1016/j.freeradbiomed.2012.09.035.
[66] W. Chen, H. Zhao, Y. Li, Mitochondrial dynamics in health and disease: mechanisms and potential targets, Signal Transduct. Target. Ther. 8 (2023) 1–25. https://doi.org/10.1038/s41392-023-01547-9.
[67] J. Nunnari, A. Suomalainen, Mitochondria: In Sickness and in Health, Cell 148 (2012) 1145–1159. https://doi.org/10.1016/j.cell.2012.02.035.

[68] O. Sommers, R.A. Tomsine, M. Khacho, Mitochondrial Dynamics Drive Muscle Stem Cell Progression from Quiescence to Myogenic Differentiation, Cells 13 (2024) 1773. https://doi.org/10.3390/cells13211773.
[69] M. Giacomello, A. Pyakurel, C. Glytsou, L. Scorrano, The cell biology of mitochondrial membrane dynamics, Nat. Rev. Mol. Cell Biol. 21 (2020) 204–224. https://doi.org/10.1038/s41580-020-0210-7.
[70] L. Miret-Casals, D. Sebastián, J. Brea, E.M. Rico-Leo, M. Palacín, P.M. Fernández-Salguero, M.I. Loza, F. Albericio, A. Zorzano, Identification of New Activators of Mitochondrial Fusion Reveals a Link between Mitochondrial Morphology and Pyrimidine Metabolism, Cell Chem. Biol. 25 (2018) 268-278.e4. https://doi.org/10.1016/j.chembiol.2017.12.001.
[71] C. Guido, D. Whitaker-Menezes, Z. Lin, R.G. Pestell, A. Howell, T.A. Zimmers, M.C. Casimiro, S. Aquila, S. Ando', U.E. Martinez-Outschoorn, F. Sotgia, M.P. Lisanti, Mitochondrial fission induces glycolytic reprogramming in cancer-associated myofibroblasts, driving stromal lactate production, and early tumor growth, Oncotarget 3 (2012) 798–810. https://doi.org/10.18632/oncotarget.574.
[72] M. Frank, S. Duvezin-Caubet, S. Koob, A. Occhipinti, R. Jagasia, A. Petcherski, M.O. Ruonala, M. Priault, B. Salin, A.S. Reichert, Mitophagy is triggered by mild oxidative stress in a mitochondrial fission dependent manner, Biochim. Biophys. Acta BBA - Mol. Cell Res. 1823 (2012) 2297–2310. https://doi.org/10.1016/j.bbamcr.2012.08.007.
[73] T.R. Figueira, M.H. Barros, A.A. Camargo, R.F. Castilho, J.C.B. Ferreira, A.J. Kowaltowski, F.E. Sluse, N.C. Souza-Pinto, A.E. Vercesi, Mitochondria as a Source of Reactive Oxygen and Nitrogen Species: From Molecular Mechanisms to Human Health, Antioxid. Redox Signal. 18 (2013) 2029–2074. https://doi.org/10.1089/ars.2012.4729.
[74] S. Iqbal, D.A. Hood, Oxidative stress-induced mitochondrial fragmentation and movement in skeletal muscle myoblasts, Am. J. Physiol. - Cell Physiol. 306 (2014) C1176–C1183. https://doi.org/10.1152/ajpcell.00017.2014.
[75] Y.-M. Kim, S.-W. Youn, V. Sudhahar, A. Das, R. Chandhri, H.C. Grajal, J. Kweon, S. Leanhart, L. He, P.T. Toth, J. Kitajewski, J. Rehman, Y. Yoon, J. Cho, T. Fukai, M. Ushio-Fukai, Redox Regulation of Mitochondrial Fission Protein Drp1 by Protein Disulfide Isomerase Limits Endothelial Senescence, Cell Rep. 23 (2018) 3565–3578. https://doi.org/10.1016/j.celrep.2018.05.054.
[76] D.-H. Cho, T. Nakamura, J. Fang, P. Cieplak, A. Godzik, Z. Gu, S.A. Lipton, S-nitrosylation of Drp1 mediates beta-amyloid-related mitochondrial fission and neuronal injury, Science 324 (2009) 102–105. https://doi.org/10.1126/science.1171091.
[77] X. Hong, J. Isern, S. Campanario, E. Perdiguero, I. Ramírez-Pardo, J. Segalés, P. Hernansanz-Agustín, A. Curtabbi, O. Deryagin, A. Pollán, J.A. González-Reyes, J.M. Villalba, M. Sandri, A.L. Serrano, J.A. Enríquez, P. Muñoz-Cánoves, Mitochondrial dynamics maintain muscle stem cell regenerative competence throughout adult life by regulating metabolism and mitophagy, Cell Stem Cell 29 (2022) 1298-1314.e10. https://doi.org/10.1016/j.stem.2022.07.009.
[78] P.M. Siu, Y. Wang, S.E. Alway, Apoptotic signaling induced by H2O2-mediated oxidative stress in differentiated C2C12 myotubes, Life Sci. 84 (2009) 468–481. https://doi.org/10.1016/j.lfs.2009.01.014.
[79] Y. Liu, S. Lu, L. Wu, L. Yang, L. Yang, J. Wang, The diversified role of mitochondria in ferroptosis in cancer, Cell Death Dis. 14 (2023) 1–12. https://doi.org/10.1038/s41419-023-06045-y.

[80] J. Khatun, J.D. Gelles, J.E. Chipuk, Dynamic death decisions: How mitochondrial dynamics shape cellular commitment to apoptosis and ferroptosis, Dev. Cell 59 (2024) 2549–2565. https://doi.org/10.1016/j.devcel.2024.09.004.
[81] Z. Wang, S. Tang, L. Cai, Q. Wang, D. Pan, Y. Dong, H. Zhou, J. Li, N. Ji, X. Zeng, Y. Zhou, Y. Shen, Q. Chen, DRP1 inhibition-mediated mitochondrial elongation abolishes cancer stemness, enhances glutaminolysis, and drives ferroptosis in oral squamous cell carcinoma, Br. J. Cancer 130 (2024) 1744–1757. https://doi.org/10.1038/s41416-024-02670-2.
[82] S.M.S. Sears, S.H. Roberts, S.J. Hewett, Hyperexcitability and brain morphological differences in mice lacking the cystine/glutamate antiporter, system xc, J. Neurosci. Res. 99 (2021) 3339–3353. https://doi.org/10.1002/jnr.24971.
[83] M.A. Iqbal, M. Bilen, Y. Liu, V. Jabre, B.C. Fong, I. Chakroun, S. Paul, J. Chen, S. Wade, M. Kanaan, M. Harper, M. Khacho, R.S. Slack, The integrated stress response promotes neural stem cell survival under conditions of mitochondrial dysfunction in neurodegeneration, Aging Cell 23 (2024) e14165. https://doi.org/10.1111/acel.14165.
[84] I. Soro-Arnáiz, G. Fitzgerald, S. Cherkaoui, J. Zhang, P. Gilardoni, A. Ghosh, O. Bar-Nur, E. Masschelein, P. Maechler, N. Zamboni, M. Poms, A. Cremonesi, J.C. Garcia-Cañaveras, K.D. Bock, R.J. Morscher, GLUD1 determines murine muscle stem cell fate by controlling mitochondrial glutamate levels, Dev. Cell 59 (2024) 2850-2865.e8. https://doi.org/10.1016/j.devcel.2024.07.015.
[85] A. Muir, L.V. Danai, D.Y. Gui, C.Y. Waingarten, C.A. Lewis, M.G. Vander Heiden, Environmental cystine drives glutamine anaplerosis and sensitizes cancer cells to glutaminase inhibition, eLife 6 (2017) e27713. https://doi.org/10.7554/eLife.27713.
[86] M.D. Neinast, C. Jang, S. Hui, D.S. Murashige, Q. Chu, R.J. Morscher, X. Li, L. Zhan, E. White, T.G. Anthony, J.D. Rabinowitz, Z. Arany, Quantitative Analysis of the Whole-Body Metabolic Fate of Branched-Chain Amino Acids, Cell Metab. 29 (2019) 417-429.e4. https://doi.org/10.1016/j.cmet.2018.10.013.
[87] N.P. Curthoys, M. Watford, Regulation of Glutaminase Activity and Glutamine Metabolism, Annu. Rev. Nutr. 15 (1995) 133–159. https://doi.org/10.1146/annurev.nu.15.070195.001025.
[88] Y.-F. Huang, Y. Wang, M. Watford, Glutamine Directly Downregulates Glutamine Synthetase Protein Levels in Mouse C2C12 Skeletal Muscle Myotubes12, J. Nutr. 137 (2007) 1357–1362. https://doi.org/10.1093/jn/137.6.1357.
[89] A.V. Zhdanov, A.H.C. Waters, A.V. Golubeva, R.I. Dmitriev, D.B. Papkovsky, Availability of the key metabolic substrates dictates the respiratory response of cancer cells to the mitochondrial uncoupling, Biochim. Biophys. Acta BBA - Bioenerg. 1837 (2014) 51–62. https://doi.org/10.1016/j.bbabio.2013.07.008.
[90] N.P. Shanware, A.R. Mullen, R.J. DeBerardinis, R.T. Abraham, Glutamine: pleiotropic roles in tumor growth and stress resistance, J. Mol. Med. 89 (2011) 229–236. https://doi.org/10.1007/s00109-011-0731-9.
[91] L. Wang, J. Li, L. Guo, P. Li, Z. Zhao, H. Zhou, L. Di, Molecular link between glucose and glutamine consumption in cancer cells mediated by CtBP and SIRT4, Oncogenesis 7 (2018) 1–10. https://doi.org/10.1038/s41389-018-0036-8.
[92] C.-S. Shin, P. Mishra, J.D. Watrous, V. Carelli, M. D'Aurelio, M. Jain, D.C. Chan, The glutamate/cystine xCT antiporter antagonizes glutamine metabolism and reduces nutrient flexibility, Nat. Commun. 8 (2017) 15074. https://doi.org/10.1038/ncomms15074.
[93] X. Ji, J. Qian, S.M.J. Rahman, P.J. Siska, Y. Zou, B.K. Harris, M.D. Hoeksema, I.A. Trenary, C. Heidi, R. Eisenberg, J.C. Rathmell, J.D. Young, P.P. Massion, xCT (SLC7A11)-mediated

metabolic reprogramming promotes non-small cell lung cancer progression, Oncogene 37 (2018) 5007–5019. https://doi.org/10.1038/s41388-018-0307-z.
[94] R. Yan, E. Xie, Y. Li, J. Li, Y. Zhang, X. Chi, X. Hu, L. Xu, T. Hou, B.R. Stockwell, J. Min, Q. Zhou, F. Wang, The structure of erastin-bound xCT–4F2hc complex reveals molecular mechanisms underlying erastin-induced ferroptosis, Cell Res. 32 (2022) 687–690. https://doi.org/10.1038/s41422-022-00642-w.
[95] N. Jyotsana, K.T. Ta, K.E. DelGiorno, The Role of Cystine/Glutamate Antiporter SLC7A11/xCT in the Pathophysiology of Cancer, Front. Oncol. 12 (2022). https://doi.org/10.3389/fonc.2022.858462.
[96] G. Pharaoh, K. Sataranatarajan, K. Street, S. Hill, J. Gregston, B. Ahn, C. Kinter, M. Kinter, H. Van Remmen, Metabolic and Stress Response Changes Precede Disease Onset in the Spinal Cord of Mutant SOD1 ALS Mice, Front. Neurosci. 13 (2019). https://doi.org/10.3389/fnins.2019.00487.
[97] J.K.C. Kreß, C. Jessen, A. Hufnagel, W. Schmitz, T.N. Xavier da Silva, A. Ferreira dos Santos, L. Mosteo, C.R. Goding, J.P. Friedmann Angeli, S. Meierjohann, The integrated stress response effector ATF4 is an obligatory metabolic activator of NRF2, Cell Rep. 42 (2023) 112724. https://doi.org/10.1016/j.celrep.2023.112724.
[98] K. Módis, C. Coletta, K. Erdélyi, A. Papapetropoulos, C. Szabo, Intramitochondrial hydrogen sulfide production by 3-mercaptopyruvate sulfurtransferase maintains mitochondrial electron flow and supports cellular bioenergetics, FASEB J. Off. Publ. Fed. Am. Soc. Exp. Biol. 27 (2013) 601–611. https://doi.org/10.1096/fj.12-216507.
[99] B. Murphy, R. Bhattacharya, P. Mukherjee, Hydrogen sulfide signaling in mitochondria and disease, FASEB J. Off. Publ. Fed. Am. Soc. Exp. Biol. 33 (2019) 13098–13125. https://doi.org/10.1096/fj.201901304R.
[100] V. Tiranti, C. Viscomi, T. Hildebrandt, I. Di Meo, R. Mineri, C. Tiveron, M. D Levitt, A. Prelle, G. Fagiolari, M. Rimoldi, M. Zeviani, Loss of ETHE1, a mitochondrial dioxygenase, causes fatal sulfide toxicity in ethylmalonic encephalopathy, Nat. Med. 15 (2009) 200–205. https://doi.org/10.1038/nm.1907.
[101] M. Libiad, V. Vitvitsky, T. Bostelaar, D.W. Bak, H.-J. Lee, N. Sakamoto, E. Fearon, C.A. Lyssiotis, E. Weerapana, R. Banerjee, Hydrogen sulfide perturbs mitochondrial bioenergetics and triggers metabolic reprogramming in colon cells, J. Biol. Chem. 294 (2019) 12077–12090. https://doi.org/10.1074/jbc.RA119.009442.
[102] B. Fräsdorf, C. Radon, S. Leimkühler, Characterization and Interaction Studies of Two Isoforms of the Dual Localized 3-Mercaptopyruvate Sulfurtransferase TUM1 from Humans, J. Biol. Chem. 289 (2014) 34543–34556. https://doi.org/10.1074/jbc.M114.605733.
[103] D. Choudhury, N. Rong, H.V.S. Kumar, S. Swedick, R.Z. Samuel, P. Mehrotra, J. Toftegaard, N. Rajabian, R. Thiyagarajan, A.K. Podder, Y. Wu, S. Shahini, K.L. Seldeen, B. Troen, P. Lei, S.T. Andreadis, Proline restores mitochondrial function and reverses aging hallmarks in senescent cells, Cell Rep. 43 (2024). https://doi.org/10.1016/j.celrep.2024.113738.
[104] B. Jones, M. Balasubramaniam, J.J. Lebowitz, A. Taylor, F. Villalta, H. Khoshbouei, C. Grueter, B. Grueter, C. Dash, J. Pandhare, Activation of proline biosynthesis is critical to maintain glutamate homeostasis during acute methamphetamine exposure, Sci. Rep. 11 (2021) 1422. https://doi.org/10.1038/s41598-020-80917-7.
[105] G. Yellen, Fueling thought: Management of glycolysis and oxidative phosphorylation in neuronal metabolism, J. Cell Biol. 217 (2018) 2235–2246. https://doi.org/10.1083/jcb.201803152.

[106] J.J. Harris, R. Jolivet, D. Attwell, Synaptic Energy Use and Supply, Neuron 75 (2012) 762–777. https://doi.org/10.1016/j.neuron.2012.08.019.
[107] G. Ashrafi, T.A. Ryan, Glucose metabolism in nerve terminals, Curr. Opin. Neurobiol. 45 (2017) 156–161. https://doi.org/10.1016/j.conb.2017.03.007.
[108] W. Liu, C.N. Hancock, J.W. Fischer, M. Harman, J.M. Phang, Proline biosynthesis augments tumor cell growth and aerobic glycolysis: involvement of pyridine nucleotides, Sci. Rep. 5 (2015) 17206. https://doi.org/10.1038/srep17206.
[109] N. Krishnan, M.B. Dickman, D.F. Becker, Proline modulates the intracellular redox environment and protects mammalian cells against oxidative stress, Free Radic. Biol. Med. 44 (2008) 671–681. https://doi.org/10.1016/j.freeradbiomed.2007.10.054.
[110] Z. Yang, X. Zhao, W. Shang, Y. Liu, J.-F. Ji, J.-P. Liu, C. Tong, Pyrroline-5-carboxylate synthase senses cellular stress and modulates metabolism by regulating mitochondrial respiration, Cell Death Differ. 28 (2021) 303–319. https://doi.org/10.1038/s41418-020-0601-5.
[111] K.W. Ryu, T.S. Fung, D.C. Baker, M. Saoi, J. Park, C.A. Febres-Aldana, R.G. Aly, R. Cui, A. Sharma, Y. Fu, O.L. Jones, X. Cai, H.A. Pasolli, J.R. Cross, C.M. Rudin, C.B. Thompson, Cellular ATP demand creates metabolically distinct subpopulations of mitochondria, Nature 635 (2024) 746–754. https://doi.org/10.1038/s41586-024-08146-w.
[112] J.D. Chung, E.R. Porrello, G.S. Lynch, Muscle regeneration and muscle stem cells in metabolic disease, Free Radic. Biol. Med. 227 (2025) 52–63. https://doi.org/10.1016/j.freeradbiomed.2024.11.041.
[113] E. Le Moal, V. Pialoux, G. Juban, C. Groussard, H. Zouhal, B. Chazaud, R. Mounier, Redox Control of Skeletal Muscle Regeneration, Antioxid. Redox Signal. 27 (2017) 276–310. https://doi.org/10.1089/ars.2016.6782.
[114] M. Segatto, R. Szokoll, R. Fittipaldi, C. Bottino, L. Nevi, K. Mamchaoui, P. Filippakopoulos, G. Caretti, BETs inhibition attenuates oxidative stress and preserves muscle integrity in Duchenne muscular dystrophy, Nat. Commun. 11 (2020) 6108. https://doi.org/10.1038/s41467-020-19839-x.
[115] P.R. Baker II, K.E. Boyle, T.R. Koves, O.R. Ilkayeva, D.M. Muoio, J.A. Houmard, J.E. Friedman, Metabolomic analysis reveals altered skeletal muscle amino acid and fatty acid handling in obese humans, Obesity 23 (2015) 981–988. https://doi.org/10.1002/oby.21046.
[116] M.C. Hughes, S.V. Ramos, P.C. Turnbull, I.A. Rebalka, A. Cao, C.M.F. Monaco, N.E. Varah, B.A. Edgett, J.S. Huber, P. Tadi, L.J. Delfinis, U. Schlattner, J.A. Simpson, T.J. Hawke, C.G.R. Perry, Early myopathy in Duchenne muscular dystrophy is associated with elevated mitochondrial H2O2 emission during impaired oxidative phosphorylation, J. Cachexia Sarcopenia Muscle 10 (2019) 643–661. https://doi.org/10.1002/jcsm.12405.

3.8. Supplementary Figures

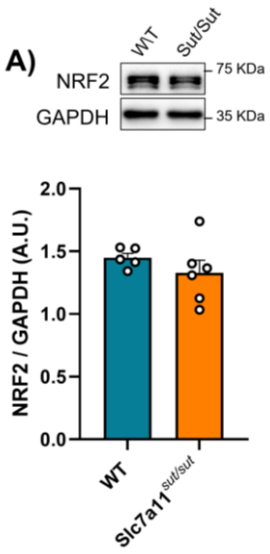

Supplementary Figure 3.1.
(A) Immunoblot of NRF2 in WT and Slc7a11$^{sut/sut}$ MuSCs. The statistical significance of the differences between groups was determined using a two-tailed Student's t-test, n = 5-6. Results are presented as mean ± SEM.

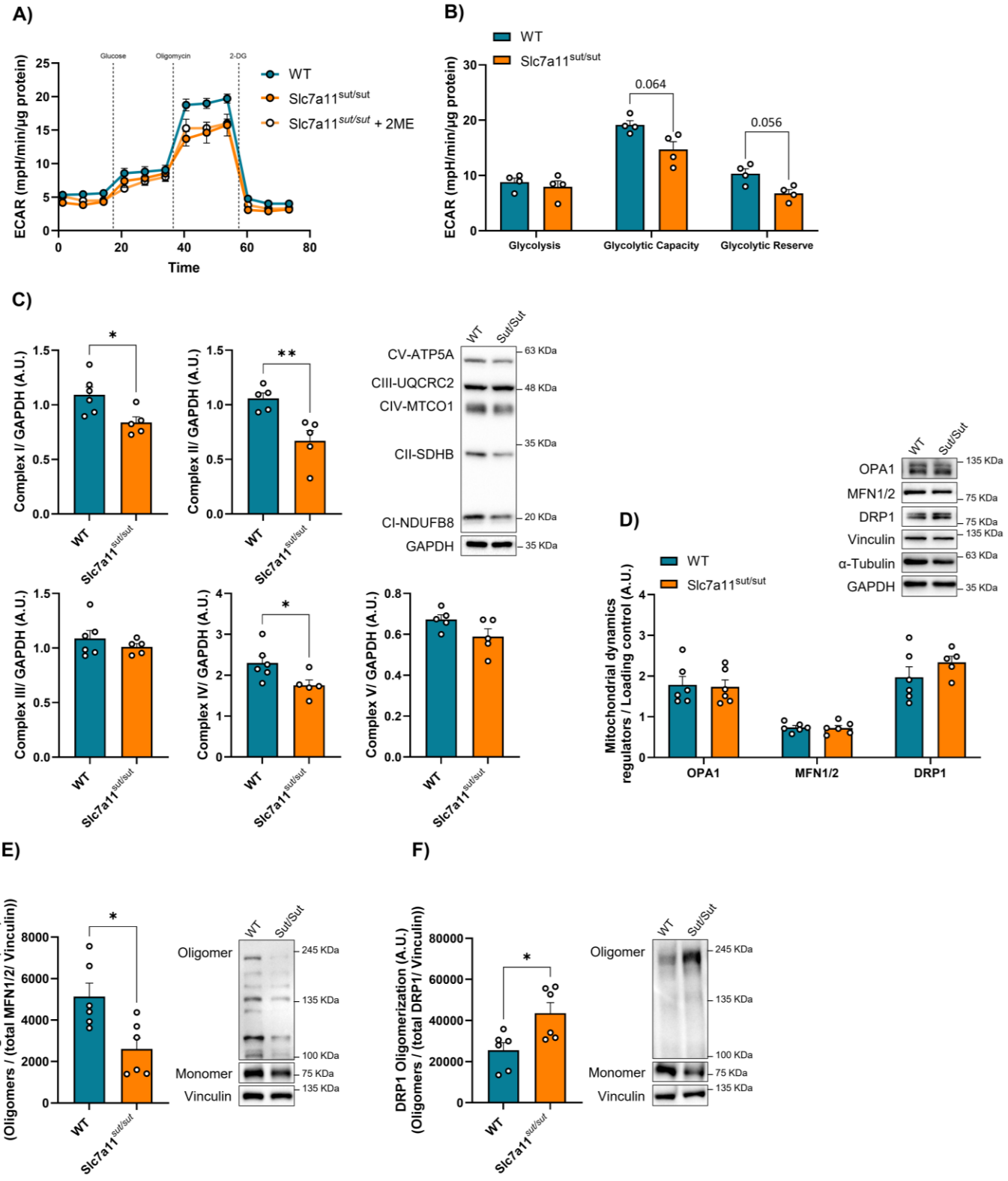
A)
Glucose
Oligomycin
2-DG
WT
Slc7a11sut/sut
Slc7a11sut/sut + 2ME
ECAR (mpH/min/µg protein)
Time
B)
WT
Slc7a11sut/sut
ECAR (mpH/min/µg protein)
0.064
0.056
Glycolysis
Glycolytic Capacity
Glycolytic Reserve
C)
Complex I/ GAPDH (A.U.)
Complex II/ GAPDH (A.U.)
Complex III/ GAPDH (A.U.)
Complex IV/ GAPDH (A.U.)
Complex V/ GAPDH (A.U.)
WT
Slc7a11sut/sut
Sut/Sut
CV-ATP5A
CIII-UQCRC2
CIV-MTCO1
CII-SDHB
CI-NDUFB8
GAPDH
63 KDa
48 KDa
35 KDa
20 KDa
D)
Mitochondrial dynamics regulators / Loading control (A.U.)
OPA1
MFN1/2
DRP1
Vinculin
α-Tubulin
135 KDa
75 KDa
63 KDa
E)
MFN1/2 Oligomerization (A.U.) (Oligomers / (total MFN1/2/ Vinculin))
Oligomer
Monomer
Vinculin
245 KDa
135 KDa
100 KDa
75 KDa
F)
DRP1 Oligomerization (A.U.) (Oligomers / (total DRP1/ Vinculin))

Supplementary Figure 3.2.
(A-B) Extracellular acidification rates (ECAR) were measured in primary WT and Slc7a11$^{sut/sut}$ MuSCs during a glycolytic stress test. **(C-D)** Immunoblots of **(C)** mitochondrial OXPHOS complexes, and **(D)** mitochondrial dynamics proteins in WT and Slc7a11$^{sut/sut}$ MuSCs. **(E-F)** Immunoblots of **(E)** MFN1/2 oligomerization, and **(F)** DRP1 oligomerization in primary WT and Slc7a11$^{sut/sut}$ MuSCs. The statistical significance of the differences between groups was determined using a two-tailed Student's t-test, n = 4-6. Results are presented as mean ± SEM, *$p < 0.05$, **$p < 0.01$.

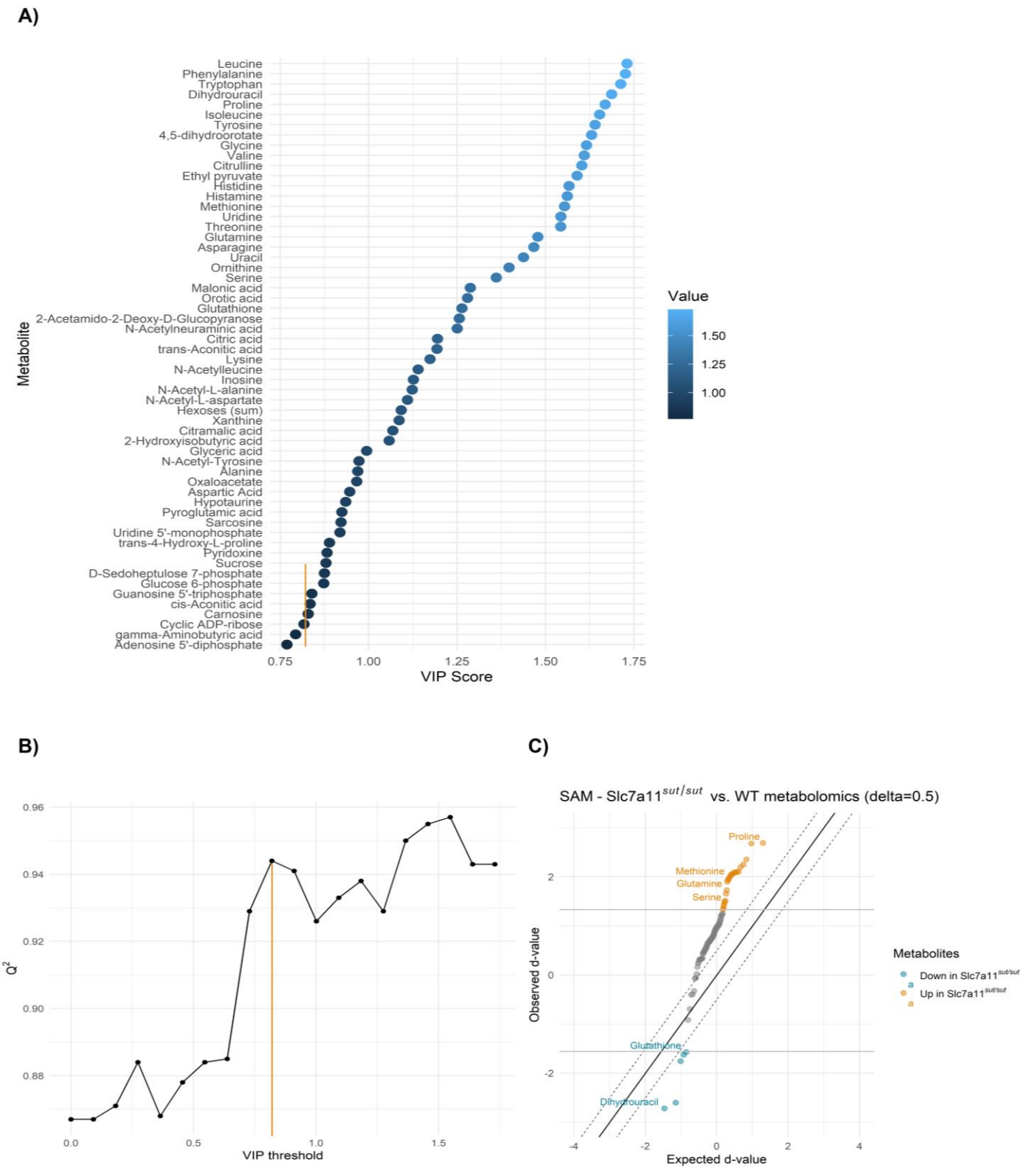
A)
Leucine
Phenylalanine
Tryptophan
Dihydrouracil
Proline
Isoleucine
Tyrosine
4,5-dihydroorotate
Glycine
Valine
Citrulline
Ethyl pyruvate
Histidine
Histamine
Methionine
Uridine
Threonine
Glutamine
Asparagine
Uracil
Ornithine
Serine
Malonic acid
Orotic acid
Glutathione
2-Acetamido-2-Deoxy-D-Glucopyranose
N-Acetylneuraminic acid
Citric acid
trans-Aconitic acid
Lysine
N-Acetylleucine
Inosine
N-Acetyl-L-alanine
N-Acetyl-L-aspartate
Hexoses (sum)
Xanthine
Citramalic acid
2-Hydroxyisobutyric acid
Glyceric acid
N-Acetyl-Tyrosine
Alanine
Oxaloacetate
Aspartic Acid
Hypotaurine
Pyroglutamic acid
Sarcosine
Uridine 5'-monophosphate
trans-4-Hydroxy-L-proline
Pyridoxine
Sucrose
D-Sedoheptulose 7-phosphate
Glucose 6-phosphate
Guanosine 5'-triphosphate
cis-Aconitic acid
Carnosine
Cyclic ADP-ribose
gamma-Aminobutyric acid
Adenosine 5'-diphosphate
Metabolite
0.75
1.00
1.25
1.50
1.75
VIP Score
Value
1.50
1.25
1.00
B)
0.96
0.94
0.92
0.90
0.88
Q²
0.0
0.5
1.0
1.5
VIP threshold
C)
SAM - Slc7a11sut/sut vs. WT metabolomics (delta=0.5)
Proline
Methionine
Glutamine
Serine
Glutathione
Dihydrouracil
Observed d-value
2
0
-2
-4
-2
0
2
4
Expected d-value
Metabolites
Down in Slc7a11sut/sut
Up in Slc7a11sut/sut

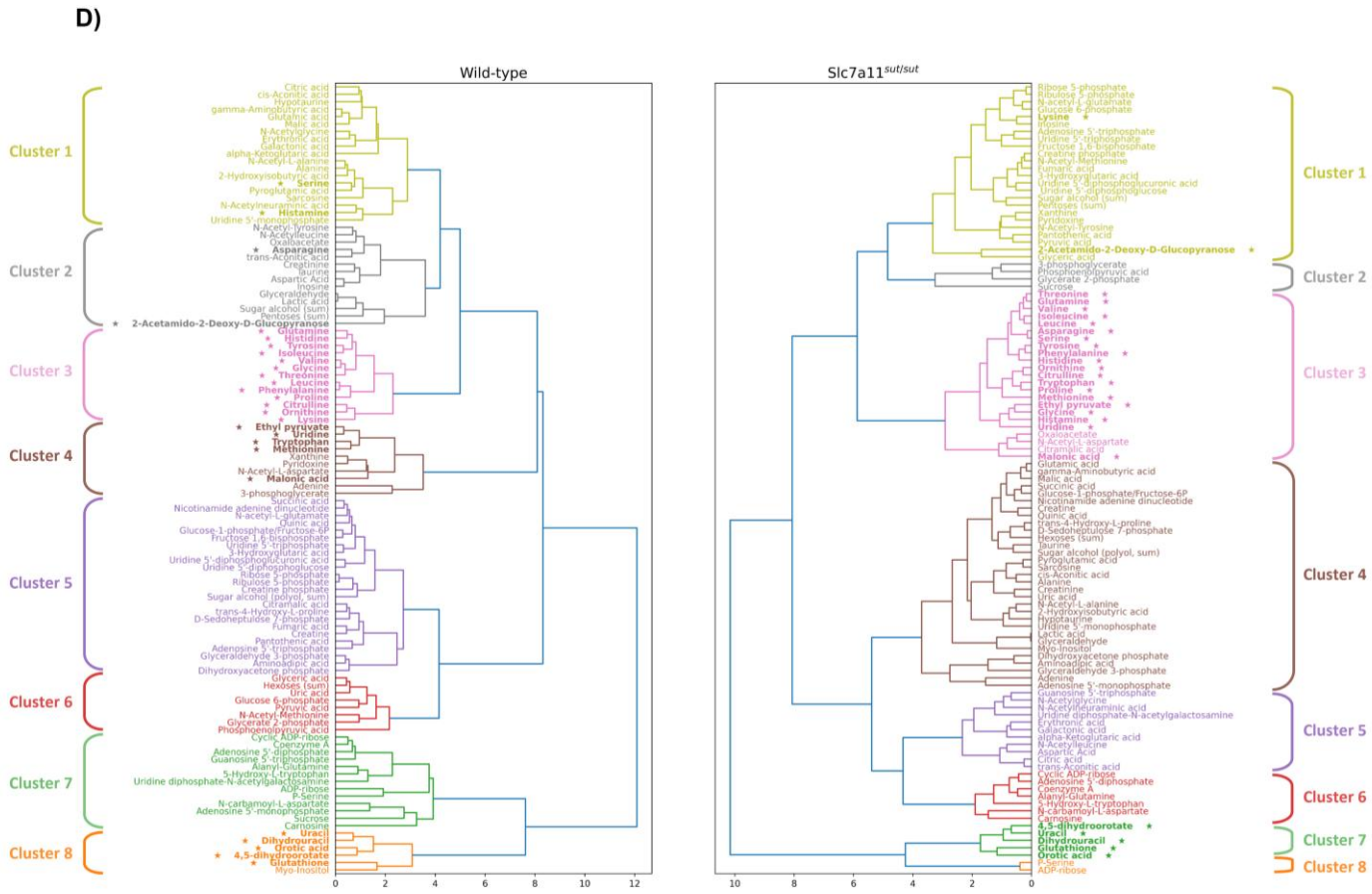

Supplementary Figure 3.3.
(A) Variable influence on projection (VIP) scores for metabolite features in OPLS-DA classification of WT and Slc7a11$^{sut/sut}$ samples, metabolites with VIP scores > 0.75 are shown. **(B)** Q^2 scores of OPLS-DA models constructed using metabolite feature subsets defined by minimum VIP score thresholds. Vertical lines indicate VIP threshold determined by peak predictive performance (Q^2) in subset models before sustained decrease. **(C)** SAM plot of WT and Slc7a11$^{sut/sut}$ groups. **(D)** Hierarchical clustering of WT and Slc7a11$^{sut/sut}$ metabolomics data. Dendrogram leafs and linkages are colored according to the assigned cluster (Euclidean distance threshold t = 4).

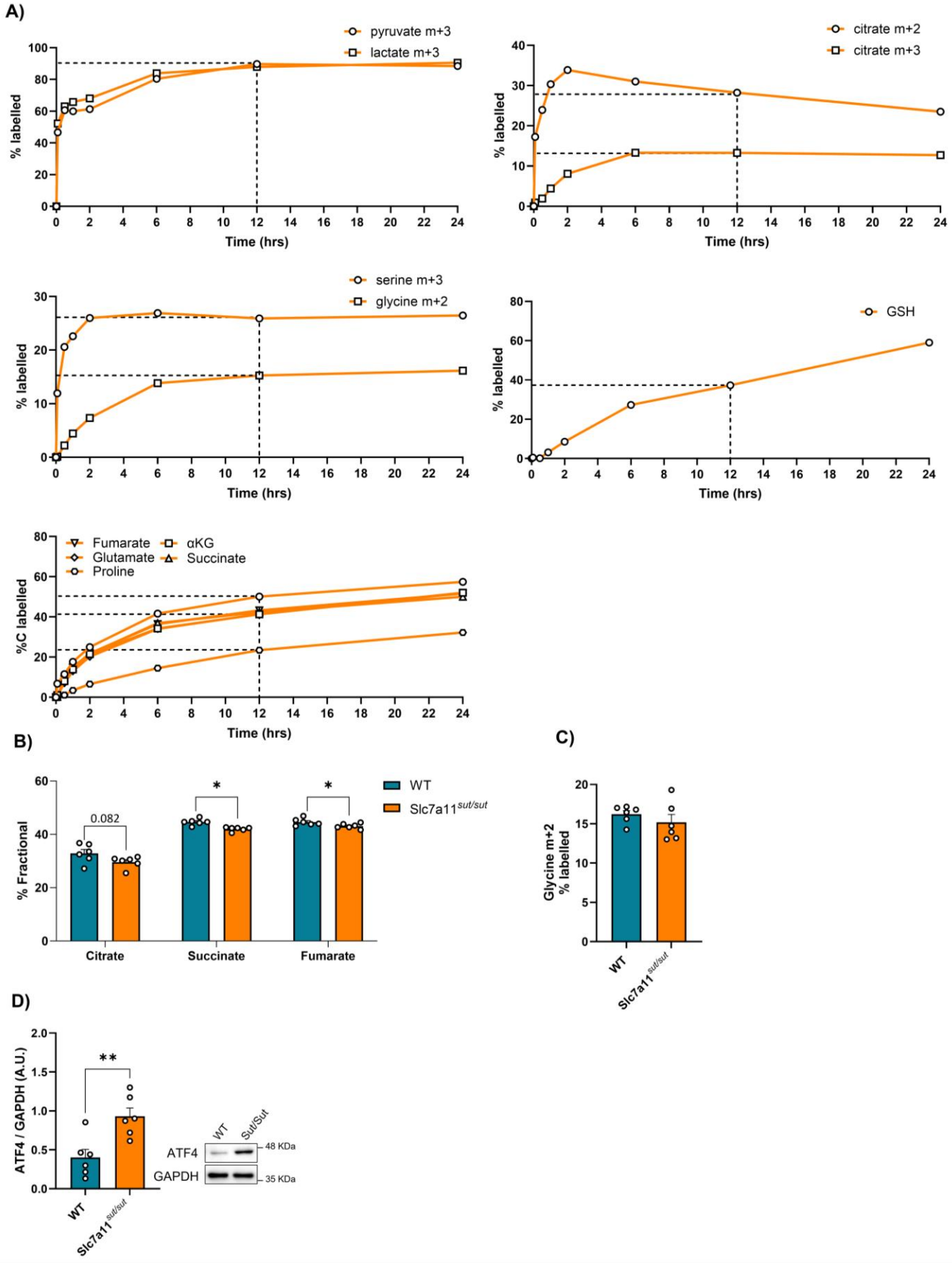
A)
pyruvate m+3
lactate m+3
% labelled
Time (hrs)
citrate m+2
citrate m+3
% labelled
Time (hrs)
serine m+3
glycine m+2
% labelled
Time (hrs)
GSH
% labelled
Time (hrs)
Fumarate
αKG
Glutamate
Succinate
Proline
%C labelled
Time (hrs)
B)
% Fractional
0.082
*
*
WT
Slc7a11sut/sut
Citrate
Succinate
Fumarate
C)
Glycine m+2
% labelled
WT
Slc7a11sut/sut
D)
ATF4 / GAPDH (A.U.)
**
WT
Slc7a11sut/sut
WT
Sut/Sut
ATF4
GAPDH
48 KDa
35 KDa

Supplementary Figure 3.4.
(A) Kinetic time-course of [U-^{13}C]-glucose labeling of relevant metabolites for 5 min, 30 min, 1 hr, 2 hrs, 6 hrs, 12 hrs, and 24 hrs in Slc7a11$^{sut/sut}$ primary MuSCs, n = 1, expressed as labelled isotopologue percentage or percentage of labelled carbon units within metabolites. **(B)** [U-^{13}C]-glucose labelling (12 hrs) of TCA cycle intermediates (citrate, succinate, and fumarate) expressed as a percentage of labelled carbon units within metabolites derived from ^{13}C precursor in WT and Slc7a11$^{sut/sut}$ MuSCs. **(C)** [U-^{13}C]-glucose labelling (12 hrs) of glycine m+2, expressed as labelled percentage of total glycine levels. **(D)** Immunoblot of ATF4 in WT and Slc7a11$^{sut/sut}$ MuSCs.

CHAPTER 4: GENERAL DISCUSSION

Muscle-related diseases like dystrophies, diabetes, and sarcopenia are a global health concern that imposes a significant financial burden on healthcare systems worldwide [1–3]. Thanks to the remarkable progress made in understanding the causes of these diseases over the last 20 years, improved preventive interventions and treatments have emerged. Despite this advancement, many fundamental aspects of their etiology remain underexplored. Research has identified disrupted redox and metabolic homeostasis as a common characteristic among these diseases. My doctoral research aimed to investigate the implications of the cystine/glutamate antiporter, xCT, in regulating the redox state and metabolism of skeletal muscle.

It is well-known that the regenerative capacity of skeletal muscle lies in the activity of MuSCs [4]. Interestingly, the functions of MuSCs and their neighbouring cells can be immensely influenced by oxidative stress, rendering skeletal muscle regeneration a redox-dependent process. For instance, high ROS levels, resulting from sustained NF-κB activity, have been shown to impair myogenic differentiation [5]. Conversely, excessive concentrations of antioxidants such as NAC and GSHee have been associated with impaired differentiation caused by reductive stress [6]. Based on these findings and considering the importance of xCT in regulating GSH levels and metabolism, we focused our research, presented in Chapter 2, on the roles of xCT in myogenesis. One of the major findings of this study was the dependence of MuSCs isolated from xCT-mutant mice, $Slc7a11^{sut/sut}$, on the reducing agent 2-mercaptoethanol (2ME) to survive and proliferate in culture. In contrast, the process of differentiation in $Slc7a11^{sut/sut}$ MuSCs was not dependent on any reducing agent. The importance of xCT in proliferating MuSCs is significant, as this confirms and extends previous findings showing that cell replication processes require high levels of GSH to maintain cellular redox and protect DNA from oxidative damage [7,8]. Additionally, it is well recognized that MuSCs have increased requirements for amino acid uptake

during proliferation to support anabolic pathways essential for cellular growth [9]. However, the metabolic role of xCT in MuSCs is poorly understood. In Chapter 3, my research examined how impaired xCT-mediated cystine uptake controls mitochondrial and metabolic remodeling in proliferating MuSCs. GSH is abundant in skeletal muscle and essential for maintaining tissue integrity and health [10]. Specifically, it has been demonstrated that depleted levels of GSH can cause cell cycle arrest by inhibiting the G1/S transition [11,12]. These findings are consistent with our results that indicate a defective proliferation in Slc7a11$^{sut/sut}$ MuSCs (Chapter 2), which can be attributable to lower intracellular availability of cysteine and subsequent decreased GSH levels. Not only proliferation but various phases of the myogenic program can be regulated by redox-dependent mechanisms in which GSH redox plays an instrumental role [13]. For instance, during differentiation, GSH undergoes an oxidative shift in which GSSG triggers several differentiation-related pathways [14,15]. Consistent with this notion, several reports have indicated the crucial role of mtROS in stimulating the initial steps of myogenic differentiation [16–21]. All these findings align with our observations of elevated GSSG and decreased GSH: GSSG ratio in Slc7a11$^{sut/sut}$ MuSCs, which exhibit enhanced *in vitro* and *in vivo* differentiation (Chapter 2). Moreover, several studies have documented that GSH levels decrease in skeletal muscle with aging [22,23]. Decreased cysteine availability is a primary cause of GSH depletion observed in muscles of older adults, where muscle cells exhibit increased oxidative stress, inflammation, and apoptosis [24,25]. Benjamin *et al*. have reported that disrupted GSH redox contributes to the age-induced deregulation of MuSCs leading to the loss of muscle regenerative capacity [26]. All these findings highlight the central role of cysteine availability and GSH in maintaining skeletal muscle function and regenerative potential, not only in aging but also in other physiological and pathological settings where cellular redox is disrupted. This raises an important question: can supplements aimed at increasing GSH levels benefit skeletal muscle health and regeneration and support adaptation to

stressors? Given the conflicting findings on the efficacy of GSH-boosting supplements in skeletal muscle, this remains an open and complex issue.

To explore this further, we will highlight findings from several studies that have investigated the impact of GSH-boosting supplements on skeletal muscle homeostasis in various contexts, including aging, muscular dystrophy, and exercise. Supplementing older adults with dietary NAC has shown positive effects on skeletal muscle, such as improved GSH levels, decreased oxidative stress, and increased strength[27,28]. It has also been demonstrated that NAC when supplemented with glycine, improves exercise capacity and muscle strength in the elderly [29]. NAC injections have been reported to mitigate fibrosis and promote muscle recovery after injury in rats [30]. Similarly, treating mice with s-allyl cysteine, another cysteine derivative, has been reported to reduce atrophy and proteolysis following muscle denervation [31]. In mdx mice, NAC treatment has been shown to improve muscle function and mitigate inflammation and oxidative stress [32]. The impact of NAC supplements on exercise performance and post-exercise muscle recovery has been extensively studied. For instance, oral NAC supplements have been shown to elevate resistance to fatigue in athletes engaging in prolonged endurance exercise. Long-term NAC supplementation has been reported to enhance exercise performance and redox homeostasis but not in individuals with sufficient levels of GSH [33]. Conversely, several reports have revealed that the excessive use of these exogenous antioxidants may have negative effects on skeletal muscle by blunting the physiological role of ROS in many cellular signaling pathways. For example, prolonged consumption of antioxidants at high doses has been shown to prevent exercise training-mediated health benefits in muscles such as hypertrophy, mitochondrial biogenesis, and increased insulin sensitivity [34,35]. Moreover, many studies have questioned the notion that dietary NAC has any benefit on tissue levels of GSH [30], and several studies support the idea that NAC is metabolized in the liver and has little impact on other tissues [36,37]. Based on these findings

and the central role of xCT in cysteine and GSH metabolism, future research should focus on exploring the implications of xCT in maintaining skeletal muscle homeostasis, particularly in physiological and pathological contexts such as aging, muscular dystrophies, and exercise-induced adaptations.

Given the conflicting outcomes reported for GSH-boosting supplementation in the context of exercise adaptation, we were interested in investigating how xCT deficiency impacts skeletal muscle metabolic response to endurance exercise. In response to physiological stressors, such as low-intensity running, skeletal muscle metabolically adapts by increasing mitochondrial metabolism and biogenesis [38,39]. Our results in permeabilized muscle fibers showed that these metabolic adaptations only occurred in WT mice. Instead, permeabilized muscle fibers from Slc7a11$^{sut/sut}$ mice displayed impaired mitochondrial metabolism and content in response to a five-week treadmill training protocol (Chapter 2). In line with our findings, *Sod2*$^{+/-}$ mice have been shown to exhibit impaired mitochondrial adaptations in response to exercise training due to elevated ROS and consequent disrupted cellular redox [40]. Therefore, we hypothesized that xCT deficiency drives mitochondrial maladaptation in response to exercise training through disrupted GSH metabolism. Surprisingly, we found that GSH levels remain unchanged across all experimental groups in basal and exercise conditions (Chapter 2). Flockart *et al*. have demonstrated that excessive exercise training leads to mitochondrial impairments in healthy subjects [41]. These impaired mitochondrial adaptations can be interpreted as a compensatory partial shutdown of mitochondrial metabolism to control ROS emission and maintain cellular redox homeostasis. In support of our previous observations of lower mitochondrial metabolism, complex I catalytic activity was lower in skeletal muscle mitochondria isolated from exercised Slc7a11$^{sut/sut}$ mice compared to exercised WT controls (Chapter 2). Notably, it has been shown that the inhibition of complex I by the anti-diabetic drug metformin results in improved skeletal muscle sensitivity to insulin [42,43], a phenotype also observed in Slc7a11$^{sut/sut}$ mice. The low catalytic activity of complex I can lead to a decline in the levels of NAD^+,

a substrate of the mitochondrial deacetylase Sirtuin3 that regulates the balance between cytosolic glycolysis and mitochondrial oxidative pathways [44,45]. In addition to higher insulin-stimulated glucose disposal, Slc7a11$^{sut/sut}$ mice displayed an increased LDH activity upon exercise training, indicating a higher glycolytic capacity (Chapter 2). These results are consistent with the conclusion that xCT-mutant mice rely on glycolytic metabolism to produce sufficient ATP, compensating for the impaired mitochondrial response to exercise training. Furthermore, by upregulating their glycolytic metabolism, xCT-deficient mice may be capable of maintaining skeletal muscle GSH levels by channeling glucose toward endogenous cysteine biosynthesis through the transsulfuration pathway. While our study only assessed the role of xCT in regulating skeletal muscle metabolism in response to endurance exercise, future research should focus on the physiological consequences of xCT deficiency in the context of other metabolic challenges, such as a high-fat diet and nutrient deprivation.

To further dissect the impact of xCT deficiency on cellular energy metabolism at the myogenic cell level, we examined the bioenergetic profiles of cultured primary muscle cells isolated from Slc7a11$^{sut/sut}$ mice and WT controls. Although high-resolution respirometry determinations showed no bioenergetic differences between xCT-mutant and WT permeabilized muscle fibers in baseline conditions (non-exercised) (Chapter 2), this was not the case in cultured primary muscle cells. Continuous real-time measurement of resting oxygen consumption rates revealed that Slc7a11$^{sut/sut}$ myoblasts exhibited lower cellular respiration during proliferation compared to WT, which was reversed during differentiation (Chapter 2). This bioenergetic difference between the *ex vivo* samples and cultured cells can be due to several factors related to the variable experimental settings. Permeabilized myofibers preserve, to a certain extent, the native intracellular environment, including mitochondrial morphology and cellular structure. In contrast, cultured primary muscle cells are dissociated from their *in vivo* environment, allowing a better manipulation of the experimental conditions [46]. During high-resolution respirometry

determinations, saturating concentrations of various substrates were sequentially provided to myofibers to assess mitochondrial respiratory capacity [47], whereas cultured primary muscle cells were maintained in culture medium containing 5 mM glucose, where substrate availability is not always saturating. Additionally, in culture conditions, the ambient O_2 percentage (21 %) is considerably higher than the physiological levels of O_2 , which may also contribute to the observed differences in the bioenergetic profiles [48,49].

Building on our findings that xCT is essential for MuSCs proliferation, we sought to further investigate in Chapter 3 the metabolic and mitochondrial remodeling mediated by xCT deficiency. Extracellular flux bioenergetic profiling revealed lower oxidative and glycolytic capacities in Slc7a11$^{sut/sut}$ MuSCs with higher proportional reliance on glycolysis than oxidative phosphorylation for ATP supply (Chapter 3). Such bioenergetic impairments may be driven by disrupted cellular redox in xCT-deficient MuSCs, attempting to control levels of ROS generation by shifting their metabolism toward glycolytic pathways [50]. In line with these observations, multiple reports have shown that elevated levels of H_2O_2 downregulate TCA cycle activity by modulating redox-sensitive enzymes such as isocitrate dehydrogenase and α-ketoglutarate dehydrogenase [51,52]. Others have found that PDK activity can be controlled through the reversible oxidation of cysteine residues in response to high levels of H_2O_2 [53,54]. In addition to redox stress, the limited intracellular availability of cysteine resulting from xCT deficiency can contribute to bioenergetic impairment. Specifically, research has demonstrated that cysteine can regulate cellular respiration in ovarian and lung adenocarcinoma cancer cells by serving as an essential component for Fe-S clusters synthesis[55,56]. Therefore, it is conceivable that decreases in ETC activity observed in xCT-deficient MuSCs are partly due to low cysteine availability and defective Fe-S clusters production.

Due to the intimate link between mitochondrial function and structure, we were also interested in investigating the effect of xCT deficiency on mitochondrial morphology and dynamics (Chapter 3). In contrast with previous reports showing that the addition of GSSG to HeLa cells promotes mitochondrial fusion and elongation in a dose-dependent manner [57], proliferating Slc7a11$^{sut/sut}$ MuSCs exhibited a fragmented mitochondrial reticulum (Chapter 3). These distinct findings may be attributed to differences in experimental conditions, as the prior outcomes were collected from an *in vitro* mitochondrial fusion assay using isolated mitochondria [57], while our observations were made in intact proliferating MuSCs. However, consistent with the decreased GSH: GSSG ratio in Slc7a11$^{sut/sut}$ MuSCs (Chapter 3), previous studies have shown that C2C12 cells initiate mitochondrial fragmentation once exposed to high levels of H_2O_2 that exceed their antioxidant capacities [58]. In line with findings from the latter mitochondrial morphology studies, our results demonstrated a higher oligomerization of DRP1 in Slc7a11$^{sut/sut}$ MuSCs (Chapter 3). Oxidative stress can induce DRP1 oligomerization through the reversible sulfenylation at cysteine residue 644 (Cys^{644}) and can also modulate its activity via the phosphorylation of serine residues 616 and 637 (Ser^{616} and Ser^{637}) [59–61]. Additionally, studies have proposed that the redox sensitivity of DRP1 is a crucial mediator of skeletal muscle mitochondrial remodeling in response to aerobic exercise training (treadmill walking and cycling) [62,63]. Recently, Pokhrel *et al*. have shown that oxidative stress causes conformational changes to Fis1 and exposes its cysteine residue 41 (Cys^{41}) to form disulfide-bond homodimers, upregulating DRP1 recruitment to mitochondria and inducing excessive mitochondrial fission [64]. All these findings further confirm that cellular redox is a key regulator of the mitochondrial dynamic machinery [65].

Taken together, the impaired mitochondrial respiration, fragmented mitochondrial reticulum, and elevated ROS emission observed in Slc7a11$^{sut/sut}$ MuSCs (Chapter 3), are all hallmarks of mitochondrial dysfunction [66]. However, these xCT-deficiency mediated mitochondrial alterations may reflect

elements of a tightly regulated but incomplete adaptive response to redox and metabolic stress [67], which will be discussed later. Importantly, considering the importance of mitochondria in a wide range of cellular and organismal functions, it is not surprising that mitochondrial dysfunction is associated with many diseases such as human inherited disorders, obesity, cancer, neurogenerative disorders, and cardiomyopathies [68]. Thus, these findings, along with our observations, highlight the relevance of further elucidating xCT roles in linking redox regulation to mitochondrial homeostasis and susceptibility to diseases in skeletal muscle.

Next, we sought to explore how the absence of functional xCT influences cellular metabolic pathways. Interestingly, our targeted metabolomic analyses demonstrated that Slc7a11$^{sut/sut}$ and WT MuSCs have distinct metabolic profiles (Chapter 3). Enrichment analysis of differential metabolites identified BCAA metabolism as one of the most altered pathways between groups (Chapter 3). BCAAs have a significant metabolic role in skeletal muscle as they can be used either for protein synthesis or transported into mitochondria for catabolism [69]. Metabolite profiling revealed that Slc7a11$^{sut/sut}$ MuSCs have a higher abundance of BCAAs (valine, leucine, and isoleucine) than WT cells. This accumulation of BCAAs in Slc7a11$^{sut/sut}$ MuSCs results from impaired catabolism, rather than increased uptake, as evidenced by lower expression levels of mitochondrial BCAT2 (Chapter 3). Elevated levels of H_2O_2 and low GSH redox observed in Slc7a11$^{sut/sut}$ MuSCs could modulate BCAT2 activity as the protein has two redox-sensitive cysteine residues 315 and 318 (Cys^{315} and Cys^{318}) [70]. While catalyzing BCAA transamination, BCAT2 produces BCKAs along with glutamate [71]. Interestingly, the upregulated levels of BCAT2 in liver cancer cells are reported to protect the cells from ferroptotic cell death, increasing intracellular glutamate release, and promoting cystine import via xCT for GSH synthesis [72]. These findings may explain the downregulation of BCAA catabolism in Slc7a11$^{sut/sut}$ MuSCs, which helps prevent excessive intracellular accumulation of glutamate due to defective xCT transport activity.

Additionally, BCAA catabolism can produce anaplerotic substrates that fuel the TCA cycle. Defects in enzymes responsible for catalyzing these catabolic pathways can cause anaplerotic stress, which is commonly associated with compromised mitochondrial metabolism [73–76]. Dysfunctional and incomplete BCAA metabolism have also been observed in various skeletal muscle-related metabolic diseases such as type 2 diabetes and obesity [77–79]. In these disease conditions, toxic metabolites derived from impaired BCAA metabolism can interfere with mitochondrial metabolism and disrupt insulin signaling through the hyperactivation of mTORC1 [73,77,80–83].

A variety of intrinsic and extrinsic stressors can influence mitochondrial metabolism, leading to drastic changes in oxidative pathways and cellular redox [84]. These alterations are not necessarily always associated with disease and can have cytoprotective purposes. Therefore, many metabolic characteristics observed in Slc7a11$^{sut/sut}$ MuSCs may be part of the adaptive mitochondrial program, referred to as the mitochondrial integrated stress response (mtISR) [85]. During mtISR, mitochondria communicate with the nucleus through complex signaling pathways to induce a reparative transcriptomic and proteomic response. ATF4, which was upregulated in Slc7a11$^{sut/sut}$ MuSCs, is known to be a key regulator of mtISR (Chapter 3) [86]. While other ATFs can also be involved in regulating the transcriptional program of mtISR, ATF4 is the primary transcriptional effector of mtISR in proliferating cells [87–90]. To promote cellular recovery and survival, mtISR induces metabolic and redox alterations. Our findings of upregulated glucose uptake and flux toward serine biosynthesis and subsequent GSH synthesis through the transsulfuration pathway in Slc7a11$^{sut/sut}$ MuSCs can be part of xCT deficiency-induced stress response (Chapter 3). Interestingly, in many muscle and heart mitochondrial disease models, mtISR-driven pathways play a central role in regulating redox homeostasis as the carbon units of glucose-derived serine have been shown to integrate rapidly into GSH biosynthesis [91]. However, others have reported that serine supplementation cannot replace serine biosynthesis induced by mtISR. This may be

attributed to the fact that the spatial localization of serine biosynthesis, possibly occurring on mitochondria, plays a crucial role during mitochondrial stress [92]. Extensive research in transgenic mouse models of mitochondrial stress has demonstrated that mtISR can systemically modulate metabolism by secreting "mitokines" such as fibroblast growth factor 21 (FGF21) and growth differentiation factor 15 (GDF15) [93]. For example, it has been demonstrated that FGF21 increases glucose uptake and lipid metabolism in the liver and white adipose tissue in mouse models of mitochondrial myopathy [94,95]. Additionally, it has been found that FGF21 can exert an autocrine effect in chronic stress, where it is needed to promote *de novo* synthesis of serine and cysteine [96]. The second secreted factor, GDF15, has been shown to have anti-inflammatory properties and the capacity to influence physiological appetite through the central nervous system [97]. Varghese *et al*. have found that a cysteine-deprived diet in a CTH knockout mouse model leads to rapid weight loss associated with stress response activation and GDF15 and FGF21 secretion [98]. However, mtISR is not always a healthy cellular adaptation; its prolonged activation can be detrimental to cells, causing cellular death and compromised organismal health [99–101]. In line with this idea, Khan *et al*. have shown that chronic induction of mtISR contributes to the progression of mitochondrial myopathy that can be reversed by rapamycin-induced inhibition of mTORC1, an upstream regulator of mtISR in muscle [102]. More recently, Bond *et al*. have demonstrated in a muscle-specific polymerase γ mutant mouse model that mtISR activation causes muscle degeneration accompanied by a perturbed folate cycle, along with FGF21 and GDF15-mediated fat reduction [103]. Interestingly, Haakonsen *et al*. found that mutations in the large E3 ligase complex, which inhibits mtISR, can contribute to the onset of neurodegenerative diseases such as ataxia and dementia [104]. Yet, how mtISR is activated and deactivated at the right time and place remains poorly elucidated. Further studies are required to explore molecular mechanisms that drive protective and maladaptive effects of mtISR on metabolism and to discover new mitokines. While

mtISR has been extensively studied in mouse models of mitochondrial stress, further translational research is required to elucidate its mechanistic and therapeutic relevance in the context of human diseases. Moreover, although significant progress has been made in understanding the implications of mitochondrial dynamics, biogenesis, and mitophagy in muscle regeneration, the role of mtISR in myogenesis is still underexplored. Thus, our in vitro xCT-deficient muscle cells can serve as a valuable model to further investigate the role of mtISR in regulating muscle cell differentiation. Specifically, it would be interesting to examine how the modulation of mtISR activity influences the transcriptomic program, as well as the mitochondrial and metabolic remodeling across different phases of the myogenic process.

Proline is another amino acid that was significantly increased in Slc7a11$^{sut/sut}$ MuSCs, as indicated by targeted metabolomic and ^{13}C-labeled glucose tracing analyses (Chapter 3). In addition to its essential role in protein structure and function, proline is pivotal in maintaining cellular redox balance, as its degradation is associated with ROS production while its biosynthesis from glutamate is reductive, and associated with NAD^+ regeneration [105]. The protein expression levels of the mitochondrial protein P5CS, which catalyzes the first step of proline biosynthesis from glutamate, were higher in Slc7a11$^{sut/sut}$ MuSCs (Chapter 3). Similar to what Jones *et al*. concluded based on their work in neuronal cells exposed to methamphetamine [106], Slc7a11$^{sut/sut}$ MuSCs may upregulate proline biosynthesis to control the intracellular excess of glutamate resulting from impaired xCT-mediated glutamate efflux. Proline biosynthesis can provide a significant bioenergetic advantage by supporting glycolysis in Slc7a11$^{sut/sut}$ MuSCs, a phenomenon commonly reported in cancer cell metabolism as well [107–109]. The reduction of glutamate to proline helps maintain high ratios of NAD^+: NADH, supporting continuous glycolytic activity and preventing the inhibition of the glycolytic enzyme GAPDH by elevated levels of NADH [110]. Similarly, lactate production and its subsequent release from muscle allow glycolysis to continue

by regenerating NAD^+ [111]. Importantly, one remarkable aspect of mitochondrial versatility lies in their metabolic heterogeneity, manifested by the ability of different mitochondria within the same cell to host distinct metabolic pathways with opposing biochemical and redox demands. For example, mitochondria can host highly oxidative pathways such as OXPHOS, alongside reductive biosynthetic processes such as proline biosynthesis [112]. Thus, our observations of upregulated proline biosynthesis in xCT-deficient muscle cells suggest that these cells can serve as a useful tool to investigate cellular mitochondrial heterogeneity further.

Despite providing novel insights into the role of xCT in regulating skeletal muscle redox and metabolism, our studies included several limitations. In Chapter 3, our bioinformatics analysis relied on available C2C12 transcriptomic datasets to assess *Slc7a11* gene expression throughout differentiation. Our results may not fully reflect the *in vivo* environment, as C2C12 cells are a transformed cell line. Additionally, results may be subject to a certain variability, caused by the different experimental conditions across the studies from which these datasets were collected. Furthermore, in Chapters 2 and 3, MuSCs were cultured under standard ambient oxygen levels (21%), which are higher than physiological levels (1-11%), and this may have influenced experimental outcomes, particularly given the redox-sensitive nature of our cell model. Future research could utilize more physiological oxygen levels to better model the *in vivo* environment of skeletal muscle. While our *in vivo* studies utilized whole-body xCT mutant mice, a MuSC-specific xCT knockout model would help minimize the potential confounding effects from other tissues of the body, which are also likely impacted by the mutation. Muscle-specific xCT knockout could be achieved by crossing floxed $Slc7a11^{f/f}$ mice with tamoxifen-inducible Pax7-specific CreER mice, enabling xCT deletion after tamoxifen injection [113,114]. Additionally, the muscle-specific xCT knockout model could determine how xCT loss in muscle modulates whole-body metabolism. Lastly, assessing the expression levels of key transcription factors during myogenesis at discrete time points (4,

7, and 21 DPI) in Chapter 2 may have missed important transient changes occurring between selected intervals or beyond 21 days, overlooking regulatory myogenic events.

Building on the findings of the present study, future work could involve the use of an additional tracer such as ^{13}C-labeled glutamine. Incorporating glutamine tracer analyses alongside our ^{13}C-labeled glucose tracing analyses would offer a more comprehensive view of xCT-driven metabolomic reprogramming, focusing on glutamine-glutamate flux, TCA cycle anaplerosis, and proline biosynthesis. As previously mentioned, xCT-deficient MuSCs offer a valuable model for enhancing our understanding of the mtISR implications in myogenesis, using pharmacological inducers and suppressors of mtISR. Moreover, to complement the *in vitro* findings on the crucial role of xCT in MuSC proliferation, future *in vivo* work could further study xCT implications by challenging the muscle stem cell pool through repeated CTX-induced injuries. Additionally, age-induced muscle loss is often linked to disrupted cellular redox and impaired MuSCs function. Therefore, investigating skeletal muscle regeneration in aged xCT-deficient mice (18-24 months old) could provide valuable insights into the role of redox regulation in age-related disrupted myogenesis. These studies could be further supported by functional assessments of muscle force production and gait analysis. While our studies in Chapter 2 used endurance exercise as a metabolic stressor, future experiments could assess the impact of xCT loss on skeletal muscle responses to other metabolic stressors, such as resistance training, nutrient deprivation, and high-fat diets. Lastly, exploring the metabolic role of xCT in the soleus muscle, which is more oxidative than the TA, could offer additional insights into its role in skeletal muscle mitochondrial metabolism.

Conclusion

In conclusion, research conducted during my doctoral studies showed that xCT is a key regulator of skeletal muscle homeostasis by controlling cellular redox and metabolism. We discovered that xCT has opposing myogenic roles; while it is essential for normal levels of muscle cell proliferation, its deficiency

enhances the differentiation process. We also revealed that during proliferation xCT deficiency drives a remarkable amount of metabolic remodeling, which appears to be an important part of a cell stress response. More research is required to better comprehend the full implications of xCT in regulating skeletal muscle health, paving the way for novel interventions to improve cellular redox and metabolism, often dysregulated in myopathies.

4.1 References

[1] C.L. Morgan, J. Godfrey, F. Chandler, E. Reuben, C.J. Currie, Epidemiology and healthcare resource utilisation associated with Duchenne muscular dystrophy, J. Rare Dis. 3 (2024) 23. https://doi.org/10.1007/s44162-024-00044-z.

[2] E.D. Parker, J. Lin, T. Mahoney, N. Ume, G. Yang, R.A. Gabbay, N.A. ElSayed, R.R. Bannuru, Economic Costs of Diabetes in the U.S. in 2022, Diabetes Care 47 (2023) 26–43. https://doi.org/10.2337/dci23-0085.

[3] K. Norman, L. Otten, Financial impact of sarcopenia or low muscle mass – A short review, Clin. Nutr. 38 (2019) 1489–1495. https://doi.org/10.1016/j.clnu.2018.09.026.

[4] Y.X. Wang, M.A. Rudnicki, Satellite cells, the engines of muscle repair, Nat. Rev. Mol. Cell Biol. 13 (2012) 127–133. https://doi.org/10.1038/nrm3265.

[5] E. Ardite, J.A. Barbera, J. Roca, J.C. Fernández-Checa, Glutathione Depletion Impairs Myogenic Differentiation of Murine Skeletal Muscle C2C12 Cells through Sustained NF-κB Activation, Am. J. Pathol. 165 (2004) 719–728. https://doi.org/10.1016/S0002-9440(10)63335-4.

[6] N.S. Rajasekaran, S.B. Shelar, D.P. Jones, J.R. Hoidal, Reductive stress impairs myogenic differentiation, Redox Biol. 34 (2020) 101492. https://doi.org/10.1016/j.redox.2020.101492.

[7] M. Poot, H. Teubert, P.S. Rabinovitch, T.J. Kavanagh, De novo synthesis of glutathione is required for both entry into and progression through the cell cycle, J. Cell. Physiol. 163 (1995) 555–560. https://doi.org/10.1002/jcp.1041630316.

[8] J. Markovic, C. Borrás, Á. Ortega, J. Sastre, J. Viña, F.V. Pallardó, Glutathione Is Recruited into the Nucleus in Early Phases of Cell Proliferation *, J. Biol. Chem. 282 (2007) 20416–20424. https://doi.org/10.1074/jbc.M609582200.

[9] A.M. Hosios, V.C. Hecht, L.V. Danai, M.O. Johnson, J.C. Rathmell, M.L. Steinhauser, S.R. Manalis, M.G. Vander Heiden, Amino Acids Rather than Glucose Account for the Majority of Cell Mass in Proliferating Mammalian Cells, Dev. Cell 36 (2016) 540–549. https://doi.org/10.1016/j.devcel.2016.02.012.

[10] L.L. Ji, R. Fu, E.W. Mitchell, Glutathione and antioxidant enzymes in skeletal muscle: effects of fiber type and exercise intensity, J. Appl. Physiol. 73 (1992) 1854–1859. https://doi.org/10.1152/jappl.1992.73.5.1854.

[11] J.P. Messina, D.A. Lawrence, Cell cycle progression of glutathione-depleted human peripheral blood mononuclear cells is inhibited at S phase., J. Immunol. 143 (1989) 1974–1981. https://doi.org/10.4049/jimmunol.143.6.1974.

[12] K.J.A. Davies, The Broad Spectrum of Responses to Oxidants in Proliferating Cells: A New Paradigm for Oxidative Stress, IUBMB Life 48 (1999) 41–47. https://doi.org/10.1080/713803463.

[13] N.S. Rajasekaran, S.B. Shelar, D.P. Jones, J.R. Hoidal, Reductive stress impairs myogenic differentiation, Redox Biol. 34 (2020) 101492. https://doi.org/10.1016/j.redox.2020.101492.

[14] J.H. Limón-Pacheco, N.A. Hernández, M.L. Fanjul-Moles, M.E. Gonsebatt, Glutathione depletion activates mitogen-activated protein kinase (MAPK) pathways that display organ-specific responses and brain protection in mice, Free Radic. Biol. Med. 43 (2007) 1335–1347. https://doi.org/10.1016/j.freeradbiomed.2007.06.028.

[15] D.J. Templeton, M.-S. Aye, J. Rady, F. Xu, J.V. Cross, Purification of Reversibly Oxidized Proteins (PROP) Reveals a Redox Switch Controlling p38 MAP Kinase Activity, PLOS ONE 5 (2010) e15012. https://doi.org/10.1371/journal.pone.0015012.

[16] M.M. Juntilla, V.D. Patil, M. Calamito, R.P. Joshi, M.J. Birnbaum, G.A. Koretzky, AKT1 and AKT2 maintain hematopoietic stem cell function by regulating reactive oxygen species, Blood 115 (2010) 4030–4038. https://doi.org/10.1182/blood-2009-09-241000.
[17] E. Owusu-Ansah, U. Banerjee, Reactive oxygen species prime Drosophila haematopoietic progenitors for differentiation, Nature 461 (2009) 537–541. https://doi.org/10.1038/nature08313.
[18] K.V. Tormos, E. Anso, R.B. Hamanaka, J. Eisenbart, J. Joseph, B. Kalyanaraman, N.S. Chandel, Mitochondrial Complex III ROS Regulate Adipocyte Differentiation, Cell Metab. 14 (2011) 537–544. https://doi.org/10.1016/j.cmet.2011.08.007.
[19] D. Malinska, A.P. Kudin, M. Bejtka, W.S. Kunz, Changes in mitochondrial reactive oxygen species synthesis during differentiation of skeletal muscle cells, Mitochondrion 12 (2012) 144–148. https://doi.org/10.1016/j.mito.2011.06.015.
[20] J.E.L. Belle, N.M. Orozco, A.A. Paucar, J.P. Saxe, J. Mottahedeh, A.D. Pyle, H. Wu, H.I. Kornblum, Proliferative Neural Stem Cells Have High Endogenous ROS Levels that Regulate Self-Renewal and Neurogenesis in a PI3K/Akt-Dependant Manner, Cell Stem Cell 8 (2011) 59–71. https://doi.org/10.1016/j.stem.2010.11.028.
[21] J.R. Hom, R.A. Quintanilla, D.L. Hoffman, K.L. de Mesy Bentley, J.D. Molkentin, S.-S. Sheu, G.A. Porter, The Permeability Transition Pore Controls Cardiac Mitochondrial Maturation and Myocyte Differentiation, Dev. Cell 21 (2011) 469–478. https://doi.org/10.1016/j.devcel.2011.08.008.
[22] W.A. Al-Turk, S.J. Stohs, F.H. El-Rashidy, S. Othman, Changes in glutathione and its metabolizing enzymes in human erythrocytes and lymphocytes with age, J. Pharm. Pharmacol. 39 (1987) 13–16. https://doi.org/10.1111/j.2042-7158.1987.tb07154.x.
[23] P.S. Samiec, C. Drews-Botsch, E.W. Flagg, J.C. Kurtz, P. Sternberg, R.L. Reed, D.P. Jones, Glutathione in Human Plasma: Decline in Association with Aging, Age-Related Macular Degeneration, and Diabetes, Free Radic. Biol. Med. 24 (1998) 699–704. https://doi.org/10.1016/S0891-5849(97)00286-4.
[24] A.D. Dam, A.S. Mitchell, J.W.E. Rush, J. Quadrilatero, Elevated skeletal muscle apoptotic signaling following glutathione depletion, Apoptosis 17 (2012) 48–60. https://doi.org/10.1007/s10495-011-0654-5.
[25] I. Sinha-Hikim, A.P. Sinha-Hikim, M. Parveen, R. Shen, R. Goswami, P. Tran, A. Crum, K.C. Norris, Long-Term Supplementation With a Cystine-Based Antioxidant Delays Loss of Muscle Mass in Aging, J. Gerontol. Ser. A 68 (2013) 749–759. https://doi.org/10.1093/gerona/gls334.
[26] D.I. Benjamin, J.O. Brett, P. Both, J.S. Benjamin, H.L. Ishak, J. Kang, S. Kim, M. Chung, M. Arjona, C.W. Nutter, J.H. Tan, A.K. Krishnan, H. Dulay, S.M. Louie, A. de Morree, D.K. Nomura, T.A. Rando, Multiomics reveals glutathione metabolism as a driver of bimodality during stem cell aging, Cell Metab. 35 (2023) 472-486.e6. https://doi.org/10.1016/j.cmet.2023.02.001.
[27] R.V. Sekhar, S.G. Patel, A.P. Guthikonda, M. Reid, A. Balasubramanyam, G.E. Taffet, F. Jahoor, Deficient synthesis of glutathione underlies oxidative stress in aging and can be corrected by dietary cysteine and glycine supplementation1234, Am. J. Clin. Nutr. 94 (2011) 847–853. https://doi.org/10.3945/ajcn.110.003483.
[28] A. Karelis, V. Messier, C. Suppère, P. Briand, R. Rabasa-Lhoret, Effect of cysteine-rich whey protein (Immunocal®) supplementation in combination with resistance training on muscle strength and lean body mass in non-frail elderly subjects: A randomized, double-blind controlled study, J. Nutr. Health Aging 19 (2015) 531–536. https://doi.org/10.1007/s12603-015-0442-y.
[29] P. Kumar, C. Liu, J. Suliburk, J.W. Hsu, R. Muthupillai, F. Jahoor, C.G. Minard, G.E. Taffet, R.V. Sekhar, Supplementing Glycine and N-Acetylcysteine (GlyNAC) in Older Adults Improves

Glutathione Deficiency, Oxidative Stress, Mitochondrial Dysfunction, Inflammation, Physical Function, and Aging Hallmarks: A Randomized Clinical Trial, J. Gerontol. Ser. A 78 (2023) 75–89. https://doi.org/10.1093/gerona/glac135.
[30] B. Yosef, Y. Zhou, K. Mouschouris, J. Poteracki, S. Soker, T. Criswell, N-Acetyl-L-Cysteine Reduces Fibrosis and Improves Muscle Function After Acute Compartment Syndrome Injury, Mil. Med. 185 (2020) 25–34. https://doi.org/10.1093/milmed/usz232.
[31] P. Gupta, V. Dutt, N. Kaur, P. Kalra, S. Gupta, A. Dua, R. Dabur, V. Saini, A. Mittal, S-allyl cysteine: A potential compound against skeletal muscle atrophy, Biochim. Biophys. Acta BBA - Gen. Subj. 1864 (2020) 129676. https://doi.org/10.1016/j.bbagen.2020.129676.
[32] G.J. Pinniger, J.R. Terrill, E.B. Assan, M.D. Grounds, P.G. Arthur, Pre-clinical evaluation of N-acetylcysteine reveals side effects in the mdx mouse model of Duchenne muscular dystrophy, J. Physiol. 595 (2017) 7093–7107. https://doi.org/10.1113/JP274229.
[33] V. Paschalis, A.A. Theodorou, N.V. Margaritelis, A. Kyparos, M.G. Nikolaidis, N-acetylcysteine supplementation increases exercise performance and reduces oxidative stress only in individuals with low levels of glutathione, Free Radic. Biol. Med. 115 (2018) 288–297. https://doi.org/10.1016/j.freeradbiomed.2017.12.007.
[34] T.-T. Peternelj, J.S. Coombes, Antioxidant Supplementation during Exercise Training, Sports Med. 41 (2011) 1043–1069. https://doi.org/10.2165/11594400-000000000-00000.
[35] T.L. Merry, M. Ristow, Do antioxidant supplements interfere with skeletal muscle adaptation to exercise training?, J. Physiol. 594 (2016) 5135–5147. https://doi.org/10.1113/JP270654.
[36] I.A. Cotgreave, N-Acetylcystei ne: Pharmacological Considerations and Experimental and Clinical Applications, in: H. Sies (Ed.), Adv. Pharmacol., Academic Press, 1996: pp. 205–227. https://doi.org/10.1016/S1054-3589(08)60985-0.
[37] M.R. Holdiness, Clinical Pharmacokinetics of N-Acetylcysteine, Clin. Pharmacokinet. 20 (1991) 123–134. https://doi.org/10.2165/00003088-199120020-00004.
[38] J.O. Holloszy, F.W. Booth, Biochemical Adaptations to Endurance Exercise in Muscle, Annu. Rev. Physiol. 38 (1976) 273–291. https://doi.org/10.1146/annurev.ph.38.030176.001421.
[39] J.O. Holloszy, E.F. Coyle, Adaptations of skeletal muscle to endurance exercise and their metabolic consequences, J. Appl. Physiol. 56 (1984) 831–838. https://doi.org/10.1152/jappl.1984.56.4.831.
[40] J.D. Crane, A. Abadi, B.P. Hettinga, D.I. Ogborn, L.G. MacNeil, G.R. Steinberg, M.A. Tarnopolsky, Elevated Mitochondrial Oxidative Stress Impairs Metabolic Adaptations to Exercise in Skeletal Muscle, PLOS ONE 8 (2013) e81879. https://doi.org/10.1371/journal.pone.0081879.
[41] M. Flockhart, L.C. Nilsson, S. Tais, B. Ekblom, W. Apró, F.J. Larsen, Excessive exercise training causes mitochondrial functional impairment and decreases glucose tolerance in healthy volunteers, Cell Metab. 33 (2021) 957-970.e6. https://doi.org/10.1016/j.cmet.2021.02.017.
[42] L. Al-Khalili, M. Forsgren, K. Kannisto, J.R. Zierath, F. Lönnqvist, A. Krook, Enhanced insulin-stimulated glycogen synthesis in response to insulin, metformin or rosiglitazone is associated with increased mRNA expression of GLUT4 and peroxisomal proliferator activator receptor gamma co-activator 1, Diabetologia 48 (2005) 1173–1179. https://doi.org/10.1007/s00125-005-1741-3.
[43] S.K. Malin, R. Gerber, S.R. Chipkin, B. Braun, Independent and Combined Effects of Exercise Training and Metformin on Insulin Sensitivity in Individuals With Prediabetes, Diabetes Care 35 (2012) 131–136. https://doi.org/10.2337/dc11-0925.
[44] M.D. Hirschey, T. Shimazu, E. Goetzman, E. Jing, B. Schwer, D.B. Lombard, C.A. Grueter, C. Harris, S. Biddinger, O.R. Ilkayeva, R.D. Stevens, Y. Li, A.K. Saha, N.B. Ruderman, J.R. Bain, C.B. Newgard, R.V. Farese Jr, F.W. Alt, C.R. Kahn, E. Verdin, SIRT3 regulates mitochondrial

fatty-acid oxidation by reversible enzyme deacetylation, Nature 464 (2010) 121–125. https://doi.org/10.1038/nature08778.
[45] L.W.S. Finley, A. Carracedo, J. Lee, A. Souza, A. Egia, J. Zhang, J. Teruya-Feldstein, P.I. Moreira, S.M. Cardoso, C.B. Clish, P.P. Pandolfi, M.C. Haigis, SIRT3 Opposes Reprogramming of Cancer Cell Metabolism through HIF1α Destabilization, Cancer Cell 19 (2011) 416–428. https://doi.org/10.1016/j.ccr.2011.02.014.
[46] A.V. Kuznetsov, V. Veksler, F.N. Gellerich, V. Saks, R. Margreiter, W.S. Kunz, Analysis of mitochondrial function in situ in permeabilized muscle fibers, tissues and cells, Nat. Protoc. 3 (2008) 965–976. https://doi.org/10.1038/nprot.2008.61.
[47] C.A. Schmidt, K.H. Fisher-Wellman, P.D. Neufer, From OCR and ECAR to energy: Perspectives on the design and interpretation of bioenergetics studies, J. Biol. Chem. 297 (2021). https://doi.org/10.1016/j.jbc.2021.101140.
[48] A. Carreau, B.E. Hafny-Rahbi, A. Matejuk, C. Grillon, C. Kieda, Why is the partial oxygen pressure of human tissues a crucial parameter? Small molecules and hypoxia, J. Cell. Mol. Med. 15 (2011) 1239–1253. https://doi.org/10.1111/j.1582-4934.2011.01258.x.
[49] M.P. Murphy, H. Bayir, V. Belousov, C.J. Chang, K.J.A. Davies, M.J. Davies, T.P. Dick, T. Finkel, H.J. Forman, Y. Janssen-Heininger, D. Gems, V.E. Kagan, B. Kalyanaraman, N.-G. Larsson, G.L. Milne, T. Nyström, H.E. Poulsen, R. Radi, H. Van Remmen, P.T. Schumacker, P.J. Thornalley, S. Toyokuni, C.C. Winterbourn, H. Yin, B. Halliwell, Guidelines for measuring reactive oxygen species and oxidative damage in cells and in vivo, Nat. Metab. 4 (2022) 651–662. https://doi.org/10.1038/s42255-022-00591-z.
[50] H.R. Molavian, M. Kohandel, S. Sivaloganathan, High Concentrations of H2O2 Make Aerobic Glycolysis Energetically More Favorable for Cellular Respiration, Front. Physiol. 7 (2016). https://doi.org/10.3389/fphys.2016.00362.
[51] L. Tretter, V. Adam-Vizi, Inhibition of Krebs Cycle Enzymes by Hydrogen Peroxide: A Key Role of α-Ketoglutarate Dehydrogenase in Limiting NADH Production under Oxidative Stress, J. Neurosci. 20 (2000) 8972–8979. https://doi.org/10.1523/JNEUROSCI.20-24-08972.2000.
[52] A.A. Starkov, G. Fiskum, C. Chinopoulos, B.J. Lorenzo, S.E. Browne, M.S. Patel, M.F. Beal, Mitochondrial α-Ketoglutarate Dehydrogenase Complex Generates Reactive Oxygen Species, J. Neurosci. 24 (2004) 7779–7788. https://doi.org/10.1523/JNEUROSCI.1899-04.2004.
[53] T.R. Hurd, Y. Collins, I. Abakumova, E.T. Chouchani, B. Baranowski, I.M. Fearnley, T.A. Prime, M.P. Murphy, A.M. James, Inactivation of Pyruvate Dehydrogenase Kinase 2 by Mitochondrial Reactive Oxygen Species *, J. Biol. Chem. 287 (2012) 35153–35160. https://doi.org/10.1074/jbc.M112.400002.
[54] Y. Tsuchiya, S.Y. Peak-Chew, C. Newell, S. Miller-Aidoo, S. Mangal, A. Zhyvoloup, J. Bakovic´, O. Malanchuk, G.C. Pereira, V. Kotiadis, G. Szabadkai, M.R. Duchen, M. Campbell, S.R. Cuenca, A. Vidal-Puig, A.M. James, M.P. Murphy, V. Filonenko, M. Skehel, I. Gout, Protein CoAlation: a redox-regulated protein modification by coenzyme A in mammalian cells, Biochem. J. 474 (2017) 2489–2508. https://doi.org/10.1042/BCJ20170129.
[55] S.C. Nunes, C. Ramos, I. Santos, C. Mendes, F. Silva, J.B. Vicente, S.A. Pereira, A. Félix, L.G. Gonçalves, J. Serpa, Cysteine Boosts Fitness Under Hypoxia-Mimicked Conditions in Ovarian Cancer by Metabolic Reprogramming, Front. Cell Dev. Biol. 9 (2021). https://doi.org/10.3389/fcell.2021.722412.
[56] N.P. Ward, S.J. Yoon, T. Flynn, A.M. Sherwood, M.A. Olley, J. Madej, G.M. DeNicola, Mitochondrial respiratory function is preserved under cysteine starvation via glutathione

catabolism in NSCLC, Nat. Commun. 15 (2024) 4244. https://doi.org/10.1038/s41467-024-48695-2.
[57] T. Shutt, M. Geoffrion, R. Milne, H.M. McBride, The intracellular redox state is a core determinant of mitochondrial fusion, EMBO Rep. 13 (2012) 909–915. https://doi.org/10.1038/embor.2012.128.
[58] X. Fan, R. Hussien, G.A. Brooks, H2O2-induced mitochondrial fragmentation in C2C12 myocytes, Free Radic. Biol. Med. 49 (2010) 1646–1654. https://doi.org/10.1016/j.freeradbiomed.2010.08.024.
[59] D.-H. Cho, T. Nakamura, J. Fang, P. Cieplak, A. Godzik, Z. Gu, S.A. Lipton, S-nitrosylation of Drp1 mediates beta-amyloid-related mitochondrial fission and neuronal injury, Science 324 (2009) 102–105. https://doi.org/10.1126/science.1171091.
[60] Y.-M. Kim, S.-W. Youn, V. Sudhahar, A. Das, R. Chandhri, H. Cuervo Grajal, J. Kweon, S. Leanhart, L. He, P.T. Toth, J. Kitajewski, J. Rehman, Y. Yoon, J. Cho, T. Fukai, M. Ushio-Fukai, Redox Regulation of Mitochondrial Fission Protein Drp1 by Protein Disulfide Isomerase Limits Endothelial Senescence, Cell Rep. 23 (2018) 3565–3578. https://doi.org/10.1016/j.celrep.2018.05.054.
[61] C. Cid-Castro, J. Morán, Differential ROS-Mediated Phosphorylation of Drp1 in Mitochondrial Fragmentation Induced by Distinct Cell Death Conditions in Cerebellar Granule Neurons, Oxid. Med. Cell. Longev. 2021 (2021) 8832863. https://doi.org/10.1155/2021/8832863.
[62] T.M. Moore, Z. Zhou, W. Cohn, F. Norheim, A.J. Lin, N. Kalajian, A.R. Strumwasser, K. Cory, K. Whitney, T. Ho, T. Ho, J.L. Lee, D.H. Rucker, O. Shirihai, A.M. van der Bliek, J.P. Whitelegge, M.M. Seldin, A.J. Lusis, S. Lee, C.A. Drevon, S.K. Mahata, L.P. Turcotte, A.L. Hevener, The impact of exercise on mitochondrial dynamics and the role of Drp1 in exercise performance and training adaptations in skeletal muscle, Mol. Metab. 21 (2019) 51–67. https://doi.org/10.1016/j.molmet.2018.11.012.
[63] C.L. Axelrod, C.E. Fealy, A. Mulya, J.P. Kirwan, Exercise training remodels human skeletal muscle mitochondrial fission and fusion machinery towards a pro-elongation phenotype, Acta Physiol. 225 (2019) e13216. https://doi.org/10.1111/apha.13216.
[64] S. Pokhrel, G. Heo, I. Mathews, S. Yokoi, T. Matsui, A. Mitsutake, S. Wakatsuki, D. Mochly-Rosen, A hidden cysteine in Fis1 targeted to prevent excessive mitochondrial fission and dysfunction under oxidative stress, Nat. Commun. 16 (2025) 4187. https://doi.org/10.1038/s41467-025-59434-6.
[65] P.H.G.M. Willems, R. Rossignol, C.E.J. Dieteren, M.P. Murphy, W.J.H. Koopman, Redox Homeostasis and Mitochondrial Dynamics, Cell Metab. 22 (2015) 207–218. https://doi.org/10.1016/j.cmet.2015.06.006.
[66] Y. Zong, H. Li, P. Liao, L. Chen, Y. Pan, Y. Zheng, C. Zhang, D. Liu, M. Zheng, J. Gao, Mitochondrial dysfunction: mechanisms and advances in therapy, Signal Transduct. Target. Ther. 9 (2024) 1–29. https://doi.org/10.1038/s41392-024-01839-8.
[67] L.J. Delfinis, S. Khajehzadehshoushtar, C.G.R. Perry, Perspectives on the interpretation of mitochondrial responses during skeletal muscle disuse-induced atrophy, J. Physiol. (2025). https://doi.org/10.1113/JP284160.
[68] A. Suomalainen, J. Nunnari, Mitochondria at the crossroads of health and disease, Cell 187 (2024) 2601–2627. https://doi.org/10.1016/j.cell.2024.04.037.
[69] T. Yoneshiro, Q. Wang, K. Tajima, M. Matsushita, H. Maki, K. Igarashi, Z. Dai, P.J. White, R.W. McGarrah, O.R. Ilkayeva, Y. Deleye, Y. Oguri, M. Kuroda, K. Ikeda, H. Li, A. Ueno, M. Ohishi, T. Ishikawa, K. Kim, Y. Chen, C.H. Sponton, R.N. Pradhan, H. Majd, V.J. Greiner, M. Yoneshiro,

Z. Brown, M. Chondronikola, H. Takahashi, T. Goto, T. Kawada, L. Sidossis, F.C. Szoka, M.T. McManus, M. Saito, T. Soga, S. Kajimura, BCAA catabolism in brown fat controls energy homeostasis through SLC25A44, Nature 572 (2019) 614–619. https://doi.org/10.1038/s41586-019-1503-x.

[70] M.E. Conway, N. Yennawar, R. Wallin, L.B. Poole, S.M. Hutson, Human mitochondrial branched chain aminotransferase: structural basis for substrate specificity and role of redox active cysteines, Biochim. Biophys. Acta BBA - Proteins Proteomics 1647 (2003) 61–65. https://doi.org/10.1016/S1570-9639(03)00051-7.

[71] K.F. LaNoue, D.A. Berkich, M. Conway, A.J. Barber, L.-Y. Hu, C. Taylor, S. Hutson, Role of specific aminotransferases in de novo glutamate synthesis and redox shuttling in the retina, J. Neurosci. Res. 66 (2001) 914–922. https://doi.org/10.1002/jnr.10064.

[72] K. Wang, Z. Zhang, H. Tsai, Y. Liu, J. Gao, M. Wang, L. Song, X. Cao, Z. Xu, H. Chen, A. Gong, D. Wang, F. Cheng, H. Zhu, Branched-chain amino acid aminotransferase 2 regulates ferroptotic cell death in cancer cells, Cell Death Differ. 28 (2021) 1222–1236. https://doi.org/10.1038/s41418-020-00644-4.

[73] C. Lerin, A.B. Goldfine, T. Boes, M. Liu, S. Kasif, J.M. Dreyfuss, A.L. De Sousa-Coelho, G. Daher, I. Manoli, J.R. Sysol, E. Isganaitis, N. Jessen, L.J. Goodyear, K. Beebe, W. Gall, C.P. Venditti, M.-E. Patti, Defects in muscle branched-chain amino acid oxidation contribute to impaired lipid metabolism, Mol. Metab. 5 (2016) 926–936. https://doi.org/10.1016/j.molmet.2016.08.001.

[74] L.A. Lotta, R.A. Scott, S.J. Sharp, S. Burgess, J. Luan, T. Tillin, A.F. Schmidt, F. Imamura, I.D. Stewart, J.R.B. Perry, L. Marney, A. Koulman, E.D. Karoly, N.G. Forouhi, R.J.O. Sjögren, E. Näslund, J.R. Zierath, A. Krook, D.B. Savage, J.L. Griffin, N. Chaturvedi, A.D. Hingorani, K.-T. Khaw, I. Barroso, M.I. McCarthy, S. O'Rahilly, N.J. Wareham, C. Langenberg, Genetic Predisposition to an Impaired Metabolism of the Branched-Chain Amino Acids and Risk of Type 2 Diabetes: A Mendelian Randomisation Analysis, PLOS Med. 13 (2016) e1002179. https://doi.org/10.1371/journal.pmed.1002179.

[75] R. Bridi, C.A. Braun, G.K. Zorzi, C.M.D. Wannmacher, M. Wajner, E.G. Lissi, C.S. Dutra-Filho, α-Keto Acids Accumulating in Maple Syrup Urine Disease Stimulate Lipid Peroxidation and Reduce Antioxidant Defences in Cerebral Cortex From Young Rats, Metab. Brain Dis. 20 (2005) 155–167. https://doi.org/10.1007/s11011-005-4152-8.

[76] C. Funchal, A. Latini, M.C. Jacques-Silva, A.Q. dos Santos, L. Buzin, C. Gottfried, M. Wajner, R. Pessoa-Pureur, Morphological alterations and induction of oxidative stress in glial cells caused by the branched-chain α-keto acids accumulating in maple syrup urine disease, Neurochem. Int. 49 (2006) 640–650. https://doi.org/10.1016/j.neuint.2006.05.007.

[77] C.B. Newgard, J. An, J.R. Bain, M.J. Muehlbauer, R.D. Stevens, L.F. Lien, A.M. Haqq, S.H. Shah, M. Arlotto, C.A. Slentz, J. Rochon, D. Gallup, O. Ilkayeva, B.R. Wenner, W.S. Yancy, H. Eisenson, G. Musante, R.S. Surwit, D.S. Millington, M.D. Butler, L.P. Svetkey, A Branched-Chain Amino Acid-Related Metabolic Signature that Differentiates Obese and Lean Humans and Contributes to Insulin Resistance, Cell Metab. 9 (2009) 311–326. https://doi.org/10.1016/j.cmet.2009.02.002.

[78] C.J. Lynch, S.H. Adams, Branched-chain amino acids in metabolic signalling and insulin resistance, Nat. Rev. Endocrinol. 10 (2014) 723–736. https://doi.org/10.1038/nrendo.2014.171.

[79] J.L. Flores-Guerrero, M.C.J. Osté, L.M. Kieneker, E.G. Gruppen, J. Wolak-Dinsmore, J.D. Otvos, M.A. Connelly, S.J.L. Bakker, R.P.F. Dullaart, Plasma Branched-Chain Amino Acids and Risk of

Incident Type 2 Diabetes: Results from the PREVEND Prospective Cohort Study, J. Clin. Med. 7 (2018) 513. https://doi.org/10.3390/jcm7120513.
[80] F. Tremblay, S. Brûlé, S. Hee Um, Y. Li, K. Masuda, M. Roden, X.J. Sun, M. Krebs, R.D. Polakiewicz, G. Thomas, A. Marette, Identification of IRS-1 Ser-1101 as a target of S6K1 in nutrient- and obesity-induced insulin resistance, Proc. Natl. Acad. Sci. 104 (2007) 14056–14061. https://doi.org/10.1073/pnas.0706517104.
[81] T.R. Koves, J.R. Ussher, R.C. Noland, D. Slentz, M. Mosedale, O. Ilkayeva, J. Bain, R. Stevens, J.R.B. Dyck, C.B. Newgard, G.D. Lopaschuk, D.M. Muoio, Mitochondrial Overload and Incomplete Fatty Acid Oxidation Contribute to Skeletal Muscle Insulin Resistance, Cell Metab. 7 (2008) 45–56. https://doi.org/10.1016/j.cmet.2007.10.013.
[82] Y. Sancak, T.R. Peterson, Y.D. Shaul, R.A. Lindquist, C.C. Thoreen, L. Bar-Peled, D.M. Sabatini, The Rag GTPases Bind Raptor and Mediate Amino Acid Signaling to mTORC1, Science 320 (2008) 1496–1501. https://doi.org/10.1126/science.1157535.
[83] S.H. Um, D. D'Alessio, G. Thomas, Nutrient overload, insulin resistance, and ribosomal protein S6 kinase 1, S6K1, Cell Metab. 3 (2006) 393–402. https://doi.org/10.1016/j.cmet.2006.05.003.
[84] Y. Zong, H. Li, P. Liao, L. Chen, Y. Pan, Y. Zheng, C. Zhang, D. Liu, M. Zheng, J. Gao, Mitochondrial dysfunction: mechanisms and advances in therapy, Signal Transduct. Target. Ther. 9 (2024) 1–29. https://doi.org/10.1038/s41392-024-01839-8.
[85] M. Bilen, S. Benhammouda, R.S. Slack, M. Germain, The integrated stress response as a key pathway downstream of mitochondrial dysfunction, Curr. Opin. Physiol. 27 (2022) 100555. https://doi.org/10.1016/j.cophys.2022.100555.
[86] P.M. Quirós, M.A. Prado, N. Zamboni, D. D'Amico, R.W. Williams, D. Finley, S.P. Gygi, J. Auwerx, Multi-omics analysis identifies ATF4 as a key regulator of the mitochondrial stress response in mammals, J. Cell Biol. 216 (2017) 2027–2045. https://doi.org/10.1083/jcb.201702058.
[87] R.C. Scarpulla, Nucleus-encoded regulators of mitochondrial function: Integration of respiratory chain expression, nutrient sensing and metabolic stress, Biochim. Biophys. Acta BBA - Gene Regul. Mech. 1819 (2012) 1088–1097. https://doi.org/10.1016/j.bbagrm.2011.10.011.
[88] T. Wai, J. García-Prieto, M.J. Baker, C. Merkwirth, P. Benit, P. Rustin, F.J. Rupérez, C. Barbas, B. Ibañez, T. Langer, Imbalanced OPA1 processing and mitochondrial fragmentation cause heart failure in mice, Science 350 (2015) aad0116. https://doi.org/10.1126/science.aad0116.
[89] S. Herzig, R.J. Shaw, AMPK: guardian of metabolism and mitochondrial homeostasis, Nat. Rev. Mol. Cell Biol. 19 (2018) 121–135. https://doi.org/10.1038/nrm.2017.95.
[90] A. Mottis, S. Herzig, J. Auwerx, Mitocellular communication: Shaping health and disease, Science 366 (2019) 827–832. https://doi.org/10.1126/science.aax3768.
[91] J. Nikkanen, S. Forsström, L. Euro, I. Paetau, R.A. Kohnz, L. Wang, D. Chilov, J. Viinamäki, A. Roivainen, P. Marjamäki, H. Liljenbäck, S. Ahola, J. Buzkova, M. Terzioglu, N.A. Khan, S. Pirnes-Karhu, A. Paetau, T. Lönnqvist, A. Sajantila, P. Isohanni, H. Tyynismaa, D.K. Nomura, B.J. Battersby, V. Velagapudi, C.J. Carroll, A. Suomalainen, Mitochondrial DNA Replication Defects Disturb Cellular dNTP Pools and Remodel One-Carbon Metabolism, Cell Metab. 23 (2016) 635–648. https://doi.org/10.1016/j.cmet.2016.01.019.
[92] X.R. Bao, S.-E. Ong, O. Goldberger, J. Peng, R. Sharma, D.A. Thompson, S.B. Vafai, A.G. Cox, E. Marutani, F. Ichinose, W. Goessling, A. Regev, S.A. Carr, C.B. Clish, V.K. Mootha, Mitochondrial dysfunction remodels one-carbon metabolism in human cells, eLife 5 (2016) e10575. https://doi.org/10.7554/eLife.10575.

[93] S. Keipert, M. Ost, Stress-induced FGF21 and GDF15 in obesity and obesity resistance, Trends Endocrinol. Metab. 32 (2021) 904–915. https://doi.org/10.1016/j.tem.2021.08.008.
[94] H. Tyynismaa, C.J. Carroll, N. Raimundo, S. Ahola-Erkkilä, T. Wenz, H. Ruhanen, K. Guse, A. Hemminki, K.E. Peltola-Mjøsund, V. Tulkki, M. Orešič, C.T. Moraes, K. Pietiläinen, I. Hovatta, A. Suomalainen, Mitochondrial myopathy induces a starvation-like response, Hum. Mol. Genet. 19 (2010) 3948–3958. https://doi.org/10.1093/hmg/ddq310.
[95] M. Ost, V. Coleman, A. Voigt, E.M. van Schothorst, S. Keipert, I. van der Stelt, S. Ringel, A. Graja, T. Ambrosi, A.P. Kipp, M. Jastroch, T.J. Schulz, J. Keijer, S. Klaus, Muscle mitochondrial stress adaptation operates independently of endogenous FGF21 action, Mol. Metab. 5 (2016) 79–90. https://doi.org/10.1016/j.molmet.2015.11.002.
[96] S. Forsström, C.B. Jackson, C.J. Carroll, M. Kuronen, E. Pirinen, S. Pradhan, A. Marmyleva, M. Auranen, I.-M. Kleine, N.A. Khan, A. Roivainen, P. Marjamäki, H. Liljenbäck, L. Wang, B.J. Battersby, U. Richter, V. Velagapudi, J. Nikkanen, L. Euro, A. Suomalainen, Fibroblast Growth Factor 21 Drives Dynamics of Local and Systemic Stress Responses in Mitochondrial Myopathy with mtDNA Deletions, Cell Metab. 30 (2019) 1040-1054.e7. https://doi.org/10.1016/j.cmet.2019.08.019.
[97] V.W.-W. Tsai, L. Macia, H. Johnen, T. Kuffner, R. Manadhar, S.B. Jørgensen, K.K.M. Lee-Ng, H.P. Zhang, L. Wu, C.P. Marquis, L. Jiang, Y. Husaini, S. Lin, H. Herzog, D.A. Brown, A. Sainsbury, S.N. Breit, TGF-b Superfamily Cytokine MIC-1/GDF15 Is a Physiological Appetite and Body Weight Regulator, PLOS ONE 8 (2013) e55174. https://doi.org/10.1371/journal.pone.0055174.
[98] A. Varghese, I. Gusarov, B. Gamallo-Lana, D. Dolgonos, Y. Mankan, I. Shamovsky, M. Phan, R. Jones, M. Gomez-Jenkins, E. White, R. Wang, D.R. Jones, T. Papagiannakopoulos, M.E. Pacold, A.C. Mar, D.R. Littman, E. Nudler, Unravelling cysteine-deficiency-associated rapid weight loss, Nature (2025) 1–9. https://doi.org/10.1038/s41586-025-08996-y.
[99] J.W. Harper, E.J. Bennett, Proteome complexity and the forces that drive proteome imbalance, Nature 537 (2016) 328–338. https://doi.org/10.1038/nature19947.
[100] M. Costa-Mattioli, P. Walter, The integrated stress response: From mechanism to disease, Science 368 (2020) eaat5314. https://doi.org/10.1126/science.aat5314.
[101] M.S. Hipp, P. Kasturi, F.U. Hartl, The proteostasis network and its decline in ageing, Nat. Rev. Mol. Cell Biol. 20 (2019) 421–435. https://doi.org/10.1038/s41580-019-0101-y.
[102] N.A. Khan, J. Nikkanen, S. Yatsuga, C. Jackson, L. Wang, S. Pradhan, R. Kivelä, A. Pessia, V. Velagapudi, A. Suomalainen, mTORC1 Regulates Mitochondrial Integrated Stress Response and Mitochondrial Myopathy Progression, Cell Metab. 26 (2017) 419-428.e5. https://doi.org/10.1016/j.cmet.2017.07.007.
[103] S.T. Bond, E.J. King, S.M. Walker, C. Yang, Y. Liu, K.H. Liu, A. Zhuang, A.W. Jurrjens, H.A. Fang, L.E. Formosa, A.P. Nath, S.R. Carmona, M. Inouye, T. Duong, K. Huynh, P.J. Meikle, S. Crawford, G. Ramm, S.N. Elahee Doomun, D.P. de Souza, D.L. Rudler, A.C. Calkin, A. Filipovska, D.W. Greening, D.C. Henstridge, B.G. Drew, Mitochondrial damage in muscle specific PolG mutant mice activates the integrated stress response and disrupts the mitochondrial folate cycle, Nat. Commun. 16 (2025) 2338. https://doi.org/10.1038/s41467-025-57299-3.
[104] D.L. Haakonsen, M. Heider, A.J. Ingersoll, K. Vodehnal, S.R. Witus, T. Uenaka, M. Wernig, M. Rapé, Stress response silencing by an E3 ligase mutated in neurodegeneration, Nature 626 (2024) 874–880. https://doi.org/10.1038/s41586-023-06985-7.

[105] L.A. Vettore, R.L. Westbrook, D.A. Tennant, Proline metabolism and redox; maintaining a balance in health and disease, Amino Acids 53 (2021) 1779–1788. https://doi.org/10.1007/s00726-021-03051-2.
[106] B. Jones, M. Balasubramaniam, J.J. Lebowitz, A. Taylor, F. Villalta, H. Khoshbouei, C. Grueter, B. Grueter, C. Dash, J. Pandhare, Activation of proline biosynthesis is critical to maintain glutamate homeostasis during acute methamphetamine exposure, Sci. Rep. 11 (2021) 1422. https://doi.org/10.1038/s41598-020-80917-7.
[107] W. Liu, C.N. Hancock, J.W. Fischer, M. Harman, J.M. Phang, Proline biosynthesis augments tumor cell growth and aerobic glycolysis: involvement of pyridine nucleotides, Sci. Rep. 5 (2015) 17206. https://doi.org/10.1038/srep17206.
[108] G.R. Kardos, H.C. Wastyk, G.P. Robertson, Disruption of Proline Synthesis in Melanoma Inhibits Protein Production Mediated by the GCN2 Pathway, Mol. Cancer Res. 13 (2015) 1408–1420. https://doi.org/10.1158/1541-7786.MCR-15-0048.
[109] M.T. Grinde, B. Hilmarsdottir, H.M. Tunset, I.M. Henriksen, J. Kim, M.H. Haugen, M.B. Rye, G.M. Mælandsmo, S.A. Moestue, Glutamine to proline conversion is associated with response to glutaminase inhibition in breast cancer, Breast Cancer Res. 21 (2019) 61. https://doi.org/10.1186/s13058-019-1141-0.
[110] J. Fan, T. Hitosugi, T.-W. Chung, J. Xie, Q. Ge, T.-L. Gu, R.D. Polakiewicz, G.Z. Chen, T.J. Boggon, S. Lonial, F.R. Khuri, S. Kang, J. Chen, Tyrosine Phosphorylation of Lactate Dehydrogenase A Is Important for NADH/NAD+ Redox Homeostasis in Cancer Cells ▿, Mol. Cell. Biol. 31 (2011) 4938–4950. https://doi.org/10.1128/MCB.06120-11.
[111] A. Luengo, Z. Li, D.Y. Gui, L.B. Sullivan, M. Zagorulya, B.T. Do, R. Ferreira, A. Naamati, A. Ali, C.A. Lewis, C.J. Thomas, S. Spranger, N.J. Matheson, M.G. Vander Heiden, Increased demand for NAD+ relative to ATP drives aerobic glycolysis, Mol. Cell 81 (2021) 691-707.e6. https://doi.org/10.1016/j.molcel.2020.12.012.
[112] J.B. Spinelli, M.C. Haigis, The multifaceted contributions of mitochondria to cellular metabolism, Nat. Cell Biol. 20 (2018) 745–754. https://doi.org/10.1038/s41556-018-0124-1.
[113] W.-M. Choi, H.-H. Kim, M.-H. Kim, R. Cinar, H.-S. Yi, H.S. Eun, S.-H. Kim, Y.J. Choi, Y.-S. Lee, S.Y. Kim, W. Seo, J.-H. Lee, Y.-R. Shim, Y.E. Kim, K. Yang, T. Ryu, J.H. Hwang, C.-H. Lee, H.-S. Choi, B. Gao, W. Kim, S.K. Kim, G. Kunos, W.-I. Jeong, Glutamate/metabotropic glutamate receptor-5 signaling in hepatic stellate cells drives endocannabinoid-mediated alcoholic steatosis, Cell Metab. 30 (2019) 877-889.e7. https://doi.org/10.1016/j.cmet.2019.08.001.
[114] M.R. Hicks, K.K. Saleh, B. Clock, D.E. Gibbs, M. Yang, S. Younesi, L. Gane, V. Gutierrez-Garcia, H. Xi, A.D. Pyle, Regenerating human skeletal muscle forms an emerging niche in vivo to support PAX7 cells, Nat. Cell Biol. 25 (2023) 1758–1773. https://doi.org/10.1038/s41556-023-01271-0.

CHAPTER 5: APPENDIX

Michel Kanaan, PhD

Ottawa, ON, Canada
LinkedIn: MichelKanaan

PERSONAL SUMMARY

Enthusiastic and results-driven Research Scientist with over eight years of progressive experience driving organizational success through effective project leadership, cross-functional collaboration, and innovative problem-solving. Demonstrated ability to bridge scientific expertise and strategic communication, as evidenced by my dual experience as a doctoral researcher and former medical representative. Committed to continuous learning and team-oriented progress, I bring deep expertise in skeletal muscle-related disease, including muscular dystrophy, diabetes, and aging, while maintaining strong scientific interests in immunology, oncology, inflammation, and rare diseases.

KEY SKILLS

✓ Cross-Functional Leadership	✓ Presentation Delivery	✓ Training & Mentoring	✓ Conflict Resolution
✓ Project Management	✓ Scientific Writing	✓ Relationship Building	✓ Process Optimization
✓ Scientific Communication	✓ Workflow Delegation	✓ Data Analysis	✓ Trilingual (EN, FR, AR)

RELEVANT PROFESSIONAL EXPERIENCE

Doctoral Researcher **01/2019 -08/2025**
University of Ottawa, Faculty of Medicine Ottawa, ON, CA

- Maintained up-to-date knowledge of skeletal muscle research and therapeutic areas.
- Managed resources for study designs, data analysis, and preparation and submission of abstracts and manuscripts, leading to two scientific publications, all as the first author.
- Presented research findings at multiple national and international scientific conferences, engaging diverse audiences of scientists, clinicians, and field experts.
- Established collaborative relationships with Canadian Nuclear Laboratories (CNL).
- Exceeded quantitative metrics, receiving Dr. Eric Poulin Center for Neuromuscular Disease STaR award totaling 10,000 CAD.
- Provided scientific counsel to colleagues, facilitating project development for junior researchers, resulting in three co-authored publications.

Teaching Assistant **01/2020 - 12/2024**
University of Ottawa, Faculty of Sciences Ottawa, ON, CA

- Conducted lectures and lab sessions for undergraduate courses, addressing student inquiries promptly.
- Organized review sessions to enhance student understanding and performance.
- Proctored and assessed exams to ensure academic integrity and fairness.
- Delivered specialized lectures on cellular bioenergetics measurements for 4th-year TMM program students.

Medical Representative **06/2015 - 08/2018**
Bellapharma Beirut, Lebanon

- Established professional relationships with physicians to enhance collaboration and engagement.
- Delivered scientific and clinical education on company products and research initiatives.
- Collaborated with cross-functional teams to align medical strategies with business objectives.
- Formulated and executed sales strategies while monitoring market conditions and competitor activities.
- Recognized as the **Best Achiever (in 2016)** for consistently exceeding sales targets and ranking as the top-performing medical representative in North Lebanon.

Lab Instructor **09/2012 - 05/2015**
University of Balamand, Faculty of Science Tripoli, Lebanon

- Organized undergraduate lab curriculum through active participation in working groups.
- Supervised and instructed undergraduate lab sessions for various courses.
- Designed, administered, and evaluated quizzes and exams to assess student understanding.

Chemistry Instructor **09/2009 - 05/2010**
United Nations Development Program (UNDP) Tripoli, Lebanon

- Participated in the United Nations Development Program initiative to support grade 9 students in public schools preparing for Lebanese official exams.
- Developed and delivered a condensed chemistry curriculum for grade 9 students.

EDUCATION

PhD in Biochemistry **Expected in 07/2025**
University of Ottawa, Faculty of Medicine, Ottawa, ON, Canada

Master's Degree in Biology **06/2015**
University of Balamand, Faculty of Science, Tripoli, Lebanon

Bachelor's Degree in Biology **07/2012**
Lebanese University, Faculty of Science III, Tripoli, Lebanon

PUBLICATIONS

- Cystine/glutamate antiporter xCT controls skeletal muscle glutathione redox, bioenergetics, and differentiation., **Michel N. Kanaan**, Chantal A. Pileggi, Charbel Y. Karam, Luke S. Kennedy, Claire Fong-McMaster, Miroslava Cuperlovic-Culf, Mary-Ellen Harper, Redox Biology, 2024
- Impaired xCT-mediated cystine uptake drives serine and proline metabolic reprogramming and mitochondrial fission in skeletal muscle cells., **Michel N. Kanaan**, Charbel Y. Karam, Chantal A. Pileggi, Luke S. Kennedy, Miroslava Cuperlovic-Culf, Mary-Ellen Harper, Redox Biology, 2025, *under review*
- The integrated stress response promotes neural stem cell survival under conditions of mitochondrial dysfunction in neurodegeneration., Mohamed Ariff Iqbal, Maria Bilen, Yubing Liu, Vanessa Jabre, Bensun C Fong, Imane Chakroun, Smitha Paul, Jingwei Chen, Steven Wade, **Michel Kanaan**, Mary-Ellen Harper, Mireille Khacho, Ruth S Slack, Aging Cell, 2024
- OPA1 mediates cardiac function and metabolism: in silico and in vivo evidence., Claire Fong-McMaster, Serena M. Pulente, Luke Kennedy, Tyler K.T. Smith, Stephanie Myers, **Michel Kanaan**, Charbel Karam, Matthew Cope, Ilka Lorenzen-Schmidt, Craig J. Goergen, Morgan D. Fullerton, Miroslava Cuperlovic-Culf, Erin E. Mulvihill, Mary-Ellen Harper, Journal of Translational Medicine, 2025, *in progress*

VOLUNTEER EXPERIENCE

Scout Leader **10/2013 - 10/2017**
Scout du Liban Association Beirut, Lebanon

- Organized and led scout-related activities for younger members, fostering cultural awareness, community participation, and leadership principles.
- Participated in many musical events and concerts.

Choir Founder and Leader **04/2019 - Present**
Saint Charbel Church Ottawa, ON, CA

- Founded and continue to lead a dynamic youth choir, fostering musical talent and community engagement.
- Organized and directed performances for various church services, cultural events, and local community activities
- Built a cohesive team environment that promotes collaboration, discipline, and artistic expression.